NOTE TO USERS

DISSERTATION

The Role of mDia1 During the Initiation of Polarization and Migration of Chick Embryo Cardiac Fibroblasts

Submitted by

Lubna Tahtamouni

Department of Biology

In partial fulfillment of the requirements

For the Degree of Doctor of Philosophy

Colorado State University

Fort Collins, Colorado

Summer 2005

COLORADO STATE UNIVERSITY

July 8, 2005

WE HEREBY RECOMMEND THAT THE DISSERTATION PREPARED UNDER OUR SUPERVISION BY LUBNA TAHTAMOUNI ENTITLED THE ROLE OF MDIA1 DURING THE INITIATION OF POLARIZATION AND MIGRATION OF CHICK EMBRYO CARDIAC FIBROBLASTS BE ACCEPTED AS FULFILLING IN PART THE REQUIREMENTS FOR THE DEGREE OF DOCTOR OF PHILOSOPHY.

Committee on Graduate Work

Advisor

Co-Advisor

Department Head

Abstract of Dissertation

The Role of mDia1 During the Initiation of Polarization and Migration of Chick Embryo Cardiac Fibroblasts

During directional migration, cells exhibit a polarized morphology with leading edge protrusion and retraction at the rear. Polarization requires coordinated reorganization of actin and microtubules. mDia1, a member of the formin family of proteins, coordinates both actin and microtubule cytoskeletons through its FH1-FH2 unit. We hypothesized that both constitutively active (CA) and dominant negative (DN)-mDia1 will disrupt the polarization and thus the migration of chick embryo cardiac fibroblasts (CECF) through their effects on actin and microtubules. We used adenoviral mediated gene expression coupled with GFP and RFP expression for 24 h prior to plating the explants or 48 h prior to plating dissociated cells. Our results indicate that 24.9%and 4.8% of cells expressing CAmdia1 or DNmDia1, respectively, exhibited polarized morphology (protrusion of a single lamellipodium) compared to 52% in uninfected and control adenovirus-infected cells. Cell migration in culture was followed by time-lapse microscopy. Polar and bipolar cells infected with CA-mDia1 adenovirus retained the capacity to migrate, but they were slower (0.49 μm/min and 0.11 μm/min, respectively) than their control-infected counterparts (1.14 μm/min and 0.34 μm/min, respectively).

Overexpression of CAmDia1 increased the size (41.8%, and 159.6% increase for polar and bipolar CECFs, respectively), number (53.1% increase for polar CECFs), and total area (112.7%, and 61.9% increase for polar and bipolar CECFs, respectively) of focal adhesions in CECFs, and increased the formation of stabilized microtubules (Glu-microtubules), but had no effect on G-actin/F-actin balance in these cells. Together, our data demonstrate that mDia1 regulates cell adhesion and microtubule dynamics in CECFs, both of which are critical for cell migration. More than 60% of CAmDia1-infected dissociated CECFs had circumferential F-actin phenotype after 1 h of plating, compared to 23% in control uninfected and GFP-infected dissociated CECFs. CAmDia1-expressing dissociated CECFs that were blocked at the circumferential stage had a higher phosphoAC/cofilin ratio than the control uninfected cells. Furthermore, when CECFs expressing CAmDia1 were co-infected with adenovirus expressing an active non-phospho-regulated ADF/cofilin, cells progressed to the next stage of polarization, the F-actin oriented phenotype. Thus, CAmDia1 overexpression in dissociated CECFs results in the block of progression from the circumferential to the oriented stage by inactivating ADF/cofilin.

Cells infected with DN-mDia1 failed to migrate out of the explants, and DNmDia1-infected dissociated CECFs failed to adhere. Thus it was impossible to obtain data on focal adhesions size and number. However, co-infection of DNmDia1-expressing CECFs with adenovirus expressing wild-type paxillin (a focal adhesion protein), rescued the ability of the cells to migrate out of the explants, suggesting that the migration defects of these cells results from faulty adhesion.

The CAmDia1-mediated enhanced microtubule stabilization minimized the ability of microtubules to target focal adhesion leading to their disassembly, which in turn caused loss of polarization and reduction in migration rate of CECFs. On the other hand, the absence of mDia1 resulted in faulty adhesion and migration defects.

Lubna Tahtamouni
Department of Biology
Colorado State University
Fort Collins, CO 80523
Summer 2005

To my Mom and Dad,
I am blessed to have you as my parents

Acknowledgements

I devote my deepest gratitude to my super-advisor Dr. James R. Bamburg for giving me the opportunity to work in his exceptional "around the clock, 24/7" lab, and for guiding me into the world of science. I appreciate all the time that he gave to teach me and share his scientific thinking and knowledge in molecular cell biology. I would like to thank my thesis committee members, Dr. Patricia A. Bedinger, Dr. Donald L. Mykles, Dr. Noreen E. Reist, and Dr. A.S.N Reddy for their valuable time and comments. I thank Dr. Louise Cramer for giving me the opportunity to work in her lab and for her valuable input.

The studies in this thesis would not have been completed without the help of Laurie Minamide, the first person in the lab to teach me and guide me through the world of cell culture, but more importantly for being such a great inspiration. Our skillful technician Alisa Shaw for helping me in cloning and constructing the adenovirus. My deepest gratitude goes to Dr. Joseph Fass for his ongoing help and support, for reviewing and improving this thesis, but mainly for putting up with me.

I owe my giant thanks to all the Bamburg lab members "The JRB'ls", Dr. Barbara Bernstein, Dr. Judy Boyle, Dr. O'Neil Wiggan, Kevin Flynn, Janel Funk, Hui Hung, Chi Pak, Hilary Bowden, James Burback, and Katie McDermott. Also my thanks to those who have left the lab during my stay: Sankar Maiti, Patrick Sarmiere, and Andy Kinley. I would like to express my special thanks for giving me such a memorable working place.

An extremely important part of my life, my family, I am grateful to my parents, the greatest parents any one can have, without their support I would never have made it. To my sisters and brothers, their love and support were unconditional. I thank my dearest best friend Hanan Al-Zraikat, for being there for me during my ups and downs. I would like to especially thank my cousin Raef Tahtamuni for his fantastic support and sharing his positive way of looking at life.

Finally, I would also like to thank all of those, who due to my memory were not mentioned, thanks for the help and friendship.

Table of contents

List of Figures

List of Tables

Table of Abbreviations

aa	Amino acid
Ab	Antibody
ABPs	Actin binding proteins
AC	ADF/cofilin
APC	Adenomatous polyposis coli
Arp2/3 complex	Actin-related protein 2/3 complex
CA	Constitutively active
Cas	Crk-associated substrate
CaM kinase-II	Calcium calmodulin-dependent protein kinase II
CCD	Coiled-coil domain
CECF	Chick embryo cardiac fibroblast
CIID	C-terminal intramolecular interaction domain
CLASPs	Cadherin-like asymmetry proteins
CLIP-170	Cytoplasmic linker protein-170
DAD	Diaphanous autoregulatory domain
DID	Diaphanous inhibitory domain
DIP	Diaphanous-interacting protein
DN	Dominant negative
DOCK-180	Dedicator of cytokinesis-180
DRF	Diaphanous related formin
EB1	End binding-1
Ena	Drosophila Enabled
FH	Formin homology
FH-1	Formin homology domain-1
FH-2	Formin homology domain-2
FH-3	Formin homology domain-3
FITC	Fluorescein
GAP	GTPase-activating protein
GBD	GTPase-binding domain
GEF	Guanine nucleotide exchange factor
GFP	Green fluorescent protein
GSK-3β	Glycogen synthase kinase-3β
HEK 293	Human kidney cell line 293
IRSp53	Insulin receptor substrate protein- 53
LIMK	LIM kinase
MAP	Microtubule-associated protein
MCAKs	Mitotic centromere-associated kinesins

Mena	Mammalian Enabled
MLC	Myosin light chain
MTOC	Microtubule organizing center
PAK1	p21-activated kinase 1
PAR	Partition defective
PIP2	Phosphatidylinositol-4,5-bisphosphate
RBD	Rho-binding domain
RFP	Red fluorescent protein
ROCK	p160 Rho-coiled coil kinase
S.E.M.	Standard error of the mean
SH3	Scr-homology domain-3
SRF	Serum response factor
Tβ4	Thymosinβ-4
+-TIPs	Microtubule Plus end- tracking proteins
TM	Tropomyosin
Tmod	Tropomodulin
Tppp/p25	Tubulin polymerization promoting protein/p25
TR	Texas Red
VASP	Vasodilator-stimulated phosphoprotein
WASp	Wiskott-Aldrich syndrome protein
WAVE	WASP family Verprolin-homologous protein
WT	Wild-type

Glossary

Adenomatous polyposis coli (APC): a tumor suppressor protein. Mutations in the adenomatous polyposis coli (*APC*) gene contribute to colorectal tumorigenesis and are commonly associated with sporadic colon cancers. APC is required for the Wnt-regulated degradation of ß-catenin, an important regulator of transcriptional activation and cell adhesion; it plays a role in chromosome segregation during mitosis and is implicated in regulating microtubule dynamics.

Arp2/3 complex: a complex of seven proteins, two of which (Arp2 and Arp3) share 50% sequence homology with actin. Arp2/3 complex nucleates the assembly of a new actin filament at an angle of 70^{o} to the preexisting filament and thus creates a branched network. It is activated by proteins of the WASp and Scar family.

CLASPs: microtubule plus-end tracking proteins. They are localized preferentially to the plus ends and regulate microtubule dynamics.

CLIP-170: the first protein that was identified as a microtubule-plus end tracking protein. It loads on the plus-end region of microtubule by recognizing a yet unknown feature and falls off from a more minus-end location. It associates with IQGAP1 which links microtubules to actin.

Crk-associated substrate (Cas): a scaffold protein at focal adhesions. It associates with mDia1 and mediates phosphorylation of Src-dependent and localization of Crk and DOCK-180 to focal adhesions.

Crk: an adapter protein that contains an SH2 domain and two SH3 domains, it binds Src kinase and Cas in a phosphorylation-dependent manner. Phosphorylated Crk localizes DOCK-180 to focal adhesion.

Diaphanous-interacting protein (DIP): an 80kDa protein that associates with mDia1 and is required for mDia1-mediated activities such as stress fiber and focal adhesion formation and Rac activation.

Diaphanous- related formins (DRF): a subclass of formin family of proteins. The members of this subclass share an N-terminal Rho-binding domain and a C-terminal autoregulatory domain.

DOCK-180: a member of the CDM (Ced-5 of Caenorhabditis elegans, mammalian DOCK-180, Mbc of Drosophila melanogaster) family of proteins. Following integrin receptor activation, Cas, Crk and DOCK-180 form a complex that is targeted to focal adhesions. DOCK-180 functions as a GEF or recruits a GEF to activate Rac. The CrkII/DOCK-180/Rac cascade promotes the reorganization of the actin network, membrane ruffling, and lamellipodial protrusions.

EB1: a microtubule plus-end tracking protein that forms a complex with APC and mDia1. This complex captures and stabilizes microtubules at the leading edge of migrating cells.

Ena: a member of the Ena/VASP family of proteins that stimulates straight actin filament assembly by competing with capping proteins.

GTPase-activating proteins (GAPs): proteins that induce inactivation of Rho through GTP hydrolysis.

Guanine nucleotide dissociation inhibitors (GDIs): GDIs preferentially bind to GDP-bound form of Rho and prevent both spontaneous and GEF-catalyzed release of nucleotide, thus maintaining the Rho-GTPases in the inactive state.

Guanine nucleotide exchange factors (GEFS): proteins which catalyze the release of GDP from Rho.GDP allowing GTP binding and reactivation.

Glycogen synthase kinase-3β (GSK-3β): a component of the Wnt signaling pathway. Cytoplasmic β-catenin is degraded in a proteasome-dependent pathway through the formation of a "destruction complex," which contains GSK-3, axin, and APC proteins. The phosphorylation of β-catenin by GSK3 is required for the formation of this "destruction complex." The activity of GSK3 is inhibited by protein kinase B (PKB)/Akt, a downstream effector of PI3-K. GSK is implicated in the control of a wide variety of cellular processes, such as growth, death, adhesion, and motility.

IRSp53: a scaffold protein that links the three most common Rho GTPases (RhoA, Cdc42, and Rac1). Down stream of IRSp53, Mena, WAVE2 and mDia1, IRSp53 stimulates actin polymerization and lamellipodium protrusion.

LIMK: Serine/threonine kinase that phosphorylates ADF/cofilin family proteins at Ser3 thus inactivates them.

Mitotic centromere-associated kinesins (MCAKs): are unusual kinesins (Kin1 family). They use ATP to bind the ends of microtubules rather than move along them. MCAKs remove tubulin subunits from the plus ends and thus stimulate depolymerization. Overexpression of MCAKs leads to complete loss of microtubules, perhaps by increasing catastrophe frequency.

Mena: a member of the Ena/VASP family of proteins. Mena is localized to the filopodial tip and protects elongating actin filaments from tight capping.

PAK-1: a kinase downstream of Rac and Cdc42 that inhibits cofilin activity via phosphorylation and stimulation of LIM kinase (LIMK). LIMK inactivates cofilin by phosphorylating Ser3.

ROCK: a downstream effector of Rho. It phosphorylates LIMK which in turns inactivates ADF/cofilin; it also phosphorylates myosin light chain and myosin light chain phosphatase which enhance contractility.

Serum response factor (SRF): a transcription factor that controls growth factor-inducible and muscle-specific genes (e.g. vinculin, smooth muscle α-actin, and β-actin). SRF is activated in response to depletion of the cellular G-actin pool.

Thymosinβ-4: G-actin sequestering protein.

Tropomyosins (TM): a large family of 100% α-helical fibrous proteins. TMs are found in the thin filaments of vertebrate striated and cardiac muscles where they inhibit myosin binding to actin in the absence of elevated calcium. TM does not bind to G-actin but binds longitudinally along actin filaments with a molar ratio of approximately 1:7. In non-muscle cells, TM is localized to stress fibers in bands of 1-2 μm, alternating with 0.5 μm bands of α-actinin. Some isoforms of TM stabilize actin filaments by decreasing the off-rate constant for actin at the pointed end.

Tropomodulin: a pointed-end capping protein of actin filaments which decreases the dynamics of pointed ends.

VASP: a protein that regulates actin assembly and elongation by competing with capping proteins.

WASp and WAVE family proteins: promote actin polymerization by stimulating Arp2/3-complex-dependent filament nucleation.

Chapter one

Introduction

Actin and microtubule dynamics during cell polarization and migration

Cell polarization and migration:

Cell polarization and movement are fundamental features of embryonic development in multicellular organisms. They are required for establishing tissue patterns and in other processes such as the response of macrophages to pathogens and for wound healing. They are also important for abnormal processes such as the metastases of tumor cells. Cells change their shape and migrate in response to guidance cues. In directional migration, cells exhibit polarized morphology, protrusion at the leading edge, and retraction at the rear (Nobes and Hall, 1999). The establishment of cell polarity and cell migration requires the coordinated communication of G-proteins to both the actin and microtubule cytoskeletons. It is generally accepted that cell movement is mostly dependent on the dynamic reorganization of the actin cytoskeleton, which entails polymerization of actin at the leading edge, and actin bundling and myosin-based contractility at the rear (Machesky and Cooper, 1999; Nobes and Hall, 1999; Habas *et al.,* 2001; Ishizaki *et al.,* 2001). However the mechanisms by which microtubules contribute to cell migration are still elusive and it seems likely that their contribution is cell type-dependent.

In some cell types, the microtubule array is needed for the maintenance of polarization in that the application of microtubule-depolymerizing drugs leads to random migration due to the formation of multiple protrusions (Eddy *et al.*, 2002; Omelchenko *et al.,* 2002). During the migration of fibroblasts, microtubule plus ends penetrate the lamellipodium and are stabilized transiently. This selective stabilization of the plus ends of microtubules enables the microtubule-organizing center (MTOC) to reorient towards the leading edge (Etienne-Manneville and Hall, 2001), which results in a polarized microtubule array that maintains directional cell migration (Magdalena *et al.,* 2003; Kodama *et al.,* 2004). However, migration of fish keratocytes is unaffected by microtubule disassembly and neutrophil motility is even increased in the absence of microtubules (Palazzo *et al.,* 2001; reviewed in Etienne-Manneville, 2004).

This thesis will focus on defining a role of a protein that interacts with both the microtubule and actin cytoskeletons. To be able to understand how this protein, mammalian diaphanous (mDia1), carries out its functions, it will be necessary to review aspects of both the actin and microtubule cytoskeletons and the proteins that regulate each of these.

Actin cytoskeleton

A. Actin structure:

Monomeric (G-) actin is a globular protein of a molecular mass of nearly 43 kDa. The overall structure consists of four quasi-subdomains, each having a repeating motif comprising a multi-strand β-sheet, a β-turn, and a right-handed βαβ-unit (Aguda *et al.,* 2005). Almost 40% of the structure is α-helical. A tightly bound nucleotide lies in a deep cleft in the center of G-actin, which is usually occupied by ATP or ADP-Pi rather than

ADP (Figure 1.1a) (Otterbein *et al.,* 2001; reviewed in dos Remedois *et al.,* 2003). G-actin assembles under physiological salt concentrations to form filamentous (F-) actin (reviewed in Steinmetz *et al.,* 1997; Gungabissoon and Bamburg, 2003). No atomic structure has yet been determined for F-actin, but some possible models have been proposed. These models include: (1) the Holmes fiber diffraction model (Holmes closed model; Holmes *et al.*, 1990), (2) the Egelman electron microscopy reconstruction model (Belmont *et al.*, 1999), which is a Holmes-like model that comprises open-cleft actin protomers (Holmes-like open model), and (3) the unrelated ribbon-to helix model that is based on actin:actin crystal contacts within profilin:actin crystals (Schutt *et al*, 1993). The conventional view is a two-start, right-handed long-pitch helix. In this model, there are 12-14 monomers per half turn and a half pitch of 360-390 . Actin filaments have a distinct structural polarity that was first noticed when the filaments were decorated with the heavy meromyosin or S1 fragments of myosin, both of which appear as arrowheads along the filament (Huxley, 1963; Nachmias and Huxley, 1970; Svitkina and Borisy, 1998), and thus the opposite ends of the filament were called "barbed" and "pointed" ends (Figure 1.1b). Assembly studies on decorated actin filaments showed the barbed end to be the faster growing end (Wegner, 1982; Fujiwara *et al.,* 2002).

B. Actin dynamics:

Actin polymerization in vitro shows an initial delay (lag phase) due to the instability of actin dimers and the slow formation of stable actin trimers (nucleation). This phase is followed by an elongation phase during which actin monomers are assembled into filaments that grow from both ends, but faster at the barbed end (plus end). A lag phase in assembly does not occur in vivo because spontaneous nucleation is

Figure 1.1
Monomeric G-actin structure and F-actin decoration.
A) Ribbon representation of monomeric actin molecule, in the ADP-bound state. Adapted from Otterbein *et al.,* Science 293, 2001.
B) Decoration of actin filaments with myosin S1, 1) S1-decorated actin filament displays a helical rope-like appearance, the thicker part of a turn is directed to the pointed end of a filament (direction of the arrow head). Adapted from Svitkina and Borisy, Methods in Enzymology 298, 1998. 2) Schematic representation of (1).

A)

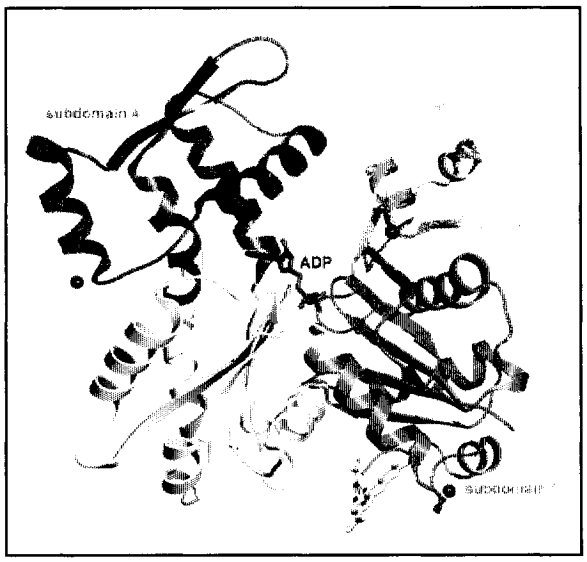

B)

1)

2)

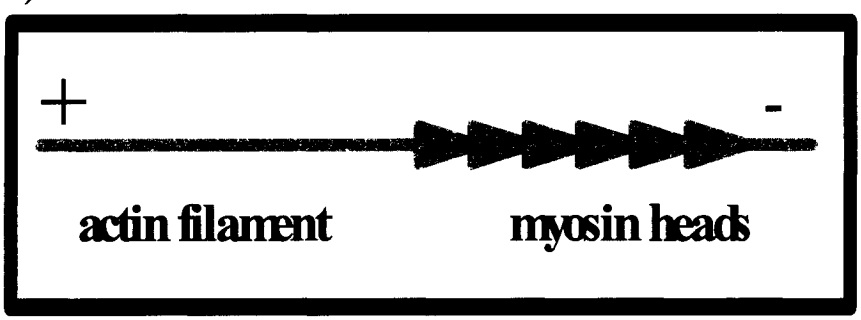

suppressed by actin monomer sequestering proteins. G-actin is incorporated into a growing filament in its ATP-bound form. ATP is then hydrolyzed to ADP-P_i. A conformational change accompanies the release of the phosphate, which is a much slower step *in vitro*. At a monomer concentration between the critical concentration of the plus/barbed end (0.1 μM) and the minus/pointed end (0.7 μM), the barbed ends grow while the pointed ends shrink, resulting in a steady-state process called treadmilling (Wegner, 1982; Fujiwara *et al.,* 2002).

C. Actin binding proteins:

Actin polymerization and depolymerization must be regulated spatially and temporally to produce motility. Polymerization requires free barbed ends, the production of which is tightly regulated in vivo (DesMarais *et al.,* 2005). New free barbed ends can arise from uncapping (Hartwig *et al.,* 1995) or severing of existing filaments (Chen *et al.,* 2000) and *de novo* nucleation (Pollard *et al.,* 2000; Pruyne *et al.,* 2002). Actin binding proteins (ABPs) regulate the different aspects of these processes. Some of the ABPs are discussed below.

1. Monomer-binding proteins:

a) Thymosin β4 (Tβ4) is a small protein (5 kDa) that belongs to a family of conserved proteins originally isolated from the thymus gland but later found to be widely distributed (Yu *et al.,* 1993; Huff *et al.,* 2004). Tβ4 is deficient in hydrophobic residues and almost 50% of its amino acids are charged (Domanski *et al.,* 2004). Tβ4 is abundant in neuronal tissue as well as circulating cells (Yu *et al.,* 1993). Free Tβ4 is predominantly unstructured but increases its α-helical content when it binds actin (Safer *et al.,* 1997; Domanski *et al.,* 2004). Tβ4 sequesters actin monomers and inhibits nucleotide exchange

(Huff *et al.,* 2004). Tβ4 competes with profilin and gelsolin for binding to actin (Ballweber *et al.,* 1997; 1998), and Tβ4 and profilin compete with WASp for binding to actin monomers and presumably have overlapping binding sites (reviewed in dos Remedios *et al.,* 2003). Also, DNase I can displace Tβ4 from the actin monomer (Ballweber *et al.,* 1997).

b) DNase I is a calcium/magnesium dependent nuclease, mainly produced by digestive tissues (Chhabra *et al.,* 2002). A 22 amino acid signal peptide at the N-terminal of the protein directs the nascent peptide to the secretory pathway organelles (Kraehenbuhl *et al.,* 1977). This enzyme is highly expressed by the acinar cells of pancreas and parotid but it is also found in non-digestive tissues such as kidney, lymph node, heart, and pituitary, as well as in serum (Shimada *et al.,* 1998). DNase I has a well-known role in digestion (DNA metabolism), and because of its wide distribution it has been proposed to have other functions, particularly DNA degradation in apoptosis and DNA clearance from extracellular fluid (Napirei *et al.,* 2000). DNase I has been found in the nuclei of apoptotic thymocytes (Peitsch *et al.,* 1993) and of apoptotic prostate epithelial cells after androgen deprivation (Rauch *et al.,* 1997).

On the basis of DNase I activity and distribution in tissue, the mammalian enzymes have been classified into three types (pancreatic, parotid and pancreatic–parotid) (De Maria and Arruti, 2003). Enzymes of the pancreatic type are more sensitive to low pH than those of the other types, and they are packaged with G-actin which has been identified as a potent DNase I inhibitor; when a carboxy peptidase removes the C-terminal amino acids from actin, DNase I is released in the gut (Mori *et al.,* 2001).

c) Profilins are a family of small proteins with an approximate molecular weight of 19 kDa, which bind to ATP-actin in a 1:1 complex (reviewed in Schluter *et al.,* 1997; dos Remedios *et al.,* 2003). Profilin has several functions. First, it has the ability to promote the exchange of nucleotide on actin monomers by opening the nucleotide-binding cleft (Lu and Pollard, 2001). Usually cleft opening results in exchange of ATP for ADP but the reverse exchange activity can also occur under conditions of stress when ADP pools are high. Profilin enhances filament turnover in the presence of cofilin by converting the ADP-actin to ATP-actin with which cofilin has much weaker interaction. Profilin can promote polymerization by transporting G-actin to the filament plus ends (Blanchoin and Pollard, 1998; Didry *et al.* 1998) where it can bind to proteins containing proline-rich regions, such as those in the Ena/VASP family (Reinhard *et al.*, 1995; Ahern-Djamali *et al.*, 1999) or WASp/Scar family (Suetsugu *et al.*, 1998), as well as formins (Watanabe *et al.,* 1997). Profilin also binds to the Arp2 protein in the Arp2/3 complex (Lu and Pollard, 2001). Finally, binding of PIP_2 or PIP to profilin causes its dissociation from actin and its localization to the plasma membrane (Goldschmidt-Clermont *et al.,* 1990). Profilin has three isoforms: profilin I, profilin IIa, and profilin IIb (profilin I and II share ~ 62% sequence similarity). Profilin I is expressed ubiquitously suggesting that it is the major form in almost all tissues. Profilin IIa is expressed abundantly only in the brain, and the expression of profilin I and IIa overlap in the adult brain. Profilin IIb is a minor form. The three isoforms have similar affinities to α-actin, but both forms of profilin II have reduced affinity to PIP_2 binding as compared to profilin I (Lambrechts *et al.,* 2000).

2. F-actin capping proteins:

Capping proteins bind tightly to a particular end of an actin filament, which under normal conditions prevents the addition or exchange of actin monomers at that end. Additionally, barbed end capping proteins stabilize trimers of actin forming nuclei for polymerization (reviewed in Schluter *et al.,* 1997; dos Remedios *et al.,* 2003).

a) CapZ: Several proteins can bind to the plus-end of actin filament such as villin and CapG, but the most abundant is CapZ. CapZ also called barbed-end capping protein is a widely distributed, highly conserved, heterodimeric (α, and β subunits) protein that binds to the filament barbed ends, but does not sever filaments. In skeletal muscle, it localizes to the Z-line (Casella and Torres, 1994).

CapZ nucleates actin assembly and captures preexisting filament barbed ends, preventing assembly (Maun *et al.,* 1996). Uncapping can occur in response to transmembrane signals that leads to the generation of PIP_2, which inhibits the actin binding of capping proteins (Schafer *et al.,* 1996).

b) Tropomodulin (Tmod) caps the pointed ends of actin filaments (Kostyukova *et al.,* 2005). In vertebrates, there are four isoforms that are conserved across species. The genes for all isoforms encode proteins of 40 kDa, with two major domains, an N-terminal unstructured domain that binds tropomyosin and a C-terminal folded domain that consists of five leucine-rich repeats. Tmod1 and Tmod3 are expressed in many tissues and cell types, while the expression of Tmod2 and Tmod4 is restricted to neuronal and skeletal muscle tissues, respectively (reviewed in Fischer and Fowler, 2003).

Tmod capping of pointed-ends occurs in a high- or low-affinity states, and in both cases, capping by Tmod is able to decrease the dynamics of pointed ends; capping by Tmod decreases the polymerization of pointed ends by slowing monomer addition

(Greenfield *et al.,* 2005), which leads to an increase in nucleotide hydrolysis thus increasing the critical concentration for addition at the pointed ends of actin filaments (reviewed in Perry, 2001; dos Remedios *et al.,* 2003).

3. Filament stabilizing proteins:

Tropomyosins (TM) make up a large family of 100% α-helical fibrous proteins. There are four human TM genes, and each gene can produce multiple tissue-specific mRNA transcripts via alternative splicing and different 3' processing (Marston and Redwood, 2003). TMs are found in the thin filaments of vertebrate striated and cardiac muscles (Corsi and Perry, 1958) where they inhibit myosin binding to actin in the absence of elevated calcium (Ebashi and Kodama, 1966; Kress *et al.,* 1986; Bryce *et al.,* 2003). TM does not bind to G-actin but binds longitudinally along actin filaments with a molar ratio of approximately 1:7. In non-muscle cells, TM is localized to stress fibers in bands of 1-2 μm alternating with 0.5 μm bands of α-actinin (reviewed in Gunning *et al.,* 1998). TM is also located in the adhesion belts of epithelial cells. At least some isoforms of TM stabilize actin filaments by decreasing the off-rate constant for actin at the pointed end (assisted by Tmod) (Almenar-Queralt *et al.* 1999). TM is often absent from regions where actin filaments are undergoing reorganization such as the leading edge of migratory cells (reviewed in Perry, 2001; DesMarais *et al.,* 2002), but some isoforms of TM may be compatible with high turnover (Bryce *et al.,* 2003).

4. Filament nucleators:

Actin filaments *in vivo* can be found in either branched or straight networks. In the leading edge of many motile cells, actin filaments form a branched network, while they form straight bundles in microvilli, contractile rings and stress fibers. The Arp2/3

complex is responsible for the formation of branched actin network, while the formins induce the polymerization of straight actin filaments.

a) Arp2/3 complex is a stable complex of seven subunits with two actin-related proteins Arp2 and Arp3, and five novel proteins (Arc) that do not appear to be related to other known proteins (Machesky *et al.,* 1994; 1997; Bailly *et al.,* 1999). The complex is abundant, essential and conserved among eukaryotes. Both Arp2 and Arp3 have nucleotide-binding and cation-binding regions (Mullins *et al.,* 1997), and Arp2 has a profilin-binding domain (Lu and Pollard, 2001). Arp2/3 complex is associated with dynamic cortical regions of cells, and colocalizes with actin filaments that form the "comet tails" of *Listeria* and *Shigella* where actin polymerization propels these bacterial pathogens through the cytoplasm (Brieher *et al.,* 2004).

Arp2/3 complex nucleates the assembly of a new actin filament at an angle of 70^{o} to the preexisting filament and thus creates a branched network (Svitkina and Borisy, 1999). The proteins of the WASp/Scar family stimulate the nucleating activity of Arp2/3 complex (Reviewed in Vartiainen and Machesky, 2004). WASp is the protein defective in Wiskott-Aldrich syndrome, a human genetic disease in which actin cytoskeleton is deficient in platelets and leukocytes (Derry *et al.,* 1994). The members of the WASp family share a central poly proline-region that binds profilin and SH3-containing proteins, a C-terminal WH2 domain which binds actin monomers and prevents their addition to filament minus but not plus ends. Also, WASp/Scar proteins share a C-terminal "A" domain that interacts with one of the Arc proteins in the Arp2/3 complex. WASp/Scar proteins differ in their N-termini (reviewed in Miki and Takenawa, 2003; Stradal *et al.,* 2004). On the N-terminal side of the proline-rich region, these proteins

have a GTPase-binding domain (GBD) and are activated by the Rho GTPases; WASp and N-WASp are effecters of Cdc42, while Scar is a Rac effector (Symons *et al.,* 1996; Higgs and Pollard, 2000). WASp and Scar thus function as mediators between the Rho GTPases and the Arp2/3 complex.

b) Formins are large multidomain proteins that share two regions of homology: formin homology-1 (FH1), and FH2 (Castrillon and Wasserman, 1994). Formin was originally isolated as the gene affected by the murine limb deformity (ld) mutation, which disrupts the epithelial-mesenchymal interactions regulating patterning of the vertebrate limb autopod (Mass *et al.,* 1990). The FH proteins were defined on the basis of conservation in sequence and protein organization (reviewed in Wasserman, 1998). They are widely distributed in eukaryotes from unicellular organisms to higher plants and animal cells (Watanabe *et al.,* 1997). The budding yeast formin Bni1p is involved in the orientation of the mitotic spindle and formation of actin cables and the contractile ring. Budding yeasts lacking the formin genes are nonviable (Sagot *et al.,* 2002b). Mouse formins regulate the anterior-posterior development and patterning of fore and hind limbs (Vogt *et al.,* 1993; Chan *et al.*, 1995), and are essential for the development of both the inner ear and eye (de la Pompa *et al.*, 1995). Formins exert their effects by regulating both actin and microtubule cytoskeletons.

Formins were identified as actin nucleators that mediate the formation of straight filaments or actin cables in an Arp2/3 independent mechanism (Figure1.2) (Chang and Peter, 2002; Pollard, 2002). GST-Bni1pFH1FH2, Bni1pFH1FH2, and GST-Bni1pFH1FH2COOH constructs had similar *in vitro* nucleating activity, which indicated that neither the GST-tag nor the COOH-terminal extension contributed to the nucleation.

Figure 1.2
Nucleation of straight actin filaments by formins. Adapted from Pollard, Nature Cell Biol. 4, 2002.

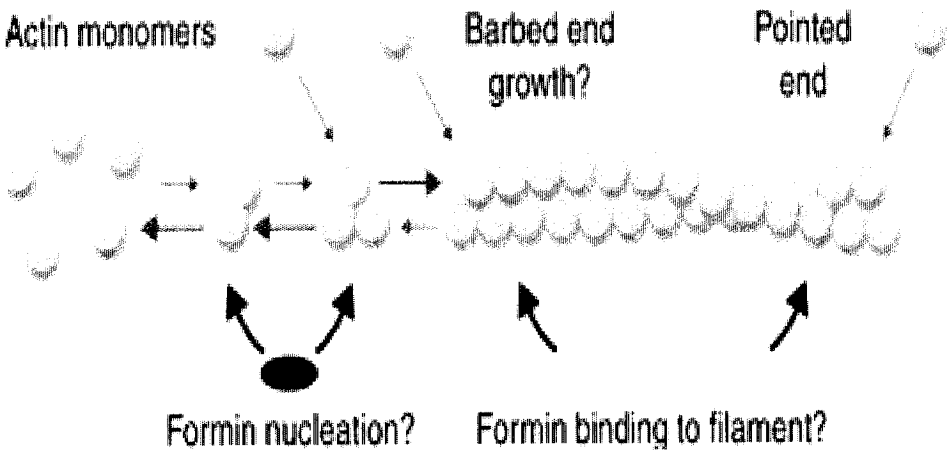

Deletion of the FH2 domain abolished the nucleating activity, and deletion of the FH1 domain diminished the activity to ~ 10%. Expression of constructs containing both FH1 and FH2 in yeast was lethal due to the aberrant accumulation of actin cables, while expression of constructs lacking either one of these domains had no effect. Thus, the FH2 domain is an actin nucleator, and the FH1 domain, which binds profilin, is important for FH2 activity *in vitro* and *in vivo* (Pruyne *et al.,* 2002; Sagot *et al.,* 2002a, b).

5. Filament depolymerizing/severing proteins:

a) ADF/Cofilin proteins have molecular masses between 13-19 kDa (reviewed in Bamburg, 1999). Actin Depolymerizing Factor (ADF) was named because of its ability to depolymerize F-actin and form a complex with G-actin in a 1:1 ratio, while cofilin was named because it co-sediments with F-actin. However, both proteins are pH-dependent in their interactions with F-actin; at pH< 7.0, both ADF and cofilin, when present in excess over actin, slightly increase the G-actin pool while binding and co-sedimenting with F-actin at a stoichemistry of 1:1 with the actin subunits. At pH above 7.3, both proteins increased the unassembled actin pool to different degrees. The activities of ADF and cofilin are regulated by multiple mechanisms including pH, phosphorylation/dephosphorylation at Ser3, PIP_2 binding, competition with TM for actin binding, compartmentalization, and mRNA stabilization (reviewed in Bamburg, 1999; Bamburg and Wiggan, 2002)

b) Gelsolin belongs to a superfamily of proteins that share one or more 120-amino acid structural repeat, which is an ADF-homology domain (reviewed in dos Remedios *et al.,* 2003). Gelsolin is an 80 kDa protein consisting of two homologous halves, each containing three domains. The isolated N-terminal half can bind two G-actin subunits

and sever F-actin in a Ca^{2+}-independent manner, while the C-terminal half binds one actin monomer and is Ca^{2+}-dependent (Khaitlina *et al.,* 2004). After severing F-actin, gelsolin remains bound to the plus-end as a cap, preventing annealing and polymerization at the barbed end while depolymerization proceeds from the minus end until equilibrium is established between capped filaments and free gelsolin. Gelsolin binding to F-actin is inhibited by PIP_2 (Lin *et al.,* 2000) and by some TM isoforms (Nyakern-Meazza *et al.,* 2002). In vivo gelsolin can mimic the ADF/cofilin increases in actin dynamics as evidenced by the ability of gelsolin to maintain the short Listeria comet tail morphology in the absence ADF/cofilin but in the presence of calcium (Larson *et al.,* 2005)

D. Cell signaling regulating the generation of barbed ends of actin filaments in the lamellipodium:

Cell migration, polarity, cytokinesis, and vesicle transport are some of the processes that depend on the actin cytoskeleton. Proper temporal and spatial regulation of actin assembly/disassembly is crucial for such activities (reviewed in Pollard *et al,* 2000; Gungabissoon and Bamburg, 2003; DesMarais *et al.,* 2002). As mentioned previously, polarized cells exhibit a characteristic morphology, protrusion at the leading edge and centripetal contractility at the rear (Nobes and Hall, 1999). Elongation of the barbed ends (pointing towards the membrane) of actin filaments drives membrane protrusion. The assembly and disassembly of the actin filament/network at the leading edge has been formulated into a "dendritic-nucleation model" (Mullins *et al.,* 1998). In this model, actin assembles predominantly at the leading edge because the concentration of uncapped barbed ends is high and is rate-limiting for polymerization (reviewed in DesMarais *et al.,* 2002). Barbed ends can be generated by *de novo* nucleation (Pollard *et*

al., 2000; Sagot *et al.,* 2002b), severing of existing filaments (Chen *et al.,* 2000), uncapping (Hartwig *et al.,* 1995), or a combination of the three. There are two proposed mechanisms for the formation of dendritic brush: 1) WASp-activated Arp2/3 complex binding laterally along pre-existing filaments on ATP- or ADP-Pi-actin subunits, promoting growth of a new filament at a ~70° angle to the original filament (Svitkina and Borisy, 1999), or 2) barbed end branching through the interaction between the Arp2/3 complex and the barbed end of a filament (Pantaloni *et al.,* 2000).

At the rear of a leading edge, two likely mechanisms contribute to the rapid depolymerization of F-actin that supplies the G-actin monomers needed for actin polymerization at the front. The first is the removal of the Arp2/3 complex from pointed ends, a debranching enhanced by ATP hydrolysis on the Arp2/3 complex (Le Clainche *et al.,* 2003), facilitating ADF/cofilin-induced depolymerization (Bailly *et al.,* 2001). The other mechanism is actin filament severing by ADF/cofilin (Bamburg, 1999) and/or gelsolin (Larson *et al.,* 2005) (Figure 1.3)

Microtubule cytoskeleton

A. Microtubule structure:

A microtubule is a non-covalent polymer of 13 protofilaments, each composed of tubulin subunits, which are arranged in a 24 nm diameter cylindrical tube (reviewed in Desai and Mitchison, 1997). The tubulin subunit is a heterodimer of α- and β- tubulin, each about 52 kDa, which are approximately 50% identical at the amino acid level (Burns, 1991). Each tubulin dimer binds two GTP molecules; one binds irreversibly to α-tubulin and does not undergo hydrolysis (Spiegelman *et al.,* 1977), while the other binds reversibly to

Figure 1.3

Model for the turnover of the actin filament array at the leading edge of lamellipodia. The cytoskeletal network at the leading edge of motile cells consists of an extensively branched array of actin filaments with barbed ends facing forward and pointed ends making Y-junctions (about 70° angles) with other filaments. These Y-junctions are formed by the Arp2/3 complex. The treadmilling of this branched array is regulated by a number of actin binding proteins as described below. Numbers in parentheses refer to numbered steps in the diagram. (1) The barbed ends of actin filaments are usually capped by capping protein when the cell is in resting state. When cells are stimulated, free barbed ends are generated in the leading edge (shaded area) to nucleate filament growth and drive membrane protrusion and cell movement. Three potential mechanisms exist for the generation of free barbed ends: dissociation of capping proteins by elevated levels of PtdIns(4,5)P2, filament severing by ADF/cofilin, and actin nucleation dependent on Arp2/3. The Arp2/3 complex is activated on binding to WASP,one form of which is activated by Cdc42. (2) The active Arp2/3 complex nucleates actin filament assembly and/or caps the free pointed end of the ATP- or ADP-Pi-actin filaments. (3) The activated Arp2/3 complex binds to the side of the filament and then nucleates filament growth or captures pointed ends of a preexisting filament. An alternative hypothesis proposes that the activated Arp2/3 complex binds to and branches the barbed end of actin filaments. Growth of filaments is rapid and the lag in Pi disassociation leads to filaments in the leading edge that are composed mostly of ATP and ADP-Pi actin and do not bind ADF/cofilin. (4) At the rear of lamellipodium, two mechanisms may contribute to rapid depolymerization: filament severing or uncapping of pointed ends by removal of the Arp2/3 complex. Severing by AC likely occurs at junctions between regions of filaments that are saturated with AC and naked F-actin. The activated Arp2/3 complex disassociates from the pointed end of ADP-actin because of its weaker affinity for ADP-actin than for ATP- or ADP-Pi-actin. (5) Capping of barbed ends by capping proteins prevents their further elongation. AC enhances depolymerization of ADP-actin from free filament ends in the rear of the lamellipodia. (6) The complex of AC and ADP-actin that disassociates from free filaments ends is in equilibrium with AC and ADP-actin monomer. (7) The nucleotide exchange on actin monomer is a slow process, further inhibited by AC. Profilin enhances nucleotide exchange. SRV2/CAP1 is a protein that binds to the AC-actin complex and dissociates AC while enhancing nucleotide exchange. (8) ATP-actin monomers are sequestered by ß-thymosin to prevent spontaneous nucleation, but provide a pool of ATP-actin for assembly. Adapted from Gungabissoon and Bamburg, J. Histochem. Cytochem. 51, 2003.

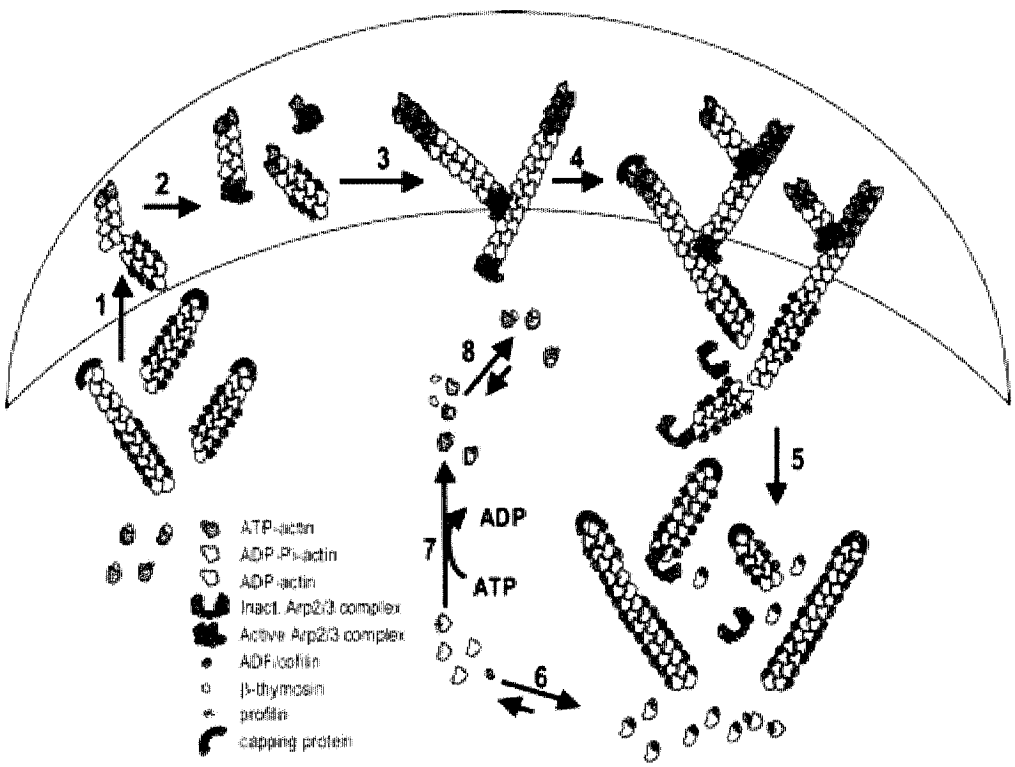

a site on β-tubulin. The β-tubulin GTP molecule can be hydrolyzed to GDP following polymerization (David-Pfeuty *et al.,* 1977). Longitudinal connections between the subunits form protofilaments and lateral connections form a curved sheet that closes into a cylinder (Lodish *et al.,* 2000). In general a singlet microtubule is formed from 13 protofilaments (Evans *et al.,* 1985) (Figure 1.4). Microtubules can also form doublets and triplets, with one complete 13 protofilament-microtubule and the other(s) composed of 10 protofilaments sharing three in a common wall (Lodish *et al.,* 2000). Doublet microtubules are found in axonemes of cilia and flagella, while triplet microtubules are found in centrioles and basal bodies (Nielsen *et al.,* 2001). Microtubules are polar structures, formed by the head-to-tail connections of the heterodimers. One end is ringed with α-tubulin and the other end with β-tubulin (Amos and Klug, 1974).

B. Microtubule dynamics:

As with actin filaments, the two ends of a microtubule have different polymerization rates. The faster growing end has exposed β-tubulin and is referred to as the plus-end, whereas the slower growing minus-end has exposed α-tubulin (Allen and Borisy, 1974). The kinetics of microtubule polymerization has similarities to that of F-actin:

1. At concentration of tubulin dimers below the critical concentration (Cc) for both ends, depolymerization occurs at both ends but more rapidly at the plus end.

2. If the dimer concentration is above Cc+ and below that of Cc-, polymerization occurs at the plus end and depolymerization occurs at the minus end, resulting in treadmilling (Margolis and Wilson, 1978).

Figure 1.4
Microtubule structure. The tubulin subunit is a heterodimer of α- and β- tubulin. Longitudinal connections between the subunits form proto-filaments and lateral connections form a sheet or a cylinder. In general a singlet microtubule is formed from 13 protofilaments. Adapted from Desai and Mitchison, Annu. Rev. Cell Dev. Biol. 13, 1997.

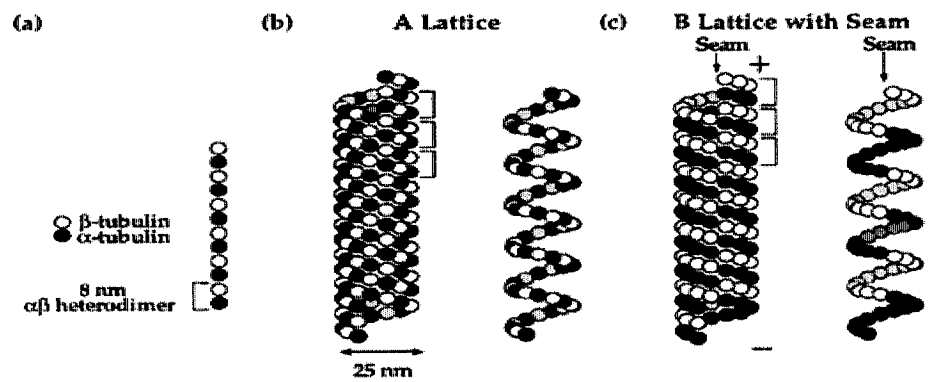

3. If the dimer concentration is above the Cc for both ends, growth occurs at both ends but more rapidly at the plus end (reviewed in Desai and Mitchison, 1997).

Microtubule nucleation usually occurs at the microtubule organizing center (MTOC), from which protofilaments assemble on ring-like structures composed in part of γ-tubulin (McKean *et al.,* 2003). As microtubules elongate at the plus end, protofilaments extend into sheets that close up into a tube as they elongate. At "steady state" there is a constant polymer mass, and catastrophes (described below) of a small percentage of microtubules provide tubulin for growth of the others (reviewed in Desai and Mitchison, 1997).

The major behavior of microtubules *in vivo* is dynamic instability (Mitchison and Kirschner, 1984), in which individual microtubule plus ends alternate between prolonged phases of polymerization (growth) and rapid depolymerization (shrinkage) (Figure1.5). The transition from growth to shrinkage is termed catastrophe, while shrinkage to growth transition is a rescue event. Under the same favorable conditions, some microtubules lengthen while other shrink and individual microtubules oscillate between shortening and growth (Horio and Hotani, 1986; Walker *et al.,* 1988). This behavior is restricted to the plus end because the minus end typically lies at the MTOC and is capped with γ-tubulin (reviewed in Dammermann *et al.,* 2003). This instability allows spatial organization and rapid remodeling of the microtubule arrays, and allows microtubule plus ends to search for their target sites (binding partners) more efficiently (search-target model) (Mitchison and Kirschner, 1984; Hayden *et al.*, 1990; Holy and Leibler, 1994). Captured microtubules, which are stable, are then subjected to further modifications that can both

Figure1.5
Dynamic instability of microtubules in which individual microtubule plus ends alternate between prolonged phases of polymerization and rapid depolymerization Adapted from Desai and Mitchison, Annu. Rev. Cell Dev. Biol. 13, 1997.

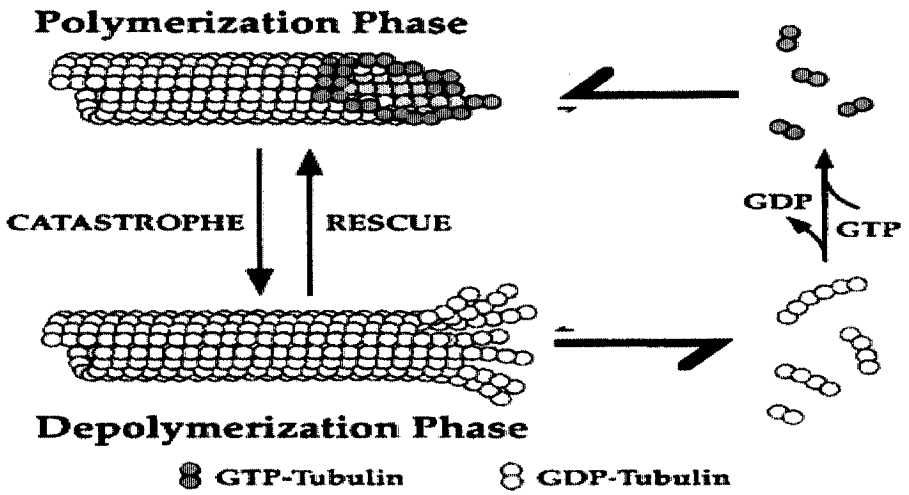

increase their stability and alter their properties- such as detyrosination and acetylation (Chang *et al.,* 2002).

In many cells it has been found that microtubules exist in two pools: (1) microtubules that undergo dynamic instability with half-lives of ~ 5-10 minutes (reviewed in McNally, 1996), and (2) stabilized microtubules with half-lives of 30 minutes to 1 hour that are formed at the onset of polarization and are aligned along the axis of polarity (Bulinski and Gundersen, 1991). Tubulin is post-translationally modified in stable microtubules. The α-tubulin undergoes a reversible removal of the C-terminal Tyr (detyrosination), exposing the penultimate Glu residue (Chang *et al.,* 2002). Antibodies specific for Tyr and Glu microtubules have been developed allowing the visualization of the stabilized and dynamic microtubule populations in cells (Gundersen *et al.,* 1984; Brown *et al.*, 1993; Kann *et al.,* 2003). Detyrosinationof microtubules permits the selective binding of certain microtubule motors, which result in polarizing the distribution of vimentin intermediate filaments (Palazzo *et al.,* 2001), among other cargo. Acetylation of certain lysine residues of both α- and β-tubulin is also another post-translational modification of stable microtubules (Bulinski and Gundersen, 1991).

C. Microtubule-binding proteins:

1. Microtubule-associated proteins:

There are several different categories of microtubule-associated proteins (MAPs) including assembly-promoting MAPs, MAPs that can bind microtubules but do not affect dynamic instability, and catastrophe-promoting MAPs (reviewed in Desai and Mitchison, 1997, Soltani *et al.,* 2005). MAPs co-purify with microtubules in a defined stoichiometry through assembly and disassembly cycles because they have microtubule binding

activity. Assembly-promoting MAPs bind along microtubules in the cytoplasm and some have the ability to cross-link microtubules (Lodish *et al.,* 2000). The cross-linking MAPs have two domains: a microtubule-binding domain, and an acidic projection domain that can bind another microtubule, membranes, or intermediate filaments (Vallee and Borisy, 1977, Aizawa *et al.,* 1989). The major neuronal MAP families are MAP1 and MAP2 (Soltani *et al.,* 2005) (its members are assembly stabilizing MAPs) (reviewed in Baas and Qiang, 2005). The major non-neuronal MAP is MAP4 (Matsushima *et al.,* 2005). MAP1A and MAP1B are multimeric protein complexes containing one heavy and several light chains. Both can bind to microtubules and F-actin, suggesting that they could mediate the interaction between actin and microtubules essential for neuronal morphogenesis and function (Noiges *et al.,* 2002). Most identified MAPs are regulated by phosphorylation (Haque *et al.,* 2004). A novel protein kinase (p110MARK), identified in brain extracts, can phosphorylate multiple MAPs *in vitro* (Drewes *et al.,* 1995; Illenberger *et al.,* 1996). Phosphorylated MAPs are inhibited in their ability to bind microtubules (Haque *et al.,* 2004).

2. Microtubule-destabilizing proteins:

A. Op18/Stathmin/P19/metablastin is a 19 kDa protein that is organized into two domains: an N-terminal regulatory domain that contains four phosphorylation sites, and a C-terminal domain that interacts with other proteins (Beretta *et al.,* 1993; Curmi *et al.,* 1994). Stathmin can induce microtubule depolymerization in a way that is dependent on its phosphorylation state (Marklund *et al.,* 1996). In its unphosphorylated state, a single stathmin can bind and sequester two tubulin heterodimers to form a "tubulin sequestering complex" (Curmi *et al.,* 1997) thereby enhancing depolymerization and increasing the

rate of catastrophe (Howell *et al.,* 1999). Phosphorylation of stathmin on different combinations of sites during the cell cycle or in response to stimuli reduces its ability to interact with tubulin. The four phosphorylation sites are at serine 16, phosphorylated by p-21 activated kinase1 (PAK1) (le Gouvello *et al.,* 1998) or calcium calmodulin-dependent protein kinase II (CaM kinase II) (Marklund *et al.,* 1994), serine 25, a substrate for MAPKs in response to stress and growth factors (Leighton *et al.,* 1993), serine 38, a target for the cyclin-dependent kinases $p34^{cdc2}$ (Beretta *et al.,* 1993) or $p33^{cdk2}$ (Brattsand *et al.,* 1994), and serine 63, the major site for the cyclic AMP-dependent protein kinase A (PKA) (Beretta *et al.*, 1993). The stathmin-related proteins SCG10 (Okazaki *et al.,* 1995), SCLIP (Ozon *et al.,* 1998), and RB3 are specifically expressed in the nervous system (Maucuer *et al.,* 1993; Ozon *et al.,* 1998). SCG10, which has a 34 amino acid N-terminal extension with a palmitoylation site to target it to membranes, is phosphorylated similarly to stathmin but RB3 is not (Gavet *et al.,* 1998; Wittmann *et al.,* 2004).

B. Mitotic centromere-associated kinesins (MCAKs) are unusual kinesins (Kin1 family). They use ATP to bind the ends of microtubules rather than move along them. MCAKs remove tubulin subunits from the plus ends and thus stimulate depolymerization. Overexpression of MCAKs leads to complete loss of microtubules, perhaps by increasing catastrophes (Howard and Hyman, 2003).

C. Microtubule-severing proteins are members of the AAA family (ATPase associated proteins with a variety of cellular activities). The AAA family is a large and diverse set of proteins that use the energy of ATP hydrolysis to catalyze the assembly or disassembly of a variety of protein complexes (Frickey and Lupas, 2004). The best characterized

microtubule-severing protein is katanin, named for the Japanese samurai sword (reviewed in Baas and Qiang, 2005). Katanin is more highly expressed in neurons than it is in many other cell types and is present throughout the neuron (Karabay *et al.,* 2004). Constitutively active katanin has been observed to break microtubules completely into subunits (Ahmad *et al.,* 1999). Katanin-based microtubule severing might be regulated by MAPs that block access of katanin to the microtubule; phosphorylation of MAPs leads to their dissociation from microtubules, thus permitting katanin access. MAP4 has been shown to suppress microtubule severing by katanin *in vitro* studies (McNally *et al.,* 2002). In dividing cells, the levels of P60-katanin (the subunit with severing properties) increase as the cell transitions from interphase to mitosis (Karabay *et al.,* 2004). In neurons, katanin levels are high during phases of rapid axonal growth and drop rapidly when the axon reaches its target and stops growing (Karabay *et al.,* 2004).

Another microtubule-severing protein is spastin. A mutation in spastin causes human autosomal dominant hereditary spastic paraplegia (AD-HSP). Expression of wild-type human spastin in transfected cell lines and cortical neurons caused disassembly of the microtubule cytoskeleton, while a mutant spastin lacking catalytic activity co-localized with tubulin (Sherwood *et al.,* 2004; Svenson *et al.,* 2005).

3. Microtubule polymerization-promoting proteins:

Tubulin polymerization-promoting protein (TPPP/p25) was identified as an intrinsically unstructured, brain-specific, and tubulin-binding protein that at sub-stoichiometric concentrations promotes the polymerization of tubulin into polymorphic aggregates and bundles of paclitaxel-stabilized microtubules in vitro (Tirian *et al.,* 2003; Kovacs *et al.,* 2004). TPPP/p25 is enriched in the Lewy bodies of Parkinson's disease

and diffuse Lewy body disease, as well as glial inclusions of multiple system atrophy (Kovacs *et al.,* 2004). Electron microscopy studies revealed clusters of TPPP/p25 immunoreactivity along filaments of the neurofibrillary tangles in Alzheimer's disease (Orosz *et al.,* 2004). At low expression levels, EGFP-TPPP/p25 specifically co-localizes with the microtubule network of HeLa cells, while at high levels of expression, it inhibits cell division and promotes cell death through the formation of aberrant microtubule arrays (Lehotzky *et al.,* 2004; Orosz *et al.,* 2004).

4. Microtubule plus-end tracking proteins:

Capture of microtubule plus-ends at special regions of the cell cortex is essential for such processes as positioning of the mitotic spindle (Miller *et al.,* 2000), cell migration (Wen *et al.,* 2004) and axon extension (Reviewed in Fukata *et al.*, 2002). Proteins of the CLIP-170 family (Perez *et al.,* 1999), EB1 family (Su *et al.,* 1995) and dynein/dynactin complex (Lansbergen *et al.*, 2004) accumulate at the plus ends and play a critical role in microtubule/cortex interaction, they have been collectively called "plus end- tracking proteins" or +-TIPs (reviewed in Schuyler and Pellman, 2001; Fukata *et al.,* 2002; Mimori-Kiyosue and Tsukita, 2003). +TIPs undergo treadmilling in which they incorporate into microtubule plus-end either by associating with newly assembled tubulin dimers or by recognition of a specific feature of these ends (the GTP-cap or the unfolded polymer sheet) (Diamantopoulos *et al.,* 1999), and subsequent release from an older, more proximal part of the microtubule (Perez *et al.,* 1999).

1. The CLIP-170 family includes CLIP-170 (cytoplasmic linker protein-170) (Perez *et al.,* 1999), CLIP-115 (Hoogenraad *et al.,* 2000), and CLIP-associated proteins or CLASPs (Akhmanova *et al.,* 2001). CLIP-170, the first plus-end tracking protein to be

identified, was found to link microtubules to endosomes in HeLa cells (Perez *et al.,* 1999). CLIP-170 binds IQGAP1 (Gundersen, 2002), which was named for its homology to GTPase activating proteins (GAPs) and its IQ (calmodulin binding) motifs. IQGAP1 binds two GTPases, Rac and Cdc42, but in contrast to regular GAPs which inhibit GTPases by increasing their GTPase activity, IQGAP1 does not act as a GAP. Rather, it appears to inhibit the GTPase activity of Cdc42, maintaining it in an active state (Bashour *et al.,* 1997; Fukata *et al.,* 1997). Also, IQGAP1 directly binds actin filaments and crosslinks them (Mateer *et al.,* 2004).

The CLIP-170/IQGAP complex then binds Rac1 or Cdc42 forming a tripartite complex that functions to link microtubule plus ends and the cortical actin network aiding in the maintenance of cell polarization. The tripartite complex may be involved in the initial attachment of microtubules to the cortex because the period of complex localization to the leading edge is short (5-10 min) (Howard and Hyman, 2003). Other mechanisms like Rho-mDia1 signaling (see below) could subsequently and/or alternatively maintain the stabilized microtubules (Wen *et al.,* 2004). CLASPs show a polarized accumulation binding preferentially to the plus ends of microtubules oriented toward the leading edge (Howard and Hyman, 2003).

2. EB1 family: EB1 (end binding-1) was identified as the protein that interacts with adenomatous polyposis coli (APC) tumor suppressor protein (Su *et al.,* 1995; Lu *et al.,* 2001). The EB1/APC complex resembles the CLIP-170/IQGAP1 complex (Howard and Hyman, 2003). EB1 and EB3, another member of this family (Stepanova *et al.,* 2003), were found to accumulate preferentially at the plus ends of neuronal microtubules and can be used as markers for microtubule growth when expressed at low concentrations

with a fluorescent protein tag. At high concentrations EB1 and EB3 will bind along microtubules (Stepanova *et al.,* 2003). Formin family members bind EB1/APC complexes and aid in their localization only to microtubule plus ends (Wen *et al.,* 2004). In budding yeast the formin Bni1p interacts with EB1 and APC homologues to cap microtubules that pull the spindle to the bud (Miller *et al.,* 2000). A complex of the formin mDia1 with EB1/APC captures and stabilizes microtubules during migration of cells from vertebrates (Wen *et al.,* 2004). In mammalian cells, the EB1/APC complex mediates the capture of mitotic microtubules at the kinetochore to ensure the precise distribution of chromosomes to dividing cells (Louie *et al.,* 2004).

3. APC: Adenomatous polyposis coli (APC) is an important tumour suppressor in the human colon, and is conserved in various organisms (Steigerwald *et al.,* 2005). One of its main functions is the destabilization of β-catenin, a key effector of the Wnt signaling pathway. Phosphorylation of APC by glycogen synthase kinase-3β (GSK-3β) inhibits APC action (reviewed in Doucas *et al.,* 2005). APC proteins are also associated with the plasma membrane of epithelial cells where they maintain the integrity of adherens junctions and orient mitotic spindles in the epithelial plane (reviewed in Bienz and Hamada, 2004).

APC was shown to bind throughout its C-terminal basic region directly to microtubules and to stabilize microtubules *in vitro* and *in vivo* (Barth *et al.,* 2002). APC binds preferentially to the plus ends of microtubules; EB1 colocalizes with APC only at these ends (Honnappa *et al.,* 2005). APC binds and activates Asef (a Rac1 GEF), and may promote membrane extension by recruiting Rac1 to the cell cortex (Kawasaki *et al.,* 2000; 2003).

D. How do microtubules control cell polarization?

There are three major hypotheses regarding the role of microtubules in cell polarization: 1) During migration cells orient their MTOC toward the leading edge and thus allow microtubules to provide tracks for the supply of building materials; 2) microtubules stabilize the leading edge of a migrating cell and thus maintain a directed movement; and 3) microtubules sequester Rho-GEF H1 which prevents local activation of Rho (see below) leading to the disassembly of adhesions and detachment of the leading edge (reviewed in Fukata *et al.,* 2002; Stepanova *et al.,* 2003).

Rho GTPases

Rho GTPases are molecular switches that cycle between two conformational states: an active, GTP–bound state, and an inactive state in which GDP is bound. Rho GTPases belong to the Ras superfamily whose members are classified into five groups: Ras, Rho, Rab, Arf, and Ran and regulate many cellular processes (reviewed in Etienne-Manneville and Hall, 2002). The switch between the active and the inactive states of Rho GTPases is regulated by guanine nucleotide exchange factors (GEFs) which catalyze the release of GDP allowing GTP binding and reactivation (Adams *et al.,* 1992; reviewed in Zheng, 2001), and GTPase-activating proteins (GAPs) which induce GTP hydrolysis (an inherent but slow catalytic activity of the G-proteins) and thus inactivation (Hu *et al.*, 2005). There are also guanine nucleotide dissociation inhibitors (GDIs) that can sequester Rho GTPases in the inactive state. GDIs preferentially bind to GDP-bound form of Rho, and prevent both spontaneous and GEF-catalyzed release of nucleotide, maintaining the Rho-GTPases in the inactive state (DerMardirossian and Bokoch, 2005)

(Figure 1.6). The Rho-GTPase family has 16 members, the three best characterized of which are RhoA, Rac1, and Cdc42 (reviewed in Van Aelst and Symons, 2002). Rho-GTPases regulate different cellular activities including cell polarity, gene transcription, microtubule dynamics, vesicular transport, and actin cytoskeleton dynamics. Rho induces acto-myosin contractility and the formation of stress fibers (Watanabe *et al.,* 1999), whereas Rac1 and Cdc42 stimulate the formation of lamellipodia and filopodia, respectively (Ridley and Hall, 1992; Nobes and Hall, 1995).

PAR proteins in cell polarity

The establishment of cell polarity depends on the asymmetrical distribution of organelles, and signaling proteins and the reorganization of the cytoskeleton (Nobes and Hall, 1999). A group of proteins that are essential for the establishment of cell polarization are the PAR (partition defective) proteins (Duncan *et al.,* 2005). These proteins interact with key regulators of the actin and microtubule cytoskeletons.

PAR proteins show polarized localization in embryos and vertebrate cells; PAR-1 and PAR-2 localize to the posterior cortex in embryos and to the basolateral membrane of epithelia, while PAR-3 and PAR-6 localize apically in epithelia, and to the anterior cortex (animal pole) of embryos (Duncan *et al.,* 2005). PAR-3 has three PDZ domains (the PDZ domain is globular fold that mediates protein–protein interactions and supramolecular complex assembly), and PAR-6 has one PDZ domain, as well as a CRIB-like domain that facilitates binding to Cdc42 and Rac GTPases. PAR-3 and PAR-6 form a tripartite complex with PKC-3 (atypical PKC) (Nishimura *et al.,* 2005).

Figure 1.6
The Rho GTPase cycle. Rho GTPases switch between an active form bound to GTP and an inactive form bound to GDP. The switch between the active and inactive state is regulated by guanine nucleotide exchange factors (GEFs, activators), GTPase-activating proteins (GAPs, inactivators) and guanine nucleotide exchange inhibitors (GDIs). GDIs preferentially bind to Rho-GDP form and prevent spontaneous and GEF-catalyzed release of nucleotide, maintaining the Rho-GTPases in the inactive state. Adapted from Etienne-Manneville and Hall, Nature 420,2002

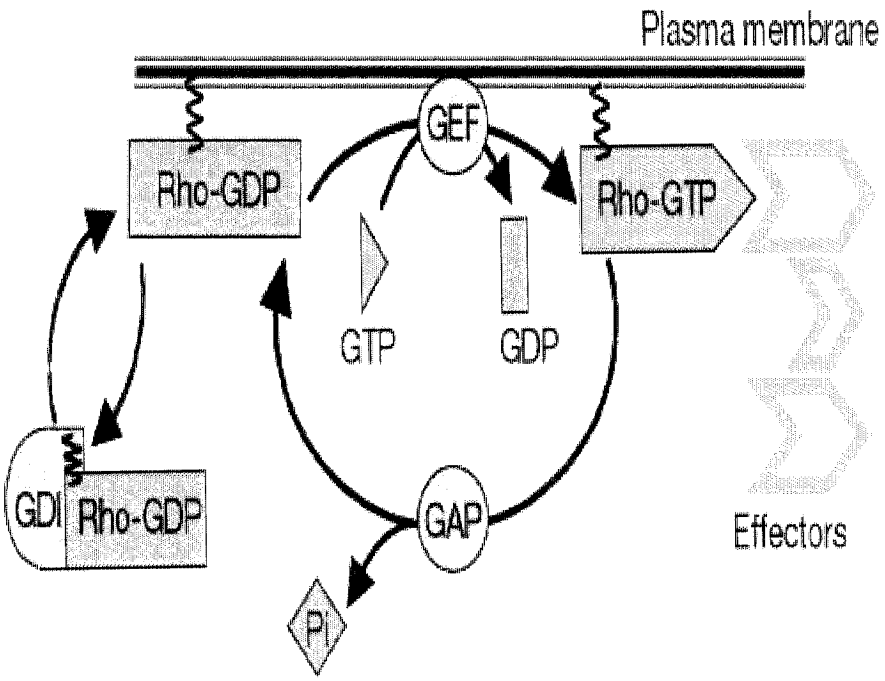

During cell migration, PAR-3 is targeted to the leading edge, and it restricts the localization of PAR-6 and PKC-3 to that region. Cdc42 then binds to PAR-6 and PKC-3 activating the latter, which in turn phosphorylates GSK-3β, inactivating it. Inactivation of GSK-3β leads to microtubule stabilization by APC and MTOC re-localization to face the leading edge (Etienne-Manneville and Hall, 2003). This complex also regulates the establishment of anterior-posterior polarity in *C. elegans* zygotes by controlling the position of the mitotic spindle (Doe, 2001; Wodarz, 2002).

Crosstalk between actin and microtubule cytoskeletons during cell polarization

In general, the actin cytoskeleton has been considered the main cytoskeleton responsible for cell motility. Recently, several studies highlighted the role of microtubules in cell migration, a role that appears to be is cell-type dependent. Cooperation and coordinated regulation of these two dynamic cytoskeletons are essential for cell migration. During cell polarization, actin and microtubules influence the dynamics of each other directly or through regulation of signaling molecules. Formation of filopodia and lamellipodia is driven by actin polymerization (Pollard and Borisy, 2003). Penetration of microtubule plus-ends into the leading edge contributes to membrane delivery and thus could promote membrane extension (Bretscher, 2003). Microtubule polymerization affects the activity of the Rho GTPases Rac and Cdc42, both of which promote actin polymerization (reviewed in Etienne-Manneville and Hall, 2002). Rac-GTP binds to unpolymerized tubulin but not to microtubules (Best *et al.,* 1996), microtubule polymerization could thus release Rac-GTP. Rac may also be activated by the Rac-GEF ASEF (Kawasaki *et al.,* 2000; 2003). The GEF activity of ASEF is

regulated by its binding to adenomatous polyposis coli (APC), which accumulates in clusters at the microtubule plus-ends in protruding regions (Barth *et al.,* 2002). IQGAP, a Cdc42 and Rac effector, may also be transported to the leading edge via its binding to CLIP-170, which associates with the plus-end of growing microtubules (Fukata *et al.,* 2002). In yeast, the association of EB1 and APC with the actin-associated motor Myo2p is required for the transport of microtubules along actin filaments (Evangelista *et al.,* 1997; Sagot *et al.,* 2002b). The microtubule plus ends are then captured at the bud tip leading to the orientation and pulling of the spindle pole body (the yeast MTOC) to the bud (Lee *et al.,* 1999, Fujiwara *et al.,* 1999).

RhoA GTPase induces the formation of stress fibers and focal adhesions, leading to increased contractility (Nobes and Hall, 1995).The crosstalk between stress fibers and focal adhesion and microtubules is bidirectional; microtubule growth leads to the dissolution of focal adhesions, whereas disruption of microtubules leads to an increase in cell contractility and to the formation of stress fibers and focal adhesions (Krendel *et al.,* 2002; Zenke *et al.,* 2004). Microtubule depolymerization induced by nocodazole treatment activates Rho (Zenke *et al.,* 2004). This effect is likely to be mediated by microtubule-associated GEF-H1; binding of GEF-H1 to microtubules inhibits its ability to activate Rho (Ren *et al.,* 1998; Krendel *et al.,* 2002). Microtubules are aligned along stress fibers, and, upon contact with focal adhesions, microtubules are transiently stabilized (Palazzo *et al.,* 2004). Regulation of microtubule stability is controlled by Rho and its effector mDia1 (Palazzo *et al.*, 2001; Wen *et al.,* 2004).

Mammalian homologue of *Drosophila* Diaphanous 1 (mDia1)

mDia1 is a member of the diaphanous-related formin homology proteins (DRFs), which are large multidomain proteins with molecular masses in excess of 200 kDa (Tominaga *et al.,* 2000). DRFs constitute a subclass of formin homology proteins (mentioned above) that bind activated Rho (Alberts, 2001). The *diaphanous* (*dia*) gene plays a critical role during cytokinesis; various combinations of *dia* mutations result in multinucleate spermatids and adult follicle cells, and pupal lethality in Drosophila (Castrillon and Wasserman, 1994). Testes of *dia* flies are thinner (translucent) and shorter than wild type (Castrillon *et al.,* 1993), hence the diaphanous name. Metazoan formins are grouped in seven distinct groups; this classification is based on phylogenetic analyses of the formin homology-2 (FH2) domain. The seven groups are: (1) Dia (Diaphanous); (2) FMN (ForMiN); (3) FHOD (Formin HOmology Domain-containing protein); (4) delphilin; (5) INF (INverted Formin); (6) FRL (Formin-Related gene in Leukocytes); and (7) DAAM (Dishevelled-Associated Activator of Morphogenesis). Mouse and human formins segregate into the seven groups, while avian formins (two proteins) fall under two groups (Table 1.1) (Higgs and Peterson, 2005).

The avian formin protein Gg1, a member of the FMN group (Higgs and Peterson, 2005), is localized to the nucleus of different embryonic cell types, and is expressed in the developing chicken limb bud and in the epithelial compartment of the pronephros and mesonephros. Gg1 protein plays an essential role during the morphogenesis of limbs and kidney (Trumpp *et al.,* 1992). The other avian formin Gg2 belongs to the Dia group (Higgs and Peterson, 2005), and is a cytosolic protein with a molecular weight of 140 kDa (1253 aa). No biochemical or cellular studies have been done to characterize this

Table 1.1 Mouse and chicken formin proteins

Species	Protein	Identifying #	group	Common name
Mus musculus (Mouse)	Mm FRL1	AF215666 (np005883)	FRL	FRL1
Mouse	Mm FRL2	XM_128263 (np443137)	FRL	FRL2
Mouse	Mm FMN2	NP_062318 (xp371352)	FMN	Formin2
Mouse	Mm mDia2	NP_062644 (Q9NSV4)	Dia	mDia2
Mouse	Mm FMN1	NP_034360 (bac86815)	FMN	Formin1
Mouse	Mm mDia1	NM_007858 (o60610)	Dia	mDia1
Mouse	Mm Delphelin	NP_579933 (xp294249)	delphilin	delphilin
Mouse	Mm INF1	XP_130991 (xp034262)	INF	INF
Mouse	Mm FHOD1	bac27106 (aao38757)	FHOD	FHOD1
Mouse	Mm mDia3	bac40476 (o60879)	Dia	mDia3
Mouse	Mm DAAM1	aar05118 (np055807)	DAAM	DAAM1
Mouse	Mm DAAM2	aar05119 (np056160)	DAAM	DAAM2
Mouse	Mm FHOD2	bac98303 (xp371114)	FHOD	FHOD2
Mouse	Mm FRL3	XP_288949 (np783863)	FRL	FRL3
Mouse	Mm INF2	NP_940803 (bc008756)	INF	INF2
Gallus gallus (Chicken)	Gg2	BAB20321	Dia	
Chicken	Gg1	A41724	FMN	

protein. mDia1 and Gg2 share 54.1% sequence identity that spans the FH3, FH1, FH2, and DAD domains (Table 1.2), while mDia1 share 27.9% sequence identity with Gg1.The best characterized formin proteins are the yeast formin Bnip1 and the mouse formin mDia1.

DRFs share the three formin-homology domains (FH1, FH2, and FH3) and two additional domains: an N-terminal Rho-binding domain (RBD) and a C-terminal diaphanous-autoregulatory domain (DAD) (Watanabe *et al.,* 1997; Palazzo *et al.,* 2001). Three mammalian DRF genes have been identified in mice and human respectively: *DRF1=mDia1/DFNA1*, *DRF2=mDia3/DIA* and *DRF3=mDia2/Dia2*. A mutation in the *DFNA1* gene (the C-terminal 52 amino acids are substituted by 21 aberrant amino acids), is responsible for non-syndromic deafness with defects in hair cells within the inner ear, while a mutation in the *DIA* gene results in premature ovarian failure (Watanabe *et al.,* 1999; Alberts, 2001; and Palazzo *et al,* 2001).

A. Structure of mDia1:

mDia1 (p140mDia) was identified as a downstream effector of activated Rho-GTPase. It contains 1255 amino acids with a molecular weight of ~140 kDa (Figure 1.7) (Watanabe *et al.,* 1997).

Domains of mDia1:

1. RBD: Rho-binding domain, (aa 63-260). Diaphanous proteins bind preferably to activated Rho-GTPases (Li and Higgs, 2003). mDia1 binds Rho, while mDia2 binds Rho and Cdc42 (Peng *et al.,* 2003).

2. FH3: Formin-homology domain 3, (aa 157-456). This domain is less well conserved among different formin proteins. FH3 overlaps with the RBD and is essential

Table 1.2 Alignment of mDia1 and Gg2 amino acid sequence

```
          10          20          30          40          50
mDia1  SGGGLGPGRGTR--DKKKGRSPDELPATGGDGGKHKKFL-----ERFTSMRIKK-EKEKP
       ::::  :   :.   :..::: .:   .    . . : :     .:.::.: .  .::::
Gg2    SGGGDEPPGPTKMNAKRSGRSSEEETRNKTKLNIQIKTLADDVRDRITSFRKSTVRKEKP
       10        20        30        40        50        60

          60          70          80          90         100
mDia1  NSAHR-NSSASYGDDPTAQSLQD-----ISDEQVLVLFEQMLVDMNLNEEKQQPLREKDI
          :. ...   .. : ::.: :     .:...:. :::.:. :::::::.. ::::::.
Gg2    LIQHHVDTQPPISEIPLAQALLDERCMNLSEKEVMDLFEKMMEDMNLNEERKAPLREKDL
       70        80        90       100       110       120

     110       120         130         140       150       160
mDia1  VIKREMVSQYLH-TSKAG--MNQK-ESSRSAMMYIQELRSGLRDMHLLSCLESLRVSLNN
       ::::: ::.  :.:.:   :.: : . :.. ::.::::::. . .::.::::::::..
Gg2    STKREMVVQYISATAKSGGLKNSKHECTLSSQEYIHELRSGIAEEKLLNCLESLRVSLTS
      130       140       150       160       170       180

         170       180       190       200       210       220
mDia1  NPVSWVQTFGAEGLASLLDILKRLHDEKEETSGNYDSRNQHEIIRCLKAFMNNKFGIKTM
       :::::::.:: :::. ::: :.:: :.:..   : :..::::.:.::::::::.:.. .
Gg2    NPVSWVNNFGHEGLGLLLDALERLLDKKQQE--NIDKKNQHKLIQCLKAFMNNKYGLQRI
      190       200       210         220       230       240

                                      FH3
         230       240       250       260       270       280
mDia1  LETEEGILLLVRAMDPAVPNMMIDAAKLLSALCILPQPEDMNERVLEAMTERAEMDEVER
       :  :...::: ::.::  :.:: ...:.:::.::. . : . ..:: :.:  :: .. ::
Gg2    LGDERSLLLLSRAIDPKQPHMMTETVKILSAICIVGE-ERILDKVLGAITTAAERNNRER
        250       260       270       280       290       300

         290       300       310       320       330       340
mDia1  FQPLLDGLKSGTSIALKVGCLQLINALITPAEELDFRVHIRSELMRLGLHQVLQELREIE
       :.:...::..   . :.:.:.:.::::.:  ::::::.:.:.:..: ::...:  :.: :
Gg2    FSPVVEGLENHEFLQLQVACMQFINALVTSPEELDFRIHLRNEFLRCGLKKILPALKEKE
         310       320       330       340       350       360

         350       360       370       380       390       400
mDia1  NEDMKVQLCVFDEQGDEDFFDLKGRLDDIRMEMDDFGEVFQIILNTVKDSKAEPHFLSIL
       ::.. .:: :::::. .:::...:. ::.:::.:::: .:::::.. : .::...: ::::::
Gg2    NEELDIQLKVFDESKEEDLIELSHRLNDIRVEMDDVNEVFQFLYNMLKDTSSENHFLSIL
         370       380       390       400       410       420

         410       420       430       440        450       460
mDia1  QHLLLVRNDYEARPQYYKLIEECVSQIVLHKNGTDPDFKCR-HLQIDIERLVDQMIDKTK
       ::.::.:::: .:::::::.:::::::::::: .: ::::.:: ....:. .:.:  .::::
Gg2    QHFLLIRNDYYVRPQYYKIIEECVSQIVLHTSGMDPDFSCRGRMDVDFSHLIDASVDKTK
         430       440       450       460       470       480

          470       480       490          500       510       520
mDia1  VEKSEAKATELEKKLDSELTARHELQVEMKKMEN---DFEQKLQDLQGEKDALDSEKQQI
       ::.:: ::.:. ::.: :. ::.: :. ..: :.   ..: ... :...     : .
Gg2    VEESEKKAAEFSKKFDEEFIARQEAQAALQKREEKIKELETEIKRLRSQVPPPASVNVLP
         490       500       510       520       530       540
```

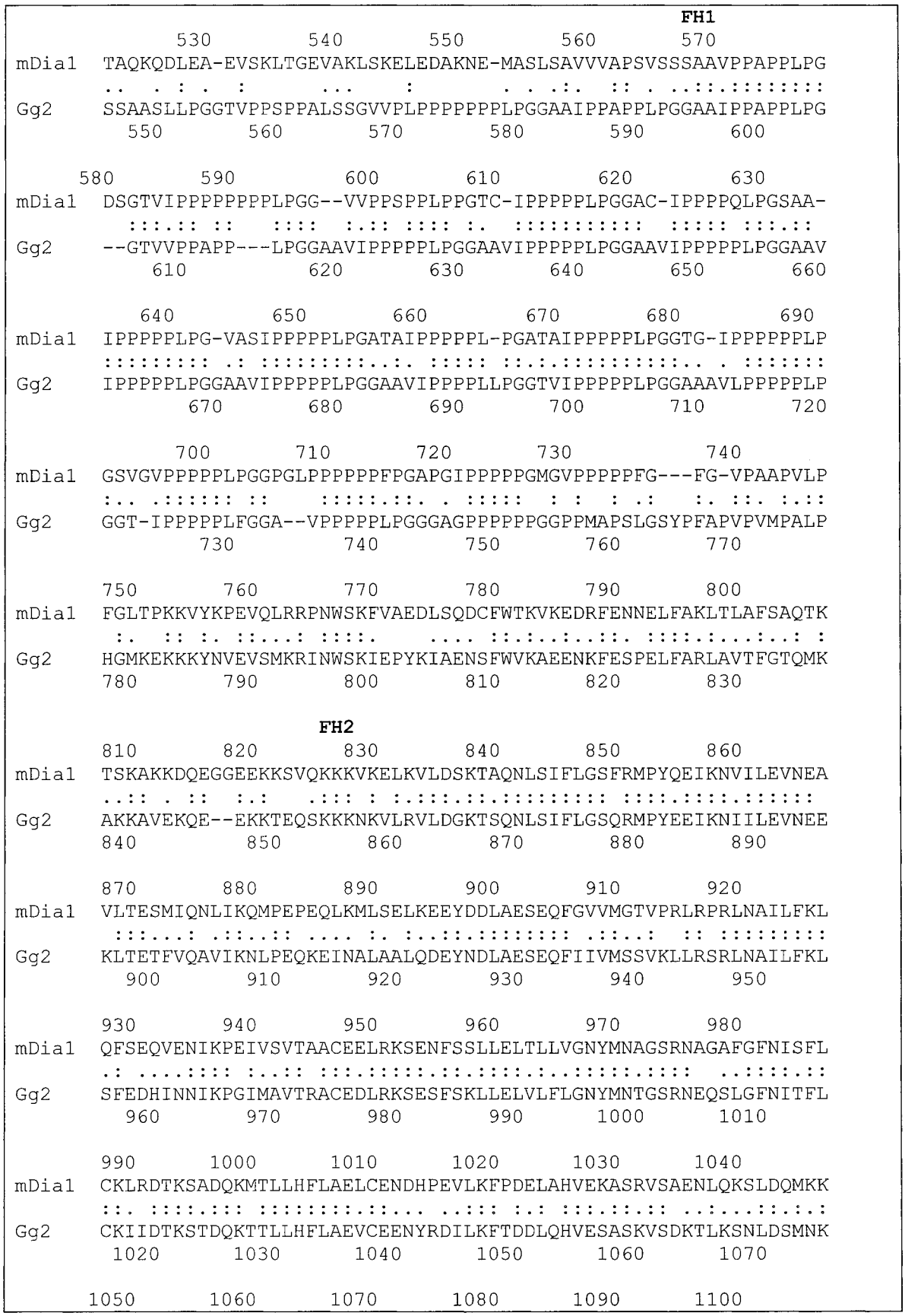

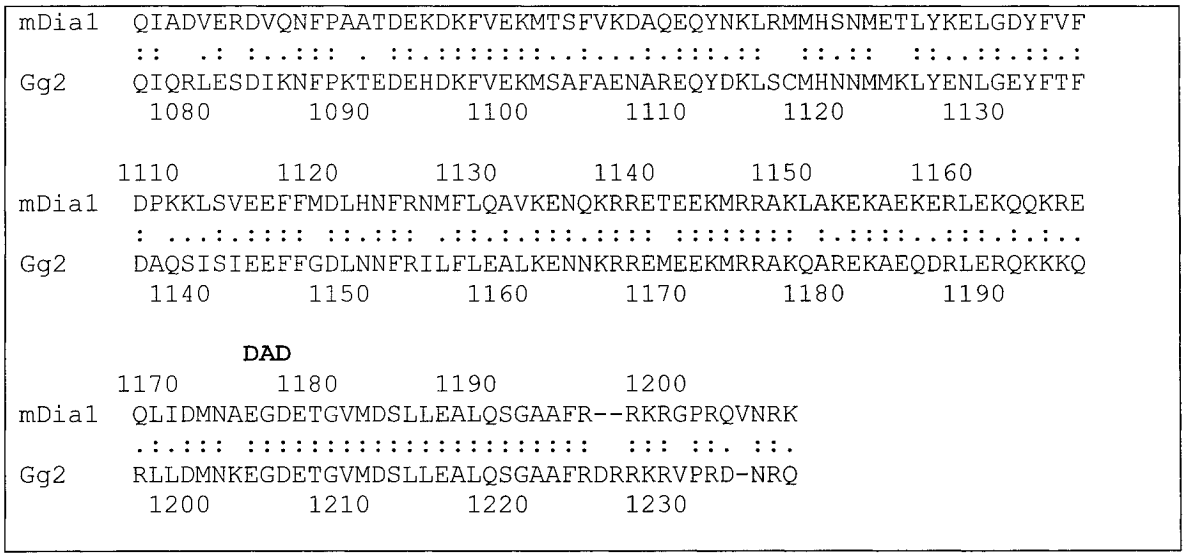

Figure 1.7
mDia1 domain structure. The numbers refer to amino acid position.

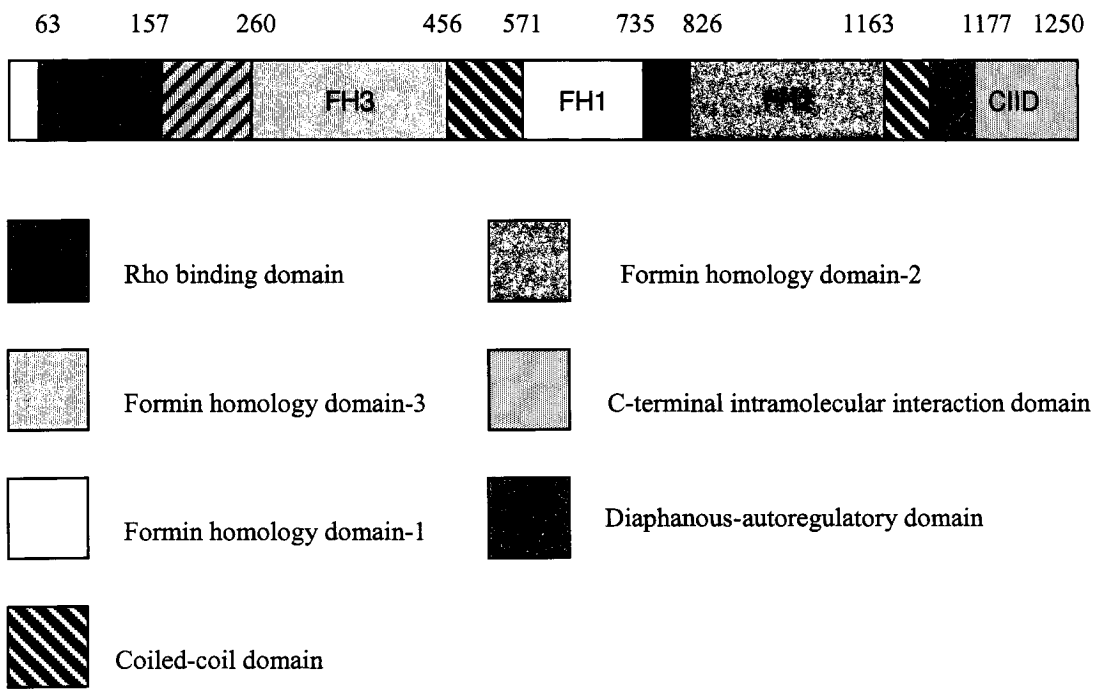

for targeting the relevant fission yeast diaphanous protein to the polar tips of mating cells and the spindle pole body (Krebs *et al.,* 2001). In HeLa cells, it is responsible for the association of mDia1 with mitotic spindles. Kato *et al.* (2001) identified a 173 amino acid-long sequence containing the C-terminal part of FH3 as a critical region in determining the spindle localization of mDia1.

3. DID: Diaphanous inhibitory domain, (aa 129-369). This domain mediates the major auto-inhibitory interaction with the mDia1 C terminus (see below) (Li and Higgs, 2005).

4. CCD: Coiled-coil domain: mDia1 has two of these domains: one at amino acids 457-571 and the other at 1111-1192. These structures are common in cytoskeletal proteins and could provide protein-protein interfaces facilitating dimerization or oligomerization (Krebs *et al.,* 2001).

4. FH1: Formin-homology domain 1, (aa 571-735). FH1 contains 14 repeats of a proline-rich region that mediates binding to profilin (Krebs *et al.,* 2001). Targeting of profilin-actin complexes to FH1 domains might recruit actin to specific sites and stimulate polymerization (Watanabe *et al.,* 1997; Sagot *et al.,* 2002a; Kovar and Pollard, 2004). This domain also links mDia1 to Src-tyrosine kinase signaling, and binds several SH3-containg proteins involved in growth regulation (Copeland and Treisman, 2002). The FH1 and FH2 domains in all family members are separated by ~100 aa, whereas the lengths of the flanking regions vary considerably (Wasserman, 1998).

5. FH2: Formin-homology domain 2 was initially characterized as a short (aa 945-1010) stretch of conserved sequence with a central GNXMN motif. This domain has been found more recently to span a larger region ~ 400 aa (826-1163), and the original FH2 domain is now called the FH2 core (Xu *et al.,* 2004). The FH2 domain is an elongated

crescent-shaped structure composed of α-helices. The structure of the FH2 domain can be divided into three subdomains: the N-terminal subdomain, the three-helix-bundle subdomain, and the FH2 motif (FH2 core) (Figure 1.8a, b). The FH2 domain is dimeric in several formins. When viewed from the top, the FH2 dimer forms a closed ring with the two hemidimers linked together by a linker segment to form a tethered dimer. This linker provides stability between the two halves (Figure 1.8c) (Shimada *et al.,* 2004; Xu et al., 2004). The FH2 domain has been implicated in the coordination of actin and microtubule networks and, as mentioned earlier, work by Pruyne *et al.* (2002) and Sagot *et al.* (2002 a, b) showed that the FH2 domain of the yeast formin nucleates the assembly of actin filaments into actin cables.

6. CIID: The C-terminal intramolecular interaction domain, (aa 1177-1255), contains the DAD or Diaphanous-autoregulatory domain (aa 1177-1207) (Krebs *et al.,* 2001). DAD is composed of two sections: 1) a leucine-rich region that is similar to the WASP/Scar WH2 domain and likewise binds G-actin, and 2) a group of basic residues that are necessary for its autoinhibition function (Alberts, 2001; Li and Higgs, 2003; Wallar and Alberts, 2003). The mDia1 protein sequence contains a putative nuclear localization sequence just before FH2 (Tominaga *et al.,* 2002). Figure 1.9 summarizes most of the activities associated with the different domains of mDia1 and the binding partners of these domains.

B. Activation of mDia1:

Two intramolecular interactions between the N and C-terminus render mDia1 inactive. The first is between the RBD and the CIID (Li and Higgs, 2003) and the second is between DID and FH2 (Li and Higgs, 2005). The DAD domain mediates the first interaction and supplies a high affinity interaction to enable the second. Binding of

Figure 1.8
Structural analysis of the FH2 domain. a) Ribbon diagram of the FH2 domain. The NH2-terminal, three-helix-bundle, and FH2 motif sudomains are colored red, blue, and green, respectively. The highly conserved "GNXMN" motif is colored purple. b) The FH2 domain is an elongated crescent-shaped molecule. Adopted from Shimada *et al.,* Mol. Cell, 13, 2004. c) Top view (left panel) and bottom view (right panel) of the FH2 dimer, the horizontal line indicates the approximate division of the dimer into hemidimers. Adapted from Xu *et al.*, Cell, 116, 2004.

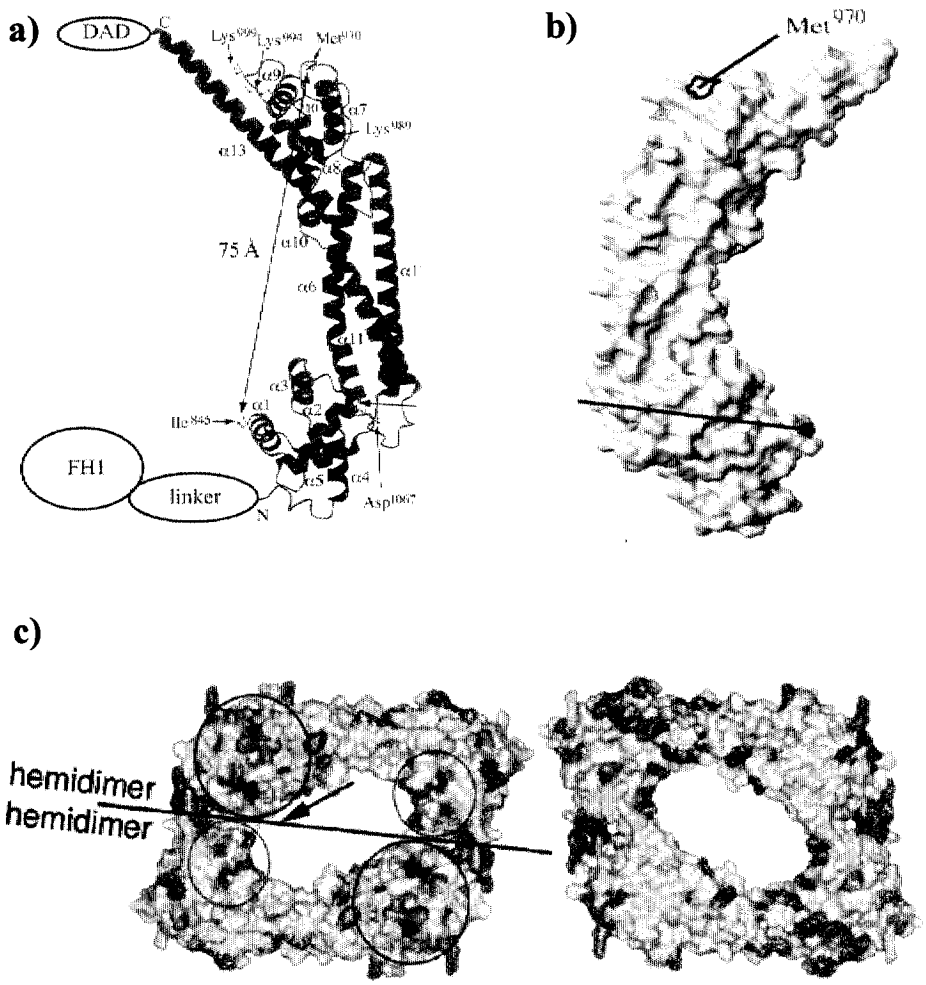

Figure 1.9 A schematic representation of mDia1 domains, their binding partners and some of the activities associated with the FH1-FH2 unit.

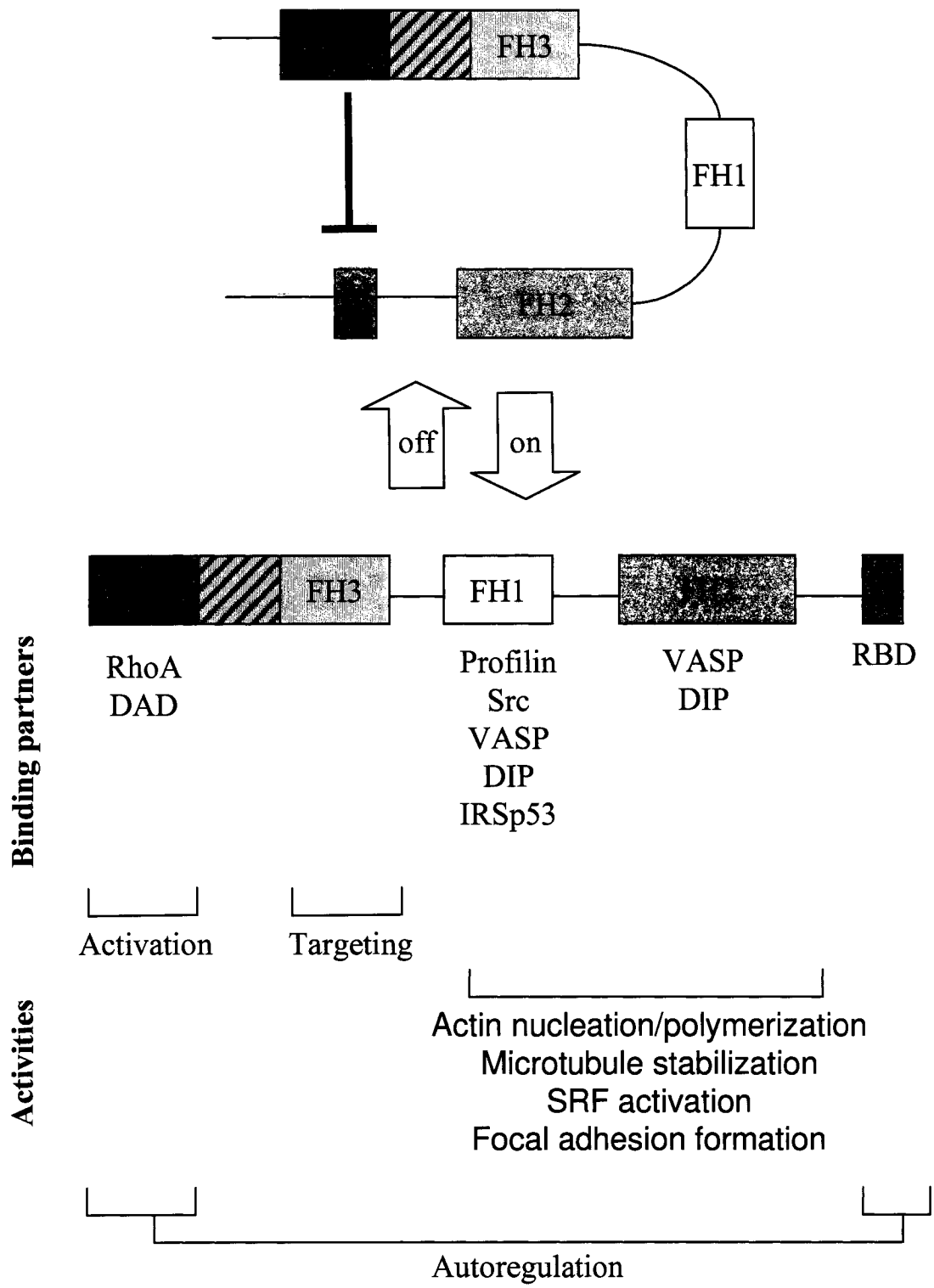

RhoA to the RBD does not relieve the autoinhibition completely which suggests a second non-RhoA-dependent interaction between the N and C terminus (DID-FH2). Inactive mDia1 has a closed conformation masking the FH1-FH2 unit, which becomes exposed upon activation (Figure1.10) (Watanabe *et al,* 1999; Alberts, 2001; Li and Higgs, 2005).

C. Localization of mDia1:

mDia1 is a cytosolic protein, which upon activation becomes localized to ruffling membranes and spreading lamellae. RhoA and profilin co-localize with mDia1 to these lamellae (Watanabe *et al.,* 1997; Krebs *et al.,* 2001). mDia1 also accumulates in a perinuclear region and at the cell periphery in HeLa cells, forming foot-like processes that contain focal adhesions (Ishizaki, *et al.,* 2001). During mitosis, mDia1 is targeted to the mitotic spindle and then to the cleavage furrow (Kato *et al.,* 2001). mDia1 and mDia2 have been found to be associated with the cytoplasmic face of endosomes, but the functional significance of this targeting is unclear (Gasman *et al.,* 2003). Recently, mDia1 was found to be enriched at the base of early initiating processes and within the growth cones of cerebellar granule cells (Arakawa *et al.*, 2003).

D. Functions of mDia1:

There are several functions for mDia1 that have been elucidated in cultured cells.

1. Effects on actin cytoskeleton:

A. Effects on actin polymerization dynamics: the FH1–FH2 unit of formins induces the enhanced formation of actin filaments in both yeast and animal cells (Evangelista *et al.,* 1997; Watanabe *et al.,* 1999). The FH1–FH2 unit initiates F-actin formation through direct actin nucleation (Pruyne *et al.,* 2002; Sagot *et al.,* 2002a, b). The FH2 region is sufficient for nucleating filaments from actin monomers *in vitro*, and the FH1–FH2

Figure1.10
A model for activation of mDia1 by Rho-GTP. Inactive mDia1 has a closed conformation masking the FH1-FH2 unit. Upon activation by Rho-GTP binding, an open conformation is induced thereby exposing the FH1-FH2 unit. Adapted from Watanabe *et al.*, Nature Cell Biol. 1, 1999.

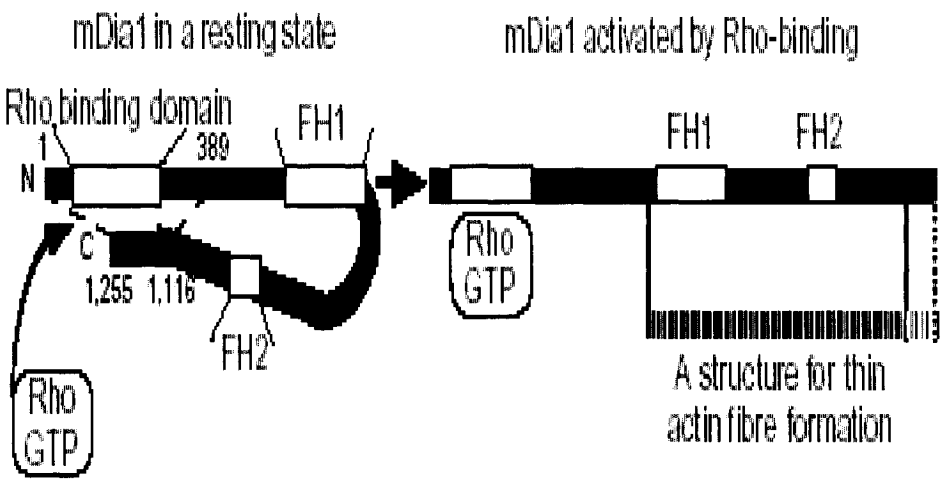

fragment can utilize the profilin–actin complex as a substrate for nucleation while FH2 alone cannot (Sagot *et al.,* 2002a; Pring *et al.,* 2003). Profilin binds actin monomers, and promotes nucleotide exchange of actin. Free actin monomers exist only at a submicromolar concentration in cells, and thus profilin prevents spontaneous actin nucleation while it allows fast actin elongation. This is perhaps one of the reasons why FH1–FH2 is much more potent inducer of the actin filament formation than the FH2 alone (Kovar and Pollard, 2004; Watanabe and Higashida, 2004).

mDia1 binds to the barbed ends of actin filaments and induces actin monomer addition. mDia1 remains attached to the barbed ends during growth and shrinkage but this binding does not block elongation making mDia1 a leaky capper. This mechanism has been known as "processive capping" (Kozlov and Bershadsky, 2004). Several models have been proposed to explain the processive capping behavior of mDia1, one of which is the "stair stepping" model (Xu *et al.,* 2004). This model recognizes the fact that the FH2 domain is a flexible tethered domain (the hemidimers are mobile relative to each other and are restrained by the linker) and each hemidimer is an actin binding head. The stair stepping mechanism implies anticooperativity in the two hemidimers, i.e. high affinity binding of one head and weak binding of the other head, and reversal of these affinities when an additional actin subunit is added (Figure 1.11) (Moseley *et al.*, 2004 ; Shimada *et al.*, 2004; Xu *et al.*, 2004)

B. Effects on actin-dependent structures/functions: In all eukaryotic cells, formins are required for cytokinesis because they are essential for the formation of the contractile ring (Severson *et al.*, 2002; Tolliday *et al.,* 2002). mDia1 cooperates with Rho kinase (ROCK, p160 Rho-coiled coil kinase) in the formation of stress fibers and focal

Figure 1.11
Stair-stepping model. Schematic illustration showing how the FH2 domain of mDia1might stair-step on the barbed end of actin filaments. Actin subunits are represented by colored ovals; the two halves of the formin dimer are colored blue and tan. Alternating dissociation, displacement, and re-binding of one half of the formin dimer could allow elongation by addition of actin monomers to the barbed end of the filament. Adapted from Xu *et al.,* Cell, 116, 2004.

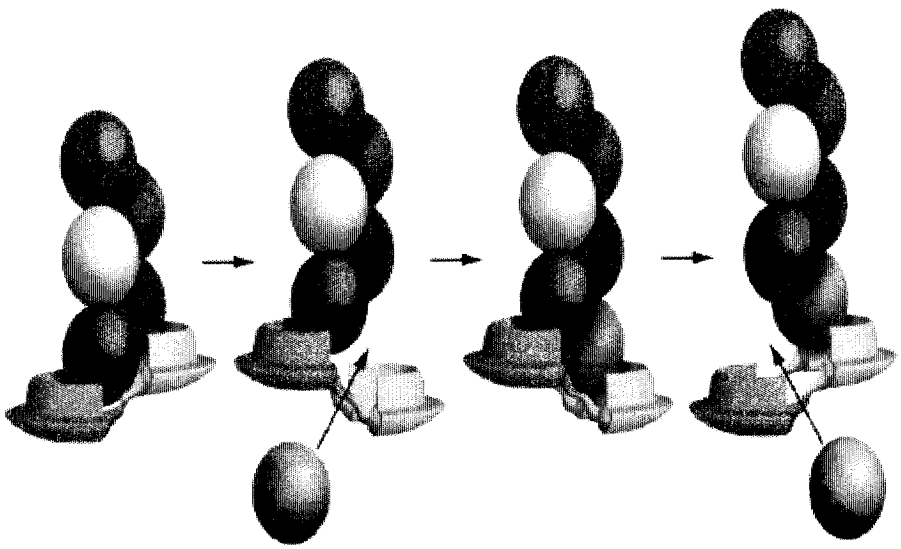

adhesions. Overexpression of a constitutively active form of ROCK stimulates the formation of stellate stress fibers that are morphologically different from the Rho-induced ones. Co-expression of a constitutively active (CA)-mDia1 corrects this defect (Narumiya *et al.,* 1997; Nakano *et al.,* 1999; and Watanabe *et al.,* 1999, Riveline *et al.*, 2001).

The FH1 domain of mDia1 binds the SH3 domain of Src tyrosine kinase (Tominaga *et al.,* 2000). Src is required for the mDia1 contribution to cooperative induction of stress fibers with ROCK (Satoh and Tominaga, 2001). The sequential activation of Rho, Src, and mDia1 is required for the formation of focal adhesions (Satoh and Tominaga, 2001). mDia2C (a splice variant of mDia2), when activated by Rho, induces a marked alignment of early endosomes along actin filaments and inhibits endosome motility through a mechanism requiring Src activity, suggesting that membrane-cytoskeleton interactions may be generally regulated by Rho-Dia-Src signaling cascades (Gasman *et al.,* 2003). mDia1 (in association with Src) along with ROCK and LIMK cooperate to regulate serum response factor (SRF) transcriptional activity. SRF is a transcription factor that controls growth factor-inducible andmuscle-specific genes (e.g. vinculin, smooth muscle α-actin, and β-actin). SRF is activated in response to depletion of the cellular G-actin pool (Tominaga *et al.,* 2000; Copeland and Treisman, 2002; Geneste *et al.,* 2002).

mDia1 interacts physically with VASP and the association is mediated by multiple domains of each protein. VASP is required for efficient operation of the mDia1 pathway that controls F-actin assembly, and VASP-induced SRF activation is dependent on RhoA and mDia1 (Figure 1.12) (Grosse *et al.,* 2003).

Figure 1.12
Proposed model for the role of mDia in SRF activation. SRF is activated in response to depletion of the cellular G-actin pool. Two of Rho effectors control F-actin polymerization.1) Rock which in turn phosphorylates LimK activating it. Activated LimK inhibits the depolymerizing activity of ADF/cofilin (AC), and 2) mDia1 which enhances actin polymerization. The exact role of VASP in the mDia1 pathway is still unclear. Adapted from Grosse *et al.*, EMBO J. 22, 2003.

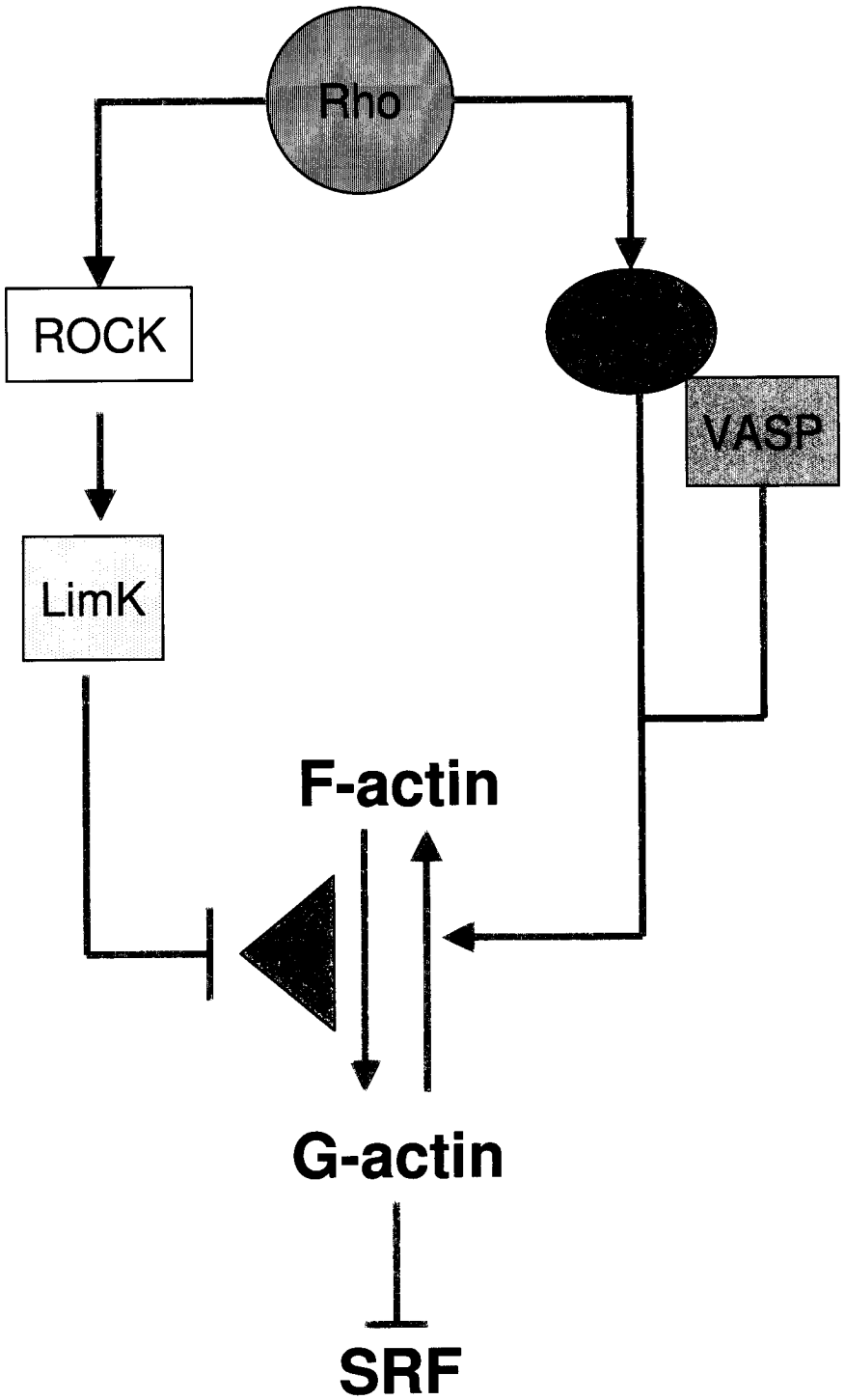

mDia1 binds Diaphanous-interacting protein (DIP), which is an 80 kDa protein that is expressed widely in different tissues (heart, brain, kidney, liver, and skeletal muscles). The FH1 domain of mDia1 binds the SH3 domain of DIP, and the FH2 domain of mDia1 binds the Leucine-rich domain (LRD) of DIP (Satoh and Tominaga, 2001). mDia1 and DIP colocalize to the cell periphery and focal adhesions in HeLa cells. mDia1 mediates the phosphorylation of DIP by Src; mDia1 mutants lacking the FH1 domain (the Src-binding domain) abolishes this phosphorylation. Upon EGF stimulation, DIP is phosphorylated by Src; then the phosphorylated DIP inactivates Rho by mediating the Src-induced phosphorylation of p190RhoGAP. In addition, phosphorylated DIP activates Rac by mediating the Src-induced phosphorylation of Vav2. Thus, DIP acts as a regulatory molecule causing Src kinase-dependent feedback modulation of Rho GTPases downstream of Rho-mDia upon EGF stimulation, and plays an important role in cell motility (Meng *et al.,* 2004).

mDia1 promotes neurite extension and branching in cerebellar granule cells. Arakawa *et al.* showed that SDF-1α (a chemokine expressed in the pia mater and a chemoattractant for migration of cerebellar granule cells) activates a ROCK-independent, C3-sensitive (C3-exoenzyme is a Rho inhibitor) pathway that leads to axon elongation (Arakawa *et al.,* 2003). When these cells were transfected with GFP-CAmDia1, axons were significantly longer compared with control cells. On the other hand, when cerebellar granule cells were transfected with a dominant-negative mutant of mDia1 or mDia1 siRNA, they had axons of significantly diminished length. Therefore, the Rho/mDia1 pathway is a potent facilitator of axon elongation (Arakawa *et al.,* 2003).

The FH1 domain of mDia1 binds the SH3 domain of the insulin receptor tyrosine kinase substrate p53 (IRSp53) (Fujiwara *et al.,* 2000). IRSp53 links Rac and WAVE2; Rac does not bind directly to WAVE; it binds to the amino terminal Rac-binding domain (RCB) of IRSp53, while WAVE binds to the SH3 domain of IRSp53. IRSp53 is essential for Rac-mediated lamellipodia protrusion, which depends on recruiting WAVE. WAVE stimulates Arp2/3-mediated actin polymerization (Miki *et al.,* 2000). Also, IRSp53 binds to Cdc42 and recruits the Ena/VASP family protein Mena to filopodia tips, which in turn protects elongating actin filaments from capping proteins (Figure 1.13) (Nakagawa *et al.,* 2003).

2. Effects on microtubule organization:

Microtubules become oriented in a polar fashion and are locally stabilized during many morphogenetic events, such as cell migration and neurite outgrowth (Etienne-Manneville and Hall, 2001). Formins bind the EB1/APC complex directing the proper localization of this complex to microtubule plus ends (Wen *et al.,* 2004). The budding yeast formin Bni1p interacts with EB1 and APC homologues to cap microtubules that pull the spindle into the bud (Tirnauer and Bierer, 2000), and mDia1/EB1/APC complex captures and stabilizes microtubules that penetrate the leading edge during cell migration (Wen *et al.,* 2004).

Overexpression of CA-mDia1 in HeLa cells caused alignment of actin filaments along the long axis of the cells and alignment of microtubules parallel to these actin filaments. Both the actin filaments and microtubules terminate at foot-like processes containing focal adhesions. This adhesion checkpoint ensures that Rho/mDia1 regulation

Figure 1.13
A proposed model explaining the interaction between IRSp53, Mena, WAVE2, and mDia1. IRSp53 binds to the proline-rich region of WAVE2 enhancing the activity of WAVE2 to stimulate the Arp2/ 3 complex. IRSp53 also binds to the proline-rich region of Mena, and the FH1 domain of mDia1. IRSp53 may represent a link between the three Rho GTPases, Rho, Cdc42 and Rac via forming a complex with their effectors (mDia1, Mena, and WAVE2, respectively). This complex could be recruited to the tips of lamellipodia or filopodia and may aid in membrane protrusion during cell motility.

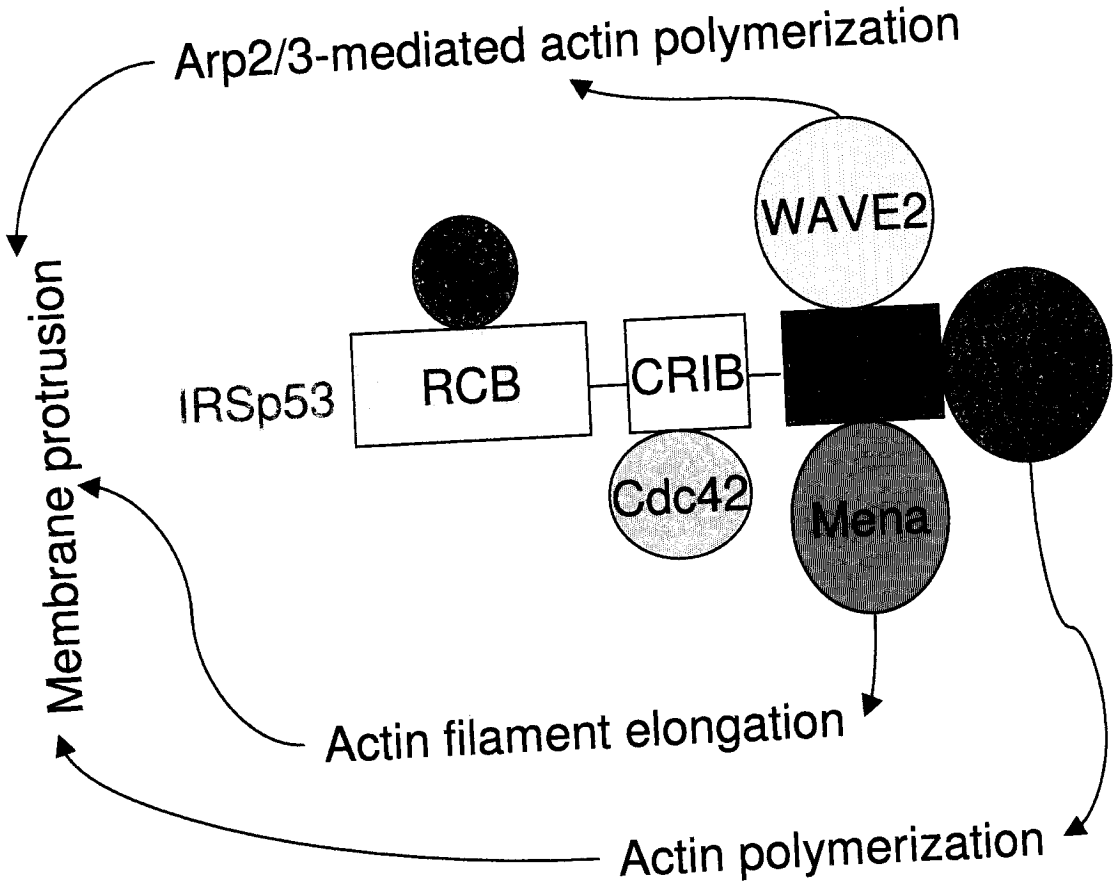

of microtubule stabilization is temporally and spatially controlled (Ishizaki *et al.,* 2001; Palazzo *et al.,* 2004).

In dividing cells, mDia1 localizes to the mitotic spindles, where it may regulate microtubules and thus the positioning of the mitotic spindle. mDia1 is then localized to the cortical region of mitotic cells in a microtubule-dependent manner (Kato *et al.,* 2001).

Figure 1.14 summarizes some of the signal transduction pathways involving mDia1 and its interacting proteins; all of these pathways culminate in the spatial and temporal regulation of the actin and microtubule cytoskeleton.

E. Postulated role(s) of mDia1 during cell migration and polarization:

Cell migration occurs through a highly regulated cycle of leading edge protrusion in the direction of migration, adhesion to the substrate, cell body translocation, and tail retraction. mDia could have a role in each of these steps. In leading edge protrusion mDia1, through its interaction with IRSp53, could be translocated to the leading edge (Fujiwara *et al.,* 2000). mDia2 binds Cdc42. Together mDia1/2 could then initiate nucleation of new filaments or they could utilize pre-existing filaments by competing with capping proteins in a VASP-dependent manner (Grosse *et al.,* 2003). Alternatively they might bind the barbed ends of filaments nucleated by Arp2/3. The newly formed filaments could then be cross-linked into large, protruding actin bundles and thus aid in the formation of lamellipodia (mDia1) or filopodia (mDia2) (Svitkina *et al.*, 2003). In the formation of stress fibers and focal adhesions, mDia1 and mDia2 cooperate with Rho kinase (ROCK) to induce stress fibers (Watanabe *et al.,* 1999; Takaishi *et al.,* 2000), and mDia1 binds Src, an interaction required for the formation of focal adhesions (Tominaga *et al.,* 2000). The cell body is translocated in the direction of migration through

Figure 1.14

Some of the signal transduction pathways involving mDia1. mDia1 is autoinhibited in vivo. Binding of activated Rho to the RBD of mDia1 relieves this inhibition. mDia1 mediates DIP- phosphorylation by Src. DIP acts as a regulatory molecule causing Src kinase-dependent feedback modulation of Rho GTPases downstream of Rho-mDia1. The phosphorylated DIP inactivates Rho by mediating the Src-induced phosphorylation of p190RhoGAP. Also, phosphorylated DIP activates Rac by mediating the Src-induced phosphorylation of Vav2. Activated mDia1 enhances actin polymerization, an activity that might be counteracted by the ADF/cofilin pathway. Also, mDia1 directs the proper localization of EB1/APC complex to the plus ends of microtubules; this tripartite complex (mDia1/EB1/APC) then captures and stabilized microtubules that penetrate the leading edge of migratory cells. On the other hand, GSK-3β phosphorylates APC preventing it from stabilizing microtubules, GSK-3β also phosphorylates MAP-1B which enhances microtubule dynamics, GSK-3β is inhibited in turn when it is phosphorylated by atypical PKC (aPKC).

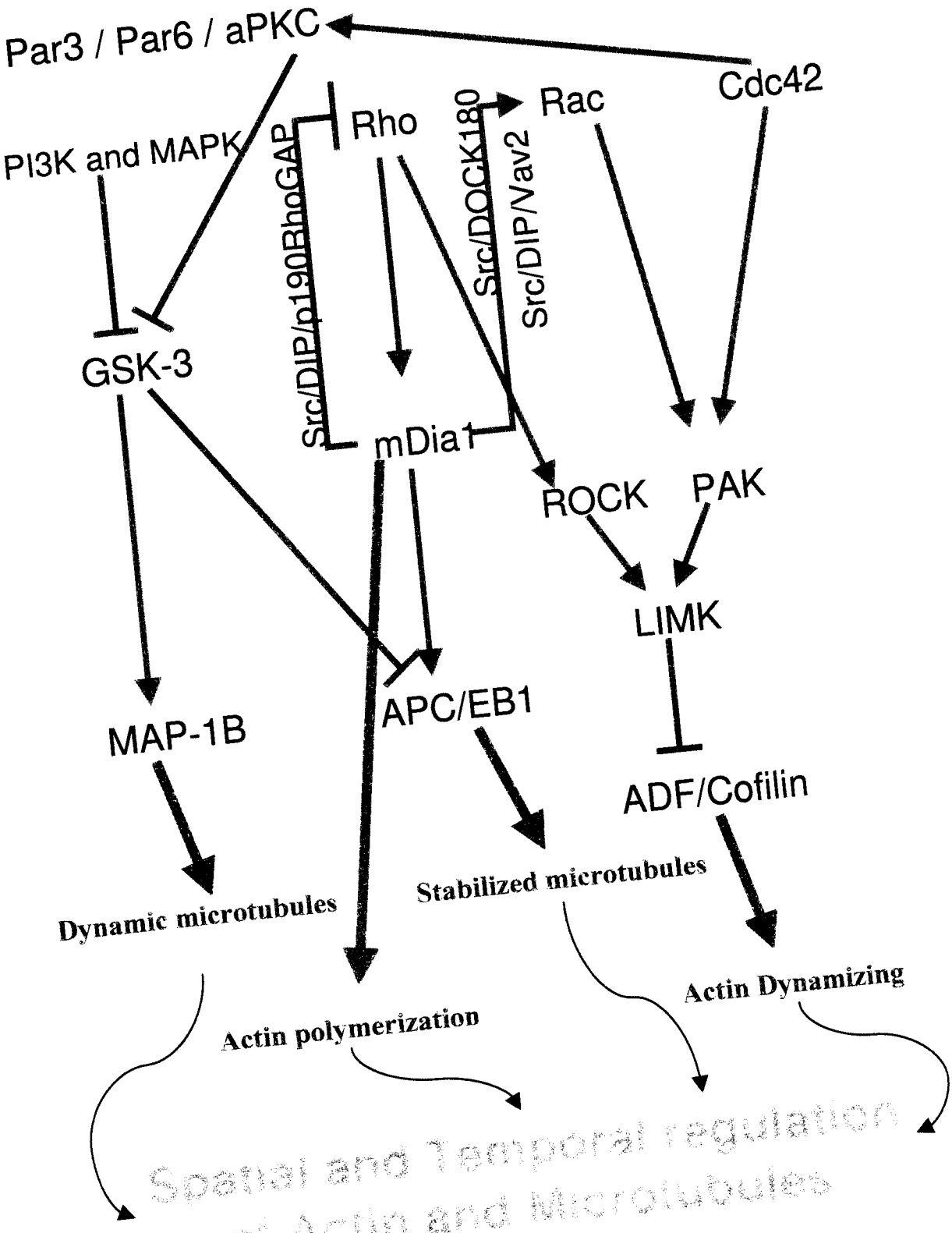

generation of tension on the new adhesion sites, an activity that has been ascribed to mDia1 in cooperation with ROCK. ROCK phosphorylates myosin and the regulatory domain of myosin-light chain phosphatase to regulate myosin-dependent contractility (Ishizaki *et al.,* 2001; Riveline *et al.,* 2001). mDia could also aid in the polarization of the microtubule network in migrating cells where the plus ends of some microtubules penetrate the leading edge and become stabilized. The mDia1/EB1/APC complex captures these plus ends (Wen *et al.,* 2004). Both mDia1 and mDia2 are targeted on endosomes with Src, but the function is unknown (Tominaga *et al.,* 2000). It has been suggested that Rho and Src might promote the transition from microtubule-dependent endosome movement to actin/myosin-dependent movement (Gasman *et al.,* 2003). Finally, tail retraction could involve ROCK/myosin-dependent contractility and/or de-adhesion of the cell rear (Worthylake and Burridge, 2003). The mDia1/Src/DIP signaling pathway alters the phosphorylation of p190RhoGAP leading to the inactivation of Rho and the dissolution of focal adhesions (Meng *et al.,* 2004) (Figure 1.15).

Conclusions and questions of the thesis

Cell polarization involves the reorganization of both the actin and microtubule cytoskeletons. mDia1 is the mammalian homolog of Diaphanous and Bni1p proteins, both of which play an important role in the establishment of cell polarity in *Drosophila* and budding yeast, respectively. Our hypothesis is that mDia1, through its ability to induce actin filament polymerization, to capture and stabilize microtubules, and its ability to coordinate the microtubule and actin cytoskeletons, is required for cell polarization and migration. Adenoviruses for expression of constitutively-active (CA), and dominant-

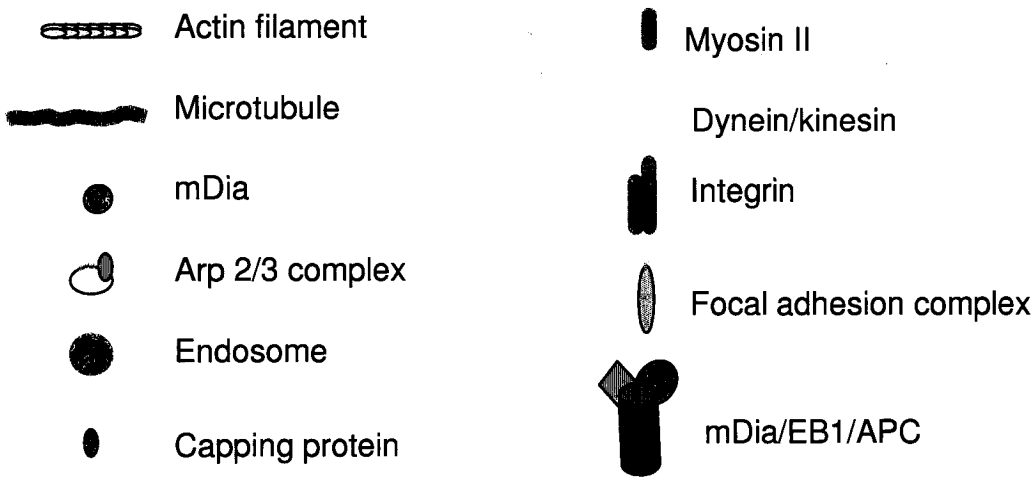

Figure 1.15
A proposed model for the role(s) of mDia in cell migration. Cell migration occurs through a highly regulated cycle of leading edge protrusion in the direction of migration, adhesion to the substrate, cell body translocation, and tail retraction. mDia could have a role in each of these steps. A) leading edge protrusion: mDia1 through its interaction with IRSp53 could be translocated to the leading edge, while mDia2 binds Cdc42. mDia1/2 then initiate nucleation of new filaments or they could utilize pre-existing filaments by competing with capping proteins in a VASP-dependent manner. Alternatively they might bind filament barbed ends nucleated by Arp2/3. The newly formed filaments are then cross-linked into large, protruding actin bundles that form filopodia. B) Stress fiber and focal adhesion formation: mDia1 and mDia2 cooperate with Rho kinase (ROCK) to induce stress fiber formation. mDia1binds Src and this interaction is required for the formation of focal adhesion. The cell body is translocated in the direction of migration through generation of tension on the new adhesion sites, an activity that has been ascribed to mDia1 in cooperation with ROCK. ROCK phosphorylates myosin and the regulatory domain of myosin-light chain phosphatase to enhancemyosin-dependent contractility. C) The microtubule network becomes polarized in migrating cells, and the plus ends of some microtubules penetrate the leading edge where they become stabilized when the mDia1/EB1/APC complex captures these plus ends.
D) Both mDia1 and mDia2 are targeted to endosomes with Src, but their function is unknown Rho and Src might promote the transition from microtubule-dependent endosome movement to actin/myosin-dependent movement.

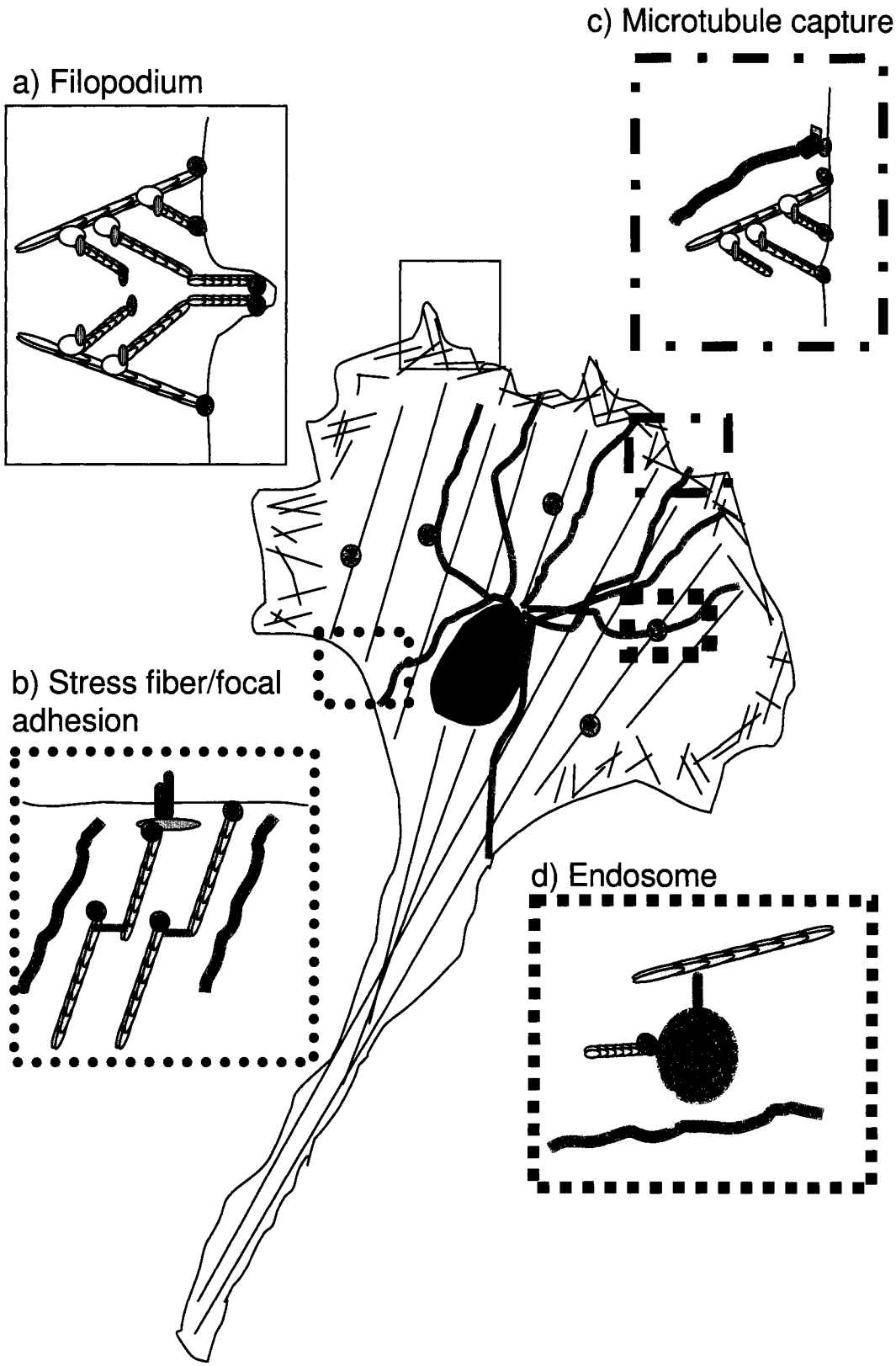

negative (DN) mutants of mDia1 were prepared. These viruses were used to test the following aims:

Aim1. To test the hypothesis that mDia1, through its in vivo interactions, is required for establishment and maintenance of cell polarity.

Aim2. To determine whether the organization of microfilaments by mDia1 is upstream or downstream of ADF/cofilin-dependent steps, and/or if the organization of microtubules by mDia1 is upstream or downstream of ADF/cofilin-dependent steps.

Choice of an experimental system:

Directional cell migration is one of many biological processes which depends on the development and maintenance of functional asymmetry (polarization) within the cell. Polarized migration is usually accomplished through the formation of protrusions and the differential distribution of organelles and signaling molecules, all aided by the cytoskeleton. In the case of migrating cells, the asymmetry is developed between two opposite ends of the cell, one of which becomes the cell's leading edge while the other becomes the tail. Most animal cells display limited (if any) directional motility in the absence of external cues, but can sense and move towards an external chemical signal (chemotaxis). Chemotaxis is an important process for many biological responses, such as the movement of leukocytes towards sites of infection or the migration of neural crest cells.

However, chick embryo cardiac fibroblasts (CECFs) are one of few cell types that display remarkable morphological polarization and rapid, persistent locomotion in the absence of an external cue (spontaneous polarization), making them a valuable tool to study cell migration and polarization *in vitro*. Another factor that makes these cells

useful for the current research is the fact that chick cells have only two formin proteins; one is a nuclear protein (Gg1) that functions as a transcription factor regulating limb and kidney morphogenesis, and the other is Gg2. Gg2 is a cytosolic protein, but no biochemical or cellular studies have been done to characterize this protein. Because there is only one cytosolic formin, over expression of a constitutively active or a dominant negative mutant of mDia1 should thus be very informative as to the role(s) of formin proteins in cell migration and polarization.

Chapter Two

Preparation and characterization of adenoviruses for expression of wild type and mutant forms of mDia1

Summary

Adenoviruses containing full-length mDia1 along with five mDia1 mutants (constitutively active (CA), dominant negative (DN), Formin homology domain 1, Formin homology domain 3, and Diaphanous Autoregulator Domain) were prepared. The work included in this thesis focuses on the effects of two mutants, CA and DN, on cell polarization and migration, and thus the activities of only these two mutants were tested in different assays and compared to literature. Adenoviral mediated overexpression of CAmDia1 in SAOS-2 cells induced cell elongation, and the formation of fine actin fibers, and the alignment of actin and microtubules parallel to the long axis of the cell. In wound-healing assays performed in both SAOS-2 and Swiss 3T3 cells, CAmDia1 expression reduced cell migration rate and thus increased the time needed to close the wound. CAmDia1-Ad-infected SAOS-2 cells migrated at a rate of 0.041 μm/min and closed the wound in 20-24 h as compared to 0.075 μm/min and 12-14 h for uninfected cells. Uninfected Swiss 3T3 cells migrated at a rate of 1.00 μm/min and needed 3-5 h to achieve wound closure, while CAmDia1-Ad-infected cells migrated at a rate of 0.43 μm/min and closed the wound in 8-9 h. In the absence of ROCK activity, achieved by

treating the cells with 30 μM of the ROCK inhibitor Y-27632, CAmDia1 induced the formation long processes in SAOS-2 cells.

DNmDia1-Ad-infected SAOS-2 cells were round, as compared to the flat, fibroblastic morphology of uninfected cells. Overexpression of DNmDia1 in SAOS-2 cells reduced stress fibers, but had no effect on microtubules. DNmDia1 overexpression in SAOS-2 and Swiss 3T3 cells had no effect on cell migration rate or the time needed to close the wound in wound-healing assay. When SAOS-2 cells were infected with DNmDia1-Ad and treated with 30 μM Y-27632 (ROCK inhibitor) to block both sides of the known Rho signaling pathways, the cells acquired a butterfly-like shape. RhoN19 (DNRho)-infected SAOS-2 acquired the same shape when treated with Y-27632, suggesting that both of the Rho pathways (via mDia and Rock) coordinate formation of the structures that give rise to the butterfly morphology. Overexpression of RhoV14 (CARho) and DNRho in SAOS-2 resulted in an enhanced and reduced stress fiber formation, respectively. CAmDia1 and DNmDia1 rescued the effects of DNRho and CARho, respectively, on stress fibers to almost normal phenotype.

Introduction

Viral vectors represent a very effective tool for efficient gene transfer into cells, both *in vivo* and *in vitro* (Gagnoux-Palacios *et al.,* 2005; Jessup *et al.,* 2005). For some cell types these vectors have been about the only effective way to obtain gene transfer (Dawe *et al.*, 2003). These viral vectors include replication-defective retroviruses and adenovirus, and recombinant adeno-associated viruses (Schmidt *et al.,* 2000). Viral vectors have been designed to be used for tissue repair, vaccination, and anticancer

treatment (Schmidt *et al.,* 2000; Gagnoux-Palacios *et al.,* 2005).The main advantages in using adenoviral vectors *in vitro* (Berkner and Sharp, 1983) are the ability to produce high titers of recombinant adenoviruses (reviewed in Yeh and Perricaudet, 1997) capable of infecting a wide variety of cell types, both dividing and post mitotic (Minamide *et al.,* 2003). Furthermore, unlike most viruses (including retroviruses) no host genes will be interrupted through chromosomal integration because the adenovirus DNA remains episomal (Verma and Somia, 1997; Harui *et al.,* 1999).

Adenoviruses are non-enveloped viruses containing a linear double stranded DNA genome. There are over 40 serotype strains of adenovirus, most of which cause benign respiratory tract infections in humans. Subgroup C serotype5 is predominantly the one used as a vector (reviewed in Russell, 2000). The life cycle does not normally involve integration into the host genome, rather they replicate as episomal elements in the nucleus of the host cell (Harui *et al.,* 1996; Verma and Somia, 1997). The wild type adenovirus genome is approximately 35 kb (Robinson *et al.,* 1977; Stillman *et al.,* 1977) of which up to 30 kb can be replaced with foreign DNA (Smith, 1995; Morsy *et al.,* 1998; Morsy and Caskey, 1999). There are four early transcriptional units (E1, E2, E3 and E4), which have regulatory functions, and a late transcript, which codes for structural proteins. Progenitor vectors have either the E1 or E3 or both genes deleted, The E3 gene is non-essential for viral replication or infection (Berkner and Sharp, 1983; Haj-Ahmad and Graham, 1986). Deleting E1 gene results in replication-defective viruses. The missing E1 gene is then supplied *in trans* by human kidney cell line 293 (HEK 293) (Graham *et al.*, 1977), a cell line that has the E1 gene integrated into the cell genome. Transgene expression from adenoviruses tends to be transient (Verma and Somia, 1997).

Introduction of foreign DNA into chick embryo cardiac fibroblasts (CECFs) using conventional transfection protocols is inefficient due to very low transfection efficiency and low cell viability after transfection (Dawe *et al.,* 2003; Cai *et al.,* 2005). Because these were the cell type to be used for my future studies, multiple adenoviruses for the expression of full-length mDia1, along with five different mDia1 mutants were constructed (Figure 2.1).

The effects of overexpression of the different mDia1 mutants on cell morphology and the cytoskeleton have been characterized in mammalian cells. When full-length mDia1 (1-1253 aa) was expressed at moderate levels, it had no effect on HeLa cell morphology or cytoskeleton, but at high level of expression it induced the formation of fine actin fibers that replaced stress fibers (Watanabe *et al.,* 1999). The overexpression of CAmDia1 (553-1253 aa), a mutant that has the N-terminal RBD deleted which prevents the N- and C-terminal autoregulation interaction, induced the formation of parallel fine actin fibers in NIH 3T3 and HeLa cells (Nakano *et al.,* 1999; Takaishi *et al.,* 2000), cell elongation (HeLa cells had a fusiform or bipolar morphology), and alignment of actin bundles and microtubules parallel to the long axis of the cell (Watanabe *et al.,* 1999; Ishizaki *et al.,* 2001). Also, CAmDia1 induced the stabilization of microtubules and formation of focal adhesions in the presence of an externally applied force (Riveline *et al.,* 2001). Finally, CAmDia1 activated the transcriptional activity of serum response factor (SRF), a transcriptional factor that is activated by depleting the cells of the G-actin pool (Copeland and Treisman, 2002). Three mDia1 mutants have been described as being DN mutants. The best characterized is the mutant that spans the region from amino

Figure 2.1
mDia1 constructs. Six different mDia1 constructs were made into adenoviruses. A) Full-length mDia1 (3.8 Kb, 1253 aa, 140 kDa), B) CAmDia1 (2.2 Kb, 718 aa, 80 kDa), this mutant has the N-terminal RBD deleted which prevents the intramolecular autoregulation, C) DNmDia1 (1.5 Kb, 503 aa, 55 kDa), this mutant is considered to be a dominant negative because the FH2 domain might 1) bind to endogenous mDia1-binding proteins such as DIP and VASP, sequestering them or, 2) it could dimerize with the endogenous mDia1-FH2 domain forming an abnormal heterodimer, and thus inhibits the formation of functional dimers of mDia1 required for its activity, D) F1mDia1 (0.91 Kb, 305aa, 33.5 kDa), E) F3mDia1 (0.91 Kb, 305aa, 33.5 kDa), and F) DADmDia1 (0.41 Kb, 137aa, 15 kDa). The DADmDia1 mutant is considered a potent activator of endogenous mDia1; overexpressed DADmDia1 mutant binds the RBD of endogenous mDia1 relieving the autoinhibition.

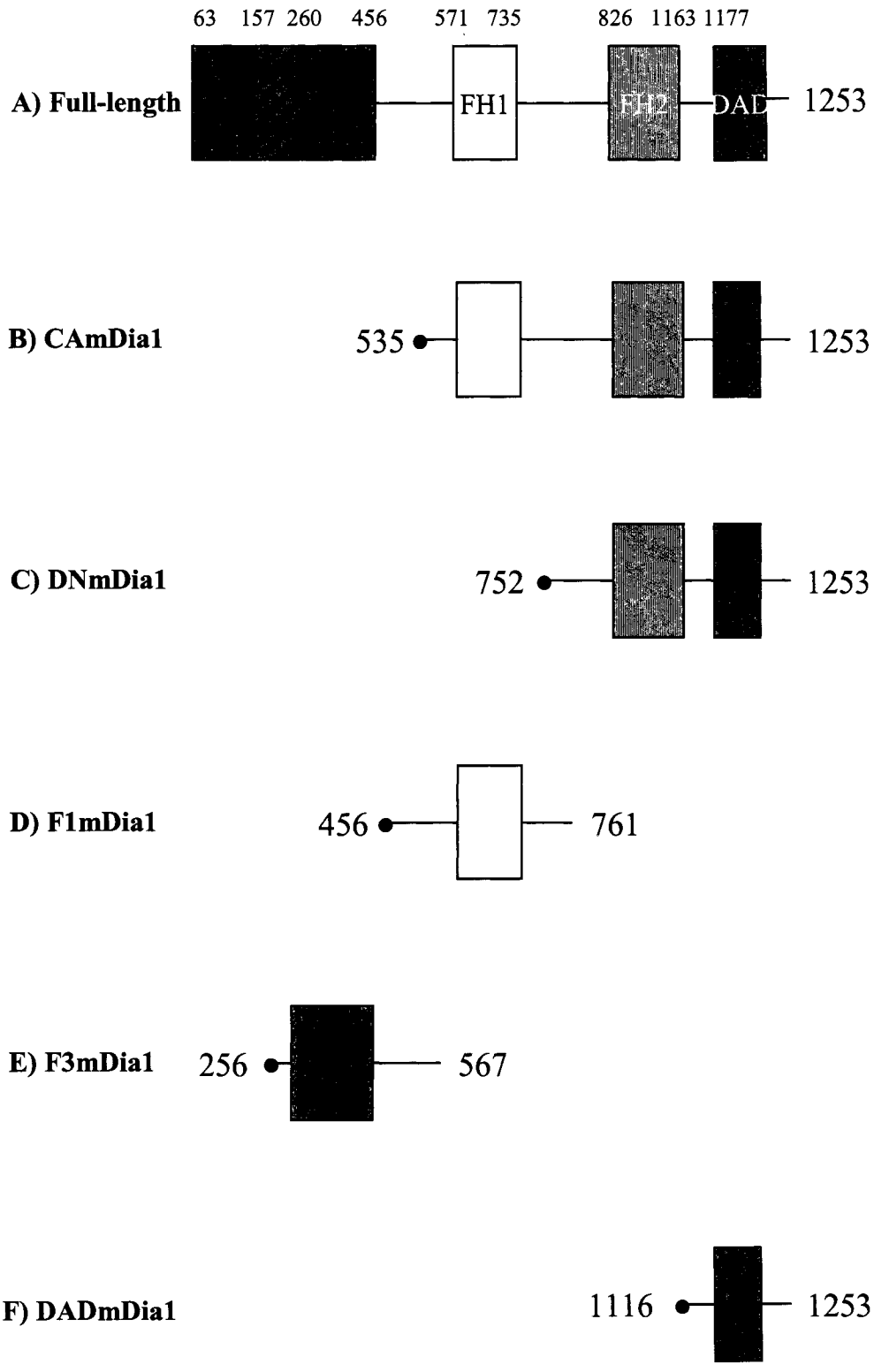

acid 772 to amino acid 1253 (FH2-CIID), hereafter referred to as DNmDia1. Although DNmDia1 was reported to inhibit the formation of actin fibers in HeLa cells (Watanabe *et al.,* 1999), others have found that it does not induce a characteristic phenotype by itself. However, when DNmDia is co-expressed with CAmDia1, HeLa cell elongation is inhibited, actin bundling or alignment is reduced, and the parallel alignment of actin and microtubules is decreased (Ishizaki *et al.,* 2001). The second dominant negative mutant, F1mDia1 (456-761 aa), induced loss of actin fiber formation, but also resulted in cell lethality (Krebs *et al.,* 2001). The effects of expressing the F3mDia1 mutant (256-567 aa) in mammalian cells have given conflicting results. The formation of stress fibers was prevented in Madin-Darby canine kidney cells (Nakano *et al.,* 1999), but in HeLa cells it had no reported effects on actin or cell shape (Watanabe *et al.,* 1999). When expressed in HeLa cells, all of the mutants induced blebbing at the cell periphery (Watanabe *et al.,* 1999).

The DADmDia1 mutant (1116-1253 aa) has been described as a potent activator of endogenous mDia1. Overexpressed DADmDia1 binds the Rho binding domain of endogenous mDia1 relieving the autoinhibition (Peng *et al.,* 2003). DADmDia1 enhanced the formation of F-actin, increased the activity of SRF (Alberts, 2001), and induced the formation of stabilized microtubules that stained positive with anti-Glu-tubulin antibody in NIH 3T3 cells. The presence of Glu-tubules is indicative of their longer half-lives and thus their stabilization. These stabilized microtubules were capped; they could not incorporate Rhodamine-tubulin at their plus ends. DADmDia1 did not induce a change in cell morphology, or alignment of actin with microtubules (Palazzo *et al.,* 2001).

This chapter discusses the construction of the different mDia1 adenoviruses and characterizes the expression of two of these (CA and DNmDia1) in different assays to compare the effects of these viruses to what has been published previously.

Material and Methods

Materials:

All of the restriction endonucleases were purchased from New England BioLabs. Calf intestinal alkaline phosphatase (CIAP) and polynucleotide kinase (PNK) were from Fisher Scientific. pBluescript and pCMV.Tag1 plasmid vectors were from Stratagene. pAdTrack.CMV, pShuttle.CMV and pAdEasy were generous gifts from the laboratory of Bert Vogelstein but are now available from Stratagene.

Molecular biological methods:

Agarose gel electrophoresis, bacterial growth, plasmid amplification and purification were performed following the protocols of Sambrook *et al.,* 1989.

Construction of mDia1.pBS vector

The plasmid pFL-mDia1 encoding flag-tagged mDia1 was a gift from Dr. Shuh Narumiya (Department of Pharmacology, Kyoto University Faculty of Medicine, Kyoto, Japan). The pFl-mDia1 vector (Figure 2.2) is 4 Kb in size with a 3.8 Kb insert (wt mDia1), that can be released by digestion with *SalI* and *BglII*. The vector and the insert have approximately the same size (4.0 Kb and 3.8 Kb, respectively), so to distinguish between them on an agarose gel, the vector was cut internally with *StuI* (non-cutter in mDia1) (Figure 2.2). The digest reaction was run on a 0.8% gel, and the larger band (slower mobility) was excised and purified using Gene Clean II (Q.BIOgene) mDia1 was

Figure 2.2 pFl-mDia1 vector map. The pFl vector is 4 Kb in size with a 3.8 Kb insert (wt mDia1), that can be released by digestion with *SalI* and *BglII*. To distinguish between the vector and the insert on an agarose gel, the vector was cut internally with *StuI* (non-cutter in mDia1). The numbers next to the arrows are residue numbers at cut sites. Adapted from Watanabe *et al.*, Nature Cell Biology 1, 1999

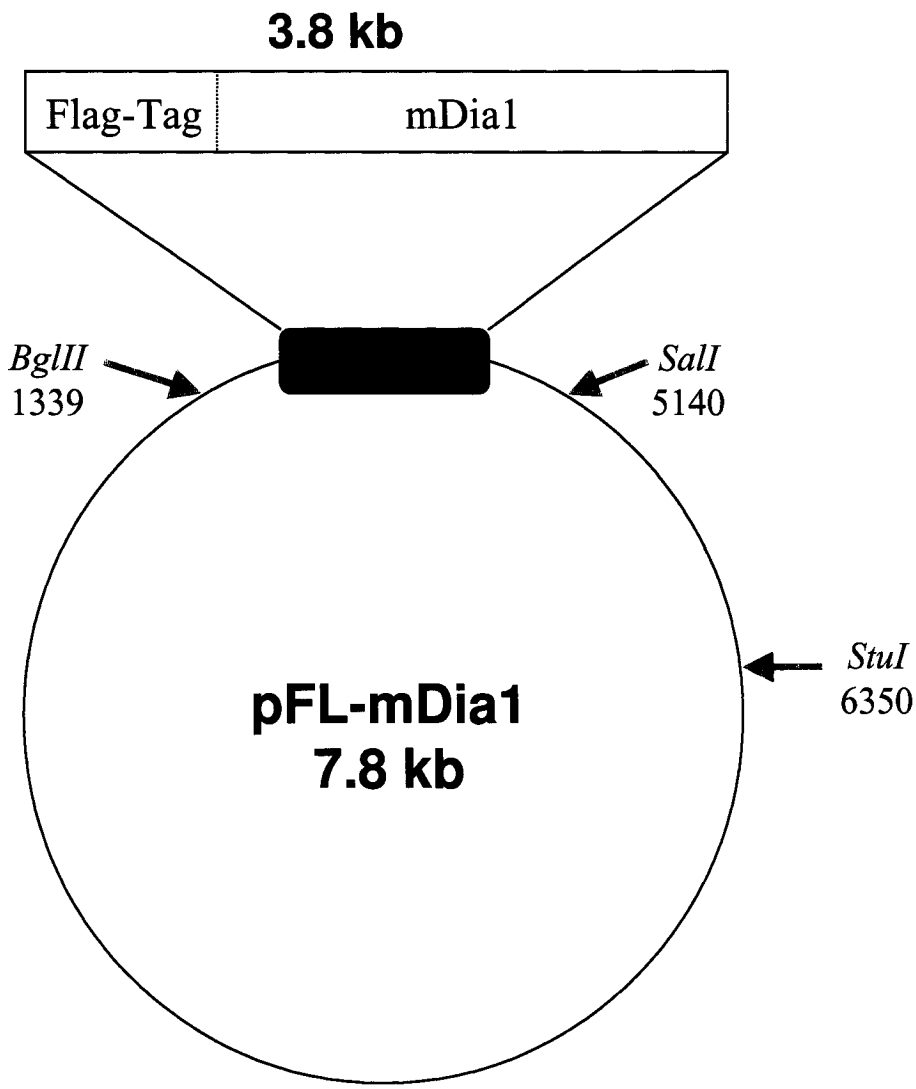

cloned in pBluescript (pBS) because the map we were provided of pFl-mDia1 was incomplete and it was unclear if the flag tag was functional.

Construction of mDia1 mutants (CA, DN, F1, F3, DAD) in pCMV-Tag1

mDia1.pBS (Figure 2.3) was used as a template for PCR amplification for the construction of the different mutants of mDia1 (see Figure 2.1 B-F). The sequences of the primers (forward and reverse) used to construct each mDia1 mutant are shown in Table 2.1 (A and B). The conditions used in the PCR amplification reaction were: denaturation at 94°C for 1 min, annealing at 60°C for 1 min, and extension at 72°C for 2.5 min, each reaction was repeated 25 times. The PCR reaction mixture contained 1 unit VENT DNA polymerase (New England BioLabs), 1X Reaction Buffer, 0.5 µl DNA template, 2.5 mM $MgSO_4$, 200 µM of each dNTP, and 0.4 µM of each primer in 50 µl total volume. All the constructs were prepared so that they have *BglII* restriction site at the 5' end, and *XhoI* restriction site at the 3' end to insert them into pCMV-Tag1 plasmid vector.

Direct cloning of the PCR products into pCMV-Tag1 vector (Figure 2.4) was not successful (cutting with *BglII* and *XhoI* followed by ligation). As an alternative, blunt end ligation was used to put these into pBS. The pBS plasmid was cut with *SmaI* and treated with alkaline phosphatase (CIAP). The PCR products were treated with T4 polynucleotide kinase (PNK) and ligated into the *SmaI* digested pBS. mDia1 mutants in pBS could then be cut with *BglII* and *XhoI* and ligated into the pCMV-Tag1 vector. The inserts were cloned between the *BglII* and *XhoI* sites, so that all the constructs should be expressed with a FLAG tag at the N-terminus. pBS and pCMV-Tag1 plasmid vectors containing mDia1 mutants were sent for sequencing at the Macromolecular Resource

Figure 2.3 mDia1 .pBS vector map

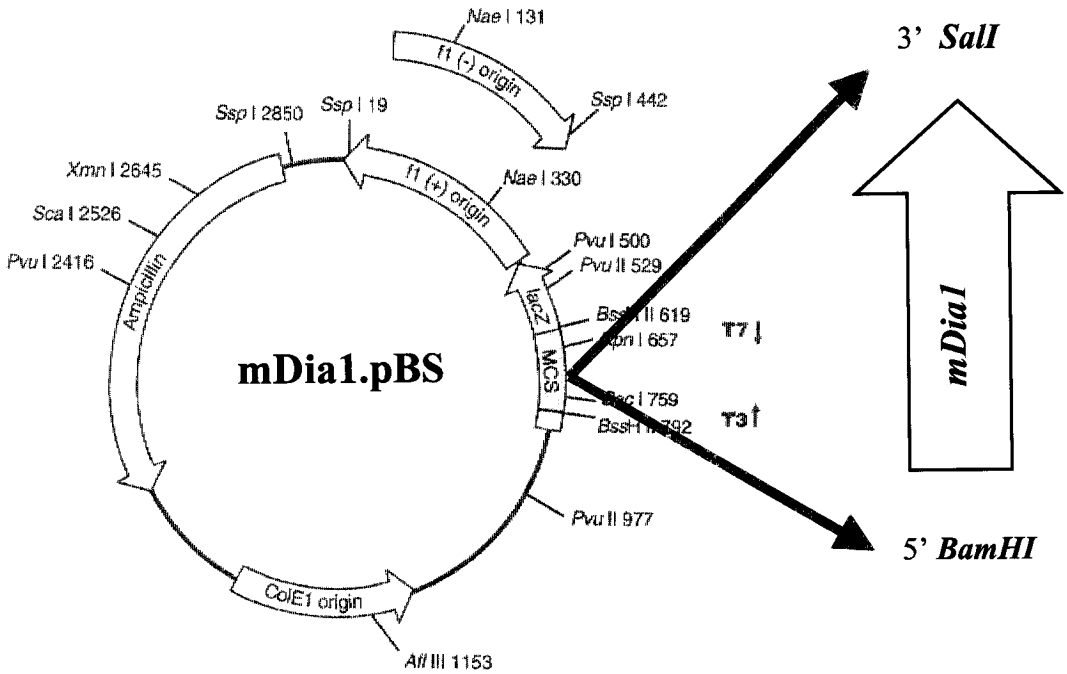

Table 2.1 DNA sequence of the PCR primers for mDia constructs

A)

mDia1 construct	Forward primer
CAmDia1	5' CGCAGATCTCGATGGGAGAGGTTGCCAAGC 3'
DNmDia1	5' CGCAGATCGATGCCCAAAAAAGTTTATA 3'
F1mDia1	5' CGCAGATCTCGATGGTTGATCAAATGATTG 3'
F3mDia1	5' CGCAGATCTCGATGGCCCTCTGTATCCTG 3'
DADmDia1	5' CGCAGATCTCGATGGAATTCTTTATGGAT 3'

B)

mDia1 construct	Reverse primer
CAmDia1	5' CGCCTCGAGTTAGCTTGCACGGCCAAC 3'
DNmDia1	5' CGCCTCGAGTTAGCTTGCACGGCCAAC 3'
F1mDia1	5' CGCCTCGAGTTACTGCACCTCTGGCTTATA 3'
F3mDia1	5' CGCCTCTCGAGTTAGCTAGAAACAGAAGGTG 3'
DADmDia1	5' CGCCTCGAGTTAGCTTGCACGGCCAAC 3'

Figure 2.4 pCMV.Tag1 vector map. The numbers are residue number at cut sites.

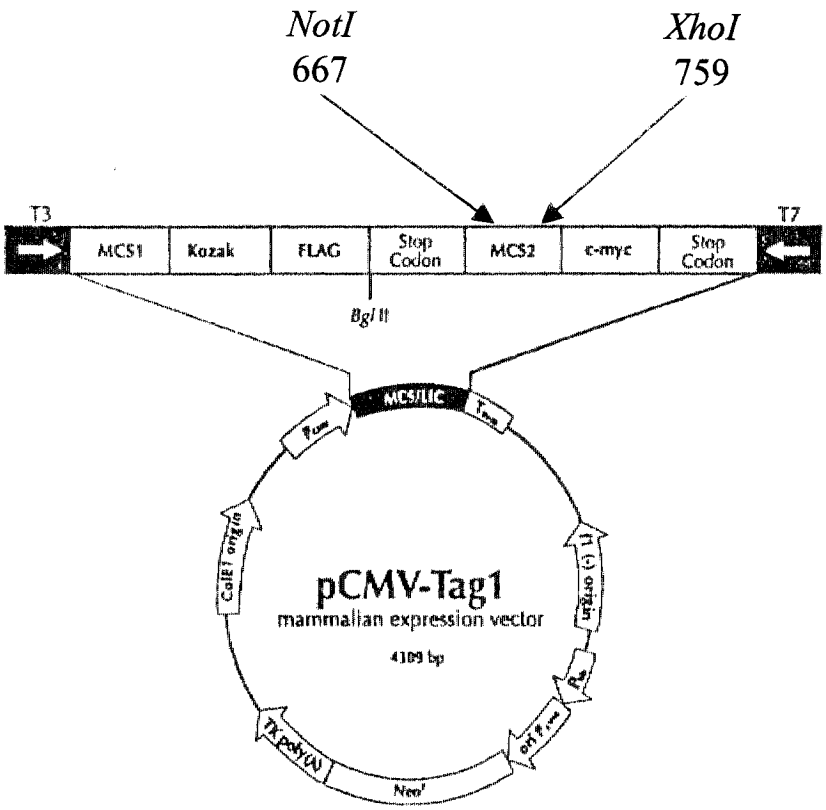

Facility (Colorado State University, Fort Collins, Co), and the results were compared to mDia1 cDNA using the Gene Runner software.

Construction of adenoviruses

Adenoviruses containing full-length mDia1 and mDia1-mutants were constructed following the protocol of Minamide *et al.*, 2003.

A. Inserting mDia1-mutants into a shuttle vector (pAdTrack, pShuttle, and pRedTrack plasmid vectors)

pCMV-Tag1 containing the mDia1 mutant cDNA was digested with *XhoI* (followed by Klenow treatment) and *NotI.* The digest reaction was run on a 1.0% agarose gel, and the fragment was excised and purified using Gene Clean II (Q.BIOgene). The purified Flag-mDia1 DNA was then ligated into the *NotI-EcoRV* sites of pAdTrack-CMV plasmid vector (this vector expresses GFP from a separate CMV promoter) (Figure 2.5). The same strategy was followed to clone the mutants into pShuttle-CMV plasmid vector (Figure 2.6) and CA- and DN-mDia1 mutants into pRedTrack-CMV vector. This vector was a modified pAdTrack-CMV, made in our laboratory by Alisa Shaw, in which the mRFP cDNA replaced the GFP cDNA (Figure 2.7). To clone the full length mDia1 into the pAdTrack-CMV and pShuttle-CMV vectors, the mDia cDNA was digested from the, pFl-mDia1 with *BglII* and *SalI*, purified from agarose gels, and ligated into the same sites in digested pAdTtrack-CMV and pShuttle-CMV vectors (Figure 2.5 and Figure 2.6).

B. Homologous recombination in BJ183 *E. coli*

Four micrograms of shuttle vector DNA containing the different mDia1 mutants were digested overnight at 37°C with 8 µl of the restriction endonuclease *PmeI.* The linearized DNA is phenol/chloroform/isoamyl alcohol extracted, ethanol precipitated

Figure 2.5
Construction of mDia1 adenoviruses. Adenoviruses containing five mDia1-mutants (CA, DN, F1, F3, and DAD) were constructed following the protocol of Minamide *et al.*, 2003. mDia1 mutants were inserted into the pAdTrack-CMV plasmid vector, which expresses GFP (green circle) from a separate CMV promoter.

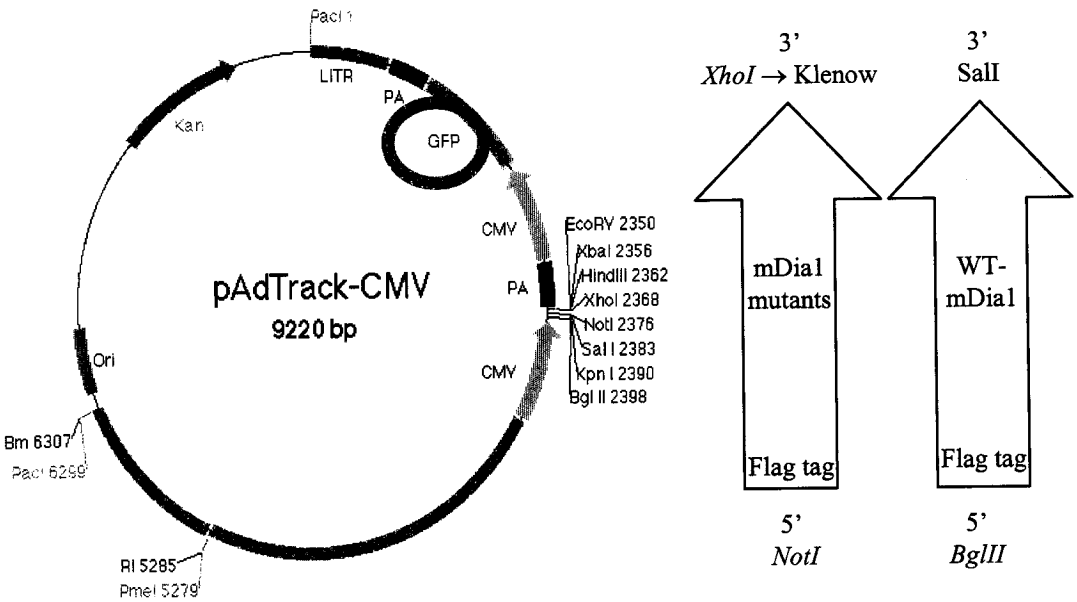

Figure 2.6
Construction of mDia1 adenoviruses. Adenoviruses containing full-length mDia1 and 5 mDia1-mutants (CA, DN, F1, F3, and DAD) were constructed following the protocol of Minamide *et al.*, 2003. mDia1 mutants were inserted into the pShuttle-CMV.

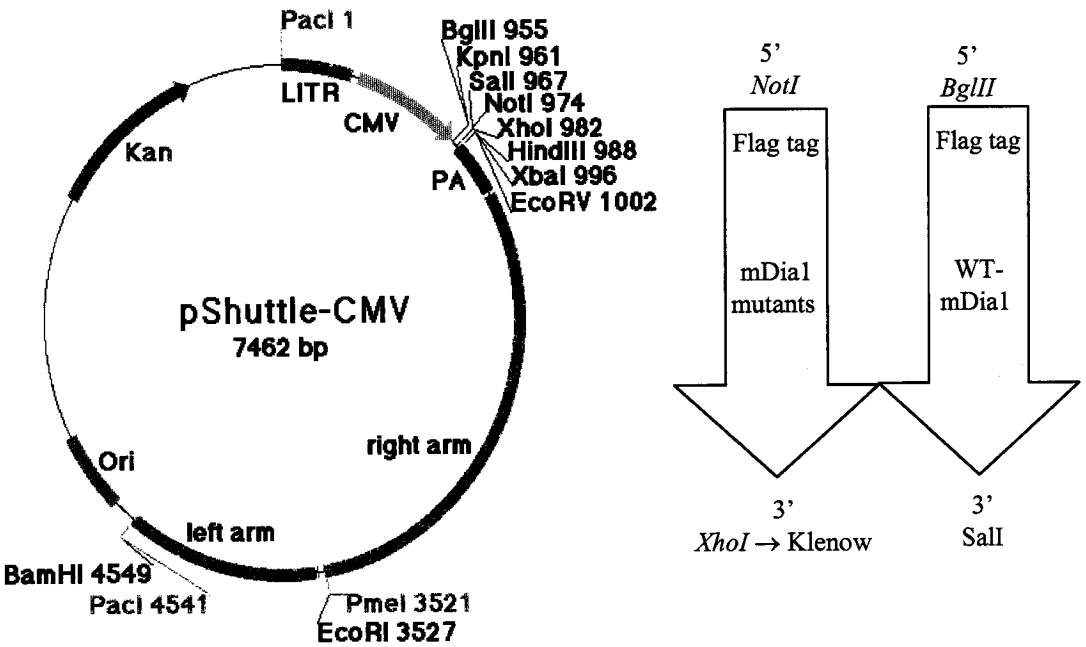

Figure 2.7
Construction of mDia1 adenoviruses. Adenoviruses containing CA- and DN-mDia1 mutants were constructed following the protocol of Minamide *et al.*, 2003. CA- and DN-mDia1 mutants were inserted into the pRedTrack-CMV vector, which expresses RFP (red circle) from a separate CMV promoter.

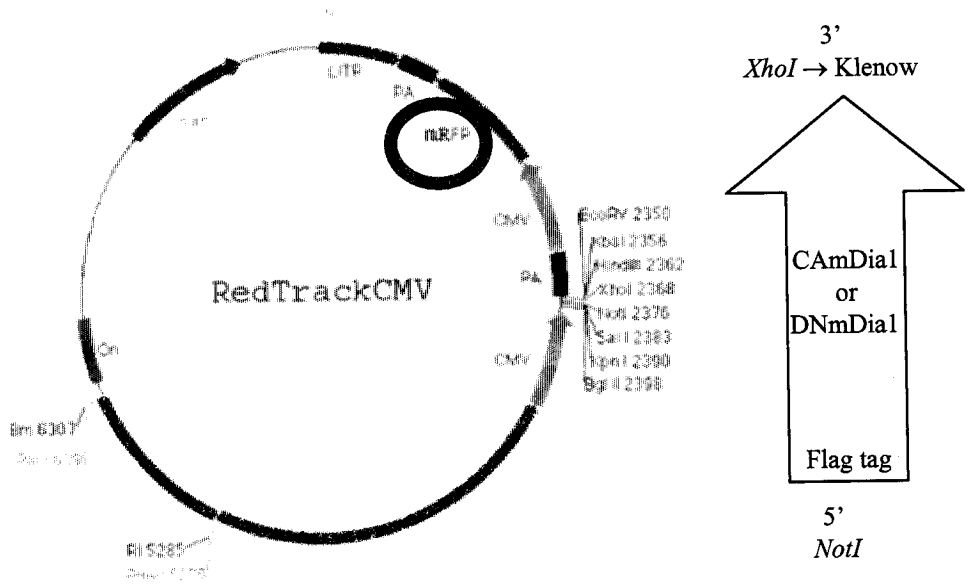

(Sambrook and Russell, 2001), and re-dissolved in sterile water at 0.1 μg/μl. 0.1-0.2 μl linearized DNA is then added to 20-25 μl electrocompetent BJ5183 cells pre-transformed with pAdEasy DNA and electroporated at 2.25 kV, 200Ω, 25 μF. 10% of the bacterial suspension was plated on a 10 cm kanamycin-containing agar plate, and the remaining 90% was plated on a second plate, to enhance the probability of obtaining isolated colonies on one or both of the plates. The plates were incubated at 37°C for about 20 h. Three sizes of colonies grew on the plates, large, medium, and small; bacteria containing the recombined DNA take longer to develop and usually form smaller colonies. Small colonies (3-5 per plate) were picked for each mutant and inoculated into a kanamycin-containing LB broth, and shaken at 37°C for less than 20 h. The plasmid DNA was isolated using standard mini-prep methods (Sambrook and Russell, 2001).

To test for the recombined AdEasy plasmid DNA (Figure 2.8), 1 μg of DNA was digested with 4 μl *PacI*. The test digest was then run on a 0.6% agarose gel; DNA from BJ5183 positive colonies should yield one large fragment of ~ 30 kb long with smaller fragment of either 3.0 kb or 4.5 kb (Figure 2.9 A), depending on whether the homologous recombination took place between the left flanking regions or at the origin of replication, both of which often occur and either of which will yield identical viruses. Because BJ5183 *E. coli* are recombination competent, the properly recombined DNA was not maintained in these bacteria. Mini-prep DNA (QIAGEN) from the BJ5183 positive clones was used to transform recA$^-$ bacteria (*E. coli* DH5α) by $CaCl_2$ transformation. A second round of *PacI* test digest was performed on mini-prep DNA from DH5α clones to confirm that no additional recombination events have occurred (Figure 2.9 B).

Figure 2.8
Schematic diagram for the production of replication-deficient adenoviral vectors using the AdEasy system. The black box represents the gene of insert, and the open boxes represent the homologous adenoviral sequences through which homologous recombination will occur. Adapted from Minamide *et al.,* 2003.

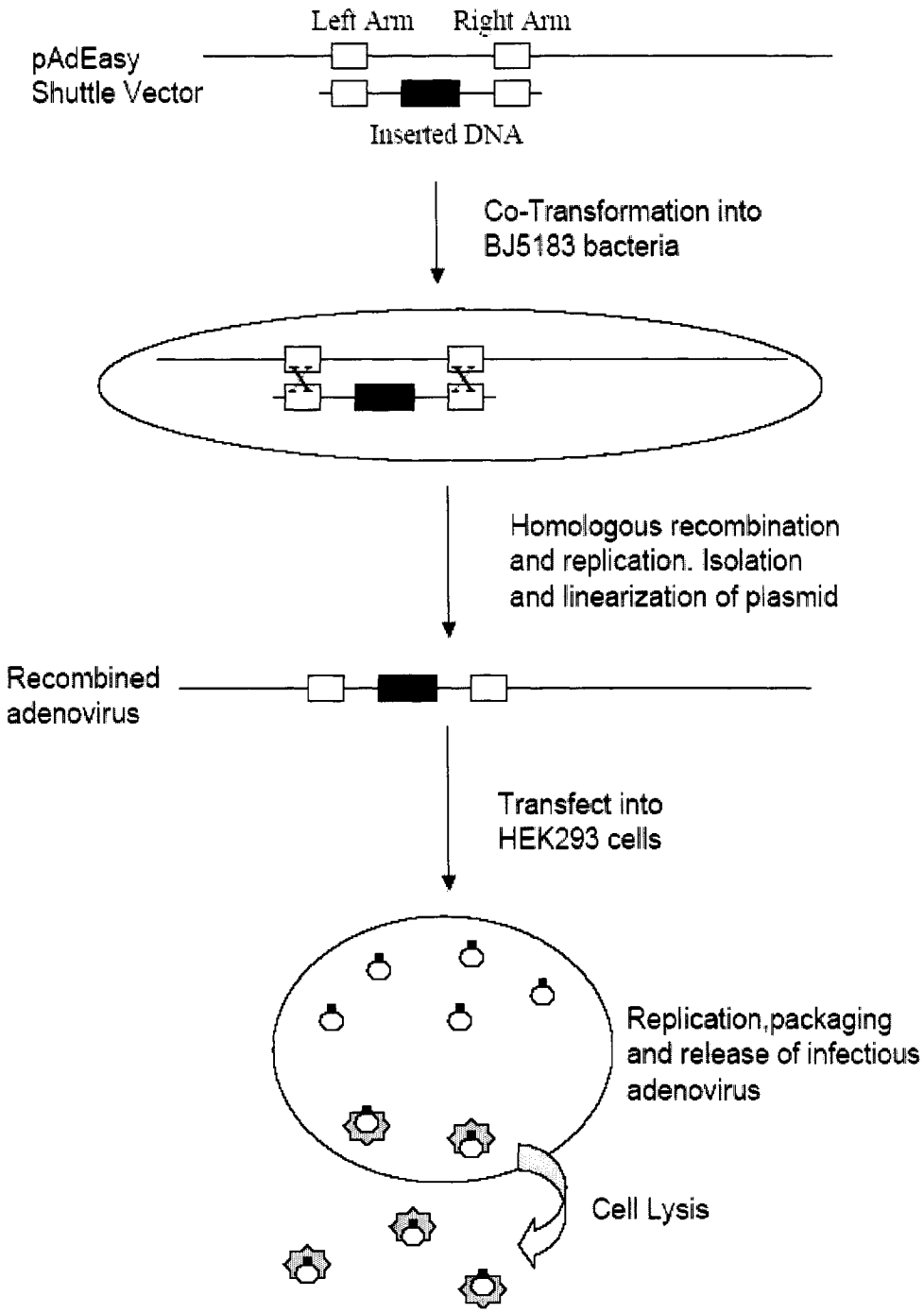

Figure 2.9
***PacI* test digests.** A) DNA from BJ5183 cells. Lanes 1,2,3,4,5,6,7, 9,10,11,14, and 15 are from positive clones; the test digest yielded one large fragment of ~ 30 kb along with smaller fragment of either 3.0 kb (lane6) or 4.5 kb (lane10) Lanes 8 and 13 show extra band at 8-9 kb, which could be due to contaminating shuttle vector, undesired recombination events, or false rearrangements of the AdEasy-1 vector. B) DNA from DH5α. Positives clones are shown in lane 2,3,4,5,and 6. M = DNA molecular marker.

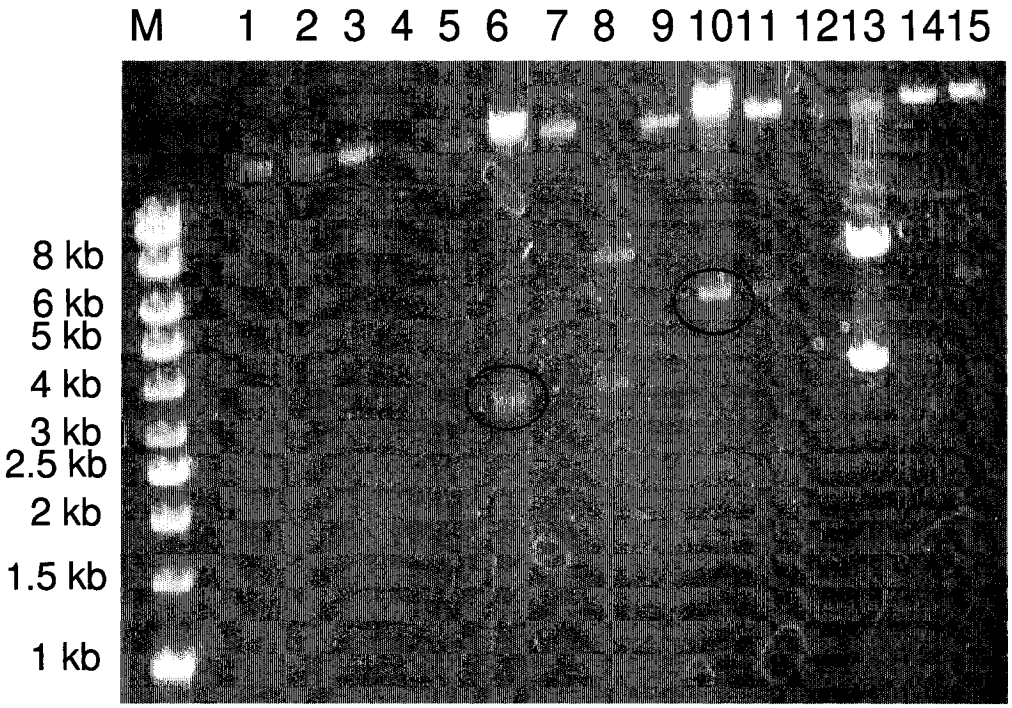

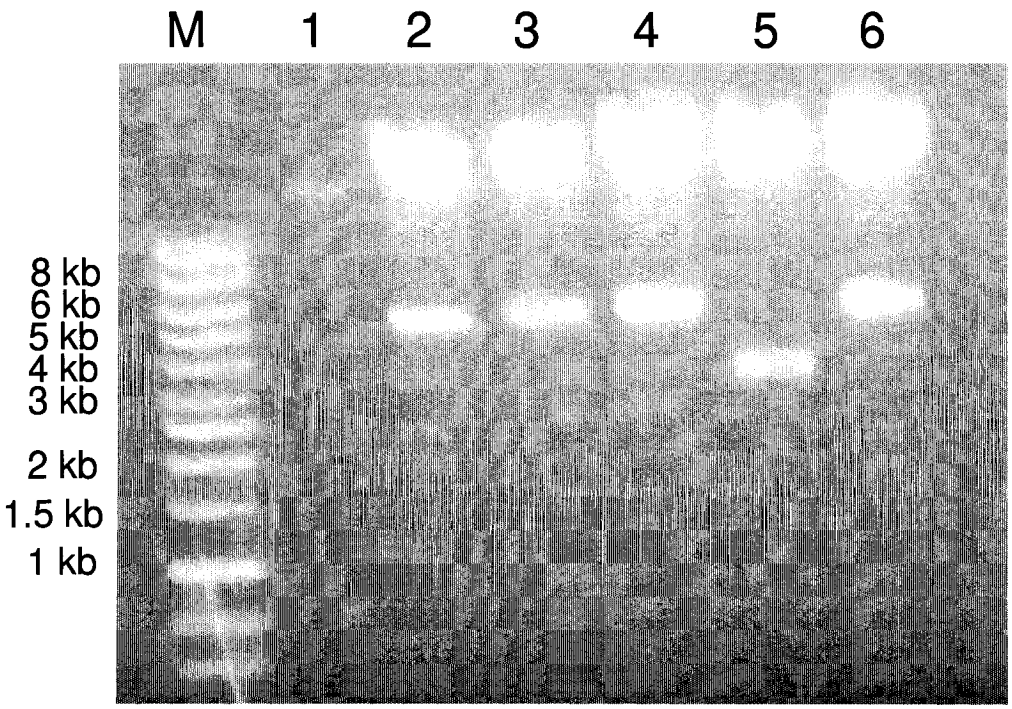

C. Production of adenovirus in HEK 293 cells

pAdEasy-1 recombinant DNA (4 μg) was digested with 40 units of *PacI* at 37°C overnight. The digest was extracted with phenol/chloroform/isoamyl alcohol and DNA precipitated with ethanol. The DNA was centrifuged at 10,000xg for 10 min at 4°C, the ethanol was removed, and the pellet was air-dried to remove any traces of ethanol. The DNA pellet was re-suspended in 20 μl sterile water. HEK293 cells (1 X 10^6) were plated in a T25 tissue culture flask 24 h prior to transfection with *PacI* linearized pAdEasy-1 recombinant DNA using the lipofectamine (Invitrogen) reagent according to the manufacutures direction.

Transfected HEK293 cells were incubated in a CO_2/air incubator at 37°C for 7-14 days. For cells transfected with vectors expressing a fluorescent protein, the fluorescence was monitored on fluorescence microscope. Signs of viral infection included rounded up cells and clear areas (plaques) surrounded by rounded cells or GFP/RFP expression were present before the cells were harvested. When the cells were ready to harvest, they were scraped off the flask, cells and medium were transferred to a 50 ml polypropylene tube, and the cells pelleted by centrifugation at 1,000xg for 3 minutes. The supernatant was discarded and the cell pellet was suspend in 2 ml sterile PBS and subjected to four cycles of freeze and thaw in a dry ice/95% ethanol bath or liquid nitrogen to release virus particles. The sample was then centrifuged at 1,500xg for 5 min to remove large cell debris, and the supernatant containing the virus was aliquoted into 0.5 ml aliquots and stored at –80°C.

To expand the transfection harvest, 0.5 ml of the primary viral harvest were added to a T25 flask inoculated 24 h earlier with 1-1.5 X 10^6 HEK293 cells. Within 2-3 days,

infected cells began to round up and lift off the flask. The cells from this first expansion flask were harvested as described above and 0.1 ml of this first expansion viral harvest was added to a T75 flask inoculated 24 h earlier with 3-4 X 10^6 HEK293 cells. Two to three days later, the cells from the second amplification rounded up and were harvested as described above, except the volume of the PBS used in the freeze-thaw cycles was 6 ml instead of 2 ml. Three rounds of virus amplification were usually sufficient to generate adenovirus with a high enough titer to use for our experiments.

Titering of Adenoviruses

Titering of the viral preparations was performed by E2 immunostaining (modified from Nevins *et al.,* 1997), which utilizes a monoclonal antibody (B6-8, Reich *et al.*, 1983) to the adenovirus E2a antigen, a nuclear protein made in infected cells. HEK293 cells were plated in 12 well plate at 6 X 10^5 cells per well. The next day, the cells covered 70-95% of the area of the wells. Three different dilutions (1:10^4, 10^5, and 10^6) of the virus to be titered were made in serum free high glucose DMEM (HGDMEM). The medium was aspirated from the HEK293 cells and 0.5 ml virus was applied per well. The plate was then incubated at 37°C in 5% CO2/95% air incubator for 45 minutes with occasional rocking to obtain the best viral dispersion over the cells. The virus solution was removed and 2 ml HGDMEM/2% fetal bovine serum (FBS; Atlas) added to each well. The plate was incubated for an additional 16 hours exactly, the medium removed by aspiration and the cells were washed once with 2 ml PBS+ (regular PBS that has 0.5 mM $MgCl_2$ and 0.9 mM $CaCl_2$ added). The cells were fixed in 3.7% EM grade formaldehyde in PBS+ for 5 min at room temperature, and then washed twice with PBS+. The cells were permeabilized in 90% methanol/10% PBS for 2 min at room temperature, and then

washed twice in PBS+ and once in 1% bovine serum albumin (BSA) in PBS+. The cells were incubated with mouse anti-E2a antibody (B6-8 hybridoma culture supernatant, 1:10 in 1% BSA in PBS+) for 45 min, and washed twice in PBS+ and once in 1% BSA in PBS+. The cells were incubated in goat anti-mouse IgG-alkaline phosphatase conjugated secondary antibody (1:1000 in 1% BSA in PBS+) for 45 min, and then washed 3X with PBS+. Finally, the cells were washed once with 2 ml high pH wash buffer (50 mM Tris pH 9.5, 100 mM NaCl, 1mM $MgCl_2$, and 0.5 ml NBT/BCIP (44 µl NBT and 33 µl BCIP in 10 ml of the high pH wash buffer) were added to each well for 30-60 minutes. The nuclei of infected cells stain dark blue. The numbers of cells with positive nuclei were counted in 5 fields using a 20X objective and 10X eyepieces on Nikon 37623 microscope.

The titer or number of focus forming units (ffu)/ml is calculated as follows: average number of positive cells/field X area conversion factor X 2 X dilution. The area conversion factor is based on the area of the field viewed through the microscope versus the area of a well in the 12-well plate. This number is 1361 for the Nikon 37623 microscope, but can be calculated for any microscope by using a stage micrometer for obtaining the full field diameter of the 20X objective and dividing this into the calculated area of a single well on a 12-well plate. Multiplying by 2 adjusts for using 0.5 ml of virus per well. As an example, if you counted an average of 25 positive cells in the 10^4 dilution, the titer would be: 25 X 1361 X 2 X 10^4 = 6.8 X 10^8 ffu/ml.

Testing adenoviruses for expression of transgenes in mammalian cells

To check for protein expression from each of the different mDia1 adenoviruses, SAOS-2 cells (human osteosarcoma) were plated at a density of 2.5 X 10^6 cells/dish for

24 h, and then infected with the different mDia1 adenoviruses at an MOI (multiplicity of infection) of 100 for 48 h. Cells were washed 3-4X with cold PBS, and lysed by applying 100-200 µl of SDS extraction buffer (2% SDS, 10 mM Tris pH 7.5, 10 mM NaF, 5 mM dithiothreitol, and 2 mM EGTA). The cell lysate was then boiled for 3-5 min, and sonicated briefly to break up the DNA and lower the viscosity of the lysate. The presence of the adenovirally expressed protein of interest was determined by immunoblotting.

SDS-PAGE and Western blotting:

The proteins in the lysates were separated by SDS-PAGE. Equal volumes of protein samples were mixed with 4X sample preparation buffer (12.5 ml 1 M Tris pH 6.8, 5 ml glycerol, 2.5 ml 20% SDS, 5 ml 2-mercaptoethanol, and bromphenol blue). The samples were loaded on a 10-well SDS-polyacrylamide mini gel (Bio-Rad) (10% resolving gel, 4% stacking gel) (Laemmli, 1970). After electrophoresis, the proteins were electroblotted onto PVDF membrane (Pall Corporation). Briefly, the membrane was pre-wet with methanol and then with transfer buffer [200 ml 10X Tris/Glycine (30.25 g Tris and 144 g Glycine in 1 liter d.H_2O), 400 ml methanol, and 1400 ml d.H_2O]. Electroblotting was performed at 300 mA for 3-4 hours. The membrane was blocked in 5% nonfat dry milk in 10 mM Tris pH 7.5, 150 mM NaCl for 1 h at room temperature, and washed 3-5X with wash buffer (10 mM Tris pH 8.0, 150 mM NaCl, 0.05% Tween 20). The blot was then incubated with monoclonal mouse anti-flag antibody (Sigma-Aldrich; 1:1000, diluted into wash buffer plus 1% BSA) for 1 h, followed by 3-5X washes with the wash buffer. The blot was then incubated with HRP-conjugated goat anti-mouse secondary antibodies (Santa Cruz Biotech.; 1:20,000, diluted into wash

buffer) for 1 h. For some experiments, the blots were stripped, re-blocked, and incubated with mouse anti-GAPDH (1:1000) (Chemicon), and then with HRP-conjugated goat anti-mouse secondary antibody. GAPDH was used as a loading marker. The bands were detected by chemiluminescence (SuperSignal West Pico, Pierce), exposing the blots to Hyperfilm (Pierce). The intensity of bands were analyzed and compared to the intensity of GAPDH bands of the same time point, using the TotalLab software.

Cells and cell culture

SAOS-2 cells were cultured in HGDMEM with 10% FBS (Atlas) medium and grown on plastic at 37°C in a humidified 95% air/5%CO_2 incubator. For most experiments the cells were plated onto drilled out dishes at a density of 2.5 X 10^6 cells/dish for 24 h prior to adenoviral infection. Swiss 3T3 cells were cultured identically except that the culture medium contained low glucose-DMEM (LGDMEM) with 10% FBS.

In some experiments the ROCK inhibitor Y-27632 [(+)-(*R*)-*trans*-4-(1-aminoethyl)-*N*-(4-pyridyl) cyclohexanecarboxamide dihydrochloride] (30 μM in H_2O) (Calbiochem) was added to the cells. For these experiments control cultures were treated with an identical volume of water.

In some experiments SAOS-2 cells were also infected with adenoviruses (at an MOI of 10) for expressing either the CARho or the DNRho for 24-48 h. Some of these cultures were also treated with 30 μM of Y-27632 or vehicle control for 30 min at which time these treated SAOS-2 cells were fixed and stained for actin and microtubules.

In some experiments SAOS-2 cells were plated on glass cover slips at 5,000 cells/dish, and then were co-infected with CARho and DNmDia1 or DNRho and

CAmDia1 at an MOI of 10 for each virus. Forty eight hours post infection the cells were fixed and stained for actin and microtubules.

Wound Healing Assay

SAOS-2 and Swiss 3T3 cells were grown on glass coverslips to about 80% confluency and then infected with CA- or DN-mDia1 adenoviruses at an MOI of 25 for SAOS-2 cells and 750 for Swiss 3T3 cells. Infected cells expressed GFP. Forty eight hours after infection, confluent cultures were wounded by scraping the monolayer with a heat polished glass pipette (~ 30-50-μm tip). Detailed observation on the behavior of live cells was monitored by acquiring images every 2 min over a period of 1 h; the images were viewed as movies. The effects of mDia1 mutants (CA and DN) on cell polarization were assessed by measuring the time and the distance migrated by infected cells to close the wound.

Cell fixation and immunostaining

Cells were fixed in 4% formaldehyde in cytoskeleton buffer (CB: 10mM MES pH 6.1, 138 mM KCl, 3 mM $MgCl_2$ and 2 mM EGTA pH 7.0) and 0.32M sucrose (CBS buffer) for 25-30 min, and then permeabilized in 0.5% Triton 100-X in PBS for 15 min. The cells were then blocked for 45 min with 2% goat serum in 1% BSA-TBS, and then stained for F-actin using Fluorescein (FITC)-phalloidin (Molecular probes) (1:50, diluted into 1% BSA-TBS), and for microtubules using anti-tubulin mouse primary antibody (Sigma-Aldrich) at 1:100 (diluted into 1% BSA-TBS) for one hour and goat anti-mouse Alexa-647-conjugated secondary antibody (1:400, diluted into 1% BSA-TBS) (Molecular Probes) for 1 h.

Time-lapse microscopy and digital image capture

Growth medium (HGDMEM or LGDMEM) was replaced with 1:1 mix of F12 and DMEM medium, and the medium was overlayered with dimethyl polysiloxane (Sigma) to prevent or reduce evaporation while allowing gas exchange. Live cell migration in wound-healing assay was followed using a 12-bit cooled CCD camera (Photometrcis Coolsnap ES) on an inverted Nikon microscope using 20X, 1.0 NA air objectives. The microscope was equipped with a homemade plexiglass incubation chamber for incubation at ~35°C. Image capture from the camera was controlled by Metamorph software (Universal imaging). Images were acquired using a 12-bit cooled CCD camera (Photometrcis Coolsnap ES) and a 40X, 1.4 NA oil objective on an inverted Nikon microscope controlled by Metamorph software (Universal imaging).

Results

Construction of adenoviruses

mDia1.pBS plasmid vector (see Figure 2.2) was used as a template for PCR amplification for the construction of mDia1 mutants. Each PCR reaction (10 μL) was run on a 1% gel for verification of results (Figure 2.10).

After cloning the different mDia1 mutants into the pCMV.Tag1 vector, pCMV-mDia1 mutants were cut with *BglII* and *XhoI* to confirm the cloning, and a 1% agarose gel was then run with the digestion reactions (Figure 2.11). Direct sequencing verified that the correct products were obtained.

The production of viruses using the three systems (pAdTrack-, pRedTrack-, and pShuttle-CMV) for all mDia1 constructs was successful except for wt-mDia1 in

Figure 2.10
PCR amplification products of mDia1 mutants. mDia1.pBS plasmid vector was used as a template for PCR amplification for the construction of mDia1 mutants. A) DNA marker, B) DNmDia1 (1.5 Kb) and F1mDia1 (1Kb), C) F3mDia1 (1Kb), D) CAmDia1 (2Kb), and E) DADmDia1 (0.5Kb). The red arrow in B,C,D and E references the position of the 1Kb size band.

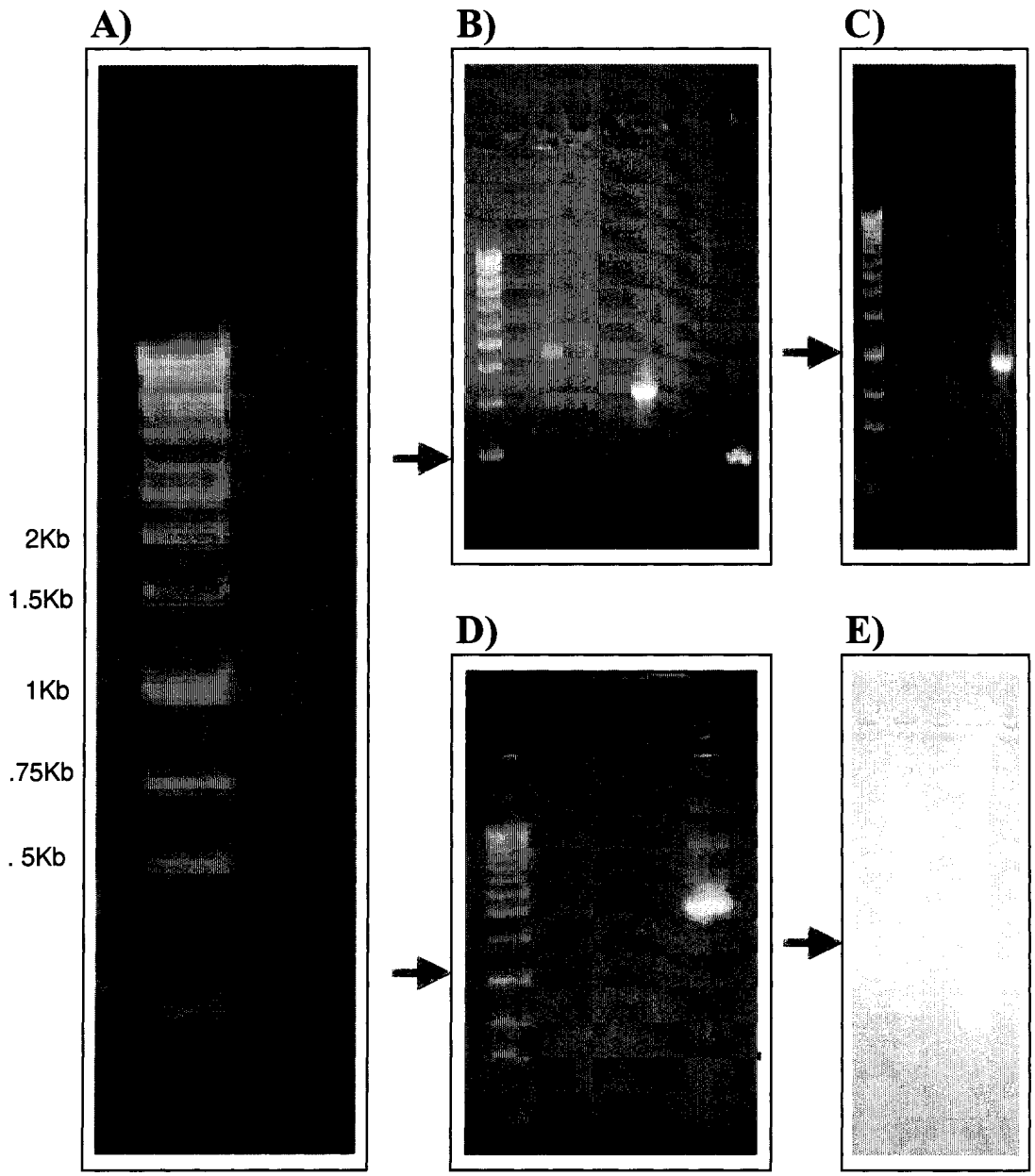

Figure 2.11
pCMV..mDia1 constructs test digest. A) DNA molecular markers. B) pCMV.CAmDia1 (pCMV.Tag1 is 4.3Kb in size, CAmDia1 is 2Kb in size). C) pCMV.DNmDia1 (DNmDia1 is 1.5 kb). D) pCMV.F1mDia1 (F1mDia1 is 1 kb). E) pCMV.F3mDia1 (F3 is 1 kb). F) pCMV.DADmDia1 (DADmDia1 is 0.5 kb). The red arrow in B, C, D, E, and F references the 1Kb size band.

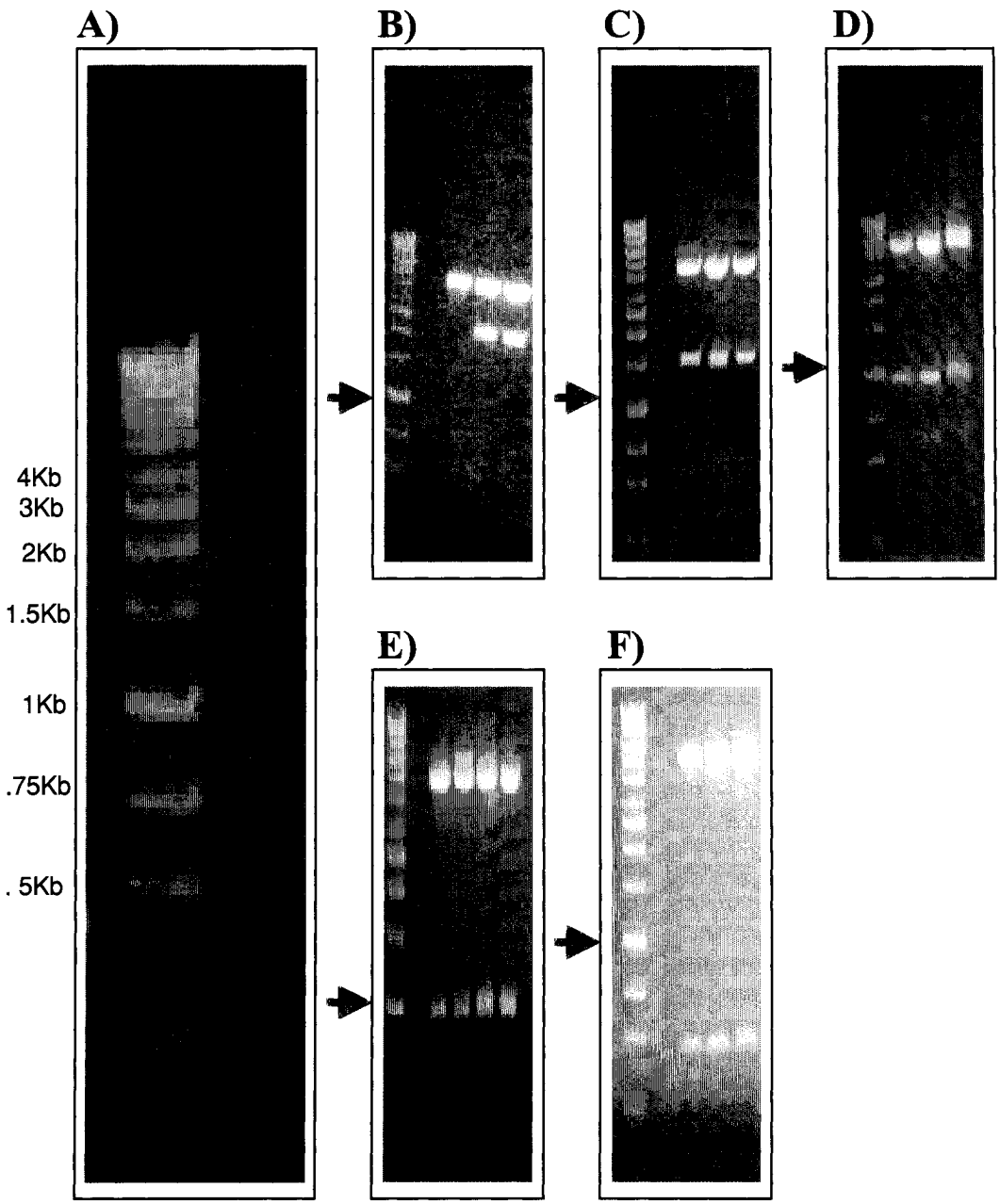

pAdTrack-CMV. All of the proteins expressed from the recombinant adenoviruses had the expected mass on SDS-PAGE when compared to standards (Figure 2.12 A, B, and C). The expressed full-length mDia as well as the F1 and F3mDia1 fragments showed some lower mass products arising either from degradation or premature termination (Figure 2.12 A).

Time course for expression of CA and DNmDia1 following adenoviral infection of cells

The time course for the expression of CA- (Figure 2.13 A) and DN-mDia1 (Figure 2.14 A) following infection of cells with the adenoviruses was determined by western blotting. SAOS-2 cells infected with either mutant were lysed every 6 h for the first 24 h and every 12 h thereafter. The intensity of CA- and DNmDia1 bands were compared to the intensity of GAPDH bands at the same time points. With both constructs, the first time point where proteins could be detected was at 12 h post infection. CAmDia1 expressing cells started to detach 24-28 h after infection requiring the collection of the cells by centrifugation of the medium in 15ml conical tubes. The loss of some cells probably explains the apparent drop in protein expression 24 h after infection (Figure 2.13 B). DNmDia1-infected cells began to detach 36-40 h post infection (Figure 2.14 B).

SAOS-2 cells were plated on 35mm drilled out dishes at two different densities, 5000 cells/dish and 20,000 cells/dish. The first sign of infection (GFP positive cells) for both mutants was 12 h post infection, which is in agreement with the western blot results. Confluent SAOS-2 cells that were infected with CAmDia1 adenovirus became elongated by 18 h post infection as compared to control uninfected or GFP-infected cells that are

Figure 2.12
Western blot of SAOS-2 lysates from cells infected with mDia1 adenoviruses. All of the constructs were expressed at the correct molecular weight: full-length mDia1 at 140kDa, CAmDia1 at 79kDa, DNmDia1 at 55kDa, F1- and F3mDia1 at 34kDa, and DADmDia1 at 15Kda. The full-length, F1 and F3mDia1 constructs showed degradation products (A).

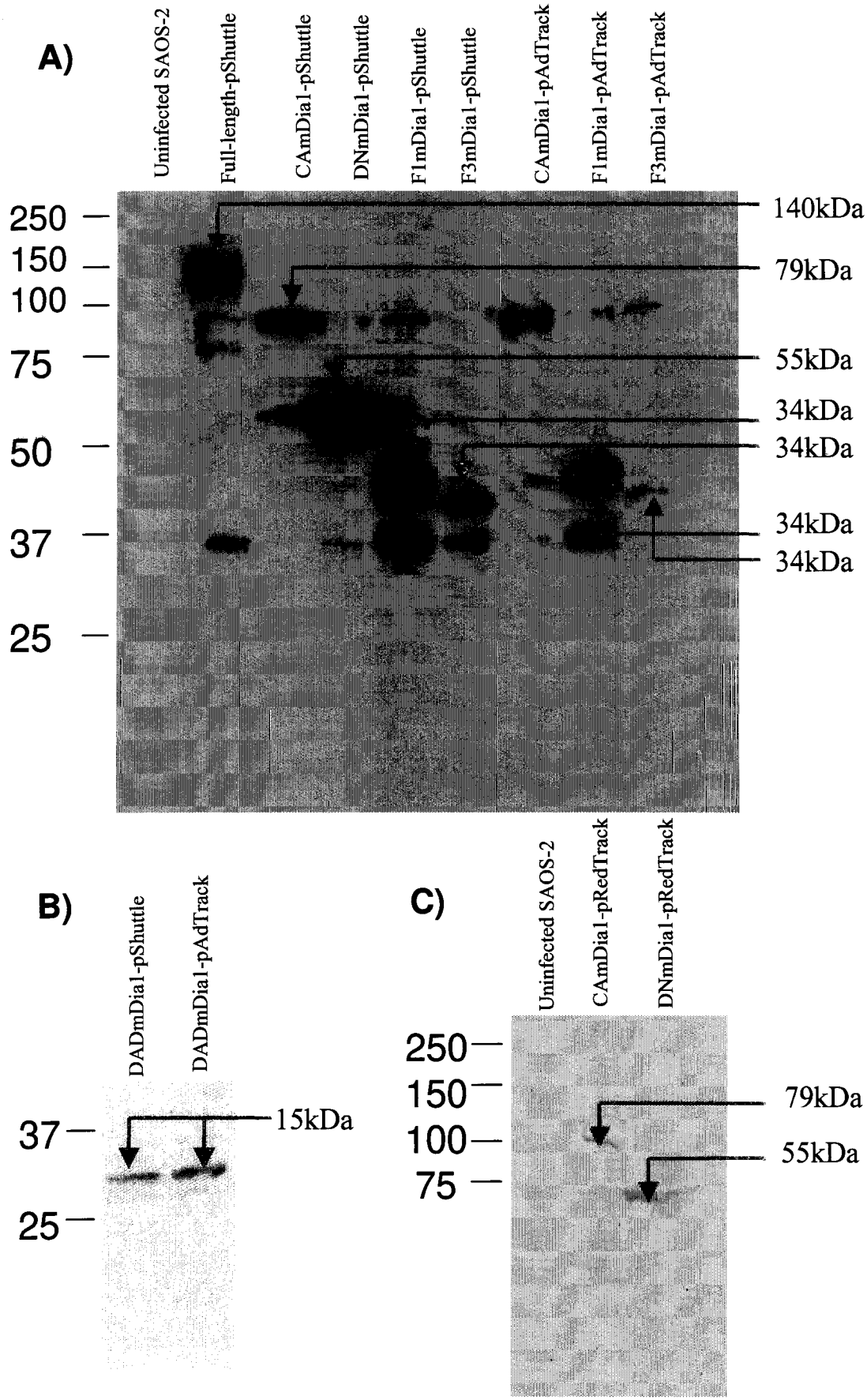

Figure 2.13
Time course of CAmDia1 expression in SAOS-2 cells.
A) Western blot of CAmDia1-infected cell lysates 6-60 h post infection stained for Flag (CAmDia1) in upper panel and GAPDH, a loading control, in lower panel. B) The intensity of CAmDia1 bands were normalized to the intensity of GAPDH bands at the same time points. The analysis was performed with the Total Lab software.

A)

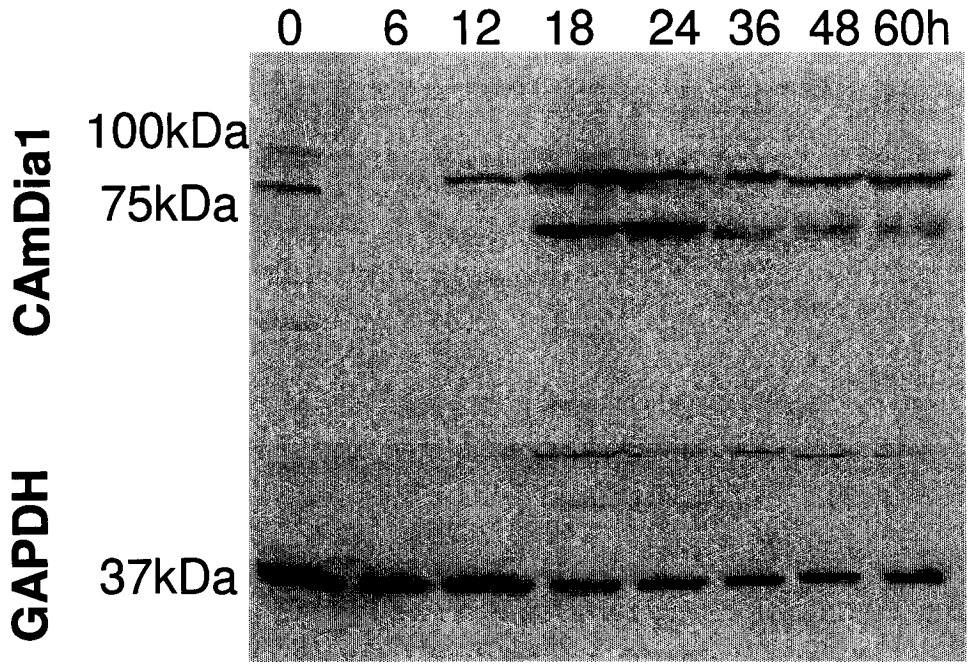

B)

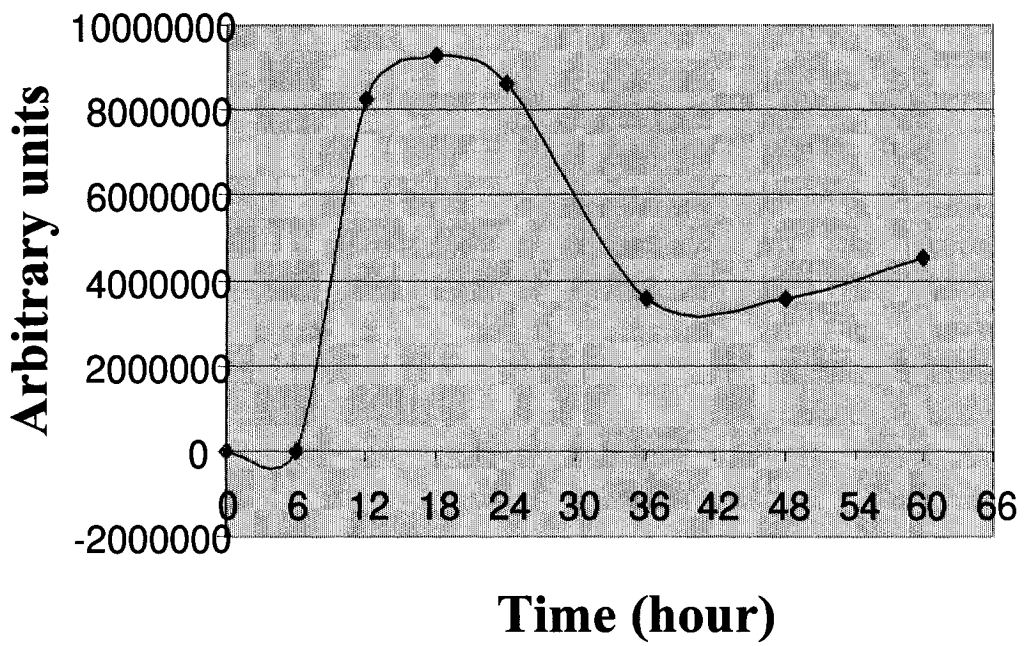

Figure 2.14
Time course of the DNmDia1 expression in SAOS-2 cells.
A) Western blot of lysates from DNmDia1-infected cells 6-60 h post infection (upper panel) and GAPDH loading control (lower panel). B) The intensity of DNmDia1 bands were normalized to the intensity of GAPDH bands at the same time points. The analysis was performed with the Total Lab software.

A)

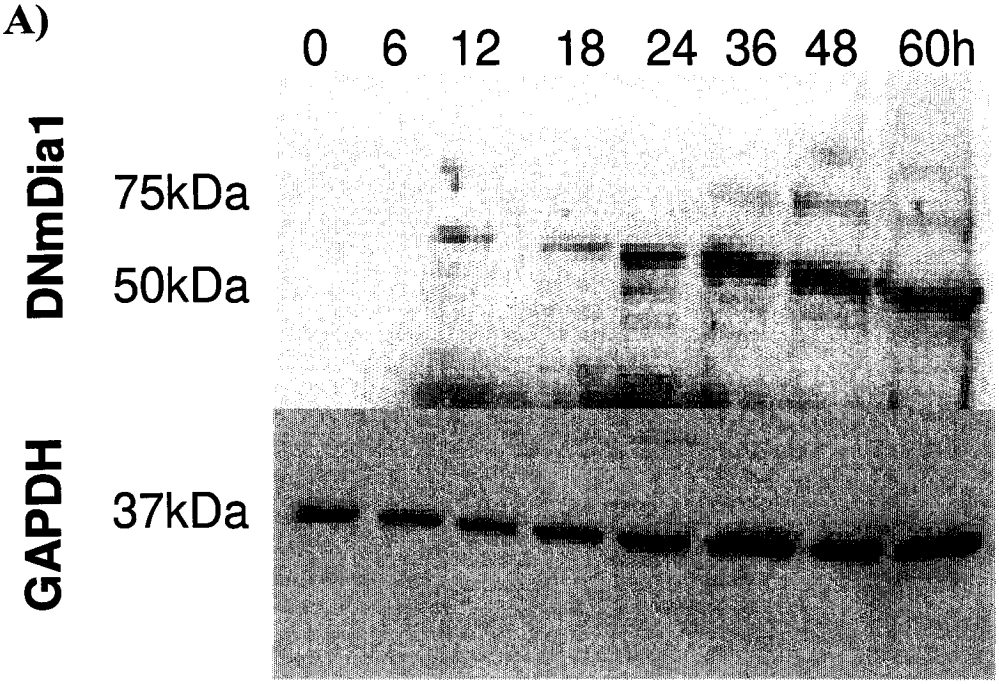

B)

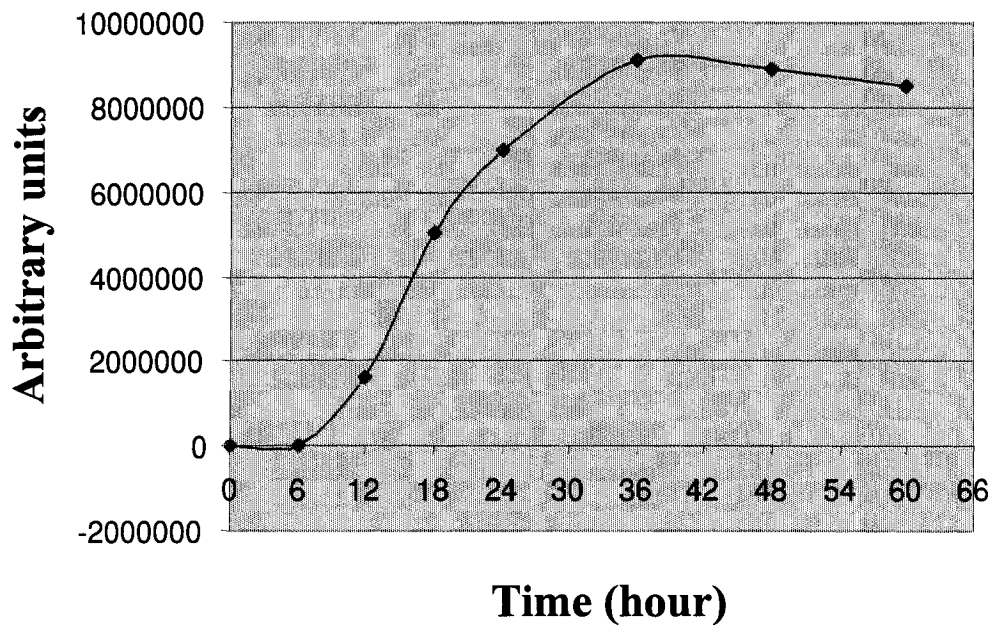

flat fibroblastic-like cells (Figure 2.15 B). By 24 h post infection, more than 70% of the cells were infected, and more than 75% of the infected cells had a fusiform morphology (Figure 2.15 C). Thirty hours after infection, the cells started to form membrane blebs at the cell periphery (Figure 2.15 D, arrows). Two days after infections, CAmDia1-infected SAOS-2 cells roundedand aggregated into clumps (Figure 2.15 E and F). For DNmDia1-infected confluent SASO-2 cells, cell morphology started to change from flat to round at 16-20 h post infection (Figure 2.16 B and C). DNmDia1-infected SAOS-2 cells retained the round shape until 30 h post-infection (Figure 2.16 D). By 36-48 h post infection DNmDia1 infected cells aggregated and were blebbing (Figure 2.16 E and F, arrows in E). Both mutants caused detachment by 60 h after infection.

Infected SAOS-2 cells, plated at low density (5,000 cells/dish) were fixed and stained for actin and microtubules. Eight cells showed signs of CAmDia1 infection 12 h post infection, half of which had a fusiform morphology (Figure 2.17 D and E) as compared to the flat, fibroblastic-like morphology of control cells (Figure 2.17 A-C). Eighteen hours after infection, 70-80% of the cells were GFP- positive. Infected cells were elongated and had a bipolar morphology. Actin filament bundles were thinner than in controls (Figure 2.17 F-I). The same phenotype persisted over the first 24 h post-infection (Figure 2.17 J-M). By 36 h, the cells were blebbing and beginning to die (Figure 2.17 N).

The first sign of DNmDia1 infection was at 12 h post-infection (4-10 GFP-expressing cells/dish), but the overexpression of DNmDia1 had no effect on cell morphology and cytoskeletal organization during the first 24 h post-infection. DNmDia1-infected cells were indistinguishable from uninfected cells (Figure 2.18 D-G, compare the

Figure 2.15
Morphology of CAmDia1-infected confluent SAOS-2. Confluent SAOS-2 cells that expressed CAmDia1 became elongated by 18h post infection (B) as compared to control uninfected or GFP-infected cells that are flat fibroblast-like cells (A). By 24h post infection, the infected cells had a fusiform morphology (C). 30 hours after infection, the cells showed signs of blebbing at cell periphery (D, arrows). 48 h post infections, CAmDia1-infected SAOS-2 cells round and aggregate (E and F).

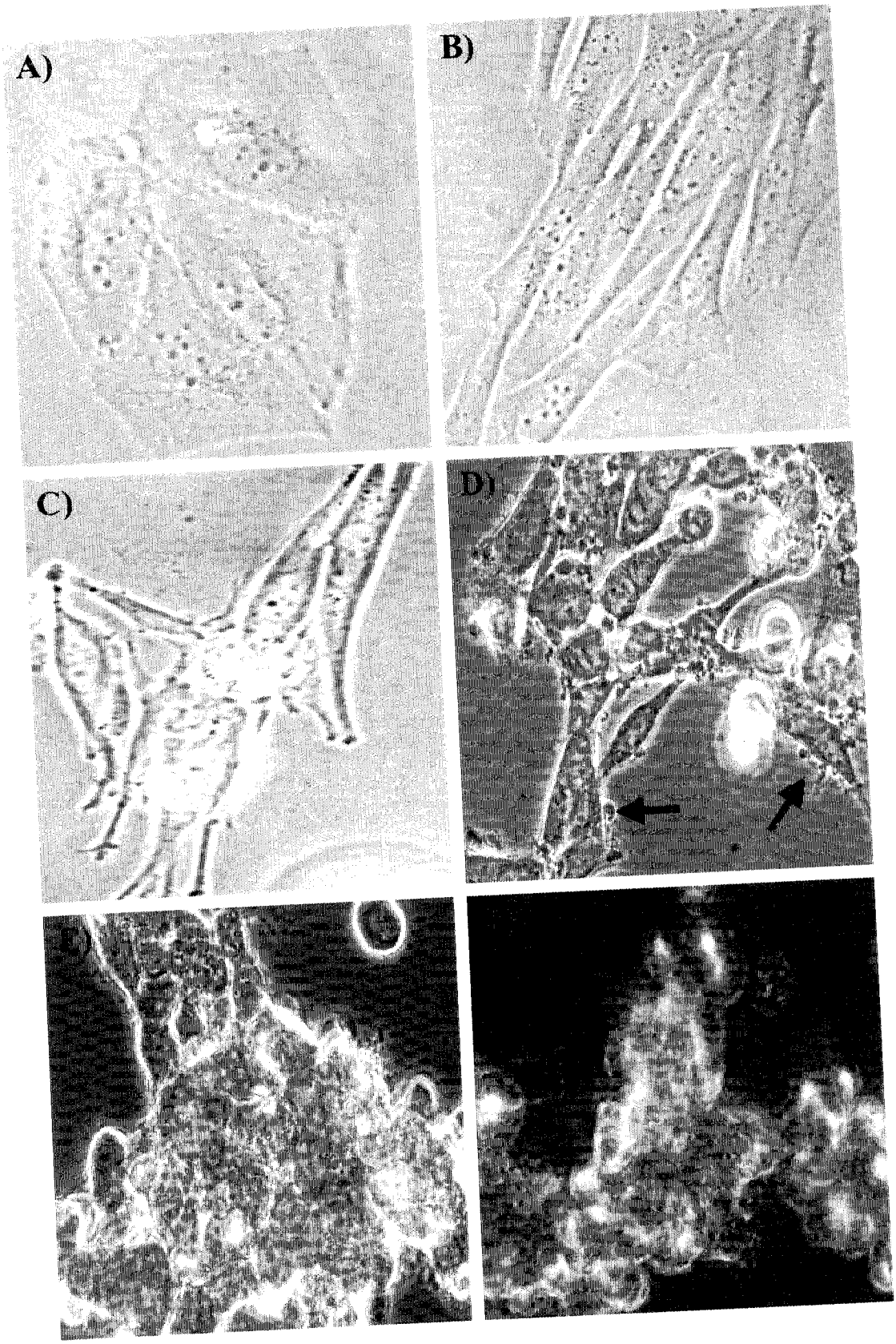

Figure 2.16
Morphology of DNmDia1-infected confluent SAOS-2. Confluent SAOS-2 cells that express DNmDia1 started to round at 18-24h (B and C) compared to uninfected or control infected cells (A). DNmDia1-infected SAOS-2 cells retained the round shape up till 30h after infection (D). 36-48h post infection, almost all cells become rounded and were blebbing (E and F, arrows in E).

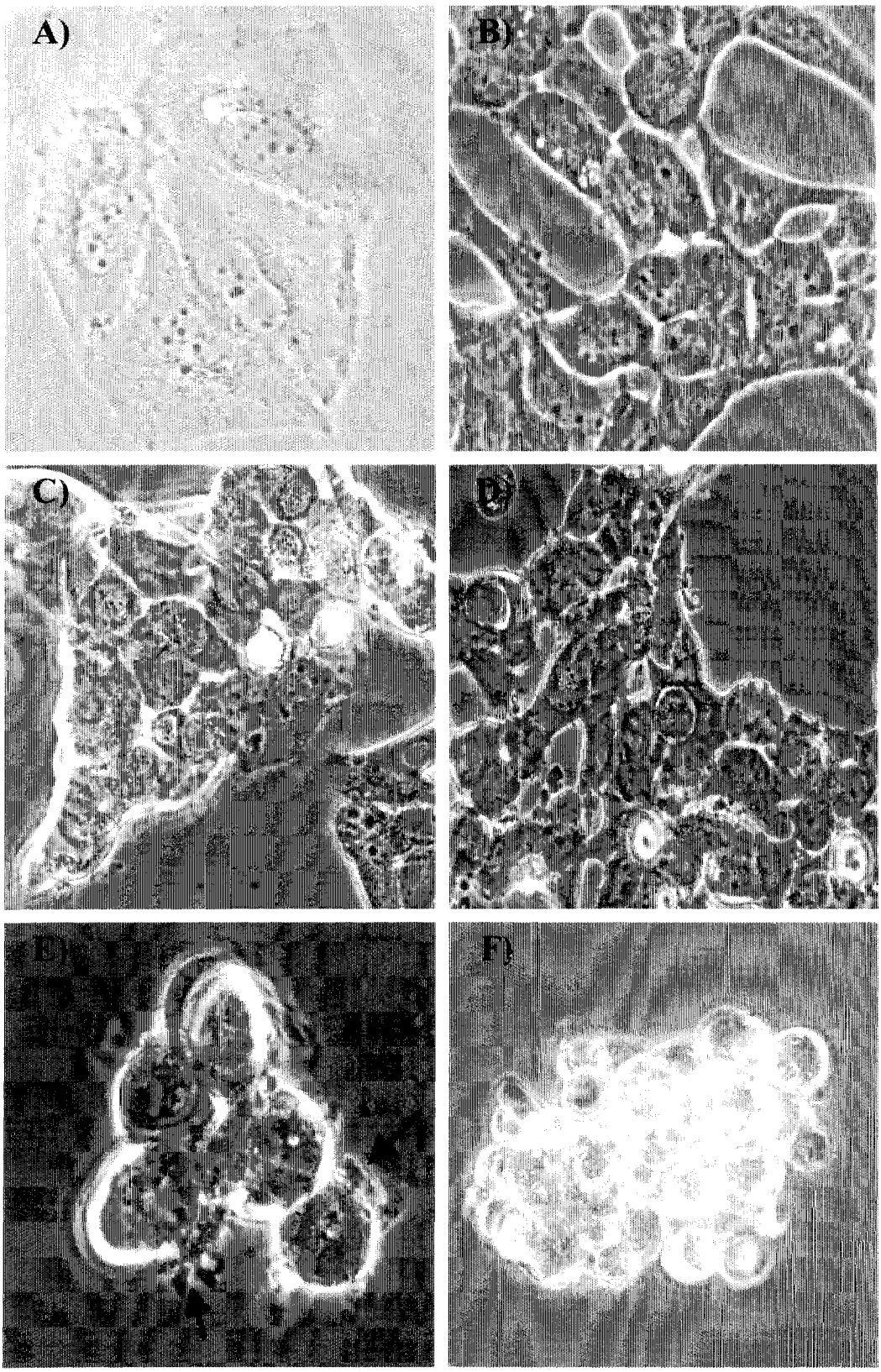

Figure 2.17
Effect of CAmDia1 overexpression on SAOS-2 cell morphology and cytoskeleton. By 12 hours post infection, half of CAmDia1-infected cells had a fusiform morphology (D and E) as compared to flat, fibroblast-like morphology of control cells (A-C). By 18 h after infection, infected cells were elongated and had a bipolar morphology (F). Actin filaments were fine and parallel to the long axis of the cells (G). Cell elongation persisted over the first 24 h post infection (J-M). By 36 h, cells were blebbing and dying (N).

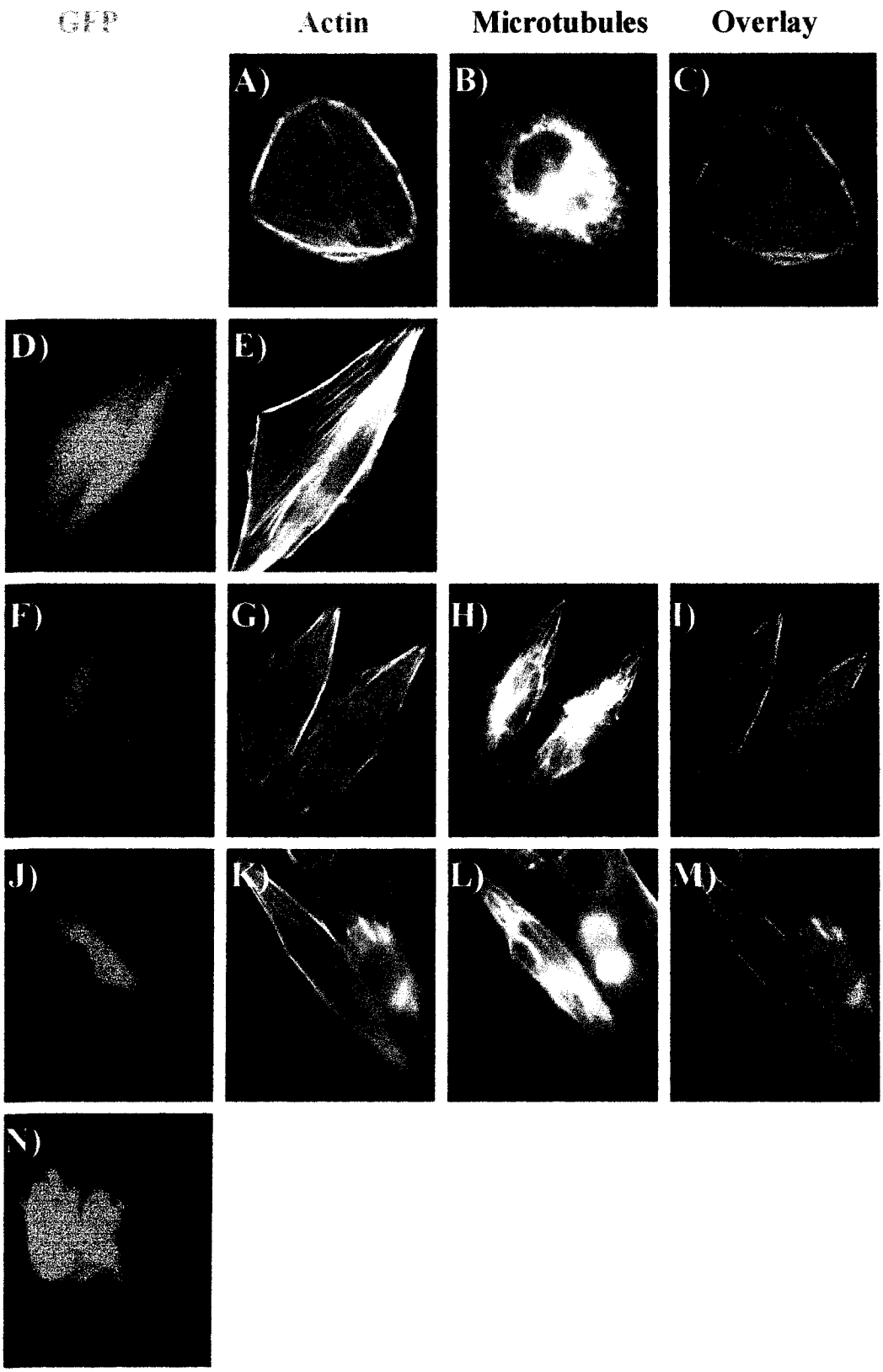

Figure 2.18
Effect of DNmDia1 overexpression on SAOS-2 cell morphology and cytoskeleton. (A-C) Uninfected control cells. DNmDia1 expression had no effects on cell morphology and cytoskeleton during the first 24 h post infection (D-G). By 36 hours post infection, stress fiber staining became faint and there was an increase in cell ruffling (I, arrows). The overexpression of DNmDia1 in SAOS-2 cells had no effect on microtubules (F and J).

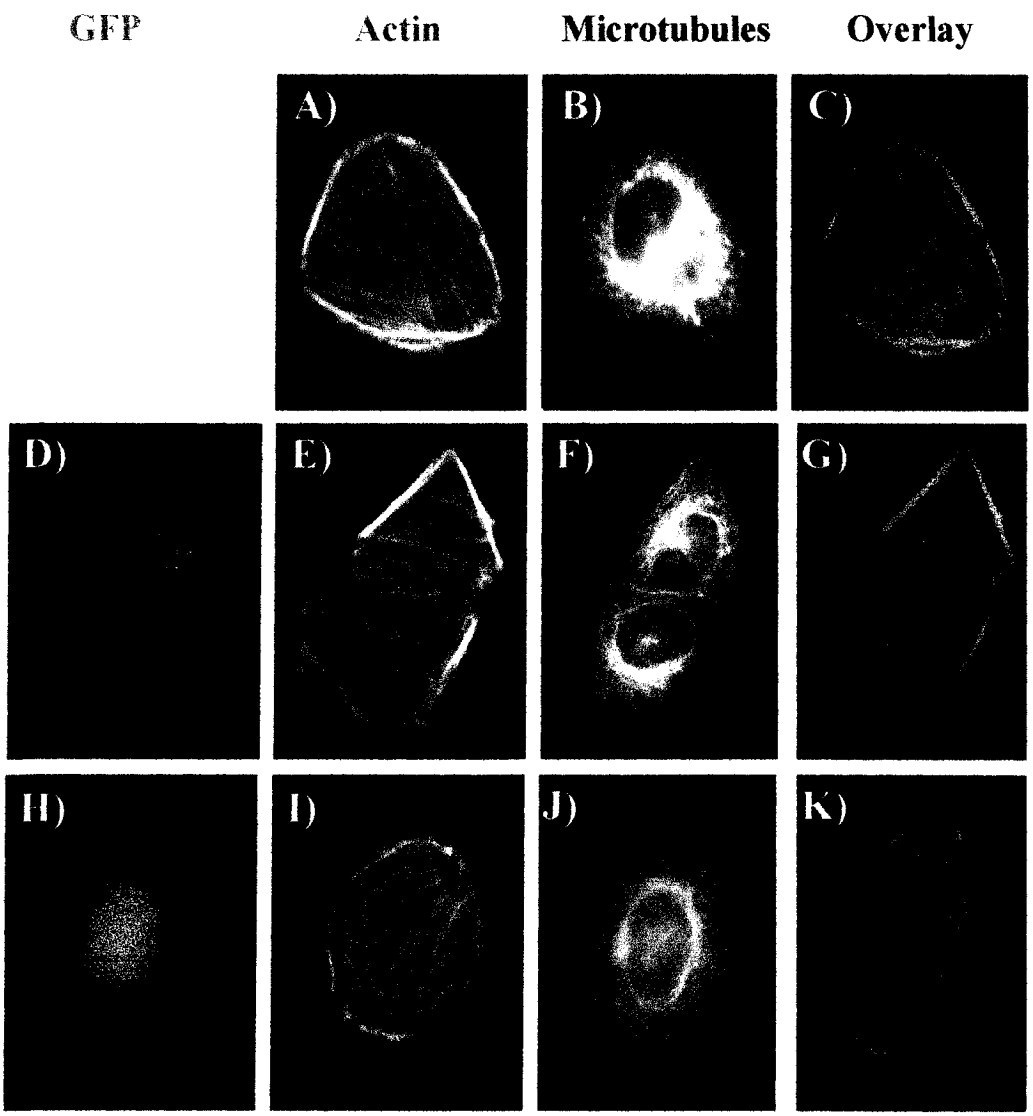

top infected cell to the bottom uninfected one). By 36 h post-infection, stress fiber staining became faint and there was an increase in cell ruffling (Figure 2.18 I, arrows). The overexpression of DNmDia1 in SAOS-2 cells had no effect on microtubule organization (Figure 2.18 F and J). Non-confluent DNmDia1- infected cells were more resistant to blebbing than confluent cells; cell blebbing was not observed before 42 to 48 h post-infection.

Overexpression of CAmDia1 but not DNmDia1 delays closure of wounds in confluent SAOS-2 and Swiss 3T3 cell cultures

SAOS-2 and Swiss 3T3 cells were grown to confluency on glass coverslips and infected with CA- or DN-mDia1 adenoviruses (MOI = 25 for SAOS-2 cells, and 750 for Swiss 3T3 cells) 48 h before wounding. All of the cells were infected (Figure 2.19 A and B). The effect of mDia1 mutants (CA and DN) on cell polarization was assessed by measuring the time and distance migrated by cells to close the wound. Control uninfected SAOS-2 cells achieved wound closure in 12-14 h on average (Figure 2.19 C-F), while it took an average of 3-5 h for Swiss 3T3 cells to close the wound (Figure 2.20 A-D). In both cell types, overexpression of CAmDia1 delayed cell migration and wound closure time. CAmDia1-infected SAOS-2 cells migrated at 0.041 μm/min whereas uninfected controls migrated at 0.075 μm/min (Figure 2.21 A), and wound closure took around 20-24 h. Similar results were obtained with Swiss 3T3 cells; when infected with CAmDia1 wound closure occurred in 8-9 h compared to 3-5 h in uninfected cells. CAmDia1-infected Swiss 3T3 cells migrated at 0.43 μm/min, compared to 1.00 μm/min for controls (Figure 2.21 B). Overexpression of DNmDia1 in both SAOS-2 and Swiss 3T3 cells had

Figure 2.19
Wound healing assay in SAOS-2 cells. Almost 100% of the cells were GFP-expressing (A). (B) The two edges of the wound (arrows). Control uninfected SAOS-2 cells achieved wound closure in 12-14 hours on average. (C) 1 h, (D) 5 h, (E) 8 h, and (F) 12 h after wounding. None of the images from C-D are showing a fully healed wound.

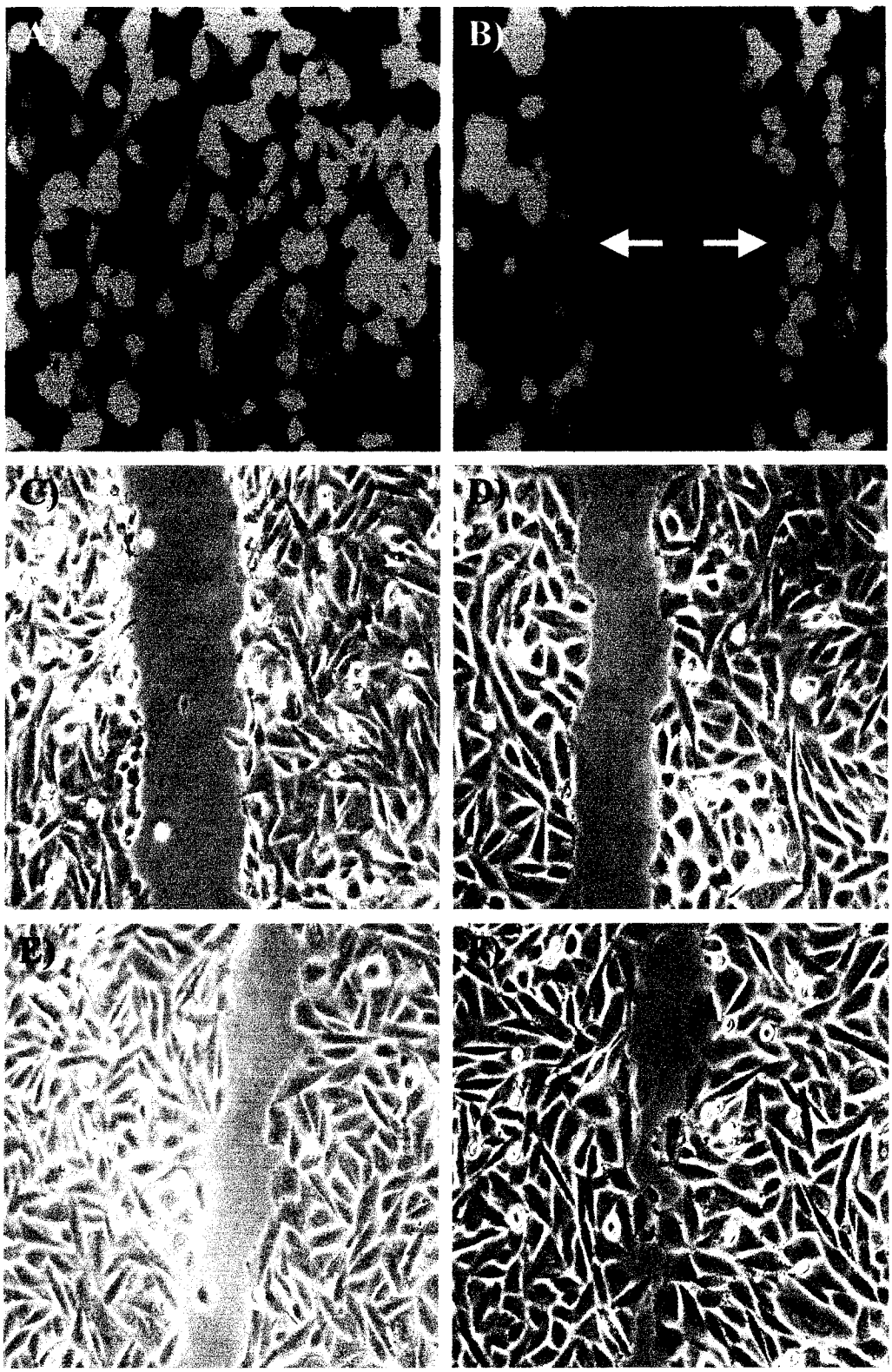

Figure 2.20
Wound healing assay in Swiss 3T3 cells. Control uninfected Swiss 3T3 cells needed 3-5 hours to close the wound. (A) 1 h, (B) 2 h, (C) 3 h, and (D) 4 h after wounding. None of the images are showing a fully healed wound.

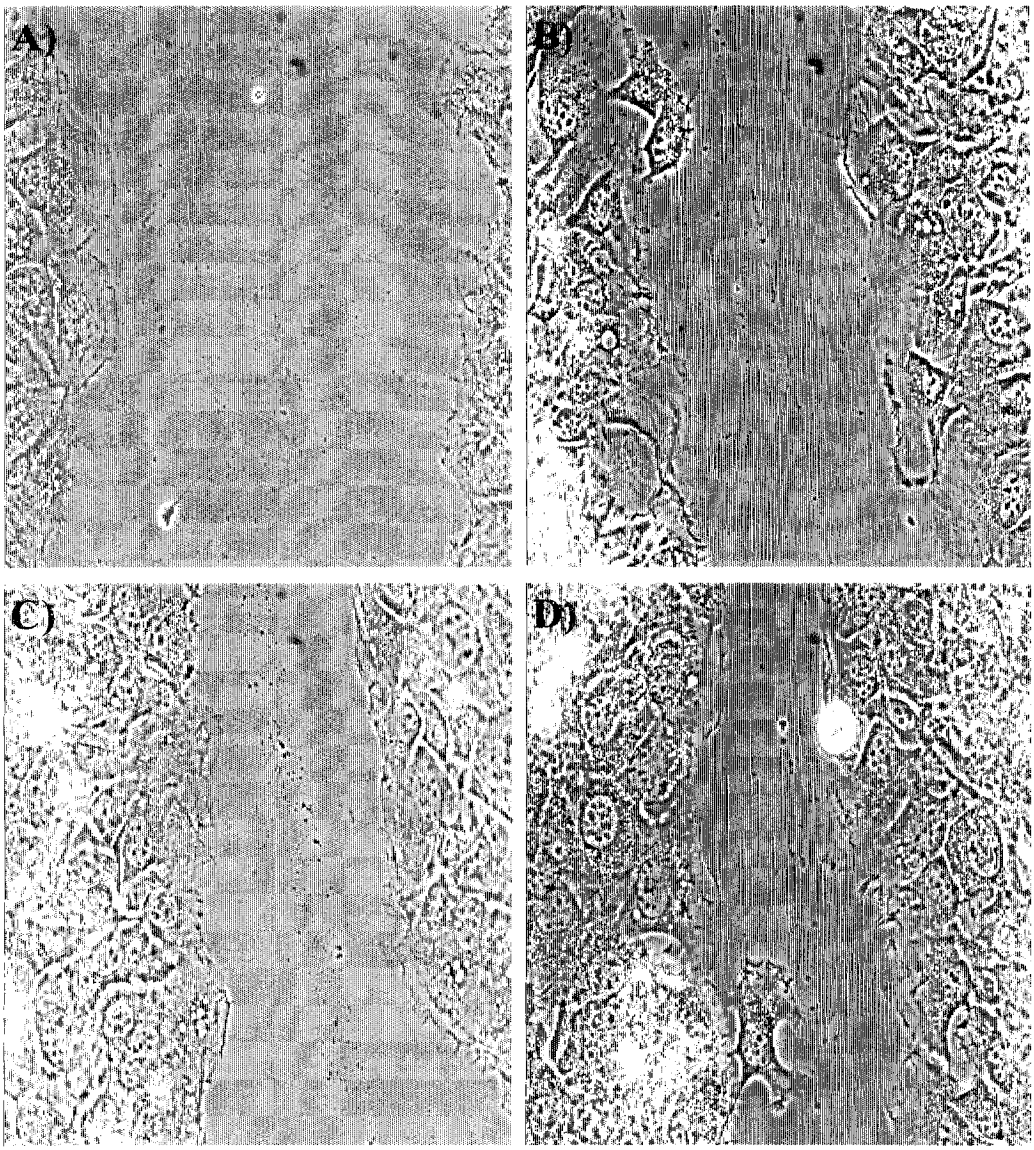

Figure 2.21
Effect of CA- and DN mDia1 on wound healing assay in SAOS-2 and Swiss 3T3 cells. Overexpression of CAmDia1 in SAOS-2 (A) and Swiss 3T3 (B) caused a delay in cell migration and thus wound closure time. Overexpression of DNmDia1 in both SAOS-2 and Swiss 3T3 cells had no effect on cell migration rate (A and B, respectively).

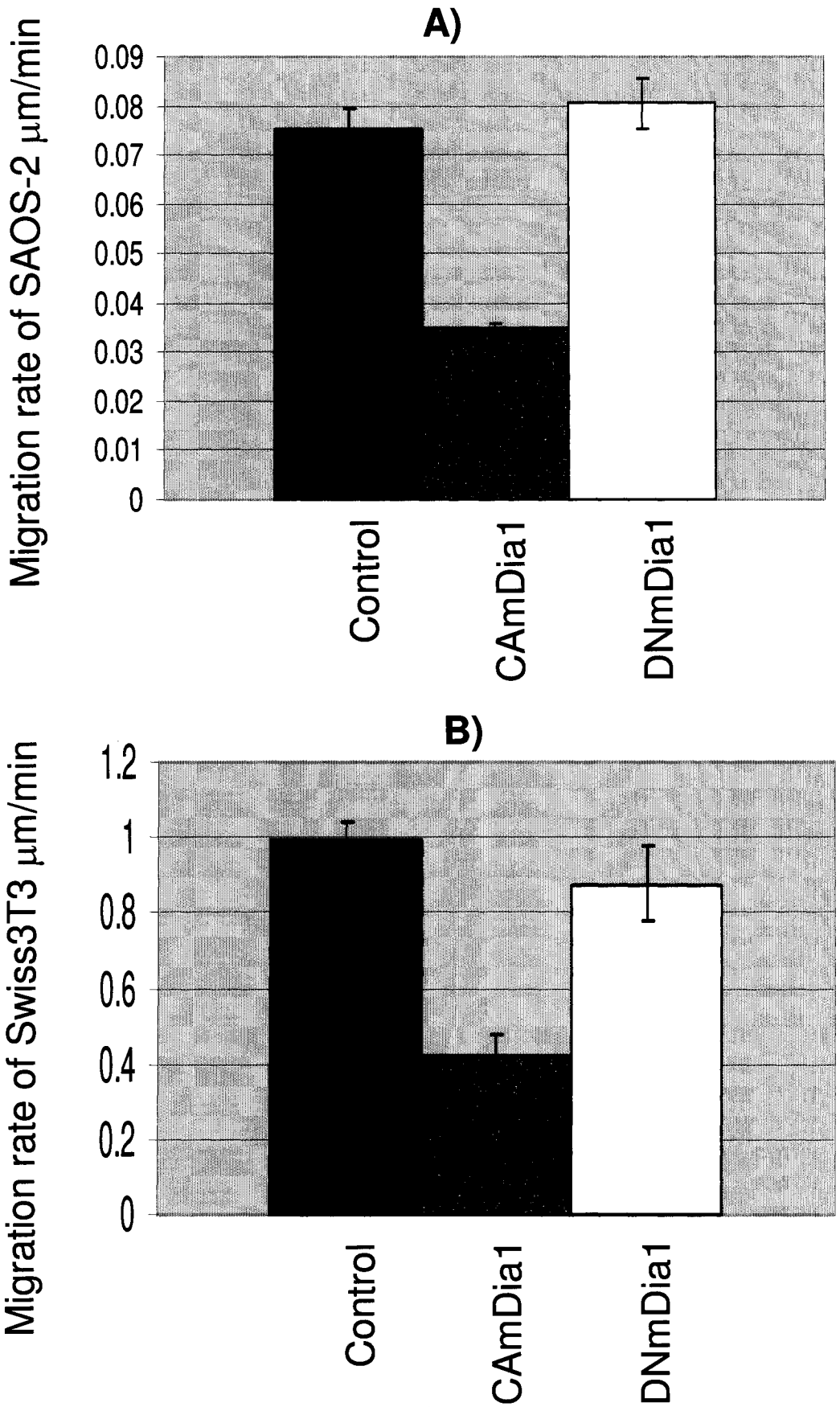

no effect on cell migration rate (Figure 2.21 A and B) or the time required to close the wound.

Inhibition of ROCK activity coupled with overexpression of CAmDia1 induces the formation of thin processes, whereas overexpression of DNmDia1 induces a butterfly-like morphology

Uninfected SAOS-2 cells were treated with the ROCK inhibitor Y-27632 (30 μM) for different periods of times and the effect of the ROCK inhibitor on cell morphology and cytoskeleton was observed. After the first 30 min, SAOS-2 cells became thin and spindle-like in shape (2.22 A). With longer incubation periods (2-15 h) the cells started extending long processes (Figure 2.22 B-D, arrows). After 15 h of incubation, the cells were fixed and stained for actin and microtubules. Actin stress fibers almost disappeared from the treated cells (Figure 2.22 F), and the long processes stained positive for microtubules (Figure 2.22 G).

SAOS-2 cells were infected with CA- and DNmDia1 for 24-48 h, and were treated with 30 μM Y-27632 for 30 min. CAmDia1-infected SAOS-2 cells extended long processes (Figure 2.23 E and F, arrows) that were filled with microtubules (Figure 2.23 G). The same phenotype was obtained when the cells were infected with CARho and treated with Y-27632 (Figure 2.23 J-N). In 78% of SAOS-2 cells, expressing DNmDia1 mutant inhibited the long- process phenotype caused by CARho expression and Y-27632 treatment. When SAOS-2 cells were infected with DNmDia1 or DNRho and treated with Y-27632, the cells spread-out and had a butterfly-like morphology (Figure 2.24 E-I and J-N, respectively). Y-27632 treatment of SAOS-2 cells that were co-infected with CAmDia1 and DNRho resulted in elongated cell morphology. All of the Y-27632 treated

Figure 2.22
SAOS-2 cell morphology in the presence of 30 μM Y-27632.
30 min after treating SAOS-2 cells with Y-27632, they exhibited a spindle-like morphology (A). With longer incubation periods 2h (B), 7h (C), and 15h (D), the cells started extending long processes (arrows). Actin stress fibers almost disappeared from the treated cells (F), and the long processes stained positive for microtubules (G). (H) is the image overlay of F and G.

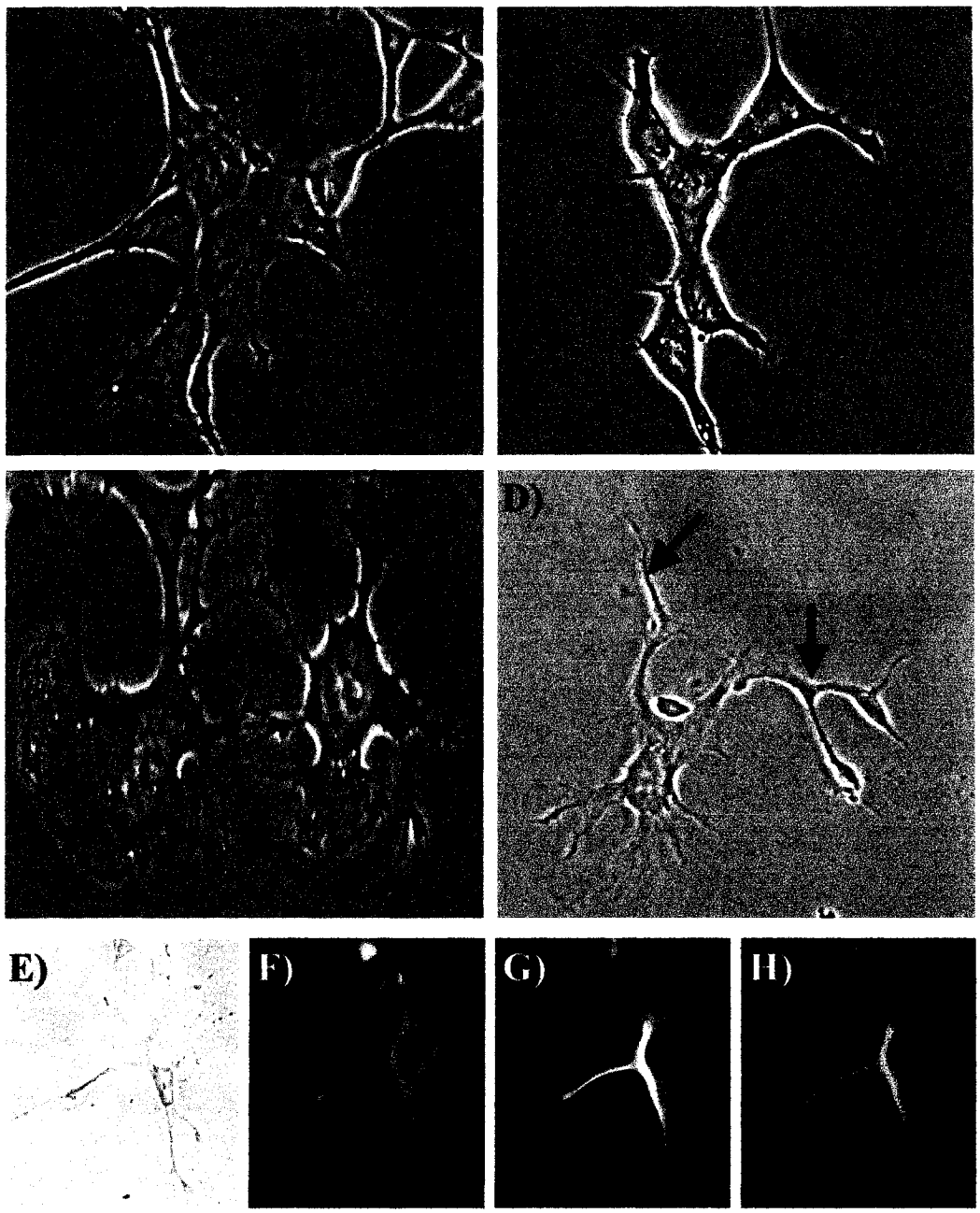

Figure 2.23
Overexpression of CAmDia1 in SAOS-2 cells in the absence of ROCK activity. (A-D) Uninfected control SASO-2 cells. CAmDia1-infected SAOS-2 cells extended long processes after 30 min of treating them with Y-27632 (E and F, arrows). These processes stained positive for microtubules (H), but actin filaments were absent (G). CARho-infected SAOS-2 cells that were treated with Y-27632 for 30 min, exhibited the same phenotype (J-N).

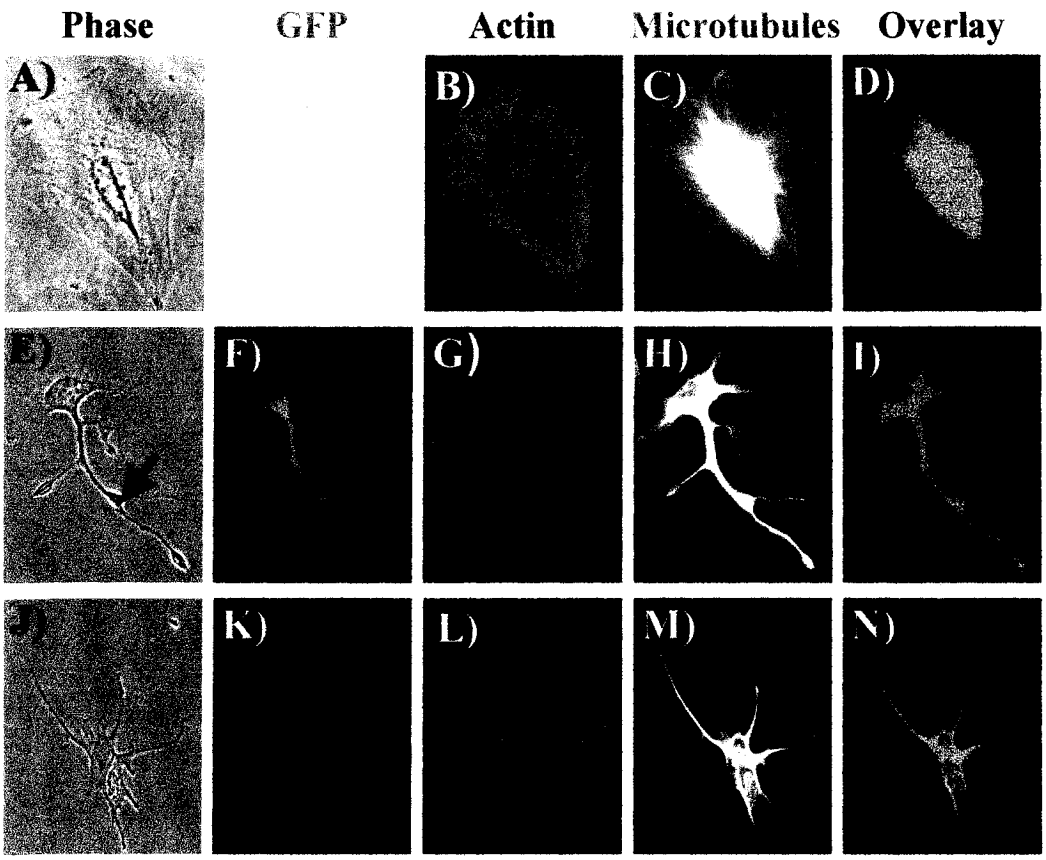

Figure 2.24
Overexpression of DNmDia1 in SAOS-2 cells in the absence of ROCK activity. (A-D) Uninfected control cells. SAOS-2 cells that were infected with DNmDia1 or DNRho and treated with Y-27632 for 30 min exhibited a butterfly-like morphology (E-I and J-N, respectively).

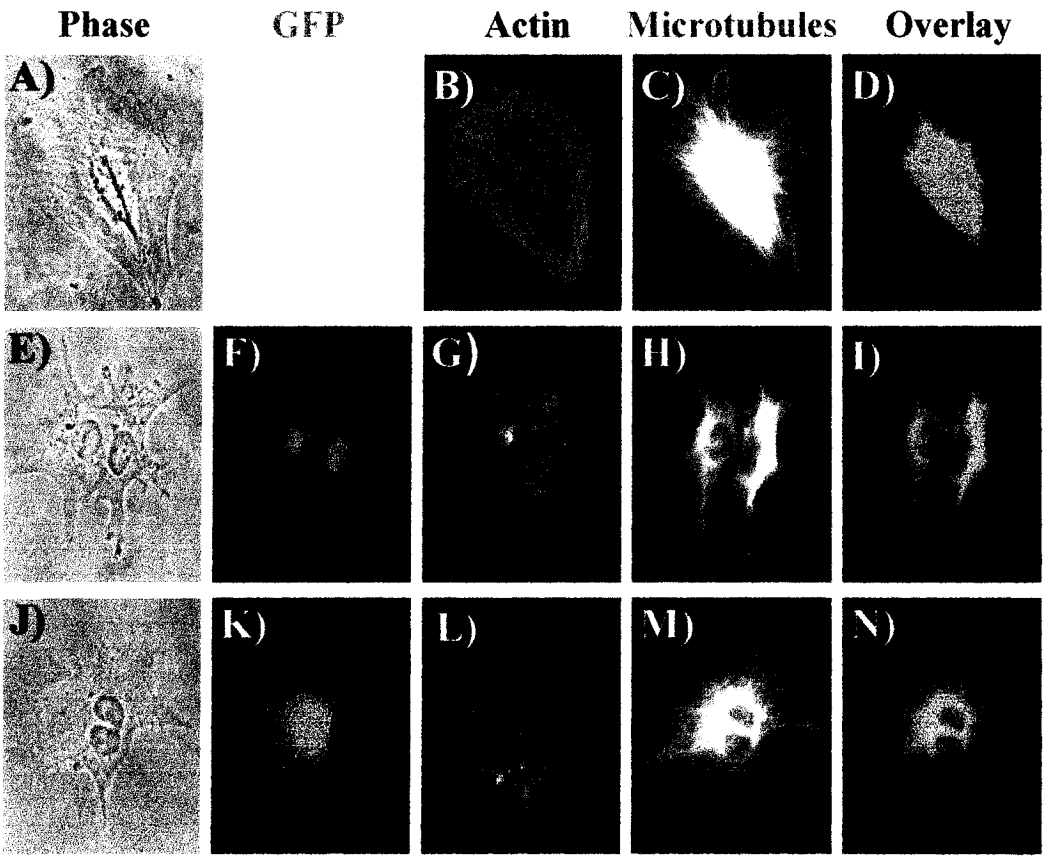

cells (regardless of other proteins expressed) had a common prominent feature, the dissolution of actin stress fibers (Figure 2.23 G and L, and Figure 2.24 G and L).

Nearly normal actin phenotypes were rescued by expression of CAmDia1 in cells expressing DN-Rho and by expression of DNmDia1 in cells expressing CA-Rho

CARho-infected SAOS-2 had a reduced size (Figure 2.25 D-G) compared to uninfected cells (Figure 2.25 A-C). The average length of the long and short axes of CARho-expressing cells was 28.8 ± 1.9 μM and 25.2 ± 2.1 μM, respectively, which is significantly smaller than that of uninfected cells (43.1 ± 1.2 μM and 34.3 ± 1.7 μM, respectively). The overexpression of CARho increased the stress fibers and cortical actin in SAOS-2 (Figure 2.25 E), but had no effect on microtubules (Figure 2.25 F). The co-infection of SAOS-2 cells with CARho and DNmDia1 reduced the stress fiber staining (Figure 2.25 J). On the other hand, DNRho reduced the stress fibers in SAOS-2 cells (Figure 2.26 E), and as with the CARho overexpression, it had no effect on microtubules (Figure 2.26 F). Expression of CAmDia1 reversed the effect of DNRho on stress fibers; CAmDia1 and DNRho co-infected SAOS-2 had nearly normal stress fiber staining (Figure 2.26 J).

Discussion

Adenoviruses containing full-length mDia1 along with five other mutant forms of mDia were prepared. All of the different mDia constructs were successfully incorporated into three different shuttle vectors (pAdTrack-CMV, pRedTrack-CMV, and pShuttle-CMV). All of these, except for the wt-mDia1 in pAdTrack-CMV, gave functionally

Figure 2.25
DNmDia1 overexpression in SAOS-2 rescued the effect of CARho on actin filaments to almost normal phenotype. CARho-infected SAOS-2 had a smaller size (D-G) when compared to uninfected cells (A-C). The overexpression of CARho increased the stress fibers and cortical actin in SAOS-2 (E), but had no effect on microtubules (F). Co-infecting SAOS-2 cells with CARho and DNmDia1 reduced the stress fiber staining (J).

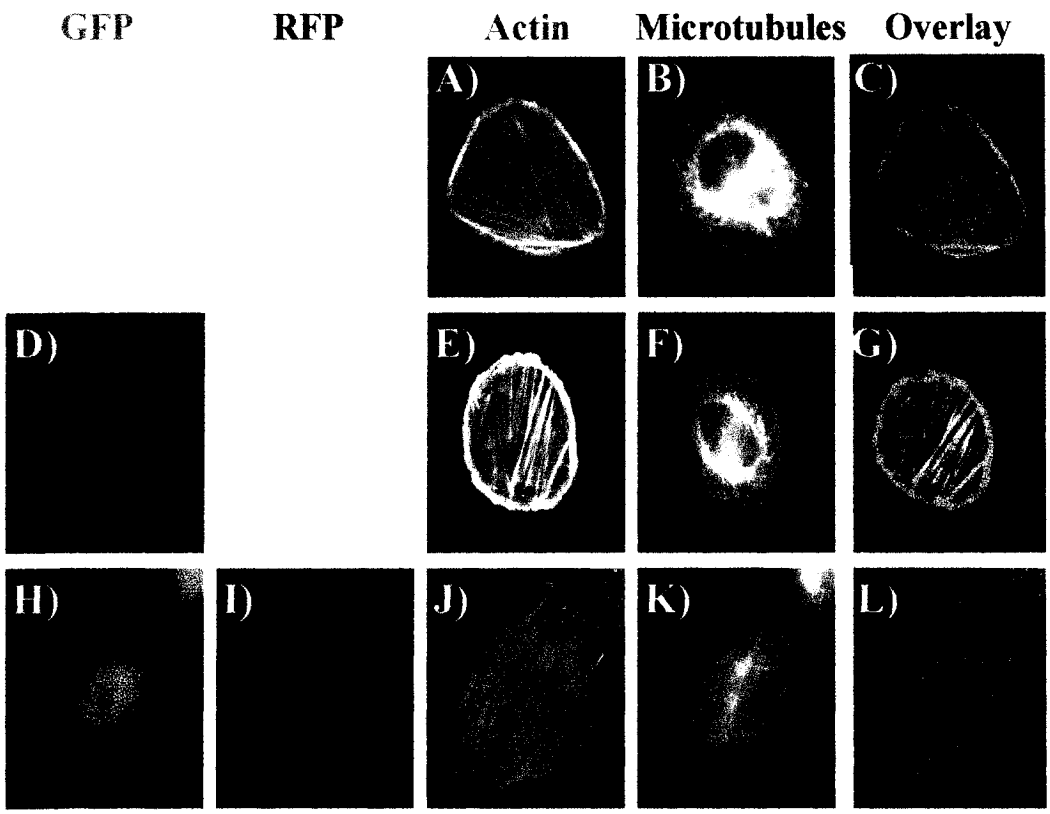

Figure 2.26
CAmDia1 overexpression in SAOS-2 rescued the effect of DNRho on actin filaments to almost normal phenotype. (A-C) Uninfected control cells. DNRho-infected SAOS-2 showed faint stress fiber staining (E), but had no effect on microtubules (F). The co-infection of SAOS-2 cells with DNRho and CAmDia1 enhanced the stress fiber staining (J).

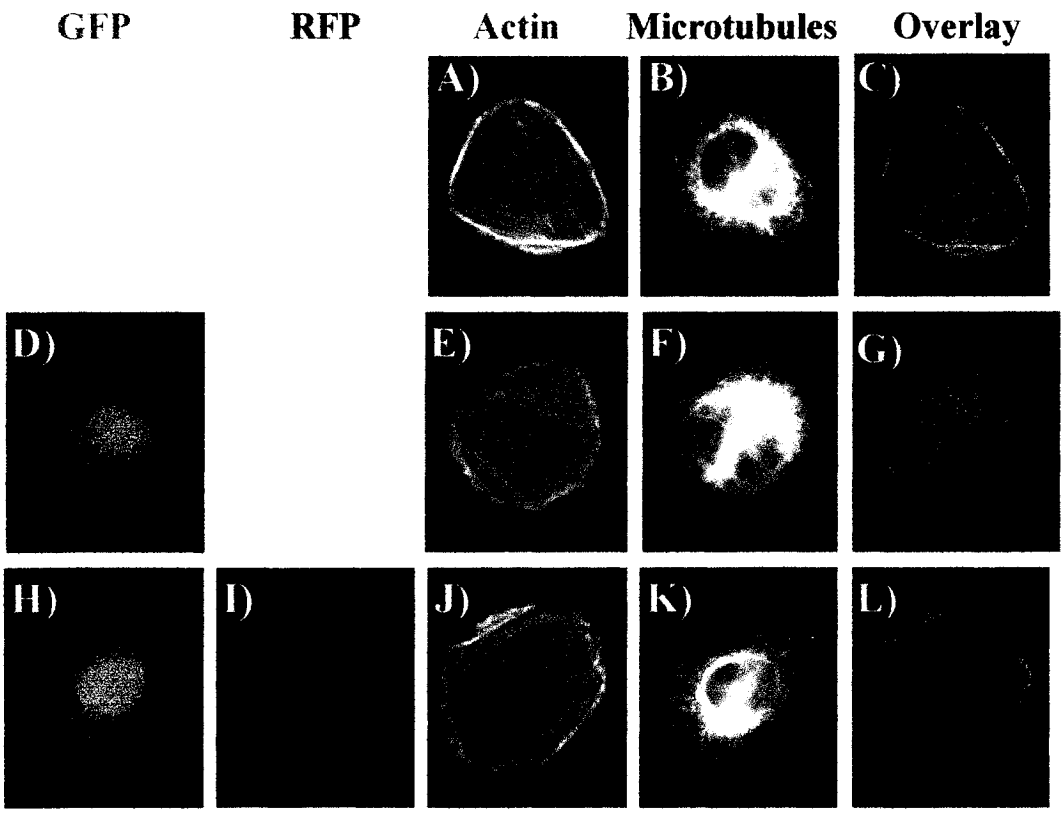

expressing adenoviruses (Figure 2.12 A, B, and C). The failure of the wt mDia1 in pAdTrack-CMV to recombine into a packagable adenovirus while the same construct put into pShuttle generated packaged and infective adenovirus suggested that the size of the full-length mDia1 insert (3.8 Kb) might exceed the accommodation capacity of the pAdTrack-CMV plasmid (Minamide *et al.,* 2003).

Two of the mDia1 mutant viruses, the constitutively active (CA) and the dominant negative (DN) ones, were selected for further characterization because these were the ones used for the additional studies reported elsewhere in this thesis. Thus, the activities of these mutants were tested in different assays and compared to what has been published in literature.

The overexpression of CAmDia1 in SAOS-2 cells induced cell elongation, (Figure 2.15 B and C) and (Figure 2.17 D-M), a phenotype that has been described previously (Watanabe *et al.,* 1999; Ishizaki *et al.,* 2001). Also, CAmDia1 expression in SAOS-2 cells induced parallel and thin bundles of actin filaments (Figure 2.17 E, G, and K), which were aligned with microtubules parallel to the long axis of cells (Figure 2.17 I and M). Both of these are characteristics for CAmDia1-expressing cells (Watanabe *et al.,* 1999, Ishizaki *et al.,* 2001; Palazzo *et al.,* 2001; Copeland *et al.,* 2004; Moseley *et al.,* 2004).

CAmDia1 expression slowed down the migration by >2X of both SAOS-2 and Swiss 3T3 cells in a wound healing assay (Figure 2.21 A and B). CAmDia1-mediated reduction of cell migration rate has been reported previously both in a wound healing assay using NIH 3T3 cells (Magdalena *et al.,* 2003) and in migrating human lymphocytes (Vicente-Manzanares *et al.,* 2003). CAmDia1 could inhibit directed motility through

inducing aberrant accumulation of actin filaments (Sagot *et al.,* 2002a, b; Li and Higgs, 2003; Copeland *et al.,* 2004; Moseley *et al.,* 2004; Watanabe and Higashida, 2004), which could enhance the level of F-actin at the expense of G-actin pool required for protrusion (Vicente-Manzanares *et al.,* 2003). Alternatively, or additionally, the CAmDia1 mutant could delocalize the stabilization of microtubule plus ends, competing with their localized capture at the leading edge (Palazzo *et al.,* 2001; 2004; Wen *et al.*, 2004), and/or inhibit Golgi apparatus polarization (Magdalena *et al.,* 2003). Polarized localization of the Golgi could be important for defining the direction of vesicular traffic (Chapin-Brion *et al.,* 2001). The overexpression of CAmDia1 also could increase the adhesiveness of the infected cells through the formation or enlargement of focal adhesions (Watanabe *et al.,* 1999; Tsuji *et al.,* 2002).

DNmDia1-infected SAOS-2 cells exhibited a rounded shape (Figure 2.16 B, C, and D), and had reduced stress fibers staining after 24 hours of infection (Figure 2.18 I), a phenotype that has been reported previously (Watanabe *et al.,* 1999). The overexpression of DNmDia1 had no effect on microtubules. Cell blebbing that was caused by the expression of CA- and DNmDia1 was reported only once in HeLa cells (Watanabe *et al.,* 1999). Overexpression of DNmDia1 in both SAOS-2 and Swiss 3T3 cells had no effect on cell migration rates or the time needed for wound closure (Figure 2.21 A and B).

The lack of effect of DNmDia1 on cell migration rates was previously observed in lymphocytes, which migrated normally when compared with the untransfected control cells (Vicente-Manzanares *et al.,* 2003). However, when NIH 3T3 cells were microinjected with DNmDia1, and then scratched in a wound-healing assay, only 30 ± 17% of the expressing cells migrated, while the rest of the DNmDia1-expressing cells

failed to migrate (Magdalena *et al.,* 2003). Control microinjected cells migrated normally. The discrepancies in these results are difficult to reconcile. Both human (SAOS-2) and mouse (Swiss 3T3) cells express multiple members of the seven groups of formin proteins (Higgs and Peterson, 2005), that could possibly compensate for the inhibition of mDia1, which explains why the overexpression of DNmDia1 did not affect the migration rates of lymphocytes, SAOS-2 cells and Swiss 3T3 cells.

DNmDia1 could exhibit its negative effects on the cytoskeleton by: 1) binding to endogenous mDia1-binding proteins such as DIP (Satoh and Tominaga, 2001) and VASP (Grosse *et al.,* 2003), sequestering them or, 2) the FH2 domain of the DNmDia1 mutant could dimerize with the endogenous mDia1-FH2 domain forming an abnormal heterodimer, and thus inhibit the formation of functional dimers of mDia1 required for its activity (Shimada *et al.,* 2004; Xu *et al.,* 2004).

Overexpression of CARho causes an increase in the number and thickness of stress fibers, and in some instances it results in the enhancement of cortical actin (Ridley and Hall, 1992; Raman and Atkinson, 1999). CARho-infected SAOS-2 cells exhibited the same phenotype (Figure 2.25 E). These effects on stress fibers downstream of Rho are mediated through both mDia1 and ROCK (Watanabe *et al.,* 1999; Tsuji *et al.,* 2002). mDia1, through its FH1-FH2 unit, is able to induce *de novo* actin nucleation and polymerization into straight actin filaments (Sagot *et al.,* 2002a, b; Pruyne *et al.,* 2002; Pollard, 2002). Actin filaments are then bundled into stress fibers, a process that is mediated by myosin-based contractility downstream of ROCK (Chrzanowska-Wodnicka and Burridge, 1996; Burridge and Chrzanowska-Wodnicka, 1996). ROCK can phosphorylate the regulatory subunit of myosin light chain (MLC), leading to myosin

activation, and MLC phosphatase, inhibiting its ability to down-regulate myosin, resulting in the enhancement of actomyosin-based contractility (Noda *et al.,* 1995; Kimura *et al.,* 1996; Kawano *et al.,* 1999; Takaishi *et al.,* 2000). Thus, ROCK and mDia1 cooperate in the formation of stress fibers (Leung *et al.,* 1996; Watanabe *et al.,* 1999; Riveline *et al.,* 2001; Tsuji *et al.*, 2002).

To distinguish between the two pathways (mDia1 and ROCK) downstream of Rho culminating in actin reorganization, one can block either the Rho-ROCK pathway with the application of the Y27632 drug, or the Rho-mDia1 pathway with DNmDia1. Alternatively, both of the Rho pathways can be blocked via expression of DNRho and then the mDia1 pathway can be rescued by expression of CAmDia1.

To investigate the effects of Rho-mDia1 pathway on cell morphology and cytoskeletal organization in the absence of ROCK activity, we infected SAOS-2 cells with CAmDia1-expressing adenovirus, and applied the ROCK inhibitor Y-27632 to the infected cells. Y-27632 is widely used as a specific inhibitor of the ROCK family of protein kinases (Kosako *et al.,* 2000; Khyrul *et al.,* 2004; Lepley *et al.,* 2005). It inhibits the ROCK family of kinases 100 times more potently than it affects other kinases, including protein kinase C, cAMP-dependent kinase and myosin light chain kinase. Y-27632 inhibits ROCK by competing with ATP for binding to the kinase (Ishizaki *et al.,* 2000). Prolonged exposure (7-15 hours) of SAOS-2 cells to 30 μM Y-27632 induced the formation of long processes (Figure 2.22 C and D). Theses processes contained microtubules (Figure 2.22 G), while actin filaments were almost absent (Figure 2.22 F). This phenotype has been reported earlier, and the processes were called neurite-like processes (Ishizaki *et al.,* 1997; Tsuji *et al.,* 2002; Arakawa *et al.,* 2003). When SAOS-2

cells were infected with CAmDia1 and then treated with Y-27632, long processes were formed within 30 min of the drug application (Figure 2.23 E-D). This result was the basis for investigating the role of mDia1 in axon elongation where it was found that CAmDia1 overexpression in cerebellar granule neurons enhanced axon length (Arakawa *et al.*, 2003). Because the same phenotype was achieved when the cells were infected with CARho and treated with Y-27632 (Figure 2.23 J-N), it is assumed that it is dependent on the activation of mDia1 downstream of Rho. Also, expressing DNmDia1 mutant inhibited the long-process phenotype caused by CARho expression and Y-27632 treatment in 78% of the co-infected SAOS-2 cells with DNmDia1 and CARho. ROCK and mDia1 antagonize during neuritogenesis; neurite outgrowth is enhanced by inhibition of the Rho/ROCK pathway (Bito *et al.*, 2000) or activation of the Rho/mDia1 pathway (Arakawa *et al.*, 2003). The long processes were formed in the absence of actin filaments because the application of Y-27632 resulted in dissolution of actin filament. This finding suggests that the formation of the long processes was a microtubule-mediated activity, and mDia1 was shown to affect orientation of microtubules in HeLa cells (Ishizaki *et al.*, 2001; Palazzo *et al.*, 2001), and to induce microtubule stability (Palazzo *et al.*, 2001; Wen *et al.*, 2004).

The phenotype induced by DNRho expression ranges from having no effect on F-actin structures (Raman and Atkinson, 1999), to complete absence of stress fibers (Massoumi *et al.*, 2002). In SAOS-2, DNRho-expressing cells exhibited reduced stress fiber staining (Figure 2.26 E), and in some cells, stress fibers were completely absent (data not shown). CAmDia1, through its ability to induce the formation of actin filaments

(Sagot *et al.,* 2002a, b; Pollard, 2002), enhanced the formation of actin filaments inhibited by DNRho (Figure 2.26 J).

On the other hand, when the activities of both mDia1 and ROCK were inhibited in SAOS-2 cells, by DNmDia1 overexpression and exposure to Y-27632, respectively, the cells exhibited a butterfly-like morphology (Figure 2.24 E-I). It is not clear why the cells develop such morphology, but cell shape changes involve many more proteins than the ones we are studying here. Cross talk between the Rho and other signaling pathways can have effects on other actin and microtubule dependent pathways that will take additional study to fully understand.

In conclusion, both of CA- and DNmDia1 mutants, when tested in different assays (effect on cell morphology and actin and microtubule cytoskeleton, in the presence or absence of ROCK activity, and wound-healing assay), induced the same phenotypes that have been published in literature. Consequently, they were used to investigate the role of mDia1 in the polarization and migration of chick embryo cardiac fibroblasts.

Chapter three

The role of mDia1 in directional migration and polarization of chick embryo cardiac fibroblasts

Summary

During directional migration, cells exhibit a polarized morphology with leading edge protrusion and retraction at the rear. Polarization involves spatial and temporal reorganization of actin and microtubules. mDia1, a member of the formin family of proteins, coordinates both actin and microtubule cytoskeletons through its FH1-FH2 unit. We hypothesized that both constitutively active (CA) and dominant negative (DN)-mDia1 will disrupt the polarization and thus the migration of chick embryo cardiac fibroblasts (CECFs) through their effects on actin and microtubules. Twenty-four hours prior to plating explants of chick cardiac fibroblasts (CECFs), explants in suspension were treated with recombinant adenovirus to express the protein of interest along with Green or Red fluorescent protein (GFP or RFP) from a separate promoter to identify infected cells. Whereas about 52% of uninfected and control adenovirus-infected cells exhibited polarized morphology (protrusion of a single lamellipodium), only 24.9% of CAmDia-expressing and 4.8% of DNmDia-expressing cells were polarized. The majority of the non-polarized, CAmDia1-infected CECFs exhibited a bipolar morphology (two distinct lamellipodia, one at each end of the cell). Almost 78% of CAmDia1-infected non-polarized CECFs were bipolar for the first 48 hours, and this percentage

dropped gradually for the following three days; 67%, 61% and 48%, respectively. Migration of the cells *in vitro* was followed by time-lapse microscopy. Directional migration in control uninfected CECFs was maintained for a minimum of 15 min and the average rate of migration was 1.14 μm/min. Polar and bipolar cells infected with CA-mDia1 retained the capacity to migrate, but they were slower than their counterparts with migration rates of 0.49 μm/min and 0.11 μm/min, respectively. On the other hand, most of the cells infected with DN-mDia1 failed to migrate out of the explants. Overexpression of CAmDia1 had no effect on G-actin/F-actin balance in CECFs, but it enhanced the formation of focal adhesions in these cells. Also, the overexpression of CAmDia1 in CECFs caused a 71% increase in the number of microtubule plus ends/unit area penetrating the lamellipodium, 65% of which were stabilized. Together, these data demonstrate that mDia1 controls CECF adhesion and microtubule dynamics, both of which are critical for their migration.

Introduction

Cell migration is a multi-step process that includes the extension of filopodia to explore the external environment, formation of a lamellipodium in the direction of migration, forward cell body translocation, and retraction of the rear end of the cell (reviewed in Raftopoulou and Hall, 2004) (Figure 3.1). Formation of filopodia and lamellipodia requires actin polymerization (Theriot and Mitchison, 1991; Ponti *et al.*, 2004; Meyer *et al.*, 2005; Schirenbeck *et al.*, 2005), whereas cell body translocation and tail retraction involve actomyosin-based contraction (Ridley and Hall, 1992; Nobes and Hall, 1995; 1999; reviewed in Mitchison and Cramer, 1996). These effects on the actin cytoskeleton are mediated via different regulatory pathways, the Rho family of GTPases,

Figure 3.1
Steps of cell migration. A migrating cell needs to perform a coordinated series of steps to move. Cdc42 regulates the direction of migration, Rac induces membrane protrusion at the front of the cell through stimulation of actin polymerization and integrin adhesion complexes, and Rho promotes actin:myosin contraction in the cell body and at the rear. Adapted from Raftopoulou and Hall, Dev. Biol. 265, 2004.

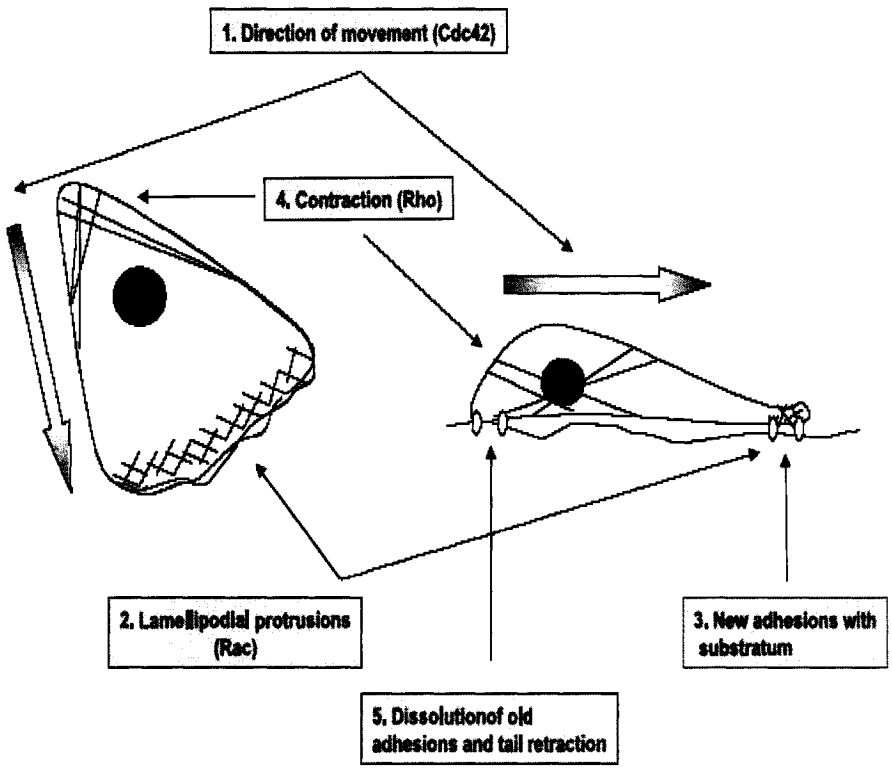

Rho, Rac and Cdc42, seems to play a dominant role in regulating the signal transduction pathways most relevant to cell migration (reviewed in Fukata *et al.,* 2003; Raftopoulou and Hall, 2004). Actin polymerization and branching at the leading edge are under the control of Cdc42 and Rac; Cdc42 is responsible for the formation of filopodia (Kozma *et al.*, 1995; Nobes and Hall, 1995) and controlling the direction of migration (Allen *et al.,* 1998; Etienne-Manneville and Hall, 2003), while Rac induces the formation of a protrusive lamellipodium (Ridley *et al.,* 1992; Nobes and Hall, 1995). On the other hand, the activities of Rho have been linked to actin filament contractility and the formation of focal adhesions (Ridley and Hall, 1992; Nobes and Hall, 1995; 1999; Watanabe *et al.,* 1999; Alblas *et al.,* 2001).

The Ser/Thr kinase PAK is activated upon either Rac or Cdc42 activation and phosphorylates and activates LIM kinase (LIMK), which in turn phosphorylates and inactivates ADF/cofilin (AC) (Arber *et al.,* 1998; Edwards *et al.,* 1999). However, enhanced activity of LIMK does not necessarily signal a decline in actin turnover or even a shift in the pool of phophorylated AC since coordinated regulation of the AC phosphatase slingshot might also occur under these conditions and the phosphocycling of the AC proteins might be coupled to enhanced actin dynamics (Chen *et al.,* 2000). AC proteins enhance the turnover of actin filaments at the leading edge by inducing filament depolymerization and severing (reviewed in Bamburg, 1999). Also, Cdc42 activates WASp and N-WASp (Rohatgi *et al.*, 2000) and Rac activates the Scar/WAVE family (Eden *et al.,* 2002), each of these effector proteins in turn can stimulate the Arp2/3 complex, which can initiate actin polymerization (Weaver et al., 2002) (Figure 3.2).

Figure 3.2
Rho-GTPase-regulated pathways affect actin filament organization. Rho promotes contractile actomyosin filament assembly through two effectors, mDia and p160ROCK. mDia induces the formation of straight actin filaments, and p160ROCK phosphorylates LIM kinase, leading to cofilin phosphorylation, and it also phosphorylates myosin light chain (MLC) and MLC phosphatase, leading to an increase in MLC phosphorylation. Rac and Cdc42 both regulate actin polymerization through the WASp/Scar/WAVE family of proteins acting on the Arp2/3 complex, and through p65PAKkinase acting on LIM kinase. Adapted from Raftopoulou and Hall, Dev. Biol. 265, 2004.

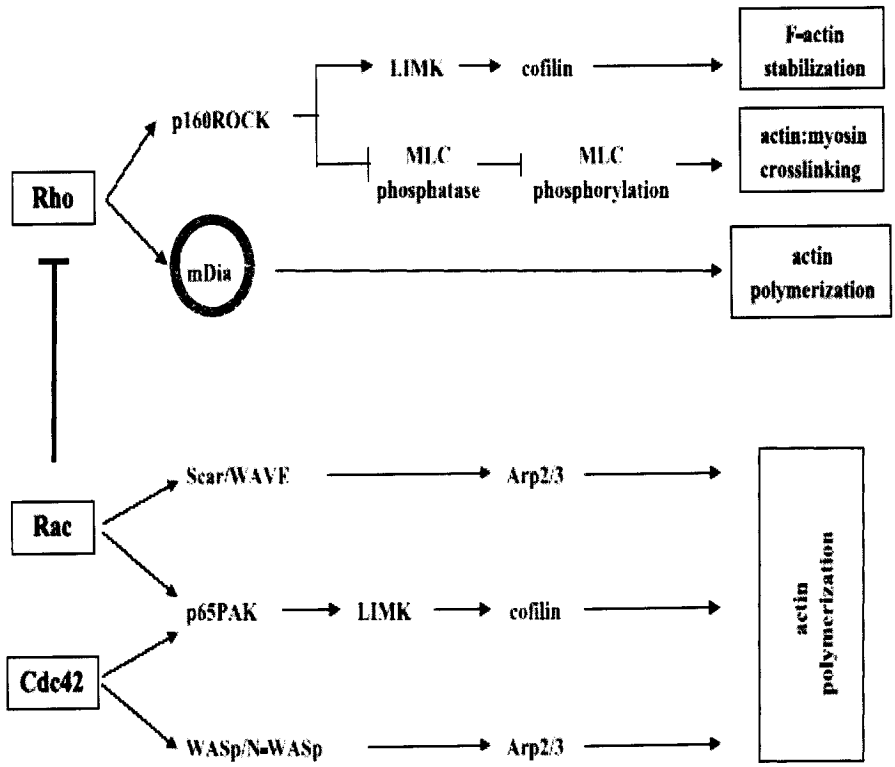

ROCK and mDia1, two downstream effectors of Rho, are mainly responsible for cell body and tail behavior during migration (Watanabe *et al.,* 1997; 1999; Ishizaki *et al.,* 2001). One important step during cell migration is the adhesion of the cell to the extracellular matrix; upon cell adhesion to the substratum, integrins are activated to bind to their ligand (Yamada *et al.,* 1997; Critchley, 2000). Once integrin binds its ligand, it forms a multi-protein complex with different cytoskeletal proteins and this focal complex is linked to actin filaments (Calderwood *et al.,* 2000). These focal complexes then aggregate to form focal adhesions and actin filaments are bundled into stress fibers (reviewed in Narumiya *et al.,* 1997). The latter process is mediated by myosin-based contractility (Chrzanowska-Wodnicka and Burridge, 1996; Burridge and Chrzanowska-Wodnicka, 1996). Beside the ability of ROCK to phosphorylate and activate LimK (Maekawa *et al.,* 1999; Sumi *et al.,* 2001), it can also enhance actomyosin contractility by phosphorylating and activating the regulatory subunit of myosin light chain (MLC), while at the same time inhibiting the activity of myosin light chain phosphatase (Noda *et al.,* 1995; Kimura *et al.,* 1996; Kawano *et al.,* 1999; Takaishi *et al.,* 2000). mDia1, through its FH1-FH2 unit is able to induce *de novo* actin nucleation and polymerization into straight actin filaments (Sagot *et al.,* 2002a; Pollard, 2002). Thus, ROCK and mDia1 cooperate in the formation of stress fibers and focal adhesions (Figure 3.3) (Leung *et al.,* 1996; Watanabe *et al.,* 1999; Riveline *et al.,* 2001; Tsuji *et al.*, 2002). The organization of actin filaments within bundles in motile cells can be classified into four different structural groups based on actin filament orientation that is determined from myosin S1 or heavy meromyosin decoration (Huxley, 1963). These groups are: uniform, alternating, graded, or mixed actin filaments (Reviewed in Cramer, 1999). In uniform actin filaments,

Figure 3.3
The Rho-mediated signal transduction pathway leading to focal adhesion and stress fibers formation. ROCK activated by Rho-GTP acts on integrins to cause their binding to the extracellular matrix and initiate cell spreading. mDia1 is then targeted to the cell periphery through its Rho binding and induces actin filament polymerization. Ligand-bound integrin forms a complex with other cytoskeletal proteins. This protein complex then binds the actin filaments. ROCK-activated actomyosin contractility causes integrin complexes to aggregate into focal adhesions that are linked by stress fibers. Adapted from Narumiya *et al.,* FEBS letters 410, 1997.

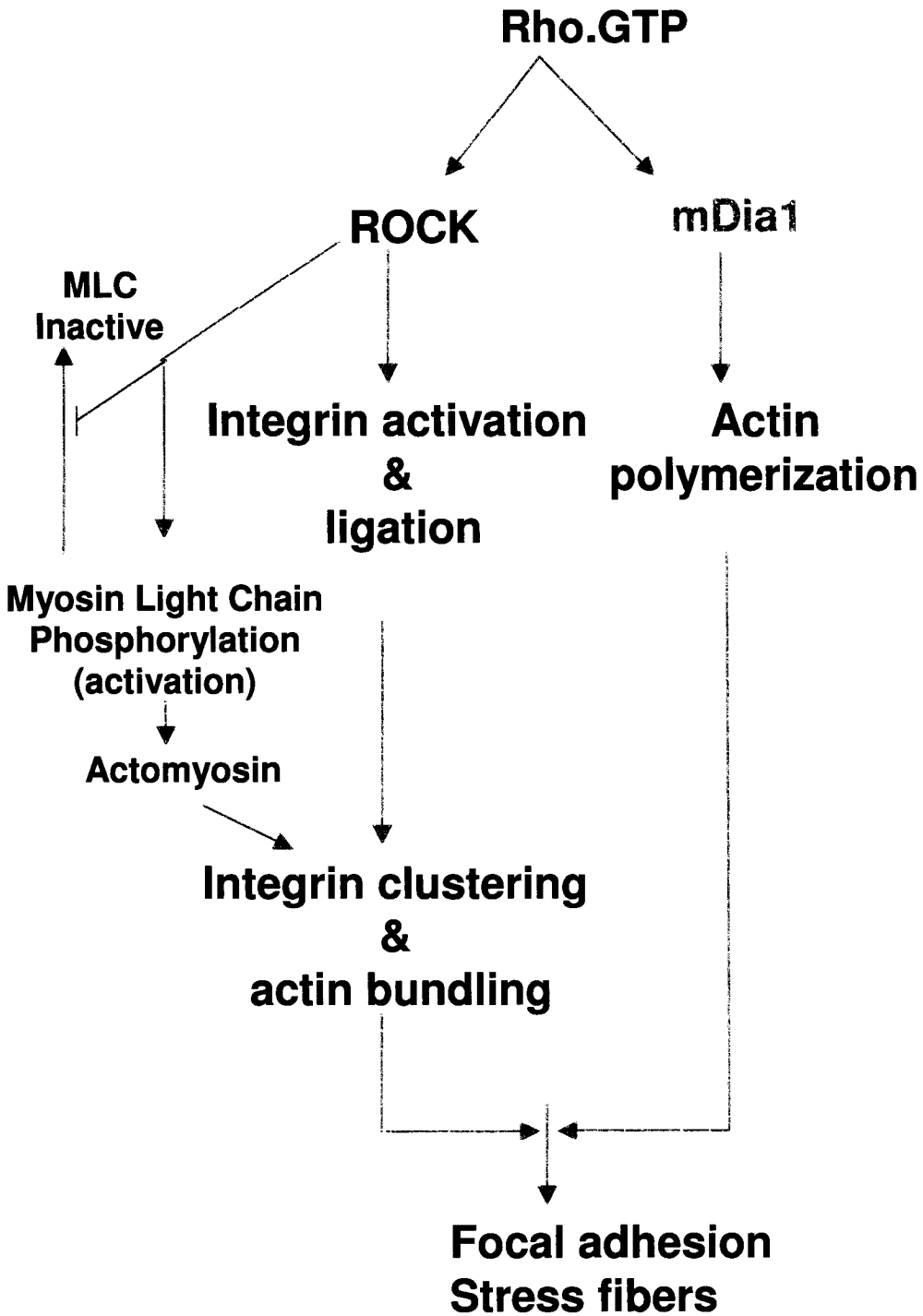

the barbed ends face away from the nucleus; these types of bundles occur in microvilli, stereocilia, filopodia, and within actin bundles (ribs) within lamellipodia (Cramer *et al.,* 1997, Svitkina *et al.,* 1997) (Figure 3.4 A). In migrating fish keratocytes, the majority of actin filaments are uniform (Svitkina *et al.,* 1997). Filament polarity in alternating-polarity actin bundles alternates over short lengths, almost every 1 μM (Figure 3.4 B). This organization occurs in stress fibers and cortical actin bundles in CECF cells (Cramer *et al.,* 1997). Graded-polarity actin bundles are the major form of actin bundles in migrating CECFs. In this type of organization, filament polarity changes gradually over the length of the bundle, and the filament polarity at any given point is dependent on the position of that point in the cell; the closer to the lamellipodium, the more filament barbed ends face forward (Figure 3.4 C) (Cramer *et al,* 1997). Finally, in mixed polarity actin bundles that occur at the lamella, roughly 50% of the barbed ends and 50% of the pointed ends face the same direction (Figure 3.4 D) (reviewed in Cramer, 1999). The work presented in this thesis did not include any ultrastructural analysis of filament bundles, and so the actin filaments in CECFs will just be referred to as actin bundles or cables.

It is generally accepted that the driving force for cell movement is provided by the dynamic reorganization of the actin cytoskeleton and myosin contraction. However, persistent migration in some cell types requires an intact microtubule (MT) network (Eddy *et al.*, 2002; Omelchenko *et al.,* 2002). All three major Rho GTPases may play a role in stabilizing the MT network (Wittmann and Waterman-Storer, 2001). Rac may enhance microtubule elongation via the PAK/stathmin pathway; PAK1 phosphorylates stathmin specifically at serine 16 and inactivates its microtubule destabilizing activity

Figure 3.4
Structural organization of actin filaments within bundles in motile cells. A) Uniform actin bundle, B) alternating-polarity actin bundle, C) graded-polarity actin bundle, and D) mixed polarity actin bundle. Adapted from Cramer, Biochem. Soc. Symp. 65, 1999.

A)

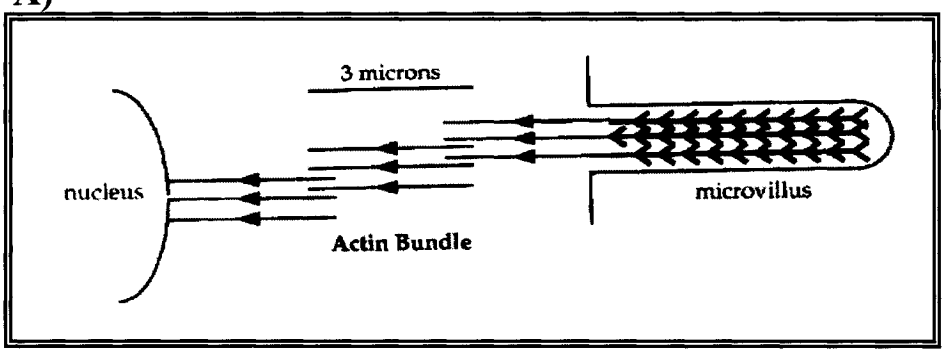

B)

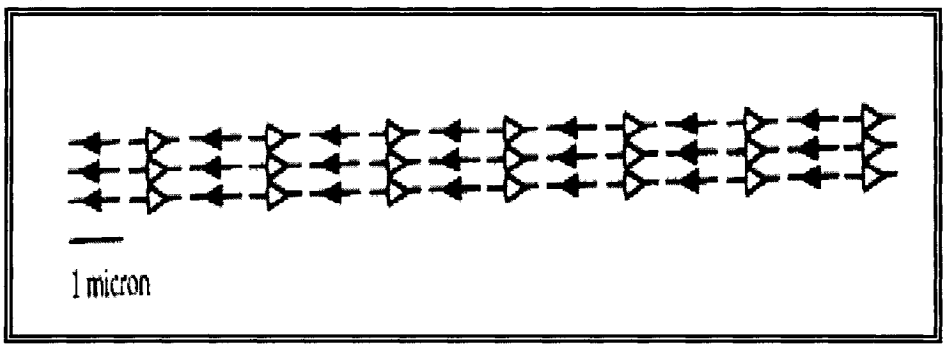

C)

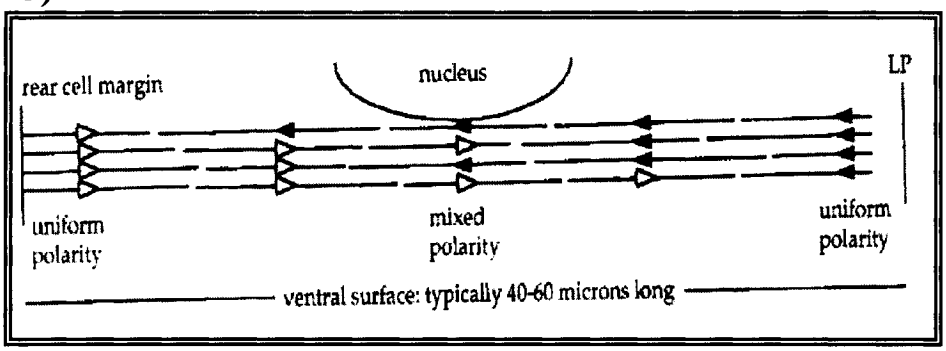

D)

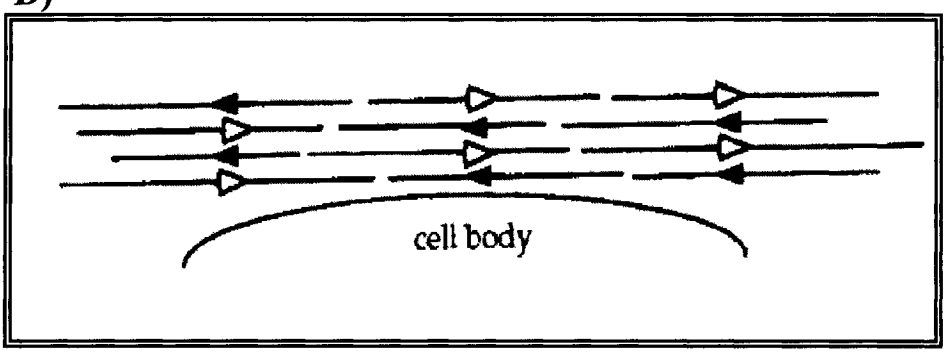

(Banerjee *et al.,* 2002; Wittmann *et al.,* 2004). Downstream of Rho, mDia1 binds EB1/APC plus-end tracking proteins and this tripartite complex then captures and stabilizes microtubule plus-ends penetrating the leading edge of migrating cells (Wen *et al.,* 2004). GSK-3β phosphorylates APC, inhibiting its activity (Rubinfeld *et al.,* 1996). Cdc42 binds PAR-6, which forms a complex with PAR-3 and PKC-3. Together this complex induces Cdc42-mediated PKC-3 activation (reviewed in Doe, 2001; Wodarz, 2002). Activated PKC-3 in turn phosphorylates GSK-3β, which inhibits its phosphorylation of APC, allowing APC to remain active and participate in MT plus-end stabilizing complexes (Zumbrunn *et al.,* 2001) (Figure 3.5).

Chick embryo cardiac fibroblasts (CECF) provide a well-established cell system in which to study cell polarization and migration. They display spontaneous polarization responding to an unknown endogenous signal. Also, chick cells have only one mDia1 homologue (Gg2) (Higgs and Peterson, 2005), and so by manipulating the expression of mDia1 in CECFs, it is easier to elucidate the role of formins during cell polarization. This chapter investigates the role of mDia1 or its homologue (Gg2) during the polarization and migration of CECF.

Material and methods

Preparation of CECF explants

CECF explants were prepared and plated according to the diagram shown in Figure 3.6 and as described below. Briefly, a day 7 to 8 (E7-E8) chick embryos were removed from the egg, opened, and the heart removed and de-membranated (Figure 3.6 A-C). The heart wall was then cut into small pieces (explants) (Figure 3.6 D), which were suspended in cloning rings (Bellco) filled with CECF medium (low glucose DMEM

Figure 3.5
Rho GTPases regulate microtubules. Rho activation leads to microtubule stabilization through mDia/EB1/APC complex. Rac activates PAK to phosphorylate and inactivate stathmin, a microtubule-destabilizing protein. Cdc42 regulates microtubule and centrosome polarity through activation of the Par6/PKC complex, which in turn leads to the inhibition of GSK-3β and the association of APC with the plus end of microtubules. Adapted from Raftopoulou and Hall, Dev. Biol. 265, 2004.

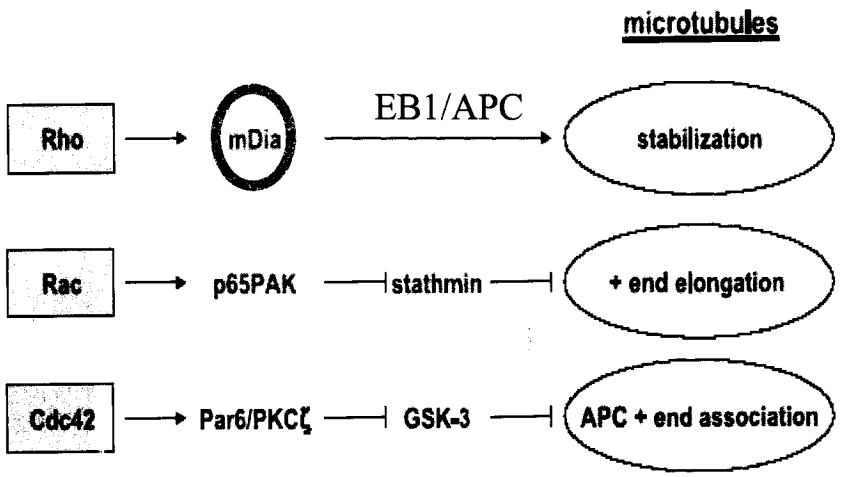

Figure 3.6
Preparation of chick embryo cardiac explants. Day 7 to 8 (E7-E8) chick embryos were removed from the egg and the heart removed and de-membranated (A-C). The heart wall was then cut into small pieces (explants, D), which were infected with adenovirus expressing the gene of interest in cloning rings for 24 h (E). The CECF explants were then plated on matrigel-coated cover slips for another 24 h (F).

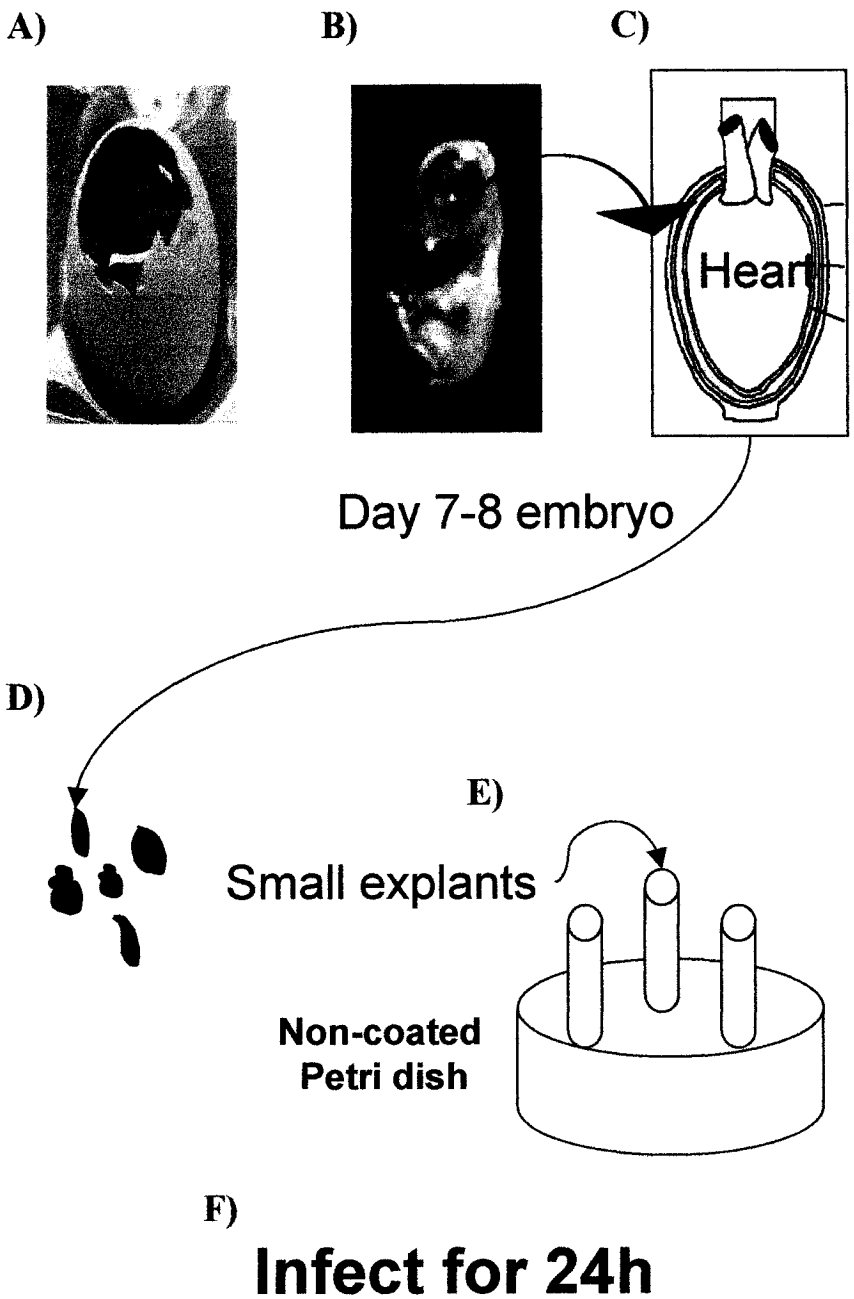

(Gibco) + 10% fetal bovine serum (FBS; Atlas, Fort Collins, CO) + 10% chick serum (Invitrogen), and placed on a Petri dish (not tissue culture coated) (Figure 3.6 E). An appropriate volume of adenovirus (determined empirically, but approximately 1.5–2X10^6 viral focus-forming units (ffu) per heart explant for single infection experiments and approximately half of that amount for each of the two viruses used for double infection experiments) was added to the cloning ring medium and the explants were incubated in suspension for 24 h at 37°C in a 5% CO_2/air incubator (Figure 3.6 F). One heart yielded enough tissue explants for 3-4 cloning rings. The CECF explants were then plated on matrigel (Becton Dickinson)-coated cover slips (glass bottom dishes) for another 24 h (Figure 3.7 A and B, arrow). Coating of the cover slips on the bottom of 35 mm drilled out dishes with matrigel was performed by first UV sterilizing the dish. Each dish was washed once with 70% ethanol, dried in the tissue culture hood, and 50-100 μl sterile 1X matrigel in PBS was added over the coverslips. After incubating at 37°C for 30-60 min, the coated cover slips were then washed 3X with PBS and once with CECF medium. Explants were then plated and allowed to attach. Fibroblasts beyond the boundary of the explant and not in contact with other cells (Figure 3.7 C, arrows) were analyzed for cell morphology (polarity, bipolarity, etc), and/or the appearance of the F-actin cytoskeleton following fixation and staining with fluorescent phalloidin (see below), or they were studied by time-lapse microscopy.

Time-lapse microscopy

CECF medium was replaced with 1:1 mix of F12 and DMEM media, and overlayered with dimethyl polysiloxane (Sigma) to prevent or reduce evaporation while allowing gas exchange. Live cell migration in culture was followed using a 12-bit cooled

Figure 3.7

Chick embryo cardiac explants. Phase contrast image of explant 24 h after plating on matrigel-coated slide (A). Fluorescence image of same explant stained with FITC-phalloidin (B). Images of cells that have migrated out of explant with arrows showing individual CECFs that are used to score polarity (C).

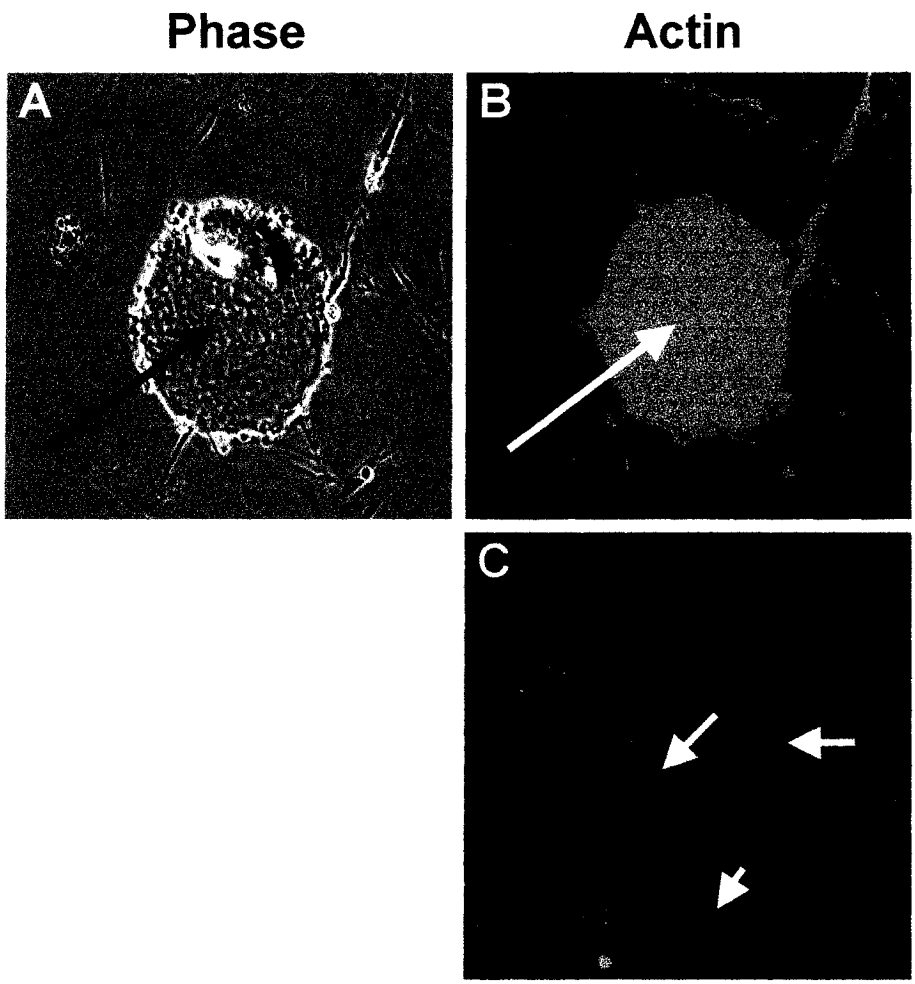

CCD camera (Photometrcis Coolsnap ES) on an inverted Nikon microscope using 20X, 1.0 NA air or 60X, 1.4 NA oil objectives. The microscope was equipped with a plexiglass incubation chamber for maintaining the cells at ~35°C. Image capture from the camera was controlled by Metamorph software (Universal imaging). Actin dynamics in live cells were also viewed on a Nikon (TE 2000-U) inverted microscope equipped with an UltraView spinning disk confocal microscope (PerkinElmer) and an Orca II-ER cooled CCD camera (Hamamatsu) controlled by Metamorph (Universal Imaging). Temperature was maintained by a Heatwave-30 temperature-controlled chamber (World Precision Instruments) and an Intracell objective heater (Bioptechs). Imaging was performed with a 60X, 1.4 NA plan-apo Nikon objective.

Immunocytochemistry

CECFs were fixed in 4% formaldehyde in cytoskeleton buffer (CB: 10mM MES pH 6.1, 138 mM KCl, 3 mM MgCl and 2 mM EGTA pH 7.0) plus 0.32 M sucrose (CBS) for 20-30 min. After fixation, the cells were permeabilized with 0.5% TritonX-100 in PBS for 5-10 min, and blocked with 2% goat serum in TBS for 45 min-1 h. CECFs were then incubated with primary antibodies for 1 h at room temperature or overnight at 4°C. The primary antibodies used were mouse anti-β-tubulin at 1:100 (Sigma-Aldrich), mouse anti-paxillin at (1:250) (Becton Dickinson), mouse anti-G-actin (N350) at 1:200 (Amersham), and rabbit anti-Glu-tubulin antibody at 1:200 (Chemicon) (all diluted into 1% BSA + TBS). After 3-5 washes with TBS, the cells were incubated with fluorescence-conjugated goat anti-mouse/rabbit secondary antibodies (1:400 into 1% BSA + TBS) (Molecular Probes). For actin staining, Alexa-350-, Texas Red (TR)-, or Alexa-647-conjugated phalloidin was used (1:50 into 1% BSA + TBS) (Molecular Probes). Images

were acquired with a 12-bit cooled CCD camera (Photometrcis Coolsnap ES) and a 60X, 1.4 NA oil objective on an inverted Nikon microscope controlled by Metamorph software (Universal imaging).

Results

Efficiency of infection of CECF

CECF explants in cloning rings were infected for 24 h with adenoviruses encoding the protein of interest. In double infection experiments, one of the viruses expressed GFP, either as a fusion protein or from a separate CMV promoter, while the other virus expressed RFP. The explants were then plated for 24 h, fixed, and scored for percentage of infection. Table 3.1 summarizes the results, which demonstrate that the second virus infects cells approximately to the percentage expected if the process is cell autonomous (i.e. infection with the first virus neither enhances nor inhibits infection with the second virus).

Overexpression of CA- and DN-mDia1 induces loss of polarization of CECF

CECF explants were infected with either DN- or CAmDia1 adenoviruses for 24 h and plated for another 24 h on matrigel-coated cover slips before fixing. Migrating cells were stained with a fluorescent phalloidin and scored for percentage of polarized cells. More than half of the control uninfected cells (53.6%) had a polarized morphology with a single lamellipodium at the front of the cell identified as the heavily phalloidin-stained region (Figure 3.8 A and B, arrow). Actin cables were oriented along the long axis of the cell. Polarized cells were either kite (Figure 3.8 A) or crescent-shaped (Figure 3.8 B). The remaining cells were "non-polarized," either bipolar with two opposing leading edges (Figure 3.8 C) or two leading edges and a tail (Figure 3.8 D), or they had multiple

Table 3.1
Efficiency of adenoviral-mediated gene expression in CECFs following single and double infections.
(n ≥100 cells in each experiment, 3 separate experiments, the numbers are percentages of expressing cells ± S.E.M.)

Construct	Single infection	Double infection
RFP	83.6% ± 3.4%	70.1% ± 4.5%
GFP	98.3% ± 4.8%	87.5% ± 3.6
XAC-E3.GFP	74.5% ± 5.1%	63.6% ± 3.1
RFP + GFP		62.1% ± 5.8%
RFP + XAC-E3.GFP		61.5% ± 4.7%

Figure 3.8
Morphologies and actin filament organization in CECFs.
Cells that have migrated out of explants were fixed and stained with FITC- phalloidin. Polarized CECFs are either kite-shaped (A) or crescent (B). Non-polarized cells are either bipolar (C) and (D), or multipolar (E).

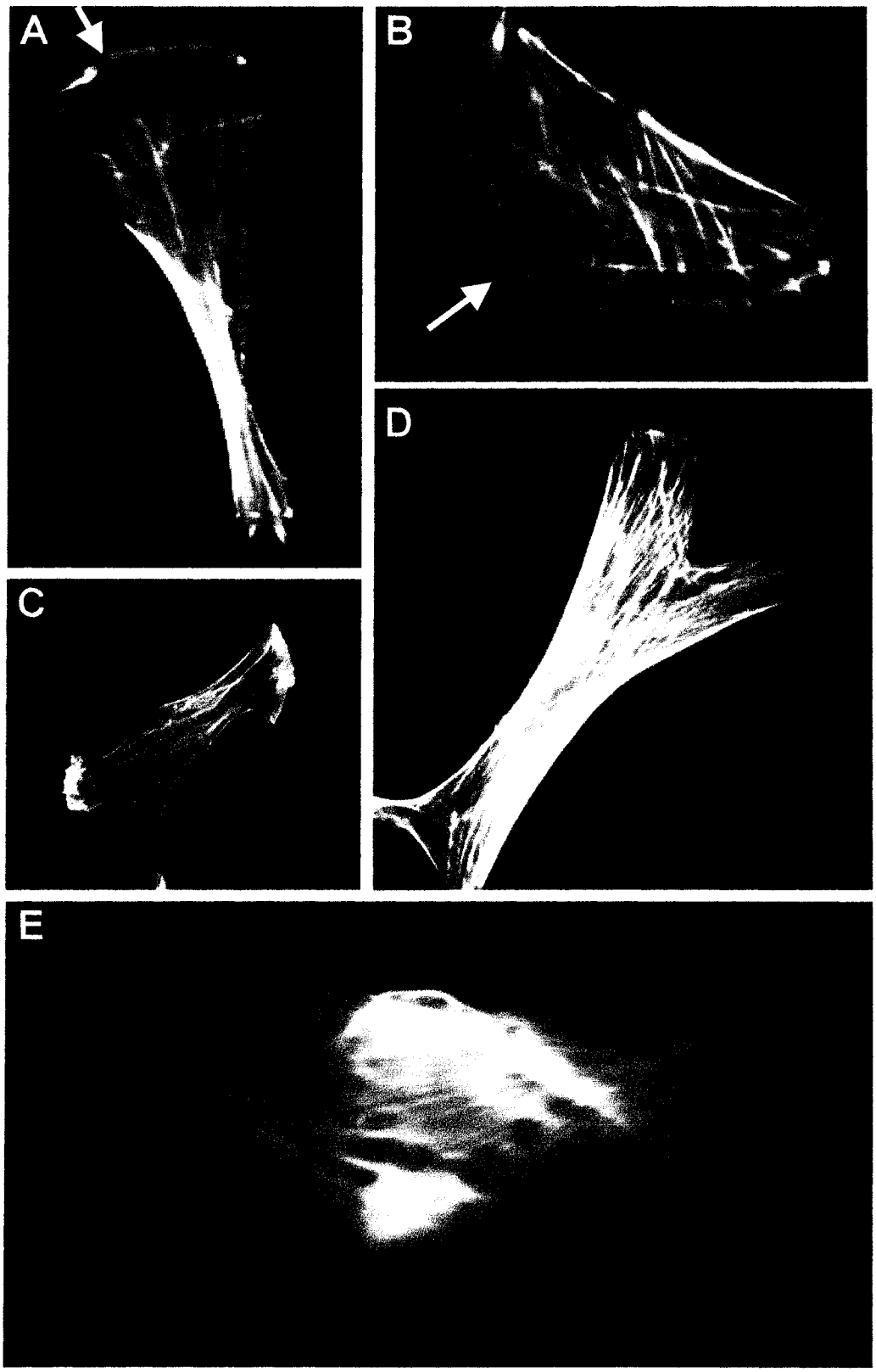

lamellipodia (Figure 3.8 E) protruding randomly from the cell surface. The percent of polarized cells in cultures infected with adenoviruses expressing only GFP or RFP were 51.3% and 53.2%, respectively (Figure 3.9), demonstrating that viral infection alone had no significant effect on cell polarity.

Most DNmDia1-expressing fibroblasts did not migrate out of the explants, and the few that did were almost all non-polarized; only 4.8% of the migrating cells exhibited polarized morphology (Figure 3.9). On the other hand, CAmDia1-expressing CECFs migrated out of the explants, and 24.9% of them were polarized compared to about 52% in various uninfected and control infected cells (Figure 3.9).

The majority of the non-polarized CAmDia1-expressing CECFs exhibited bipolar cell morphology (two lamellipodia) rather than multipolar morphology (more than two lamellipodia). Almost 78% of CAmDia1-expressing non-polarized CECFs were bipolar for the first 48 hours, this percentage dropped gradually for the following three days; 67%, 61% and 48%, respectively (Figure 3.10). More than half (57%) of the control non-polarized CECFs were bipolar 24 h after plating the explants, the percentage increased to 64% in the next day, then it dropped significantly in the following three days (33%, 16%, and 11%, respectively). By the end of the fifth day, the majority (89%) of the non-polarized control CECFs were multipolar (Figure 3.10).

Morphology and cytoskeleton of CAmDia1-infected CECFs

Kite-like migrating CECFs had four cell regions: a leading edge (lamellipodial projection in the direction of migration of the cell) or lamellipodium at the front of the cell identified by heavy fluorescent phalloidin staining, a lamella posterior to the lamellipodium which stained faintly with fluorescent phalloidin, a nuclear and

Figure 3.9
Overexpression of CA- and DNmDia1 induces loss of polarity in CECFs. Quantification of the percentages of polarized cells migrating out of explants that were uninfected, infected with adenoviruses expressing GFP or mRFP alone, or infected with adenoviruses expressing CA- or DN mDia. Error bars are standard error of the mean (S.E.M.).

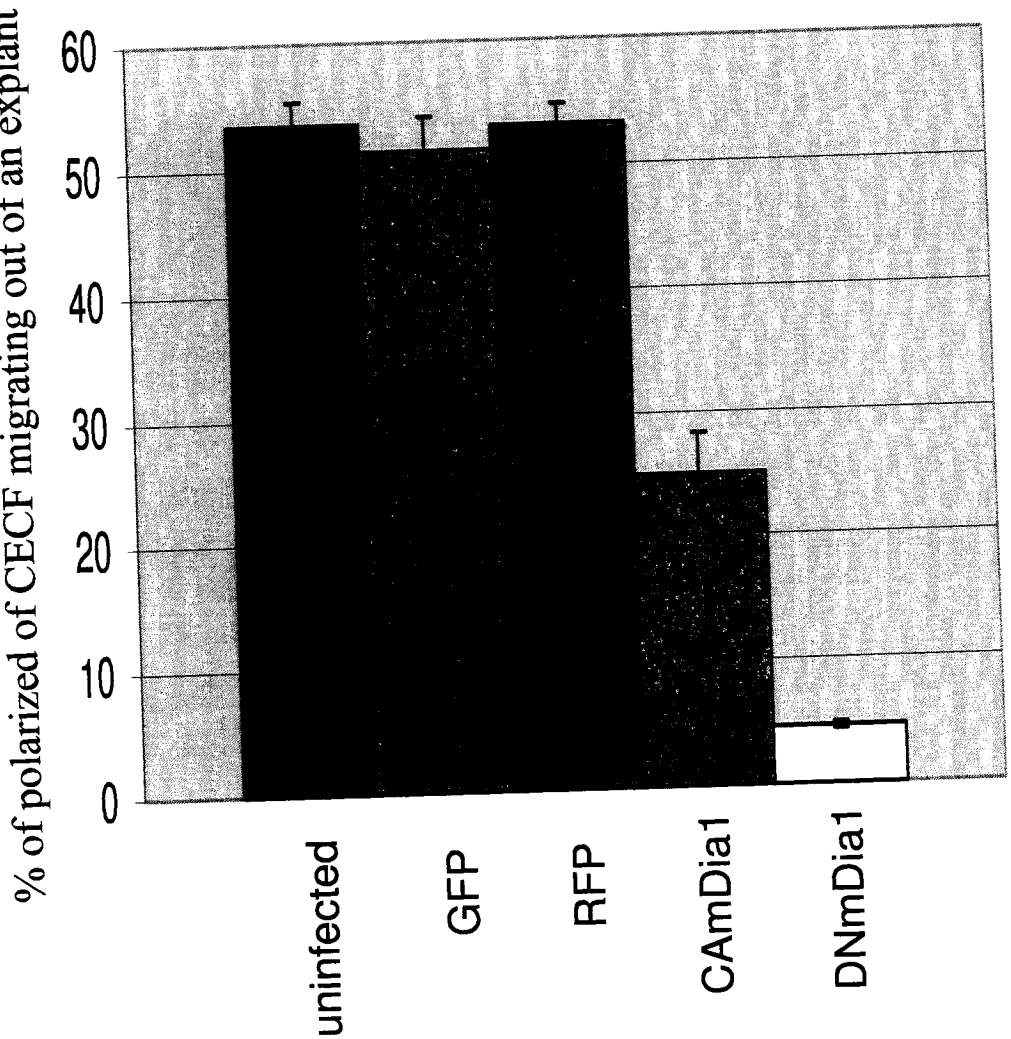

Figure 3.10
The majority of the non-polarized CAmDia1-expressing CECFs exhibited bipolar cell morphology. Chick cardiac explants were infected with CAmDia1 adenovirus for 24 h and then allowed to migrate for 1, 2, 3, 4, and 5 days. The cells were fixed after each time point, stained for actin filaments, and scored for the percentage of CECFs with bipolar and multipolar morphology. Error bars are S.E.M.

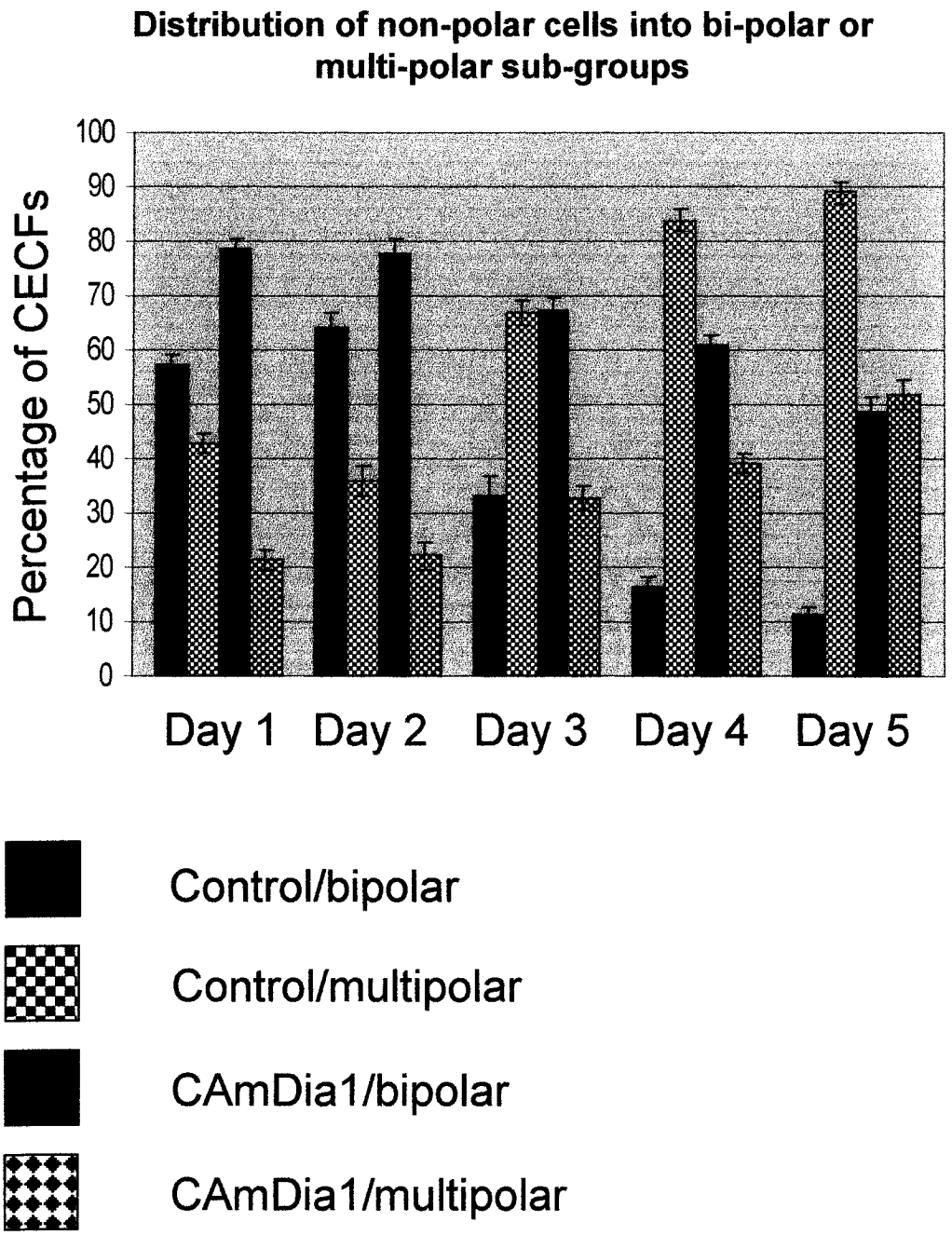

perinuclear region that occupied more than half the cell size through which actin filaments ran parallel to the long axis of the cell, and a tail at the rear of the cell (Figure 3.11) (Cramer *et al.,* 1997; 1999). Crescent CECFs had the same first three regions (lamellipodium, lamella, nuclear region) but lacked a tail (Figure 3.12 A-F). In uninfected CECFs, few of the microtubules plus ends penetrated into the lamellipodium (Figure 3.12 F and I, open arrows), while other microtubules were seen in the lamella running parallel to the lamellipodium (Figure 3.12 E, F, H, and I, arrows).

Overexpression of CAmDia1 in CECFs induced cell elongation and the formation of thin actin cables (compare Figure 3.13 B, F to Figure 3.12 A) along the long axis of the cell. The cell regions were not easily identified in CAmDia1- expressing CECFs, even in the polarized infected cells (Figure 3.13 A-D). The lamellipodium of polar CAmDia1-expressing CECFs was not well defined. It occupied 1-1.5 μm of cell size as compared to 3-5 μm in control cells (compare Figure 3.13 B to Figure 3.12 A); however, more microtubule plus ends were seen to reach the cell periphery in CAmDia1-expressing CECFs (compare Figure 3.13 D to Figure 3.12 F). Actin cables and microtubules seemed to run parallel in bipolar CECFs expressing CAmDia1 (Figure 3.13 F-H). Overexpression of CAmDia1 in HeLa cells was reported to induce alignment of actin and microtubules (Ishizaki *et al.,* 2001). To assess if the same phenotype occurs in CECFs, high magnification images (100X) were captured for bipolar uninfected and CAmDia1-expressing CECFs. The alignment of actin and microtubule in CAmDia1-expressing cells was not conclusive; the microtubules in some cells ran parallel to actin cables (Figure 3.14 H-J, white boxes), while in other CmDia1-expressing cells, the microtubules were folded (Figure 3.14 M and N, arrows). Both of these organizations

Figure 3.11
The cell regions of a kite-like CECF. A kite shaped CECF migrating out of an explant was fixed and stained for F-actin with Texas Red phalloidin.

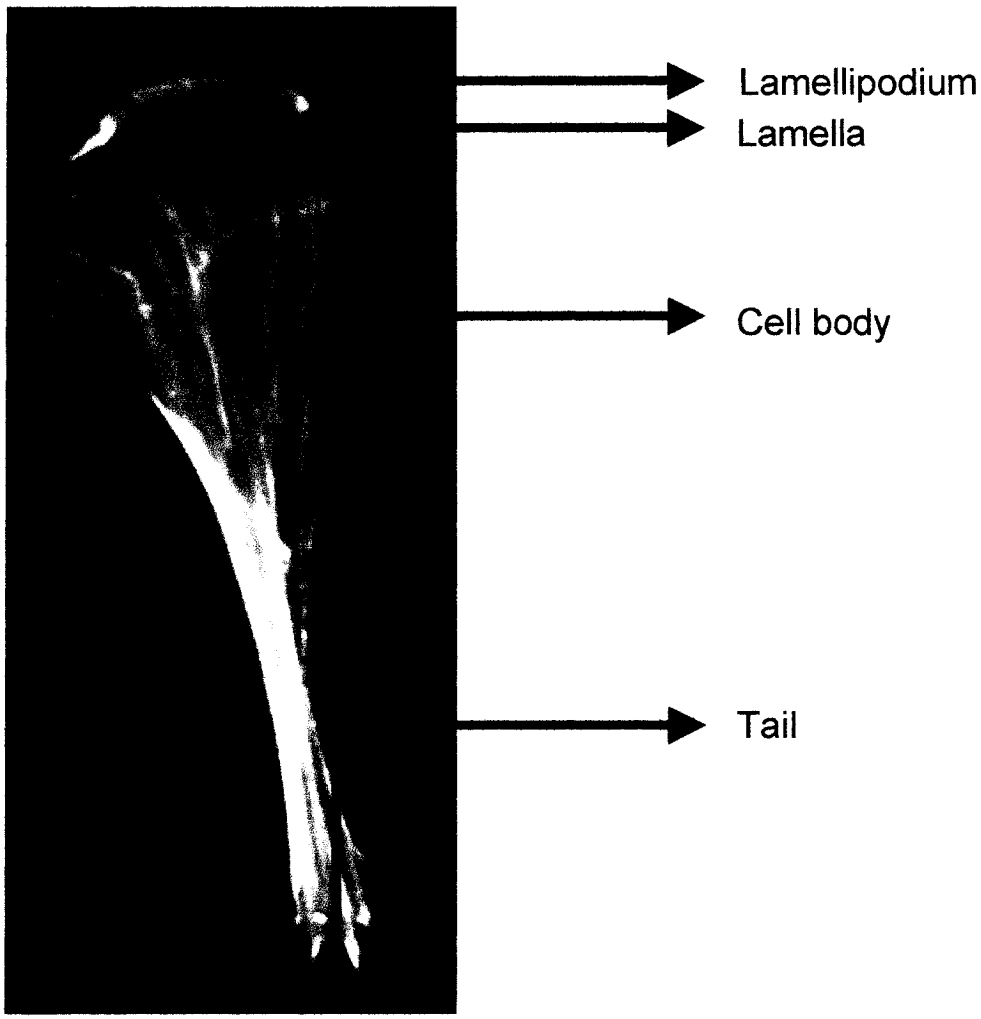

Figure 3.12
Morphology and cytoskeleton of control uninfected CECFs. Cells migrating out of an explant were fixed and immunostained for microtubules or stained with fluorescent phalloidin for F-actin. A-C) Crescent-like CECF, D-F) high magnification of a crescent-like CECF, G-I) bipolar CECF. Dashed arrows in panel F and I show microtubules penetrating the lamellipodium, and arrows in panel E, F, H, and I show microtubules running parallel to the lamellipodium.

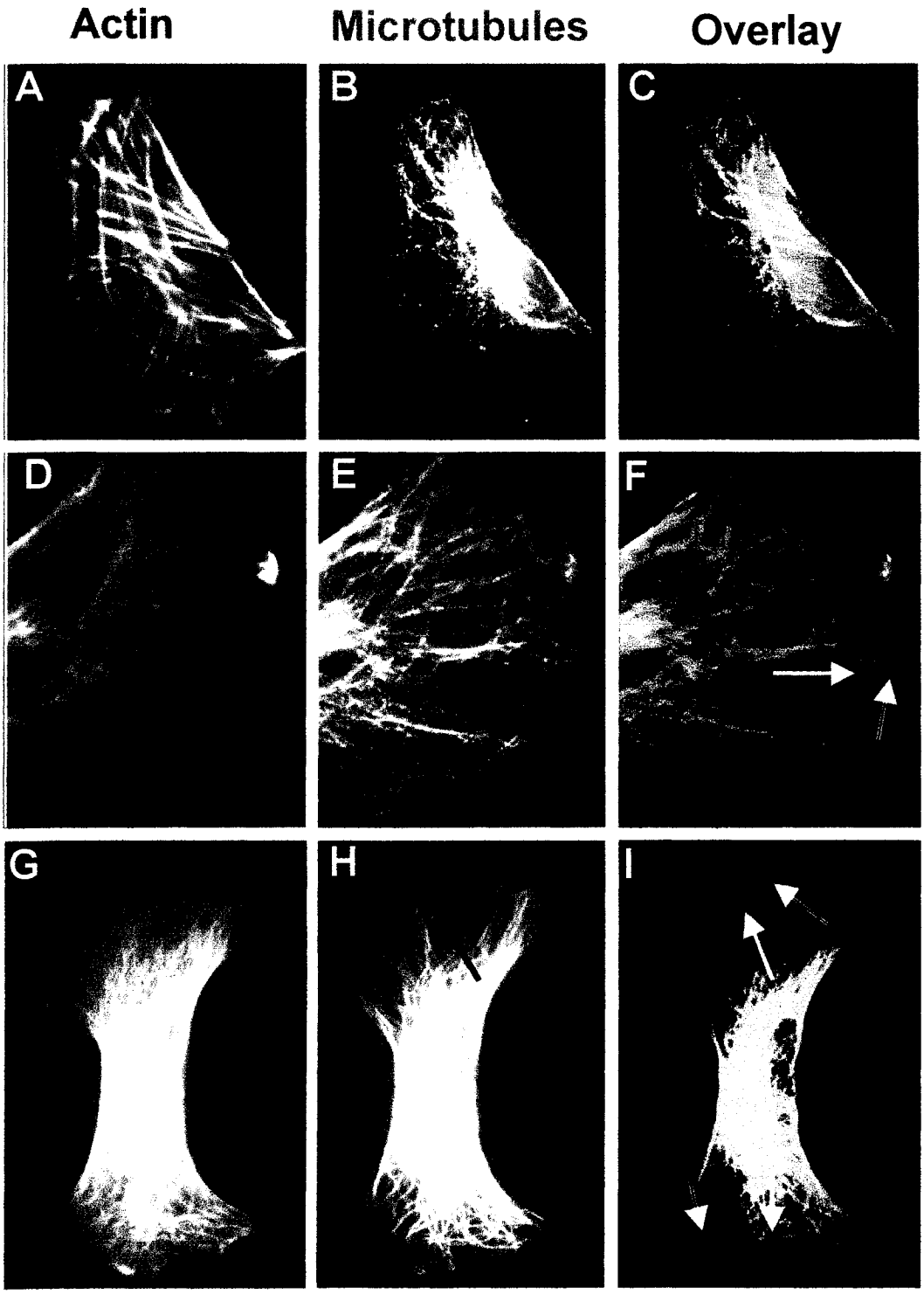

Figure 3.13
Morphology and cytoskeleton of CAmDia1-expressing CECFs.
Infected cells express GFP. Fixed cells were stained for F-actin with fluorescent phalloidin and immunostained for microtubules. A-D) Polar CECF, E-H) Bipolar CECF, I-L) CECF with a second and a third lamellipodia (arrows) generated to the sides of the original lamellipodium (dashed arrow).

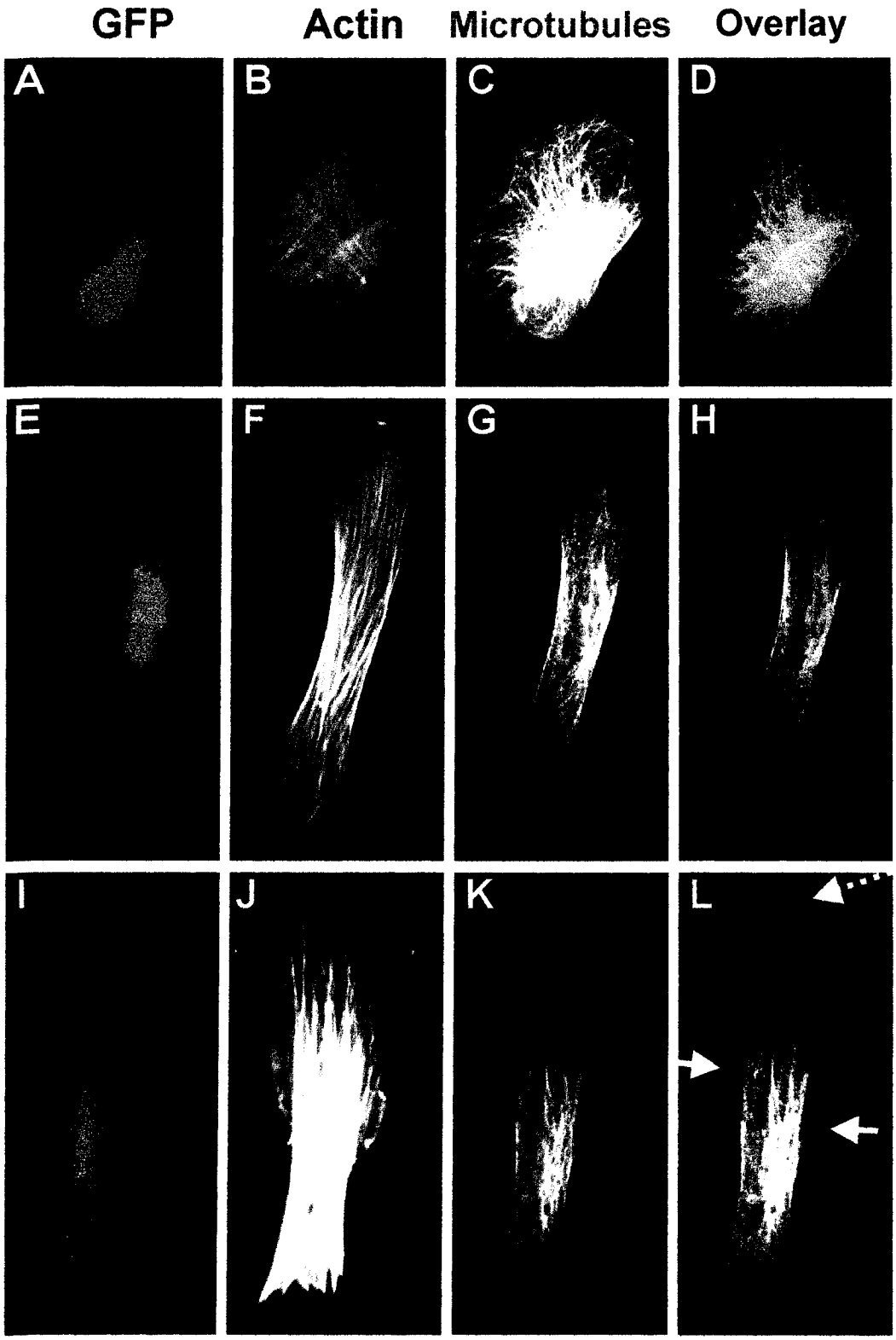

Figure 3.14
Actin filaments and microtubules alignment in CAmDia1-infected CECFs. A-F) control uninfected CECFs, G-N) CAmDia1-expressing CECFs. Cells were stained with TR-phalloidin (A, D, H, and L), and mouse anti-tubulin 1° Ab, and Alexa-647 goat anti-mouse 2° Ab (B, E, I, and M). The white boxes in H-J show parallel actin and microtubules, and the arrows in M and N show folded microtubules.

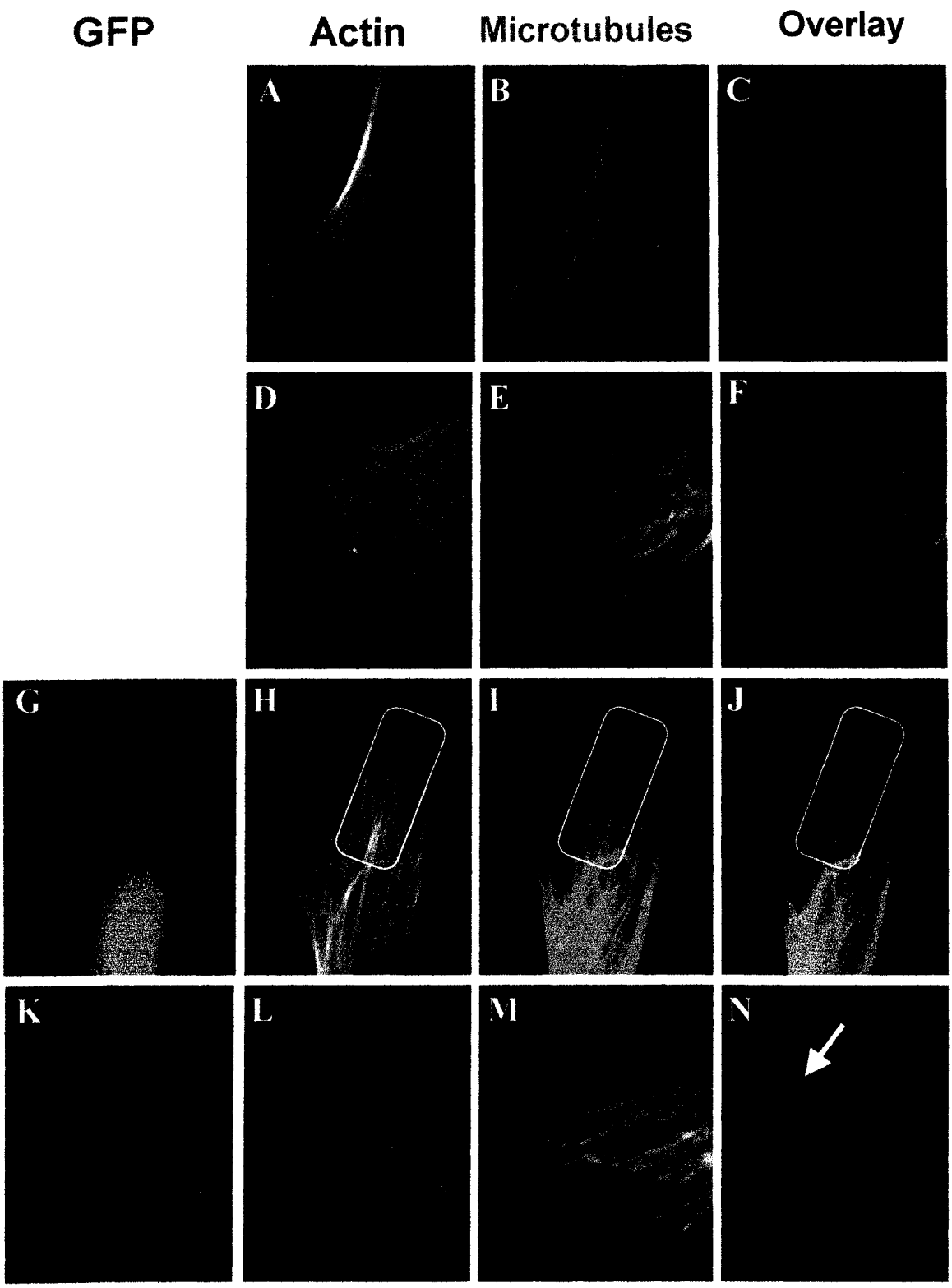

could be seen in control uninfected CECFs (Figure 3.14 A-F). In some cases, a second or a third lamellipodium could be seen to the sides of the original lamellipodium (dashed arrow) in CAmDia1-expressing CECFs (Figure 3.13 L, arrows).

Overexpression of CAmDia1 in CECF reduces the migration rate

To investigate the effect of CAmDia1 expression on chick fibroblast behavior and movement, the migration of control and infected cells was analyzed by time-lapse microscopy and using the kymograph option on Metamorph (Figure 3.15). Both polarized and bipolar CAmDia1-expressing cells retained the capacity to migrate, albeit more slowly than control uninfected polarized or bipolar CECFs (Figure 3.16). Polarized CAmDia1-expressing cells exhibited persistent directed cell movement defined as the ability of cells to migrate in one direction for 15 min (Figure 3.17), but the average migration rate (0.49 ± 0.03 μm/min) was reduced to almost half the average migration rate of polarized control cells (1.14 ± 0.06 μm/min) (migration rate ± S.E.M). Bipolar cells have two lamellipodia, usually facing opposite directions (see figure 3.13 E-H). As a result of this morphology, the two lamellipodia sometimes extend in opposite directions. At other times, one leading edge becomes dominant, and the other lamellipodium begins to retract (Figure 3.18). Bipolar cells, whether infected or not, were able to migrate, but they kept moving back and forth; bipolar uninfected CECFs changed direction more than 8 times over the 15 min, while CAmDia1-expressing bipolar CECFs changed direction more than 12 times over the 15 min (Figure 3.19). The migration rate of bipolar uninfected CECFs was slow (0.34 ± 0.05), due to the behavior mentioned earlier of bipolar cells (See Figure 3.18), and because of the high frequency of change in direction

Figure 3.15
Measuring the migration rates of migrating CECFs using the kymograph program. Individual CECFs were imaged with phase contrast objectives (low light intensity to avoid photodamage) for at least 15 min, imaging at 20 s intervals. The migration rate was measured from the center position of the cell body over 15 min using the kymograph option in Metamorph. The kymograph creates a cross-sectional view of the intensity values of a user-defined line through the planes of an image stack. This can be used to create a view of object movement in a time-based series of images. Four different regions of each cell were selected (A) and a kymograph created for each region, only one of which is shown here (B). The kymograph was then analyzed with a journal prepared by Dr. Joseph Fass and Chi Pak (Bamburg lab) which tracks the front and rear membrane positions along the line at each time point and creates an average cell center position (centroid) which is then plotted versus time (frame number), from which a slope was calculated (C). The migration rate which equals [slope (pixel/frame) X (1μM/# pixels) X (# frames/#min)], was averaged from 10 cells in each case, 4 measurements (slopes) per cell.

A)

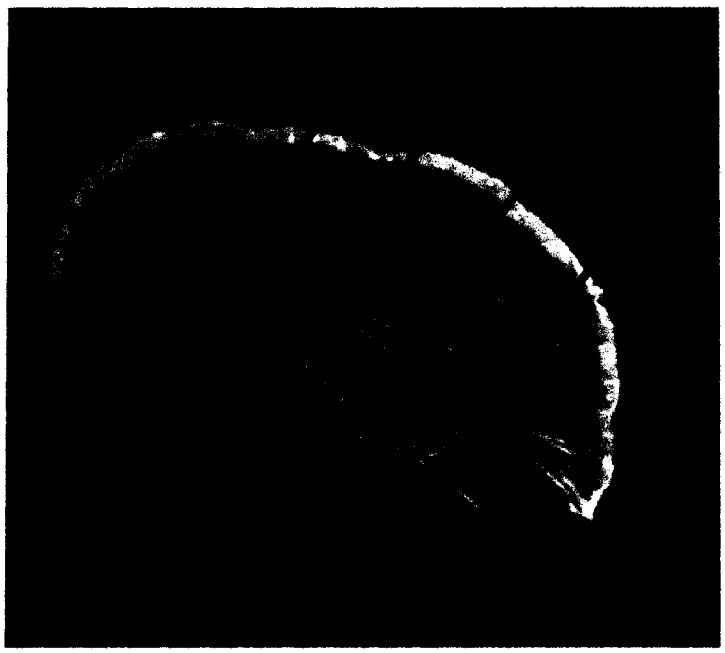

B)

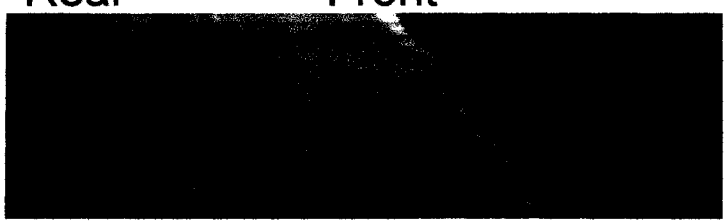

C)

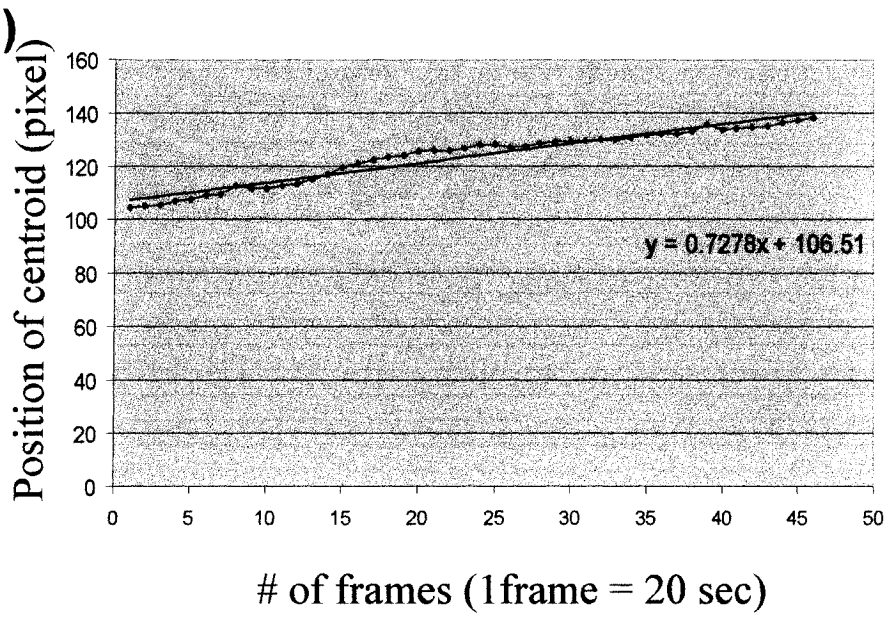

Figure 3.16
Migration rates of control uninfected and CAmDia1- expressing CECFs. The migration rate of polarized CAmDia1-expressing cells was reduced to almost half the average migration rate of polarized control cells (0.49 ± 0.03 μm/min and 1.14 ± 0.06 μm/min, respectively) (migration rate ± S.E.M). The migration rate of bipolar uninfected CECFs was slow (0.34 ± 0.05), and CAmDia1-expressing bipolar CECFs were extremely slow (0.11 ± 0.03 μm/min) (migration rate ± S.E.M).

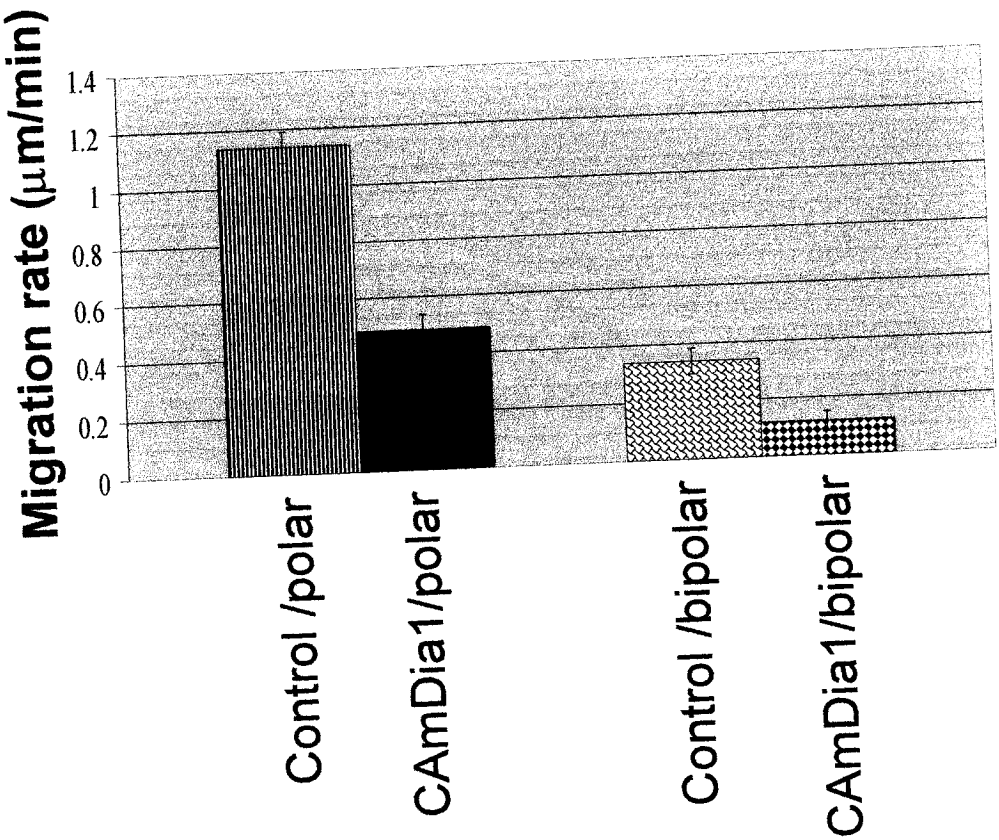

Figure 3.17
Polarized control uninfected and CAmDia1-expressing CECFs undergo directional migration. Directional migration is defined as the ability of chick cardiac fibroblast to migrate in one direction (dashed arrow) for 15 min at least. Still images of mRFP.actin-expressing polarized control CECF migrating in culture are shown. The red cell is the preceding position of the cell in each image, while the green cell is the new position, note the protrusion of the lamellipodium (arrow) over time in each image. Time shown is in (min : sec). This figure is representative of at least 10 CECFs in each of the two categories.

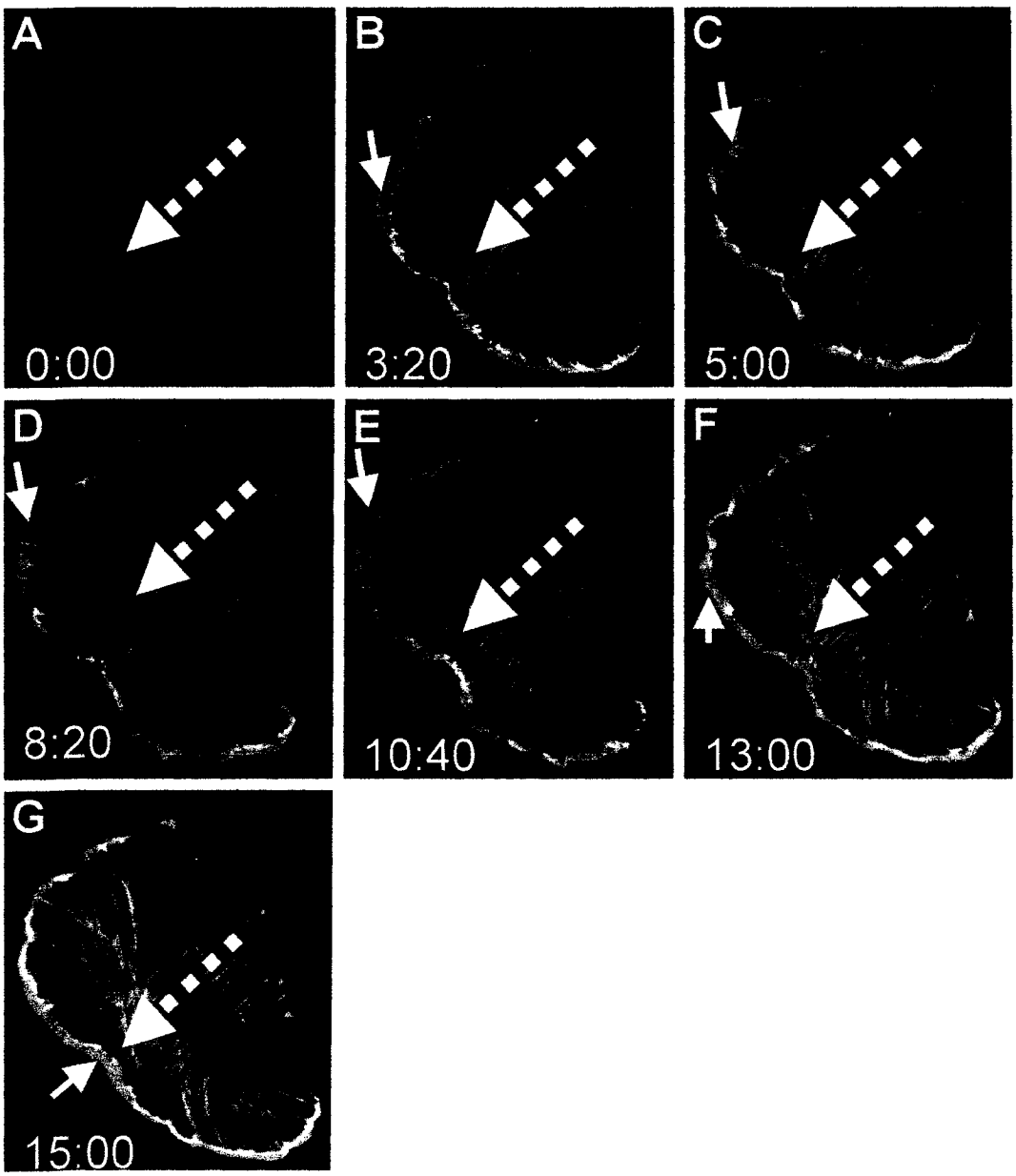

Figure 3.18
Bipolar uninfected or CAmDia1-expressing CECFs were able to migrate, but the movement frequently switches directions. Bipolar cells have two lamellipodia. One outcome of this morphology, which is depicted in the still images of a CAmDia1/GFP and mRFP.actin co-expressing CECF, is that the two lamellipodia (L1, and L2) continue to extend in opposite directions (dashed arrows), as if the cell was under the control of two pulling forces in opposite directions. However the net movement is not zero because at certain times one leading edge becomes the dominant lamellipodium, whereas the second lamellipodium starts retracting. The red cell is the preceding position of the cell in each image, while the green cell is the new position. Time is in (min : sec). This movie represents at least 10 CECFs of the two categories.

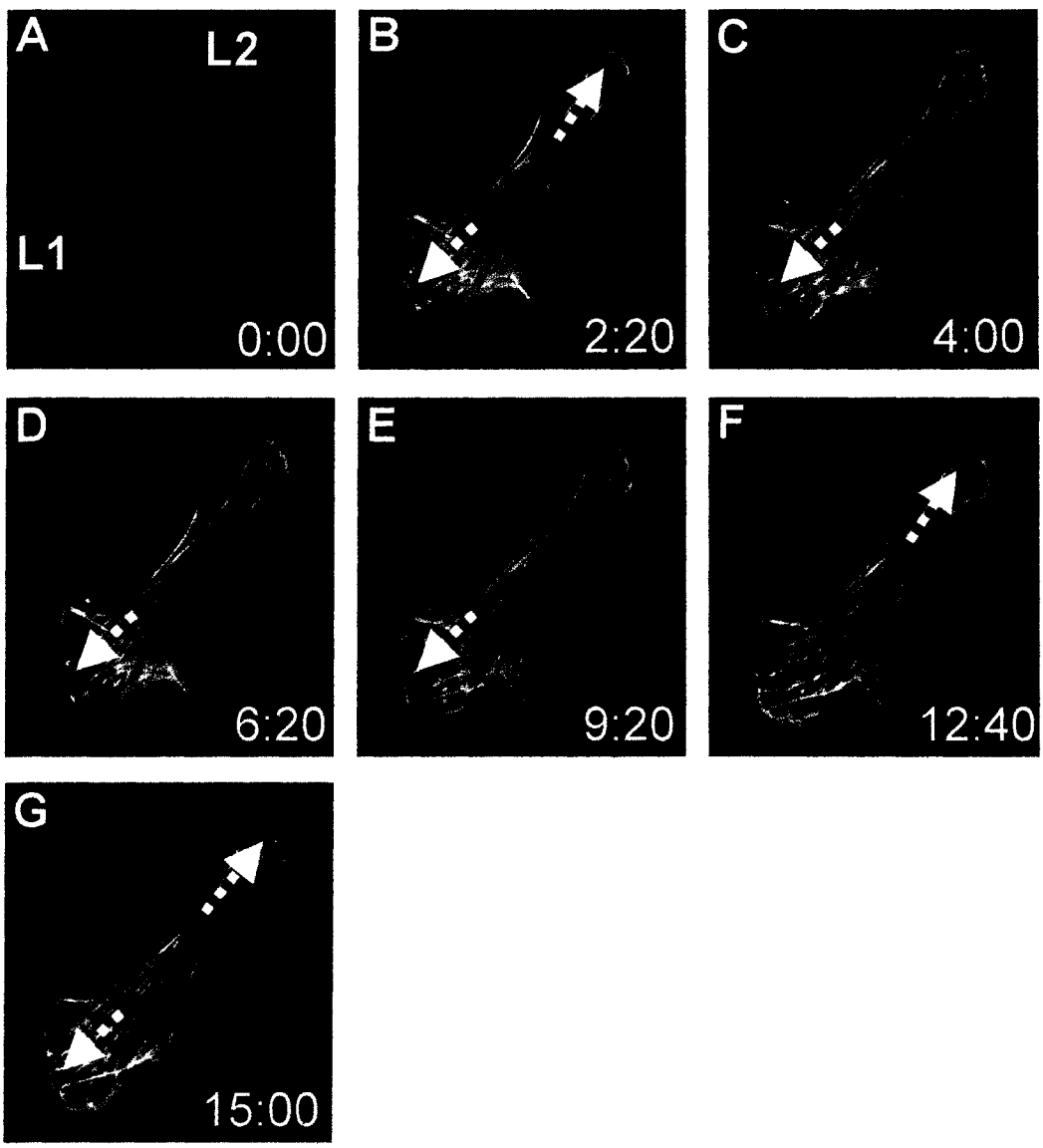

Figure 3.19
Frequency in change of direction for bipolar CECFs over 15 min.
Bipolar cells, whether infected or not, were able to migrate, but they kept moving back and forth; bipolar uninfected CECFs changed direction more than 8 times over the 15 min, while CAmDia1-expressing bipolar CECFs changed direction more than 12 times over the 15 min. Error bars are S.E.M., $p < 0.01$.

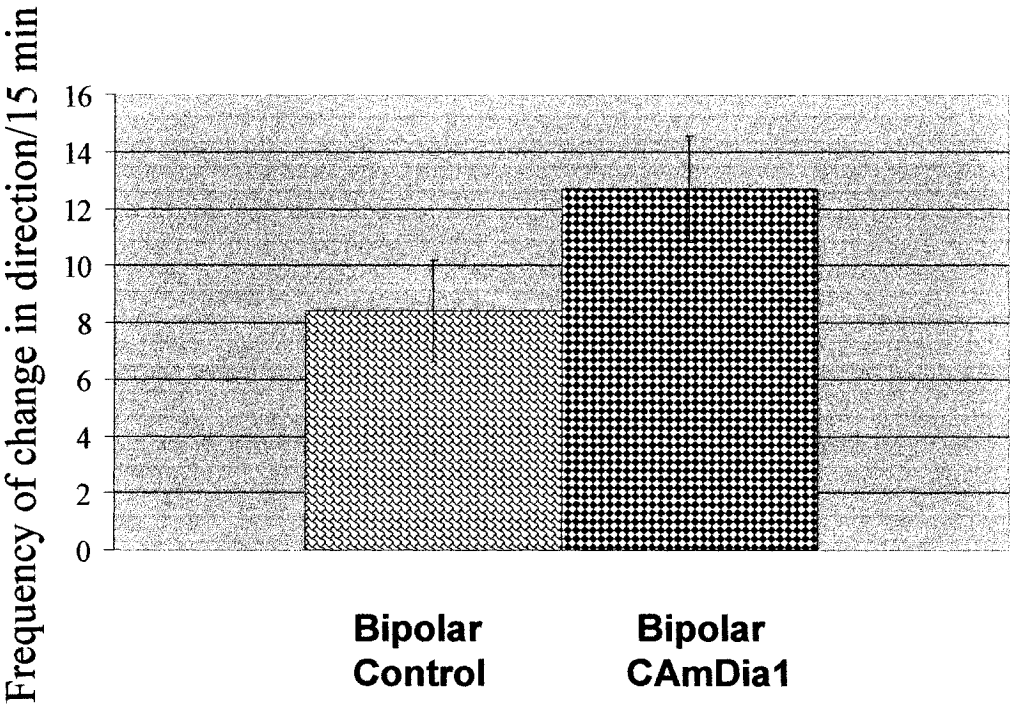

(8X/15 min). On the other hand, CAmDia1-expressing bipolar CECFs were extremely slow (0.11 ± 0.03 μm/min) (migration rate ± S.E.M) (Figure 3.16).

The lamellipodium history (protrusion, pausing, and retraction) of the migrating CECFs was also analyzed using the kymograph images and a journal prepared by Dr. Joseph Fass and Chi Pak. The leading edges of polar uninfected and CAmDia1-expressing cells were analyzed (Figure 3.20 A), while the two lamellipodia of bipolar uninfected and CAmDia1-expressing cells were analyzed (Figure 3.21 A), and graphed on Excel (Figure 3.20 B and 3.21 B). Polar uninfected CECFs spent most of the 15 min (76%) protruding, and spent the rest of the time pausing (10.5%) or retracting (13.5%) (Figure 3.22), and on average the lamellipodium fluctuated between protrusion and retraction 3 times per 15 min, while it paused one time over the same period (Figure 3.23). On the other hand, polar CAmDia1-expressing CECFs protruded 58%, paused 21% and retracted 21% of the 15 min (Figure 3.22), and on average the lamellipodium fluctuated between protrusion and retraction 5.7 times per 15 min, while it paused 2.7 times over the same period (Figure 3.23).

Bipolar uninfected CECFs spent almost equal time protruding and retracting, 38% and 37% of the 15 min, respectively, and for the rest of the time (25%), the lamellipodia were pausing (Figure 3.22). This lack of persistence was not significantly different in the bipolar CAmDia1-expressing cells (Figure 3.22). The lamellipodia of bipolar CAmDia1-expressing CECFs fluctuated between protrusion and retraction more frequently than those of bipolar control CECFs, 8.8 and 6.2 times over 15 min, respectively (Figure 3.23).

Figure 3.20
The lamellipodium history of polar migrating CECF. The lamellipodium history (protrusion, pausing, and retraction) was analyzed using the kymograph images (A) and the journal prepared by Dr. Joseph Fass and Chi Pak, and graphed on Excel (B). The kymograph image was created from a line that crosses the cell centroid, and the reference point from which the lamellipodium is measured, is the position of the lamellipodium at time point zero. This particular cell (GFP.actin-expressing) paused but did not retract.

A)

B)

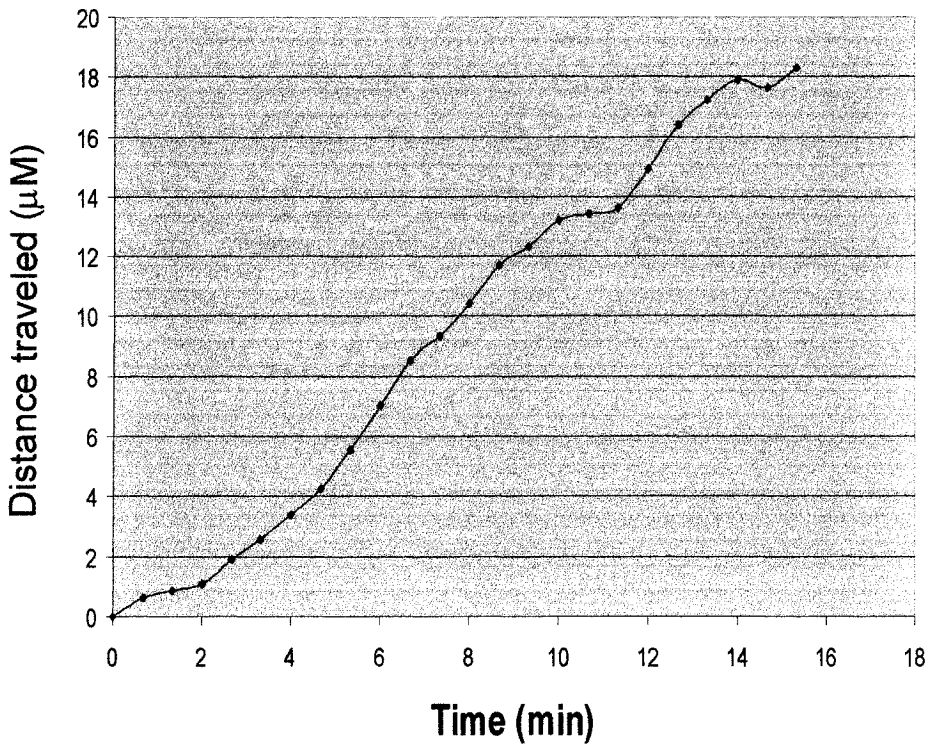

Figure 3.21
The lamellipodium history of bipolar migrating CECFs. The lamellipodium history was analyzed using the kymograph images (A) and the journal prepared by Dr. Joseph Fass and Chi Pak, and graphed on Excel (B). The pink line represents the lamellipodium on the left and the blue line the lamellipodium on the right. This cell was infected with GFP.actin-expressing adenovirus.

A)

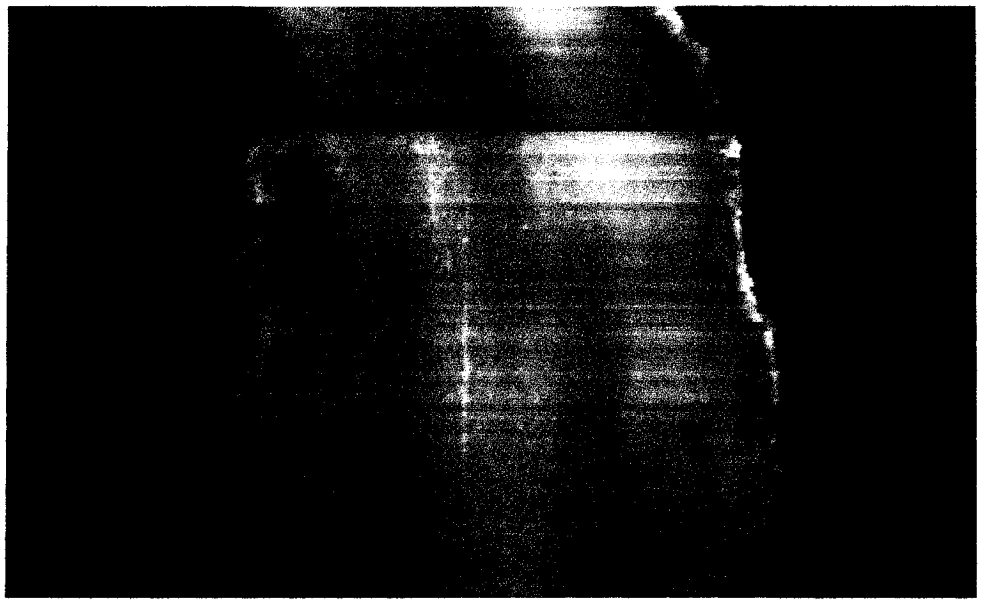

B)

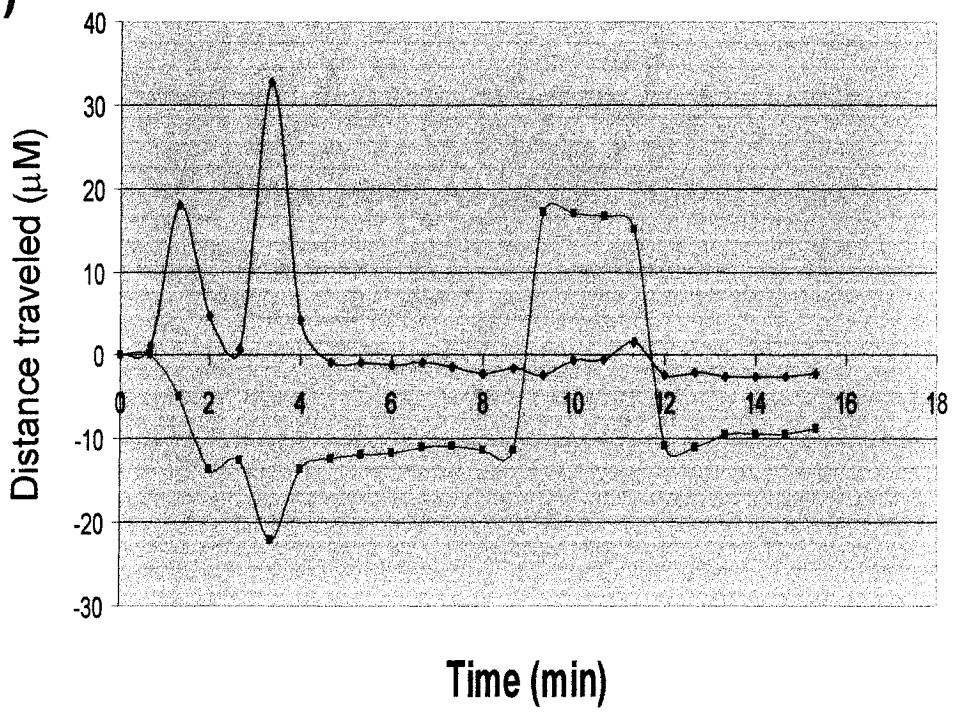

Figure 3.22
Lamellipodium history of protrusion, pausing, and retraction of migrating CECFs. Summary of quantitative data from several cells in each category.

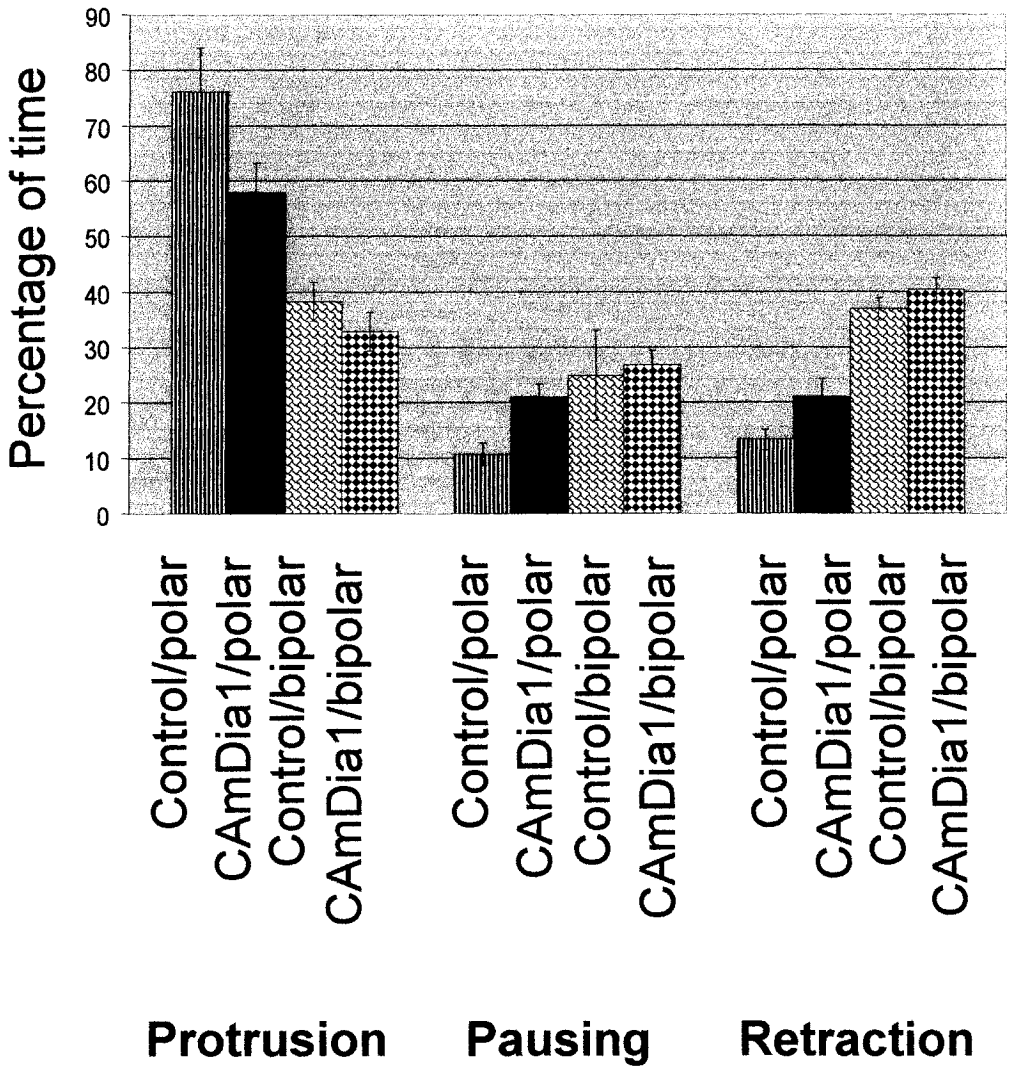

Figure 3.23
Lamellipodium history of frequency of changes between protrusion, pausing and retraction in migrating CECFs.

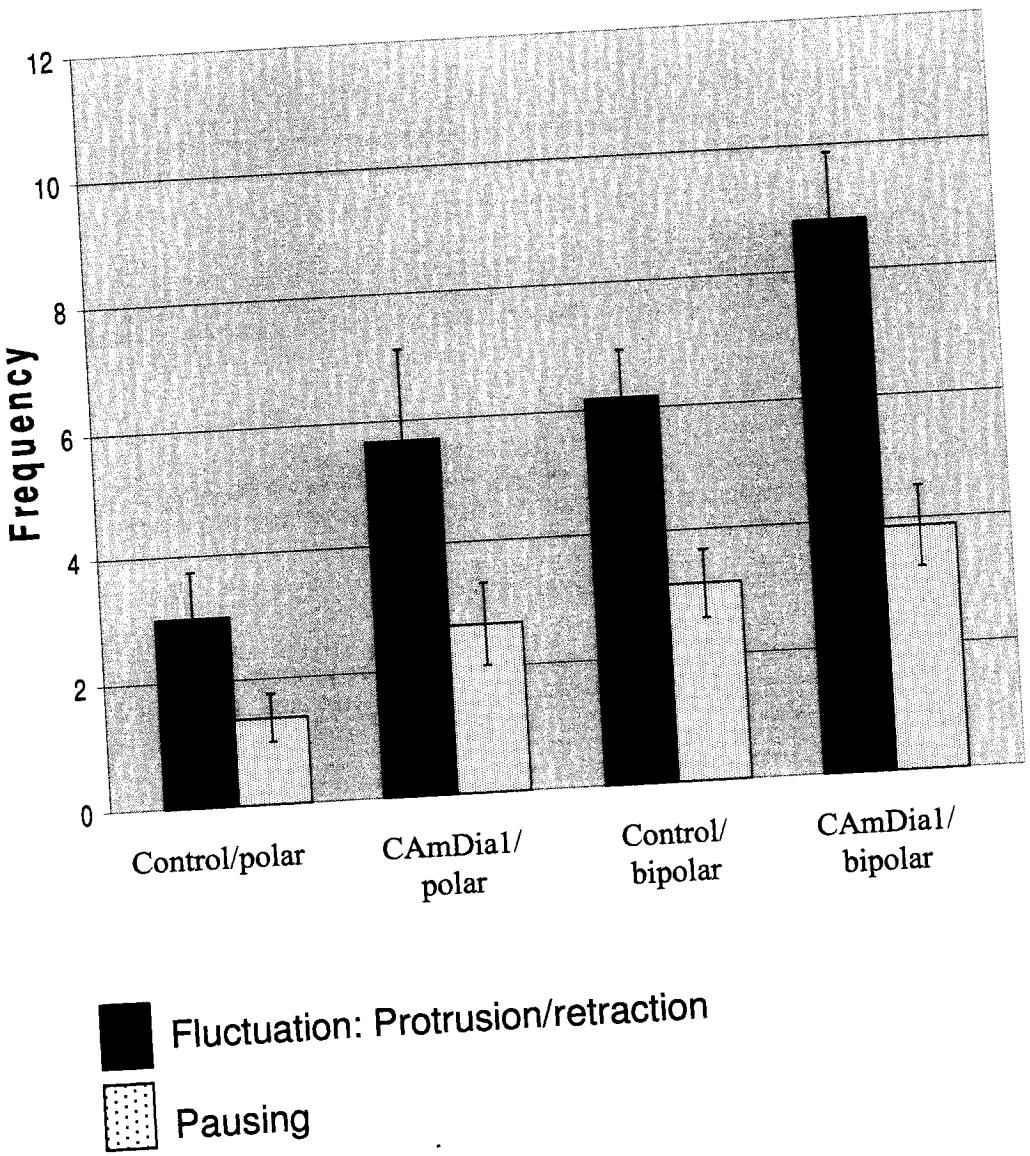

CAmDia1 could exert its effects on migration rate and the behavior of the lamellipodium via different mechanisms: 1) inducing the polymerization of F-actin (Pruyne *et al.,* 2002; Sagot *et al.,* 2002), and thus resulting in the aberrant accumulation of actin cables (Sagot *et al.,* 2002b; Evangelista *et al.,* 2002), and/or depleting the cells of the G-actin pool required for protrusion (Tominaga *et al.,* 2000; Geneste *et al.,* 2002; Copeland and Treisman; 2002; Vicente-Manzanares *et al.,* 2003); 2) enhancing the formation of focal adhesion (Takaishi *et al.,* 2000; Riveline *et al.,* 2001; Tsuji *et al.*, 2002), making the cells more adhesive to the substrate; and 3) mDia1 could induce abnormal microtubule stabilization (Palazzo *et al.,* 2001; 2004; Wen *et al.,* 2004), resulting in the sequestering of GEF-H1 and inactivation of Rho (Ren *et al.,* 1998; Krendel *et al.,* 2002), preventing contraction and forward cell body translocation. The role of mDia1 in each of these mechanisms is explored below.

Overexpression of CAmDia1 does not enhance F-actin formation in CECFs

Overexpression of CAmDia1 mutant has been shown to induce the formation of actin filaments in HeLa cells (Watanabe *et al.,* 1997; 1999), NIH 3T3 cells (Tominaga *et al.*, 2000; Satoh and Tominaga, 2001; Copeland and Treisman, 2002), Swiss 3T3 (Tsuji *et al.,* 2002); and Madin-Darby Canine Kidney cells (MDCK cells) (Takaishi *et al.,* 2000). To investigate if the overexpression CAmDia1 in CECFs resulted in the same effect leading to loss of polarization and impaired migration of the cells, the ratio of G-actin/F-actin in the lamellipodium and cell body of both uninfected and CAmDia1-expressing CECFs was measured. CECFs were fixed and stained with N350 primary antibody that recognizes G-actin, while F-actin was stained with a fluorochrome-conjugated phalloidin. The average intensity of G-actin and F-actin staining was

measured in Metamorph for both the lamellipodium and the cell body, and then the relative ratio of G-actin/F-actin was calculated which equals [the ratio of G-actin/F-actin (lamellipodium)] / [the ratio of G-actin/F-actin (cell body)]. The slight reduction observed in the relative ratio of G-actin/F-actin in the lamellipodia of CAmDia1-expressing CECFs when compared to uninfected CECFs was not significant (Figure 3.24) (n=25 cells in each category, ± S.E.M.). CECFs were co-infected with adenoviruses expressing CAmDia1 and N17 Rac (dominant negative mutant), and CAmDia1 and XAC-S3A (non-phospho-regulated ADF/cofilin), both DNRac and XAC-S3A mutants should enhance actin filament turn over. Neither N17 Rac nor XAC-S3A mutants rescued the loss of polarization caused by CAmDia1 (Figure 3.25).

Overexpression of CAmDia1 in CECF cells increases the total area occupied by focal adhesions

Overexpression of CAmDia1 enhanced the formation of focal adhesions in many cell types including MDCK cells (Nakano *et al.,* 1999; Takaishi *et al.*, 2000), HeLa cells (Watanabe *et al.,* 1999; Ishizaki *et al.,* 2001), NIH 3T3 fibroblasts (Riveline *et al.*, 2001), and Swiss 3T3 fibroblasts (Tsuji *et al.,* 2002). Overexpression of CAmDia1 could exert the same effect on chick cardiac fibroblasts making them more adhesive to the substrate which would explain the reduction of migration rate in CAmDia1-expressing cells. CECFs were fixed and stained for focal adhesions with anti-paxilin primary antibody (Figure 3.26).Both polar and bipolar CAmDia1-expressing CECFs showed increased (42% and 160%, respectively) size of focal adhesions when compared to uninfected CECFs (Figure 3.27 A) (n=25 cells in each category, ± S.E.M, $p < 0.001$). On the other hand, polar CAmDia1-expressing CECFs exhibited an increase in the number of focal

Figure 3.24
Overexpression of CAmDia1 does not enhance F-actin formation in CECFs. CECFs were fixed and stained with a primary antibody that recognizes G-actin, while F-actin was stained with fluorescent phalloidin. The average intensity of G-actin and F-actin staining was quantified with Metamorph for both the lamellipodium and the cell body, and then the relative ratio of G-actin/F-actin was calculated.

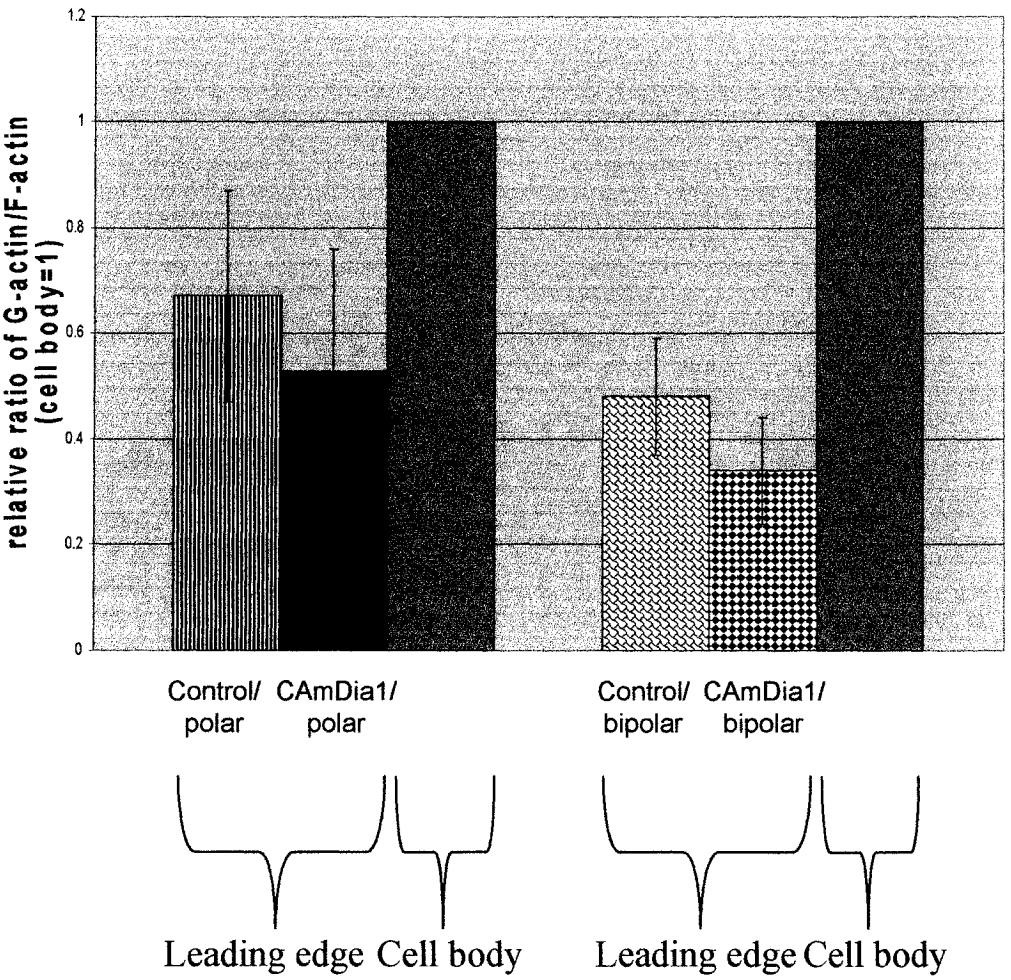

Figure 3.25
Co-expression of DN Rac or XAC-A3 with CAmDia1 in CECFs did not rescue loss of polarity. Chick cardiac explants were co-infected with CAmDia1 and DN Rac or XAC-S3A adenoviruses for 24 h, and then were allowed to migrate for another 24 h. The cells were then fixed and stained with Alexa-350-conjugated phalloidin and scored for polarity.

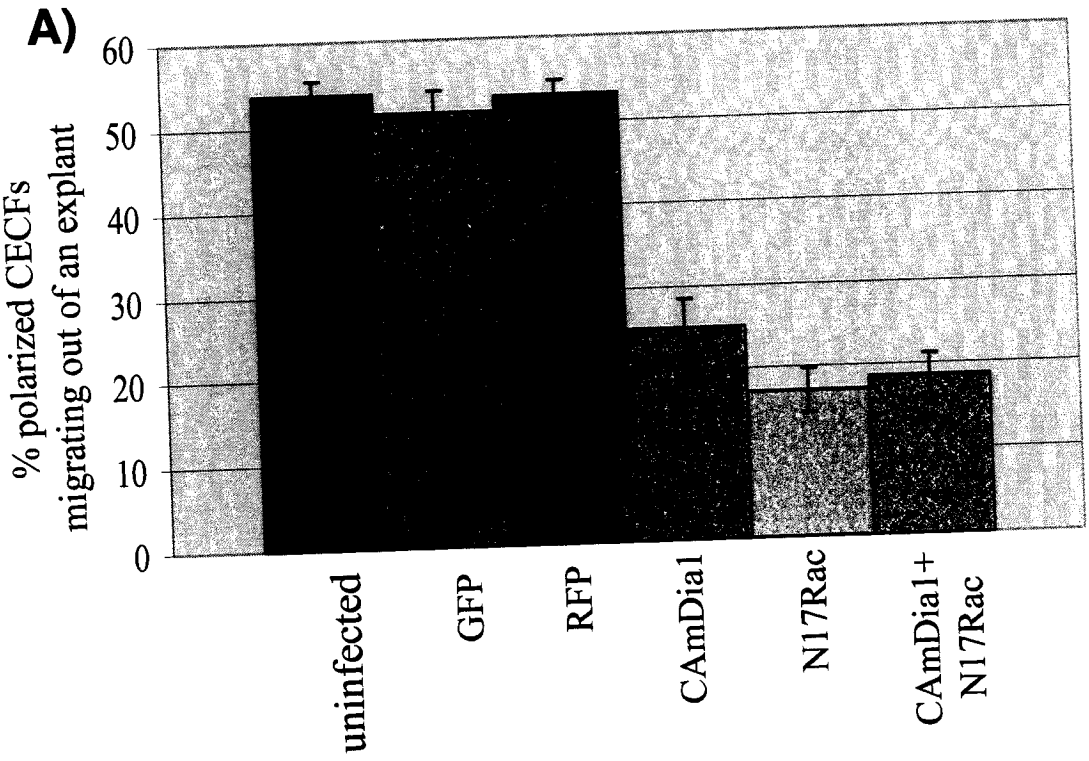

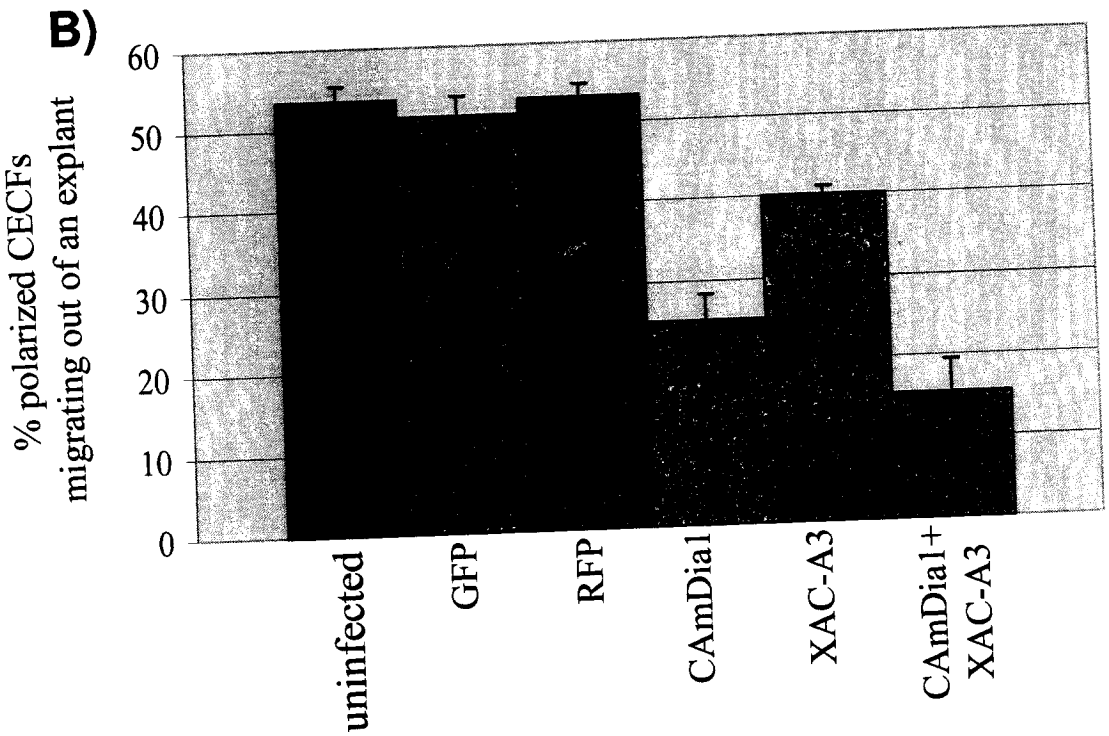

Figure 3.26
Focal adhesion staining. CECFs were fixed and stained for focal adhesion (anti-paxillin primary antibody; A), and actin (Alexa-350-conjugated phalloidin; B).C) image overlay.

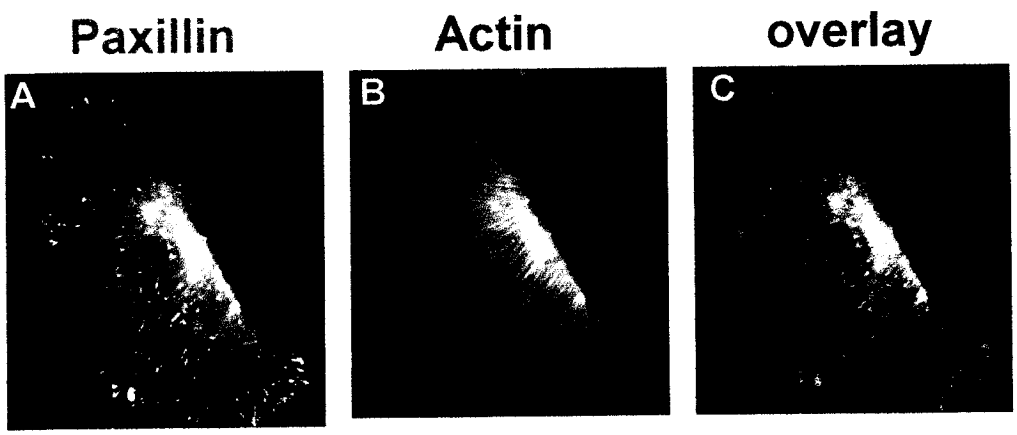

Figure 3.27
Overexpression of CAmDia1 in CECF cells increases the size and number of focal adhesions. CECFs were infected with CAmDia1 adenovirus for 24 h and allowed to migrate for another 24 h and then fixed and stained for focal adhesions with mouse anti-paxillin primary antibody. The size and number of focal adhesions per unit area (125 μm^2) was measured in Metamorph.

A)

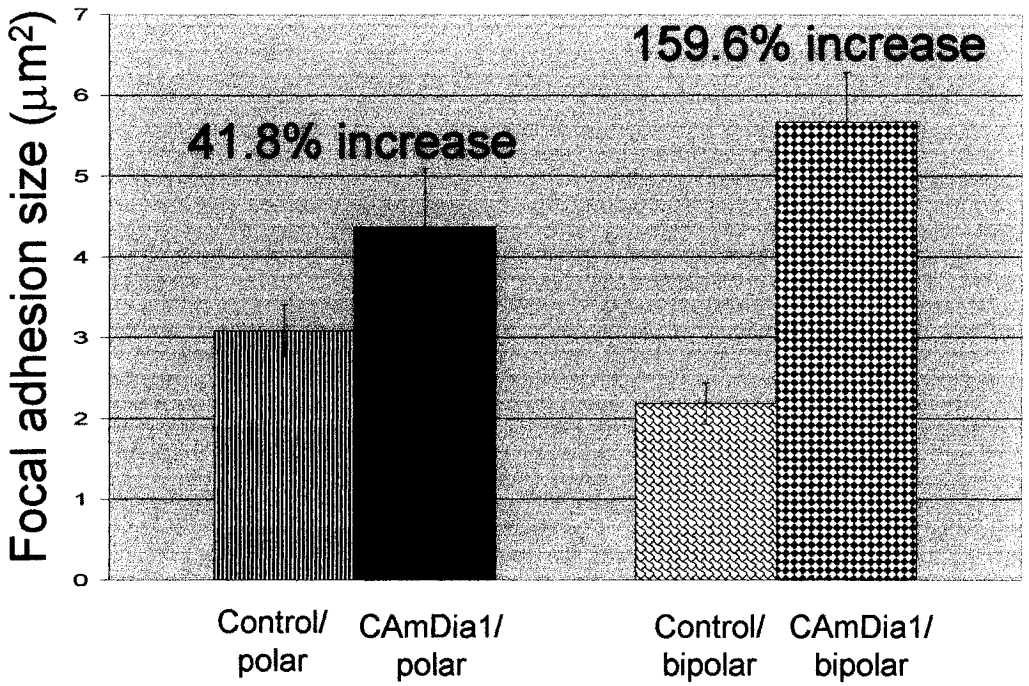

B)

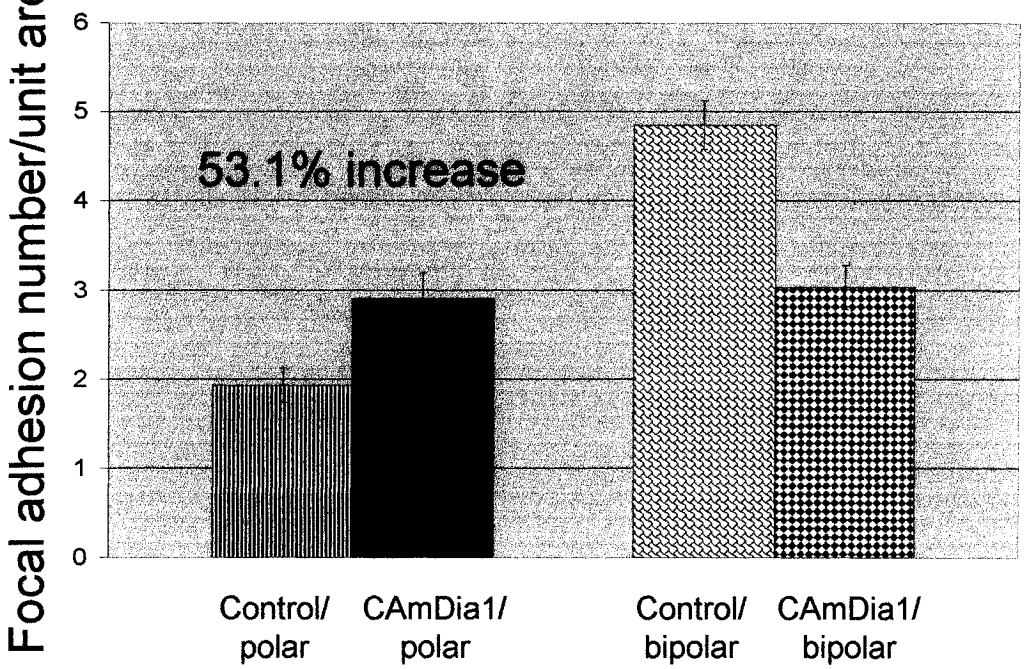

adhesions when compared to uninfected polar CECFs (Figure 3.27 B), whereas bipolar uninfected CECFs had more focal adhesions/unit area than bipolar CAmDia1-expressing CECFs (Figure 3.27 B) (n=25 cells in each category, ± S.E.M, $p < 0.001$). When data from Figure 3.27 A and B were grouped and expressed as the total area occupied by focal adhesion/unit area, the total area occupied by focal adhesions in CAmDia1-expressing CECFs was larger than that of uninfected CECFs (Figure 3.28). The majority of DNmDia1-expressing CECFs did not migrate out of the explants, and when these cells were dissociated and plated (dissociated CECFs are used to study initiation of polarization and will be explained in chapter four), they did not adhere to the substratum, suggesting a faulty adhesion. Therefore, we co-infected chick cardiac explants with DNmDia1 and wild-type (WT) paxillin-GFP adenoviruses (Figure 3.29). The co-infection increased the number of DNmDia1-expressing CECFs that migrated out of the explants from 5-10 cells to 50-70 cells, in the DNmDia1 adenovirus single infection and the DNmDia1/wt-Paxillin adenovirus double infection preparation, respectively. Almost none of the co-infected cells were polarized.

Overexpression of CAmDia1 in CECFs increases the number of microtubule plus ends penetrating the lamellipodium, and induces their stabilization

Polar uninfected and CAmDia1-expressing CECFs were stained for total and stabilized microtubules (Figure 3.30). Few microtubule plus ends were seen to penetrate the lamellipodium of uninfected cells (Figure 3.30 B, dashed arrows), very few of these plus ends were stabilized (Figure 3.30 C, arrow). The majority of the Glu-positive microtubules were seen perinuclear, where the MTOC is localized (Figure 3.29 C and D). On the other hand, more plus ends were seen to reach the cell periphery in CAmDia1-

Figure 3.28
Overexpression of CAmDia1 in CECF cells increases the total area occupied by focal adhesions. Quantification of the focal adhesion area from paxillin stained polar and bipolar control and CAmDia1-expressing CECFs. n=25 cells in each category, $p<0.001$.

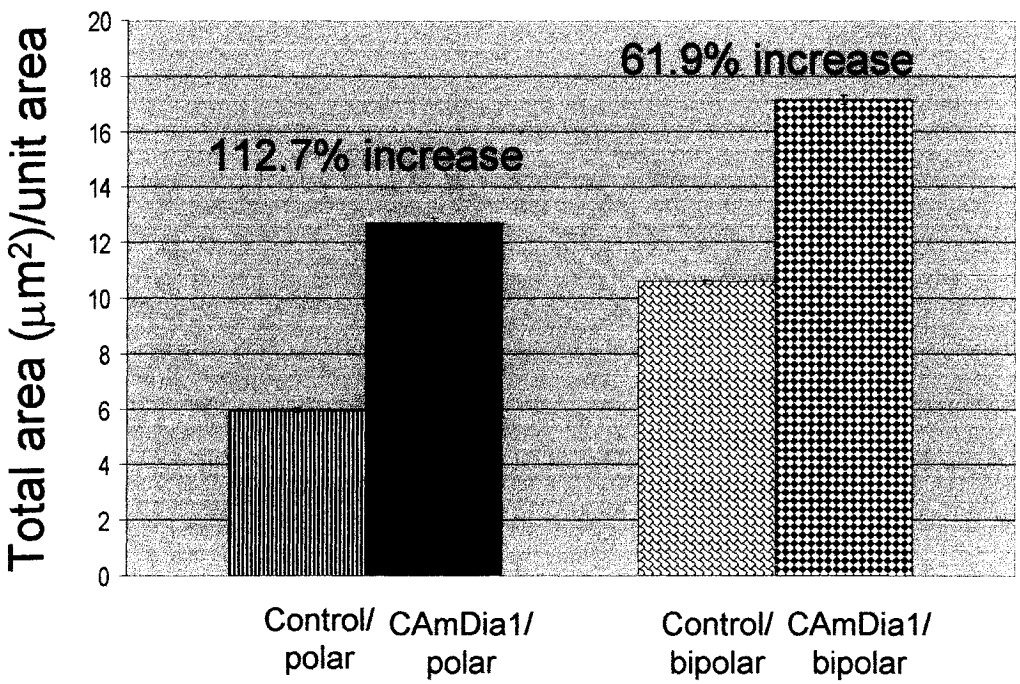

Figure 3.29
CECFs co-expressing DNmDia1 and wt-paxillin-GFP. A) DNmDia1/RFP, B) wt-paxillin.GFP. The arrows indicate focal adhesions.

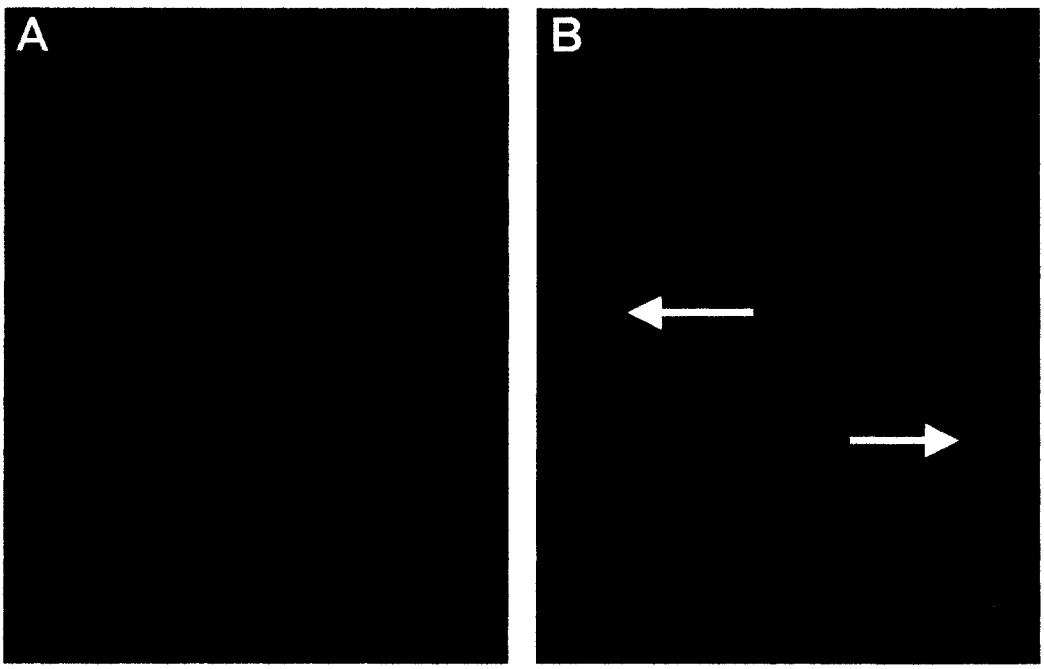

Figure 3.30
Total and Glu-positive microtubules in CECFs. Control and CAmDia1-expressing CECFs were stained with β- and Glu-tubulin primary antibodies. To count the number of plus ends penetrating the leading edge, a band was drawn (A, region 1), that is ~ 55-60 μm across, and 5 μm in width (A, region 2). The number of microtubule plus ends/unit area (20 μm^2) (A, region 3) were then counted. B-D) control uninfected CECF, E-H) CAmDia1-expressing CECF. n = 15 cells in each category, 5 areas per cell.

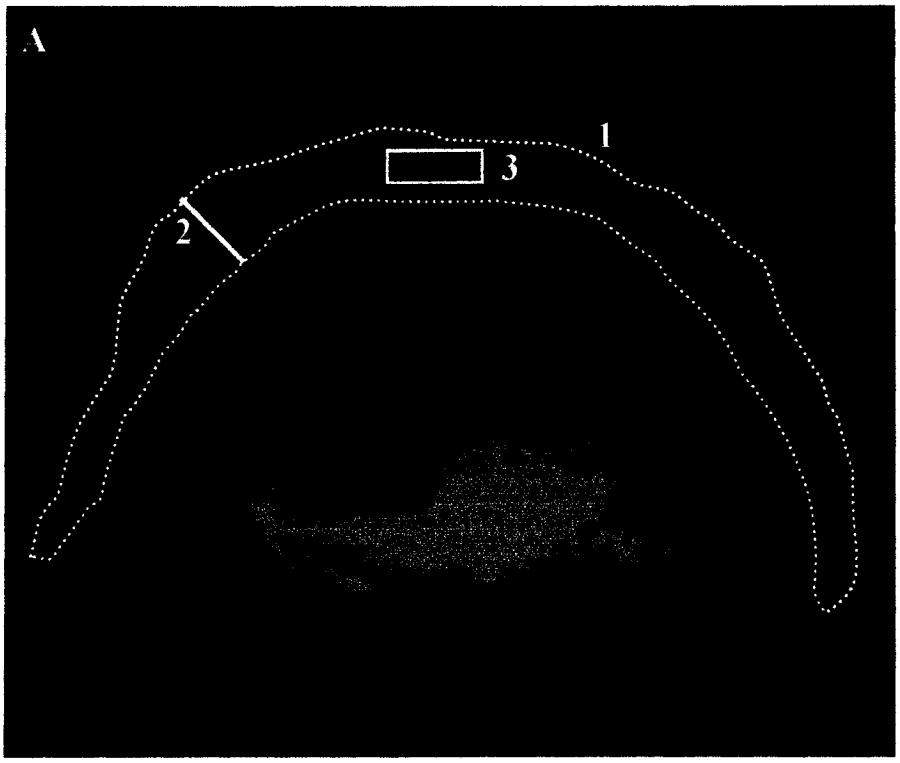

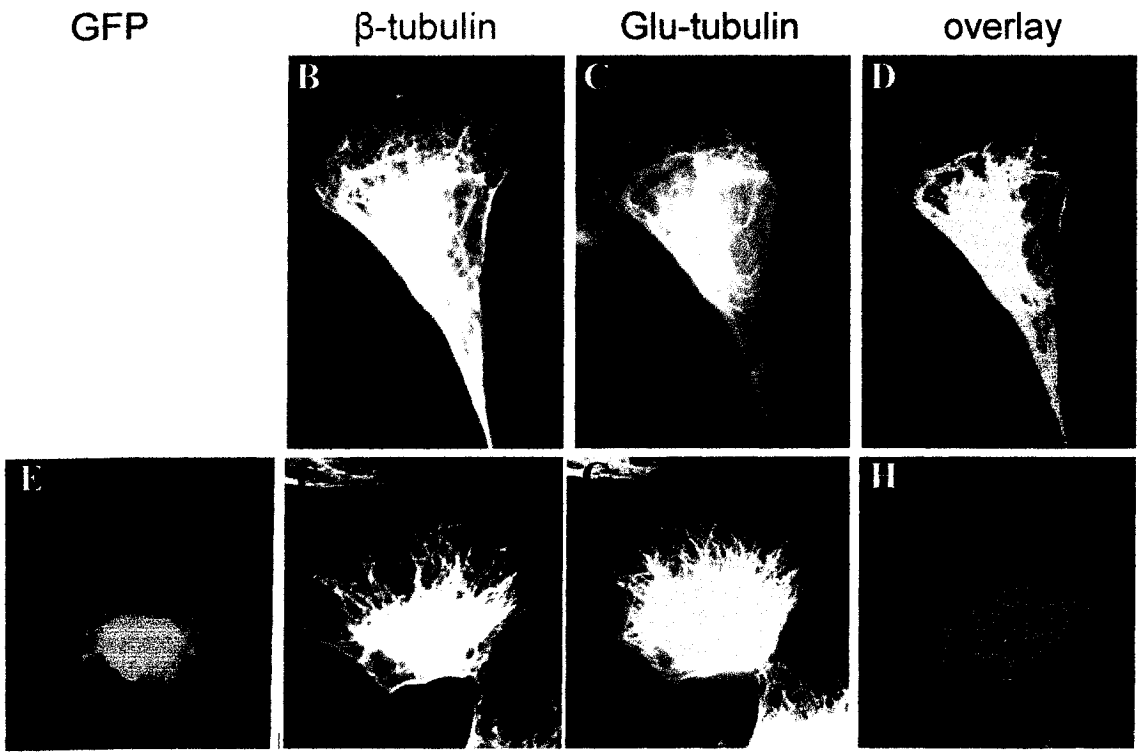

expressing CECFs (Figure 3.30 F), the majority of these microtubule plus ends were stabilized (Figure 3.30 G and H). Overexpression of CAmDia1 caused a 71% increase in the number of total microtubule plus ends penetrating the lamellipodium; the number of microtubule plus ends/unit area in control uninfected and CAmDia1-expressing CECFs was 3.1 and 5.3, respectively (Figure 3.31). About 65% of the microtubules that penetrated the lamellipodium in CAmDia1-expressing cells were stabilized (Figure 3.31), as judged from the number of microtubules that stained positive for Glu-tubulin antibody (See Figure 3.30 G), whereas only 31% of the microtubule plus ends penetrating the lamellipodium in control cells stained positive for Glu-tubulin (Figure 3.31).

Discussion

Observation of chick embryo cardiac fibroblasts migrating out of an explant allowed us to study the role of mDia1 during cell migration and polarization. CECFs from day E7 or E8 chick cardiac muscle migrating out of explants, are one of few cell types that display remarkable morphological polarization and rapid, persistent locomotion in the absence of an external cue (spontaneous polarization), making them a valuable tool to study cell migration and polarization *in vitro.*

Avian cells have two formin proteins, Gg1 and Gg2 (Higgs and Peterson, 2005). The formin protein Gg1 is localized to the nucleus of different embryonic cell types, and is expressed in the developing chicken limb bud and in the epithelial compartment of the pronephros and mesonephros. Gg1 protein plays an essential role during the morphogenesis of limbs and kidneys (Trumpp *et al.,* 1992). The other avian formin, Gg2 is an mDia1 homologue and belongs to the Dia group (Higgs and Peterson, 2005). Gg2 is

Figure 3.31
Overexpression of CAmDia1 in CECFs increases the number and stabilization of microtubule plus ends penetrating the lamellipodium.
Quantification of Glu and total microtubule ends in CECFs.
n = 15 cells in each category, $P < 0.001$.

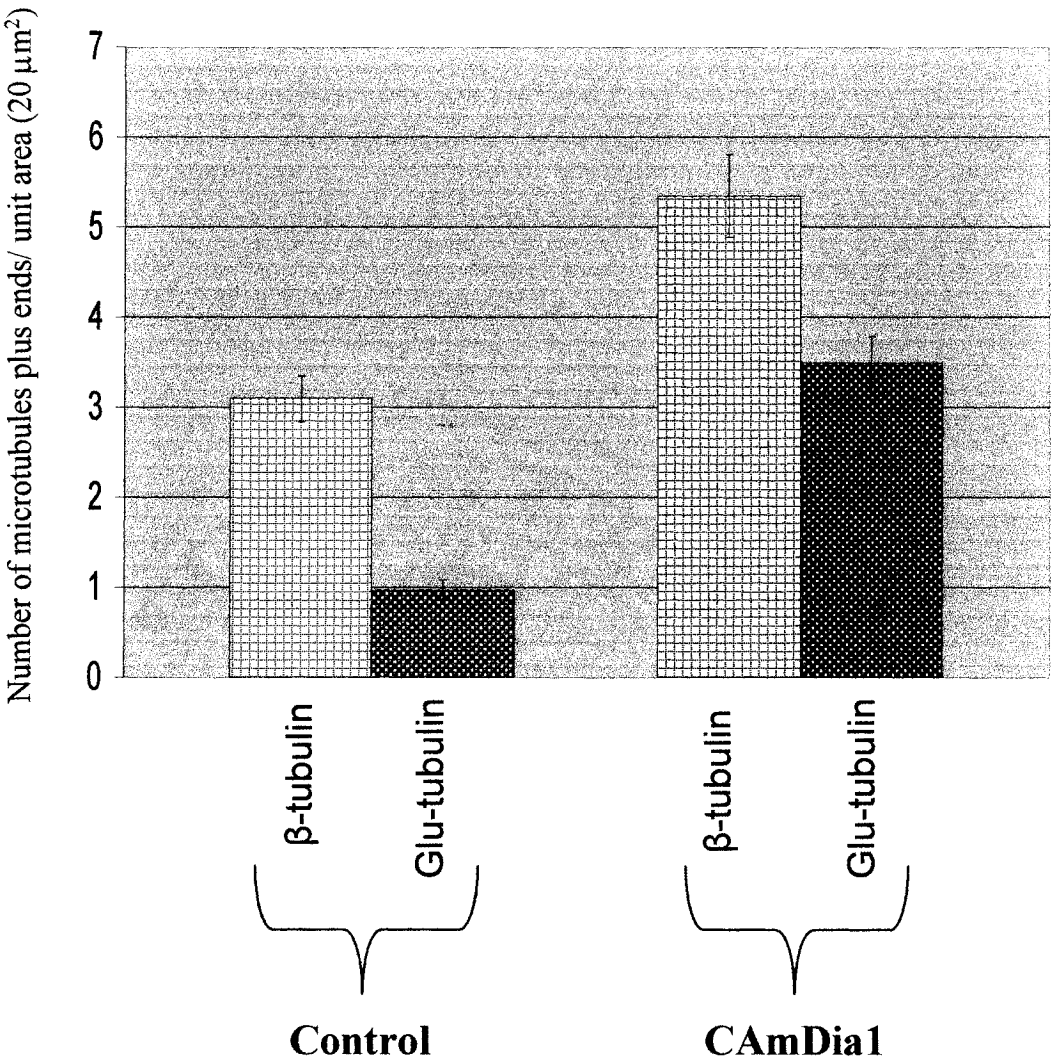

a cytosolic protein with a molecular weight of 140 kDa (1253 aa), and yet no biochemical or cellular studies have been done to characterize this protein. Overexpression of mDia1 mutants in CECFs, either the constitutively active (CA) or the dominant negative (DN) should therefore give some direct insight on what roles formin proteins might play during cell polarization and migration.

Infecting CECFs with a variety of adenoviruses yielded high infection rates. Although exact multiplicity of infections can't be calculated because the number of cells in each explant is not constant or known, relatively low MOIs (approximately 10-50 based upon the cell numbers from dissociated explants) were needed to obtain almost complete (100%) infection (Table 3.1). Because the measure of infectivity is the detection of expression of a fluorescent protein, this is also subject to some variability since scoring a cell as an expressing cell will depend on the threshold set for exposure time. Nevertheless, we are confident that a very high percentage of the cells were infected in these experiments since our camera is quite sensitive and exposure times were kept relatively short (less than 2-3 sec) comparable to what we commonly use for immunofluorescence imaging. Infecting the cells with two different adenoviruses simultaneously reduced slightly the percentage of cells infected with each virus (98.3% to 87.5% for GFP adenovirus), but the percentage of CECFs that were doubly-infected was high enough to perform the experiments (> 60%). Furthermore the infection of cells with the second virus seemed to be independent of whether or not the cell was infected with the first virus. Chick embryo fibroblasts (CEF) prepared from the whole (headless) chick embryo, required very high MOIs (up to 2000) and the maximum percentage of infected

CEFs was less than 10%. Thus the cardiac fibroblasts (CECFs) proved to be an ideal chick cell in which to exploit the advantages of adenoviral-mediated gene expression.

The chick cardiac explants were infected with a range of MOIs with the DNmDia1 adenovirus, and even with the lowest MOI (estimated to be ~ 10) almost none of the cells migrated out of the explants. This is the first report of this mutant completely blocking cell migration. Overexpression of this mutant reduced the migration of a confluent culture of NIH 3T3 fibroblasts wounded in vitro by scraping with a tip of a pipette. About 70% of DNmDia1-expressing NIH 3T3 cells were left behind the wound edge, while the remaining 30% migrated with the wound edge (Magdalena *et al.,* 2003). On the other hand, DNmDia1-expressing lymphocytes exhibited normal migration behavior (rate and directionality) (Vicente-Manzanares *et al.,* 2003). These experiments were done in mouse and human cells, respectively, both of which express several different types of formin proteins, while chick cells express only the one cytosolic formin protein (Gg2). This lack of multiple formins and Dia-proteins perhaps explains why overexpression of the DNmDia1 mutant in CECFs resulted in such a pronounced effect.

CAmDia1-expressing CECFs migrated out of the explants and about 25% of them were polarized compared to about 50% of uninfected or control adenovirus infected cells (Figure 3.9). As previously reported, CAmDia1 induced cell elongation accompanied by the formation of fine longitudinal actin cables (Figure 3.13 B; Watanabe *et al.,* 1999; Ishizaki *et al.,* 2001). Ishizaki and colleagues (2001) reported that the treatment of CAmDia1-expressing cells with nocodazole (microtubule depolymerizing drug), but not cytochalasin D (actin depolymerizing drug), induced cell shortening, suggesting that the microtubules and not actin are responsible for cell elongation. This could be explained by

the fact that microtubule depolymerization causes the release of GEF-H1, a Rho GEF, which leads to the activation of Rho/ROCK pathway resulting in contraction and cell shortening (Ren *et al.,* 1998; Krendel *et al.,* 2002; Zenke *et al.,* 2004).

The migration of CECFs was analyzed by time-lapse microscopy for at least 15 min. CAmDia1-expressing cells, either polarized or bipolar, retained the capacity to migrate, albeit in a slower fashion than uninfected polarized or uninfected bipolar CECFs, respectively (0.49 μm/min compared to 1.14 μm/min, and 0.11 μm/min compared to 0.34 μm/min (Figure 3.13). This effect of CAmDia1 on cell migration has been reported previously. In NIH 3T3 fibroblasts CAmDia1 overexpression slowed wound closure in a wound healing assay (Magdalena *et al.,* 2003), and in lymphocytes CAmDia1 expression slowed motility (Vicente-Manzanares *et al.,* 2003). Several possibilities could explain the CAmDia1-mediated reduction in cell migration rates.

The first possibility is that mDia1, through its known induction of actin polymerization (Kovar and Pollard, 2004; Moseley *et al.*, 2004; Shimada *et al.*, 2004; Watanabe and Higashida, 2004), could deplete the cell's free G-actin pool required for protrusion; this explanation correlates with the role of mDia1 in the activation of the transcriptional activity of SRF, a transcriptional factor that is activated by depleting the cells of G-actin (Tominaga *et al.,* 2000; Copeland and Treisman, 2002; Genesto *et al.,* 2002). Overexpression of CAmDia1 in T lymphocytes depleted the cells of monomeric actin, which resulted in an inhibition of both spontaneous and chemokine-induced lymphocyte motility (Vicente-Manzanares *et al.,* 2003). On the other hand, overexpression of a constitutively active mutant of a yeast formin (Bni1p) increased the formation of actin cables, which resulted in a defective polarized growth in yeast (Sagot

et al., 2002b). Both of these mechanisms were tested in CECFs but neither proved to be the CAmDia1-mediated mechanism that caused the loss of polarization induced by overexpression in CECFs. The ratio of G-actin/F-actin was measured in uninfected and CAmDia1-infected CECFs, but the difference was insignificant (Figure 3.24). Also, CECFs were co-infected with adenovirus for expressing CAmDia1 and two mutants that should increase actin filament turn over: N17 Rac or XAC-S3A. Neither mutant could rescue the loss of polarization caused by CAmDia1 overexpression (Figure 3.25). This finding suggests that the CAmDia1-mediated loss of polarization in CECFs is not due to aberrant accumulation of actin cables.

Secondly, CAmDia1 could enhance the formation of focal adhesions, making the CECFs more adhesive to the substrate (Nakano *et al.,* 1999; Watanabe *et al.,* 1999; Takaishi *et al.*, 2000; Ishizaki *et al.,* 2001; Riveline *et al.*, 2001; Tsuji *et al.,* 2002) and thus inhibiting movement. In cultured cells, integrin-based complexes form several types of adhesion structures. Small dot like (0.5– 1μm) structures known as focal complexes (Bershadsky *et al.* 1985; Tawil *et al.,* 1993) are localized at the edge of a lamellipodium (Nobes and Hall, 1995). Elongated (3–10μm in length) streak-like structures that are associated with stress fibers and are known as focal adhesions (Heath and Dunn, 1978; Rottner *et al.,* 1999; Zamir *et al.;* 2000). There are also tensin-enriched fibrillar adhesions (Zamir *et al.* 1999; 2000; Katz *et al.*, 2000). It has been shown that focal complexes appear first after cell–matrix interaction, and focal adhesions evolve from them in a Rho-dependent manner (Clark *et al.,* 1998; Rottner *et al.,* 1999). Two downstream effectors of Rho, ROCK and mDia1 mediate Rho effects on cell adhesion (Watanabe *et al.,* 1999). The Rho-ROCK pathway increases cell contractility (Kimura *et al.,* 1996; Kureishi *et al.,*

1997), which is necessary for the formation of focal adhesions (Chrzanowska-Wodnicka and Burridge, 1996; Helfman *et al.,* 1999). The mDia1-dependent pathway is necessary for focal adhesion elongation and assembly (Riveline *et al.,* 2001). Also, mDia1 plays the role of a scaffold protein that mediates the formation of a multiprotein complex at focal adhesions; Src kinase associates with mDia1, and this association results in the phosphorylation of Cas (Tsuji *et al.,* 2002). Cas is the Crk-associated substrate, a major tyrosine phosphorylated protein in cells transformed by v-crk and v-src oncogenes (Brabek *et al.,* 2005). Src kinase is responsible for integrin-dependent Cas phosphorylation (Klinghoffer *et al.,* 1999). Phosphorylated Cas provides binding sites for Crk and DOCK180 (O'Neill *et al.,* 2000), and DOCK180 (Rac-specific GEF) in turn activates Rac (Kiyokawa *et al.,* 1998). This pathway is antagonized by ROCK, which phosphorylates paxillin (Tsuji *et al.,* 2002), and phosphorylated paxillin inhibits membrane ruffling and cell migration mediated by Cas-Rac pathway (Yano *et al.,* 2000; Tsuji *et al.,* 2002), a pathway important for invasion and metastasis of src-transformed cells (Brabek *et al.,* 2005) (Figure 3.32). In migrating CECFs, we found that the overexpression of CAmDia1 resulted in an increase in focal adhesion size, number (Figure 3.27 A and B), and total area occupied by the focal adhesions/unit area (Figure 3.28).

Finally, mDia1 could induce abnormal microtubule stabilization. Microtubule dynamics are required for maintaining a pool of active ADF/cofilin at the leading edge of migrating CECFs (Cramer *et al.,* submitted). The stabilization of microtubule plus ends by mDia1 overexpression in CECFs (Figure 3.31) could reduce the level of active ADF/cofilin through regulating the dynamics of microtubule plus ends. Alternatively,

Figure 3.32
mDia1 functions as a scaffold protein at focal adhesion.

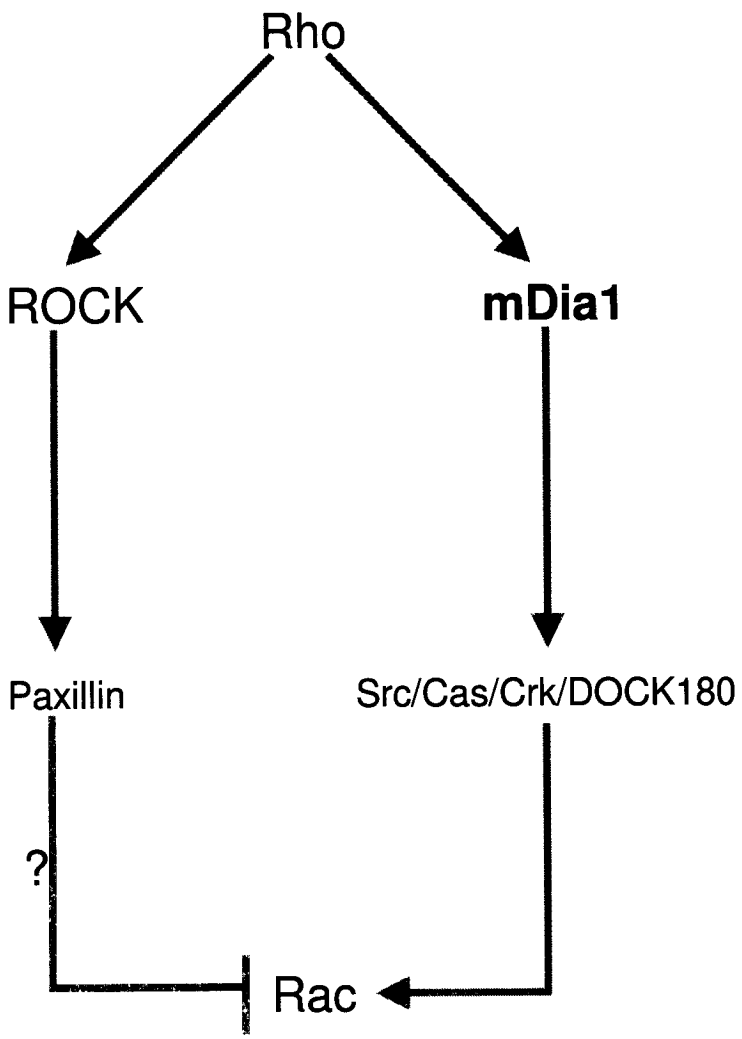

microtubule stabilization could restrict the ability of microtubules to target focal adhesion leading to their disassembly. Microtubule-induced focal adhesion disassembly could be mediated through kinesin (Krylyshkina *et al.,* 2002), or dynamin and focal adhesion kinase (Ezratty *et al.,* 2005). Also, microtubule stabilization could result in the sequestering of GEF-H1 (a Rho guanine exchange factor that is inhibited when bound to microtubules) in the cell body (Ren *et al.,* 1999; Krendel *et al.*, 2002; Zenke *et al.,* 2004). GEF-H1 sequestration could in turn lead to inactivation of Rho, preventing contraction and forward cell body translocation (Ren *et al.,* 1999; Krendel *et al.*, 2002).

It is tempting to speculate that during migration of CECFs, mDia1 activates Rac via Src to enhance membrane ruffling and migration, and it cooperates with ROCK to control the formation of longitudinal actin filaments that aid in the cell body translocation. When CECFs reach their target or become ready to stop migration, mDia1 is upregulated, resulting in an increase in focal adhesion formation, making the cells more adhesive and reducing motility.

Chapter four

The role of mDia1 in the initiation of polarization of chick embryo cardiac fibroblasts

Summary

mDia1 is a member of the formin family of proteins that plays important roles in establishing cell polarity. We tested the hypothesis that mDia1 is required for initiation of polarization in chick embryo cardiac fibroblasts (CECFs). We found that more than 60% of dissociated CECFs that were expressing constitutively active (CA)mDia1 had the circumferential F-actin phenotype, the same phenotype observed for dissociated CECFs expressing CA-LIM kinase or the inactive Xenopus ADF/cofilin (XAC)-S3E, or for cells treated with the F-actin stabilizing compound jasplakinolide. CAmDia1-expressing dissociated CECFs that were blocked at the circumferential stage had a higher phosphoAC/cofilin ratio than the control uninfected cells. Furthermore, when CECFs expressing CAmDia1 were co-infected with adenovirus expressing the constitutively active XAC-S3A, cells progressed to the next stage of polarization, the F-actin oriented phenotype. Thus, CAmDia1-expressing dissociated CECF results in the block of progression from the circumferential to the oriented stage by inactivating ADF/cofilin. These results are discussed in terms of the probable mechanism(s) by which mDia1 modulates ADF/cofilin activity.

Introduction

The establishment of cell polarity involves the asymmetrical distribution of organelles, and signaling proteins and the reorganization of the cytoskeleton (Nobes and Hall, 1999). Formin family of proteins is defined by the conserved FH1-FH2 unit (Castrillon and Wasserman, 1994; reviewed in Wedlich-Soldner and Li, 2004). Formins were identified in the early 1990s as proteins that are essential for cytokinesis (Castrillon and Wasserman, 1994; Chang, 1999; Feierbach and Chang, 2001; Tolliday *et al.,* 2002), limb development (Kleinebrecht *et al.,* 1982; Jackson-Grusby *et al.,* 1992; Vogt *et al.,* 1993), and cell polarity in yeast (Amatruda *et al.,* 1990). The main function of formin proteins during cell polarization in yeast is the nucleation and assembly of actin cables (Sagot *et al.,* 2002a; reviewed in Evangelista *et al.,* 2003). Actin cables are parallel bundles of actin filaments, stabilized by tropomyosins, which serve as tracks for myosin-driven transport of secretory vesicles, vacuoles, proteins, and mRNA to the bud neck (Bretscher, 2003). Also, actin cables deliver a microtubule plus-end complex comprising Bim1p and Kar9p (the yeast EB1 and APC homologues, respectively) to the bud (Evangelista *et al.,* 1997; Sagot *et al.,* 2002b). The spindle pole body (the yeast MTOC) is then pulled to the bud via a myosin-based motility along the actin cables (Lee *et al.,* 1999, Fujiwara *et al.,* 1999) (Figure 4.1).

The role of formin in enhancing actin assembly was discovered when CAmDia1 was overexpressed in cells; this overexpression induced the formation of stress fibers (Watanabe *et al.,* 1997; 1999; Satoh and Tominaga, 2001). Further biochemical studies indicated that the FH1–FH2 unit of formins is able to nucleate unbranched actin filaments

Figure 4.1
Formins control cell polarity in budding yeast through the assembly of actin cables. Bni1p (budding yeast formin) is activated by Rho GTPases (1). Activated Bni1p nucleates and assembles actin cables (2). Tropomyosin stabilizes the growing cables (3). Bni1p binds to the barbed ends of cables, thereby establishing their polarity. In turn, the polarized cables can then serve as tracks for myosin V, Myo2p, which migrates towards the barbed end of the actin cable to deliver secretory vesicles (4) and to orient the mitotic spindle (5). Adapted from Evangelista *et al.*, JCB 116, 2003.

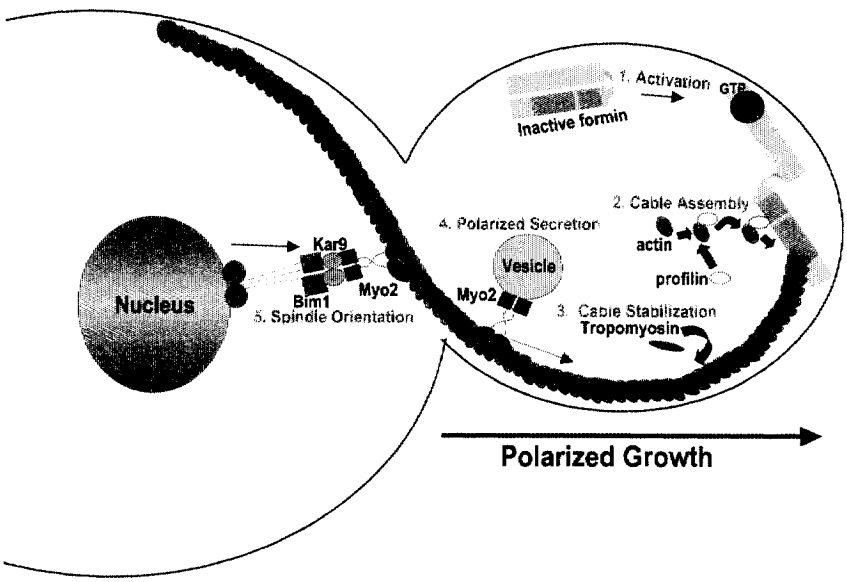

in vitro (Evangelista *et al.,* 2002; Sagot *et al.,* 2002a and b; Li and Higgs, 2003; Moseley *et al.,* 2004; Zigmond, 2003).

Proteins of the ADF/Cofilin (AC) family enhance the turnover of actin filaments by inducing filament depolymerization and severing (reviewed in Bamburg, 1999; Bamburg and Wiggan, 2002). The activities of ADF and cofilin are regulated by multiple mechanisms including pH (Yonezawa *et al.,* 1985; Hawkins *et al.,* 1993; Hayden et al., 1993), PIP_2 binding (Yonezawa *et al.,* 1990), competition with TM for actin binding (Bernstein and Bamburg, 1982; 1991; Ono and Ono, 2002), compartmentalization (Nishida *et al.,* 1987; Abe *et al.,* 1993; Ono *et al.,* 1993), mRNA stabilization (Minamide *et al.,* 1997), capping of the pointed end by spectrin (Schafer and Cooper, 1995), and phosphorylation/dephosphorylation at Ser3 (Morgan *et al.,* 1993; Agnew *et al.,* 1995).

LIM kinase (LIMK) is the kinase that phosphorylates AC at Ser3 (Arber *et al.,* 1998). Two isoforms of LIMK have been identified: LIMK1, and LIMK2. The Ser/Thr kinase PAK is activated upon binding either activated Rac or Cdc42, and phosphorylates and activates LIMK1 and LIMK2 (Edwards *et al.,* 1999). On the other hand, ROCK can phosphorylate and activate LIMK2 (Maekawa *et al.,* 1999; Sumi *et al.,* 2001).

Five different phosphatases have been identified to date that dephosphorylate AC proteins and thus activate them, although not all of these have been shown to be able to do so directly in vitro. The five phosphatases are the calcium-dependent protein phosphatase 2B (PP2B or calcineurin) (Baorto *et al.,* 1992; Okada *et al.,* 1996; Meberg *et al.,* 1998), protein phosphatase 1 and 2A (PP1 and PP2A), slingshot (SSH) (Niwa *et al.,* 2002), and chronophin (CIN), a member of the haloacid dehalogenase (HAD) superfamily (Gohla *et al.,* 2005). Three human and mouse isoforms of slingshot, SSH-1,

2, and 3, have been identified, each with long and short variants (Niwa *et al.,* 2002; Ohta *et al.,* 2003). hSSH-1L requires binding to F-actin for activity (Nagata-Ohashi *et al.,* 2004; Soosairajah *et al.,* 2005), and it can dephosphorylate active LIMK1 on Thr 508, and thus inhibit LIMK1, as well as activate AC proteins (Soosairajah *et al.,* 2005). Also, PAK4 can phosphorylate hSSH-1L inhibiting its phosphatase activity (Soosairajah *et al.,* 2005). Figure 4.2 summarizes the signal transduction pathways regulating the phosphorylation/ dephosphorylation of AC proteins.

mDia1 upregulates Rac via two different pathways, both of which are mediated by Src kinase (Tsuji *et al.,* 2002; Meng *et al.,* 2004). mDia1 and ROCK antagonize in Rho-dependent Rac activation (Tsuji *et al.,* 2002). There is a dichotomy of the signaling from Rho to Rac; one is mediated by mDia1 resulting in the phosphorylation of Cas through Src (Tsuji *et al.,* 2002). Cas is the Crk-associated substrate, a major tyrosine phosphorylated protein in cells transformed by v-crk and v-src oncogenes. Src kinase is responsible for integrin-dependent Cas phosphorylation (Klinghoffer *et al.,* 1999). Phosphorylated Cas provides binding sites for Crk and DOCK180 (O'Neill *et al.,* 2000), and DOCK180 in turn activates Rac (Kiyokawa *et al.,* 1998). This pathway is antagonized by ROCK, which phosphorylates paxillin (Tsuji *et al.,* 2002), and phosphorylated paxillin inhibits membrane ruffling and cell migration mediated by Cas-Rac pathway (Yano *et al.,* 2000; Tsuji *et al.,* 2002), a pathway important for invasion and metastasis of src- transformed cells (Brabek *et al.,* 2005) (Figure 4.3). The other signaling pathway leading to Rac activation downstream of Rho-mDia1-Src is mediated by DIP (Diaphanous interacting protein). Phosphorylated DIP activates Rac by mediating the

Figure 4.2
Signal transduction pathway regulating the phosphorylation/ dephosphorylation of ADF/Cofilin (AC) family of proteins. AC enhance the turnover of actin filaments by inducing filament depolymerization and severing. Limk phosphorylates AC at Ser3 inhibiting their activity, while slingshot (SSH) dephosphorylates AC proteins activating them. D= G-actin.ADP, DPi= G-actin.ADP.Pi, and T= G-actin.ATP. Adapted from Bamburg, Annu. Rev. Cell Dev. Biol. 15, 1999.

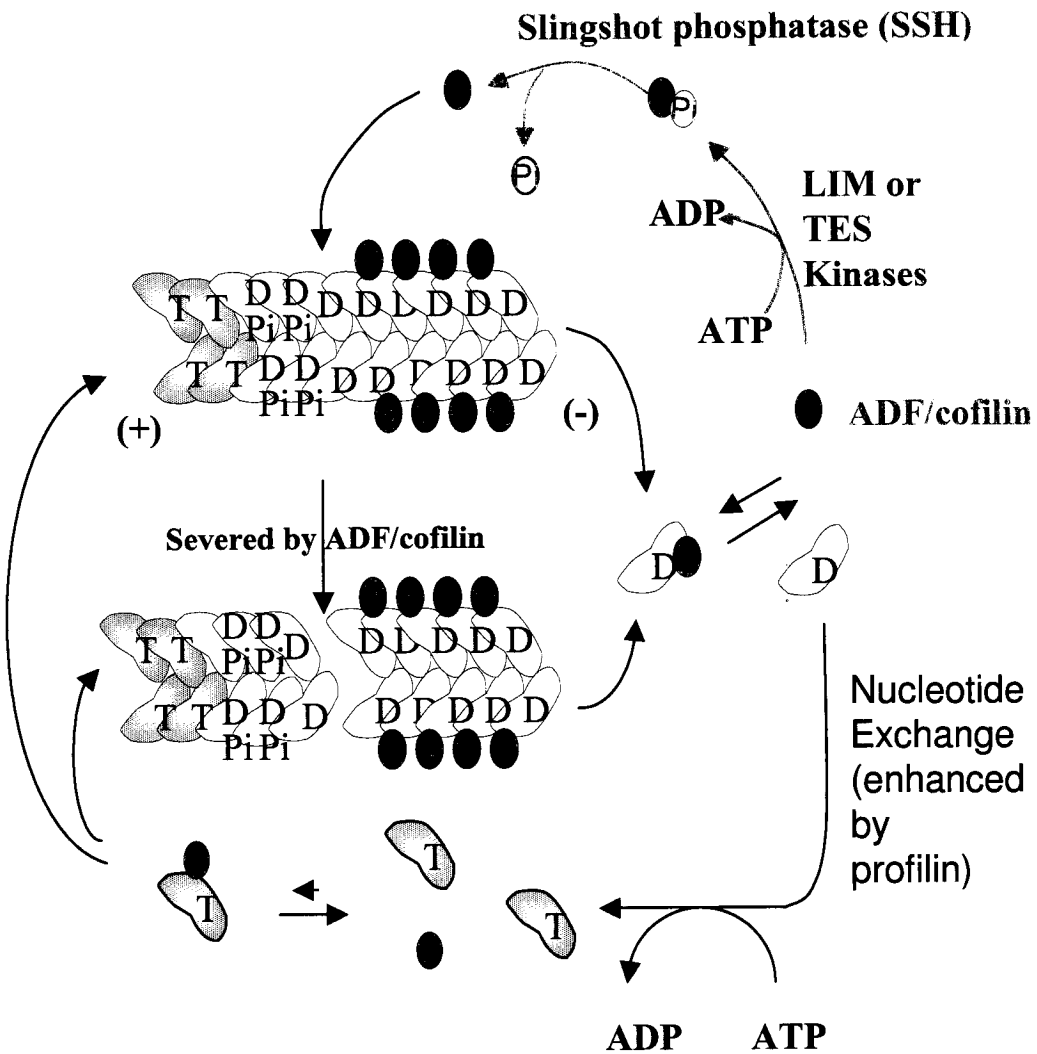

Figure 4.3
mDia1 and ROCK antagonize in Rho-dependent Rac activation.

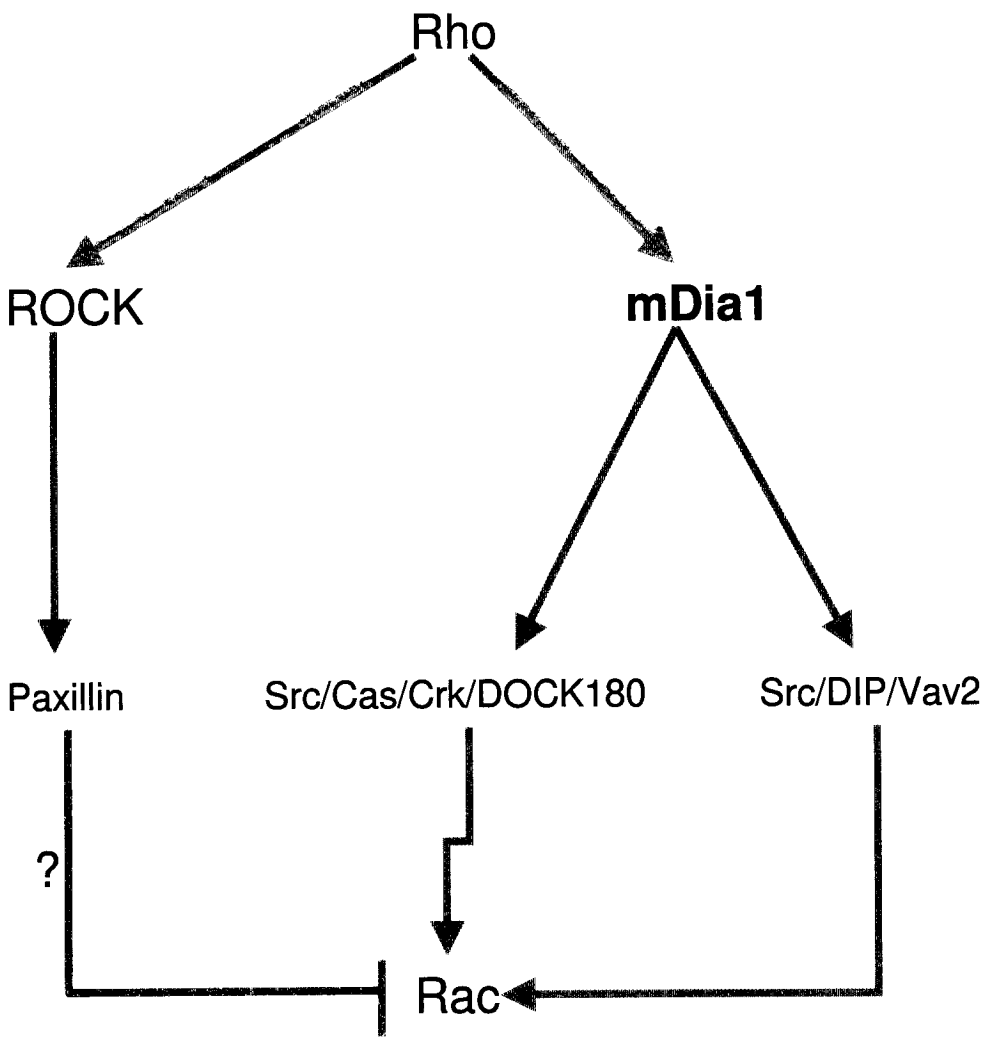

Src-induced phosphorylation of Vav2 (Figure 4.3) (Meng *et al.,* 2004). Vav2 is a Rac GEF; in its phosphorylated state it activates Rac (Crespo *et al.,* 1997).

Here we show that more than 60% of dissociated CECFs that were expressing CAmDia1 had the circumferential F-actin phenotype after one hour of plating, compared to 23% in control cells. The same phenotype observed for dissociated CECFs infected with adenovirus expressing either CA-LIMK or XAC-E3 or for cells treated with jasplakinolide. When CECFs expressing CAmDia1 were co-infected with adenovirus expressing XAC-A3, cells progressed to the next stage of polarization, the F-actin oriented phenotype. CAmDia1-infected CECFs had a higher phosphoAC/cofilin ratio than the control uninfected cells. Thus, CAmDia1-expressing CECFs blocks progression from the circumferential to the oriented stage by inactivating ADF/cofilin. The most probable mechanisms by which this occurs are discussed.

Material and methods

Preparation of dissociated CECFs

Explants from E7 or E8 chick hearts were prepared as described in chapter three. The explants were transferred into cloning rings and incubated at 37°C overnight in a 5% CO_2/air incubator. Approximately one million cells are needed for each preparation so each heart was enough for one cloning ring. The explants were infected for 48 h, followed by treatment with collagenase (2.5 mg/ml) for 30 min or until the explants are completely dissociated. The dissociated cells were then washed 3X with PBS + 10% FBS and once with CECF medium to remove the viruses and the collagenase, each washing

step was followed by centrifugation at 785x g for 3-5 min. Finally, dissociated CECFs were suspended in CECF medium and plated on matrigel-coated coverslips incubated at 37°C for 1 hour. The cells were then fixed and stained for F-actin.

Co-infection of dissociated CECFs

The cells from explants that were infected with two adenoviruses simultaneously failed to survive collagenase dissociation, although cells infected well with both viruses as determined from explant cultures. To obtain an unpolarized population of doubly infected cells, we co-infected explants in the cloning rings for 24h, plated them for another 24h and then treated the cells with 5 μM LatrunculinA (LatA) (actin depolymerizing drug) for one hour. CECFs treated with 5μM LatA for 1 h, round up, but when the LatA is removed the cells undergo the same actin organizational stages (described below) observed when explants are dissociated before plating, and the same percentage of cells re-polarize (50-75%). After the LatA washout with 3-5X PBS and 1X with CECFs medium, the cells were incubated at 37°C for an hour and then fixed and stained for F-actin.

Time-lapse microscopy

To follow the effect of mDia1 on actin dynamics during the initiation of polarization, chick cardiac explants were co-infected with adenoviruses expressing CAmDia1 and fluorescent-actin (GFP- and mRFP-actin adenoviruses; made by Alisa Shaw) for 24h, and then plated on matrigel-coated coverslips for another 24h. The cells were treated with 5 μM LatA for one hour, and the LatA then washed out. CECF medium was replaced with 1:1 mix of F12 and DMEM medium overlayered with dimethyl polysiloxane (Sigma) to reduce evaporation while allowing gas exchange. Imaging of live

cells started 5-10 min after the LatA washout. Actin dynamics in live cells were observed on a Nikon (TE 2000-U) inverted microscope equipped with an UltraView spinning disk confocal microscope (Perkin Elmer) and an Orca II-ER cooled CCD camera (Hamamatsu) controlled by Metamorph (Universal Imaging). Temperature was maintained by a Heatwave-30 temperature-controlled chamber (World Precision Instruments) and an Intracell objective heater (Bioptechs). Imaging was performed with a 60X, 1.4 NA plan-apo Nikon objective.

Immunocytochemistry

CECFs were fixed in 4% formaldehyde in cytoskeleton buffer (CB: 10 mM MES pH 6.1, 138 mM KCl, 3 mM $MgCl_2$ and 2 mM EGTA pH 7.0) plus 0.32 M sucrose (CBS) for 20-30 min. After fixation, the cells were permeabilized with 0.5% TritonX-100 in PBS for 5-10 min, and then blocked with 2% goat serum in TBS for 45min-1h. CECFs were incubated with primary antibodies for 1 h at room temperature or overnight at 4°C. The primary antibodies used were mouse anti-cofilin (Mab 22; Abe *et al.,* 1989) at 1:200 and rabbit anti-total-pAC (4321; Meberg *et al.,* 1998) (1:1000) (diluted into 1% BSA + TBS). After 3-5 washes with TBS, the cells were incubated with FITC-conjugated goat anti-mouse and Alexa-647-conjugated goat anti- rabbit secondary antibodies (both at 1:400 into 1% BSA + TBS) (Molecular Probes). For actin staining, Alexa-350-, or FITC-, or TR- conjugated phalloidin was used (1:50 into 1% BSA + TBS) (Molecular Probes). Images were acquired using a 12-bit cooled CCD camera (Photometrcis Coolsnap ES) and a 60X, 1.4 NA oil objective on an inverted Nikon microscope controlled by Metamorph software (Universal imaging).

Results

Morphology and actin organization during the initiation of polarization of dissociated CECFs

After dissociation and plating, most CECFs polarize during the first 1-2 h and then migrate at the same rate as polarized cells moving out of an explant. By 12 hours fewer than 20% of the cells remain polarized and migrating (Dawe, Ph.D. thesis); therefore to study initiation of polarization, cells were fixed 1 h after plating, or followed by time-lapse microscopy from 10 min-1 h after plating.

Time-lapse imaging and immunocytochemistry showed that dissociated CECFs polarize in distinct stages as defined by morphology and the organization of their actin cytoskeleton (Dawe, Ph.D. thesis). Cells adhere to the coverslip within 5 min of plating. The fibroblasts are initially symmetrical and discoid in shape (fried egg morphology; Figure 4.4 A, B, and C). The first sign of a break in the symmetry is an inwards movement or "bite-like" loss of part the plasma membrane (Figure 4.4 E, arrow). This "bite" enlarges over the course of approximately 10 min until a distinct crescent-shaped portion is taken out of one side of the cell (Figure 4.4 F, G). This site for the break in symmetry ultimately becomes the cell tail. Upon completion of the formation of the polarized shape, the cell begins to migrate (Figure 4.4 H, I). However, the cells are not synchronized and therefore, at any given time point, there is a mixed population of cell morphologies at different stages of polarization. Due to this fact, the percentage of fully polarized migrating cells was never more than 30-35 % at any one time.

CECFs were infected with adenovirus encoding a fluorescent protein-labeled actin so that actin organization could be followed in live cells by time-lapse microscopy.

Figure 4.4
Actin reorganization during the morphological polarization of dissociated CECFs. 5 min post plating, the cells were mostly flattened on the cover slip (Fried egg morphology; A, B). Within the cell body, actin was distributed in a radial arrangement outwards from the centre (B), and/or oriented in a circumferential array (C). From the radial or the circumferential stages, the cells became slightly ovoid with the actin filaments arranged in an oriented fashion across the longest length (D). The bite site always occurred at a position perpendicular to the actin orientation (E, arrow). The bite site enlarged through inward movement of membrane (F and G). During the stabilization of the tail, the first actin bundles oriented perpendicular to the leading edge appeared (H, arrow). These increased in number, accompanied by a decrease in the number of actin bundles oriented perpendicular to the break in symmetry, until by the time that the cell was fully polarized, the majority of the actin was oriented perpendicular to the leading edge (I).

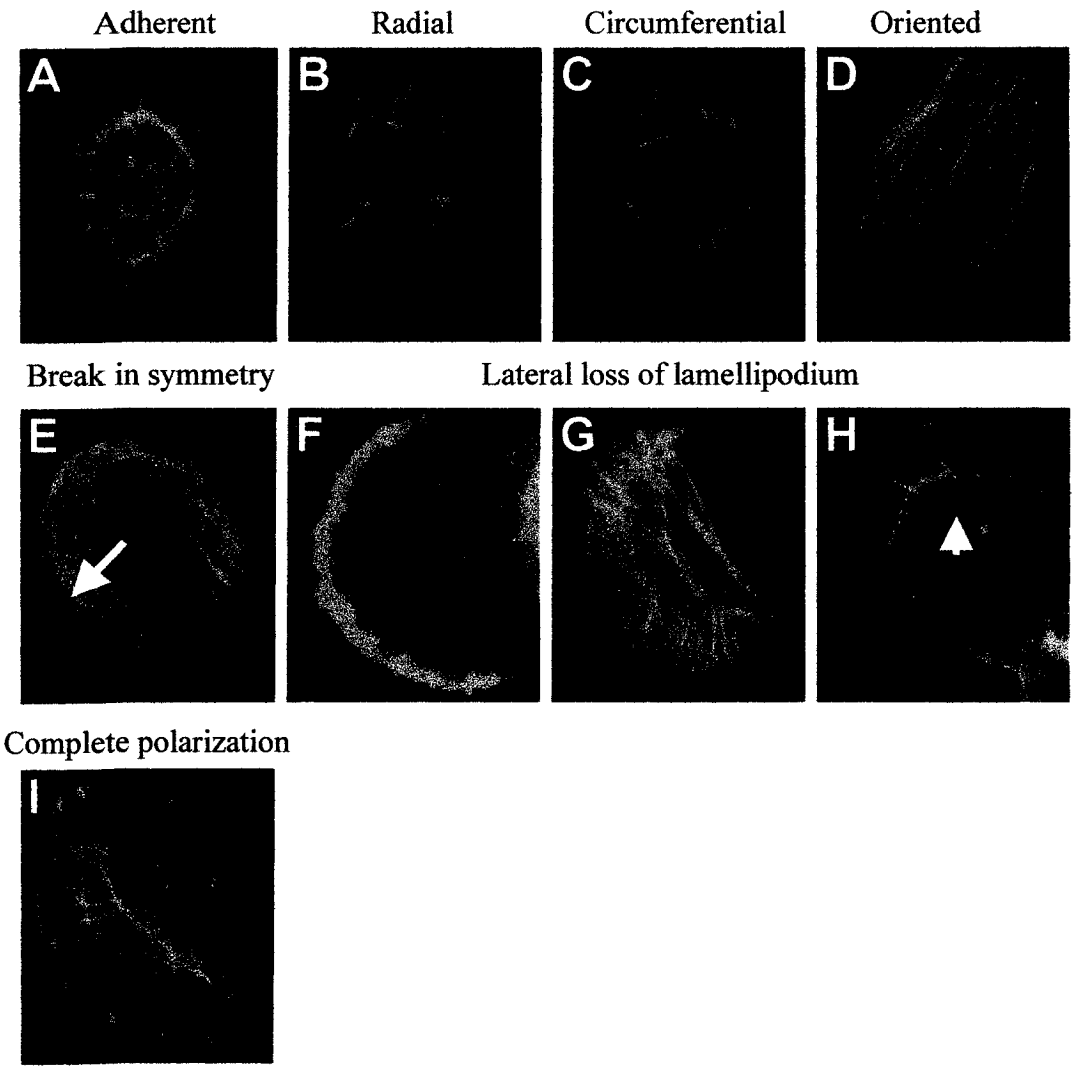

A number of actin rearrangements occurred while the cell shape was still discoid. After 5 min, the cells were mostly flattened on the cover slip (Figure 4.4 A, B). Within the cell body, actin was distributed in a radial arrangement outwards from the centre (Figure 4.4 B), and/or oriented in a circumferential array (Figure 4.4 C). From the radial or the circumferential stages, the cells became slightly ovoid with the actin filaments arranged in an oriented fashion across the longest length (Figure 4.4 D). The cells always went through this oriented stage in order for the break symmetry to occur. The bite site always occurred at a position perpendicular to the actin orientation (Figure 4.4 E). The bite site enlarged through inward movement of membrane (Figure 4.4 F and G). During the stabilization of the tail, the first actin bundles oriented perpendicular to the leading edge appeared (Figure 4.4 H, arrow). These increased in number, accompanied by a decrease in the number of actin bundles oriented perpendicular to the break in symmetry, until by the time that the cell was fully polarized, the majority of the actin was oriented perpendicular to the leading edge (Figure 4.4 I).

Overexpression of CAmDia1 inhibits the progression from circumferential to oriented stages in dissociated CECFs

CECF explants were infected with CAmDia1 adenovirus for 48 h (efficient expression of gene of interest in CECFs requires 48 hours of incubation with adenoviruses), dissociated and plated on matrigel-coated cover slips. After 1 h of incubation at 37°C, the cells were fixed and stained for actin. By 1 h after plating only 8.2% of CAmDia1-infected cells were polarized, as compared to 33% and 30.5% in uninfected and GFP-infected CECFs, respectively (Table 4.1, $n \geq 200$ from 3

Table 4.1 role of mDia1 in the initiation of polarization I.
The numbers are percentages of total expressing cells in each category ± SEM. n = at least 200 over 3 experiments. Scoring of cells in each category was done 1 h post plating.

	Control Uninfected	GFP-expressing	CAmDia1-expressing
Adherent	4.4% ± 0.7	3.8% ± 0.8	10.1% ± 2.0
Radial	4.8% ± 0.6	6.0% ± 2.0	4.0% ± 2.0
Circumferential	18.7% ± 3.0	17.1% ± 2.0	38.4% ± 4.0
Oriented	26.6% ± 8.0	27.0% ± 2.0	10.9% ± 1.0
Break of symmetry	1.1% ± 0.2	1.9% ± 0.8	5.8% ± 1.0
Lateral loss of lamellipodium	6.1% ± 0.2	4.8% ± 1.0	8.6% ± 1.0
Complete polarization	31.0% ± 2.0	30.5% ± 1.0	8.2% ± 1.0
Non-polarized	3.7% ± 0.6	5.7% ± 0.4	12.4% ± 5.0
Disorganized	3.6% ± 0.6	3.2% ± 0.3	1.6% ± 0.8

experiments). When the cell numbers were expressed as the percentages of cells before the break of symmetry (radial-oriented), and not the percentages of the whole cell population, CAmDia1-infected cells showed almost a 3- fold increase in circumferential morphology, and 2.5 fold reduction in the oriented morphology compared to uninfected or GFP-infected cells (Table 4.2). Interestingly, CAmDia1-infected CECFs that were stuck in the circumferential stage, a phenotype known as the "C.D." morphology [actin bundles fill the cytoplasm almost completely, as compared to the doughnut-like shape of control CECFs in the circumferential stage (See figure 4.4 C)] (L. Cramer, personal communication) (Figure 4.5), showed the same phenotype as cells overexpressing CA-LIMK- and XAC-S3E, as well as cells treated with the F-actin stabilizing compound, jasplakinolide. The same phenotype was also observed in cells infected with CAmDia1 adenovirus constructed in the pShuttle system (no fluorescent protein being expressed) (data not shown), and when actin dynamics of CAmDia1-expressing cells was observed by time-lapse microscopy.

Chick cardiac explants were co-infected with adenoviruses expressing CAmDia1 and GFP or mRFP-actin. Actin dynamics in these doubly infected cells was observed by time-lapse microscopy. Five min after the LatA wash out, the cells started to spread out (Figure 4.6 A), and acquire the fried egg morphology (Figure 4.6 B and C). The first sign of the circumferential F-actin phenotype appeared around 20 min after LatA wash out (Figure 4.6 D). Cells of this phenotype continued to accumulate 20 min later (Figure 4.6 E and F). Two adhesion points at opposite sides then appeared (Figure 4.6 G, arrows). A "bite" started from one side of the cell (Figure 4.6 G, open arrow), but it did not enlarge

Table 4.2 role of mDia1 in the initiation of polarization II.
The numbers are expressed as the percentages of cells before the break of symmetry (radial-oriented), and not the percentages of the whole population of cells.

	Control Uninfected	GFP-expressing	CAmDia1-expressing
Disorganized	4.7% ± 0.6	3.6% ± 1.0	3.5% ± 2.0
Radial	19.0% ± 4.0	14.0% ± 2.0	7.0% ± 5.0
Circumferential	22.7% ± 3.0	22.4% ± 2.0	66.7% ± 2.0
Oriented	53.4% ± 4.0	60.0% ± 3.0	22.8% ± 3.0

Figure 4.5
CAmDia1-expressing dissociated CECFs were blocked at the circumferential stage, and exhibited the "C.D." morphology.
A-C) CAmDia1-infected CECFs that were stained with TR-phalloidin, showing the "C.D." morphology.

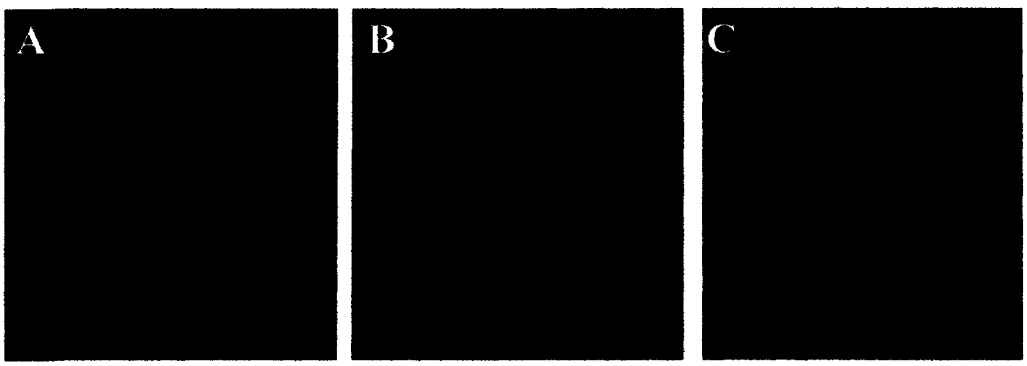

Figure 4.6
Actin dynamics in CAmDia1-expressing dissociated CECFs.
Still images of CECFs that were co-infected with GFP.actin and CAmDia1/RFP expressing adenoviruses .Time is in h: min: sec.

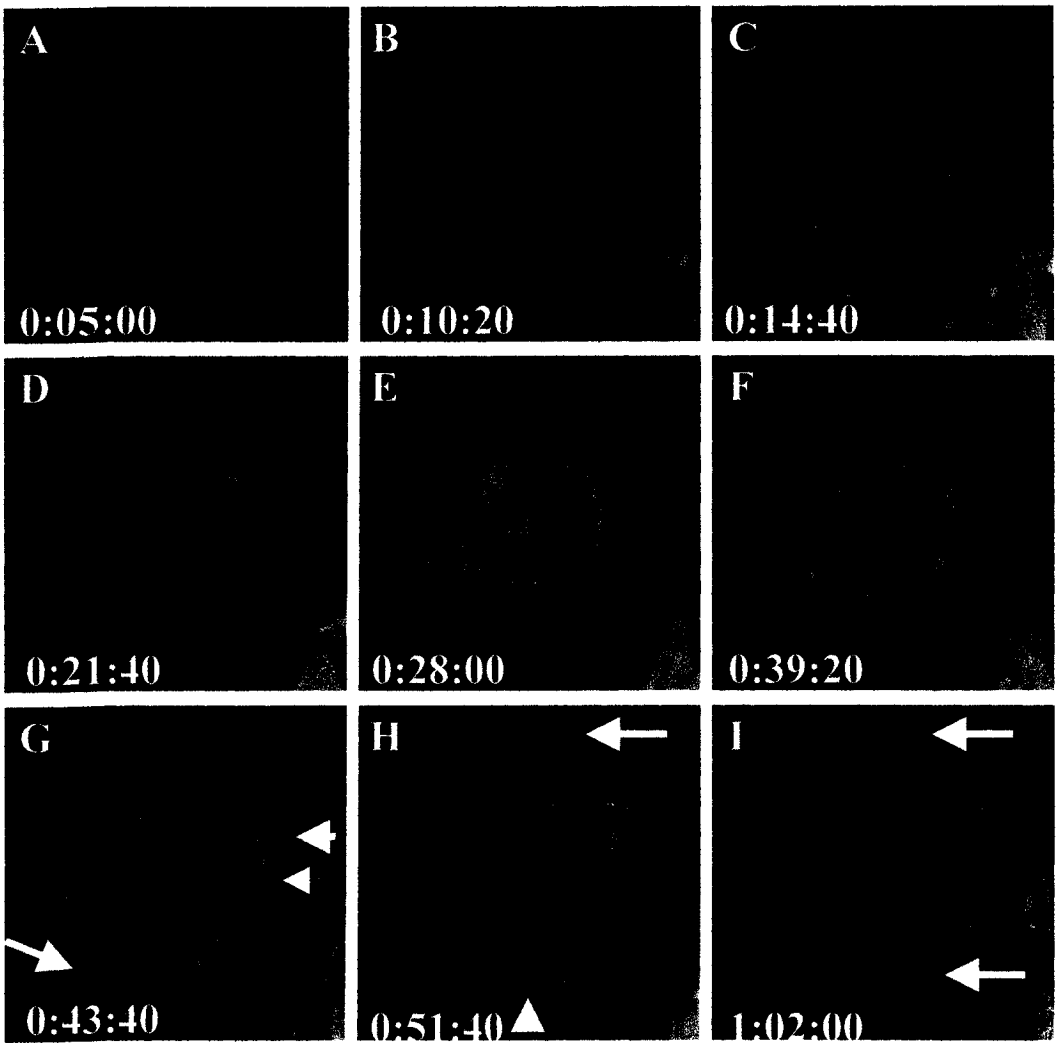

to result in a polarized morphology, and instead the cell developed two lamellipodia at opposite ends (Figure 4.6 H and I, arrows).

Because cells trapped in the CD morphology due to the overexpression of active LIMK1 could be rescued through the expression of the non-phospho-regulated form of Xenopus ADF/cofilin (XAC-S3A) (Dawe, Ph.D. Thesis), we tested to see if the coexpression of XAC-S3A could rescue the CAmDia1 phenotype. CECF explants were co-infected for 24 h with both CAmDia1 and XAC-A3 adenovirus, plated for another 24h and then treated with LatA for an hour. LatA was washed out, and the cells were incubated for an extra hour at 37°C. The cells were then fixed and stained for actin. Cells that co-expressed XAC-S3A progressed to the oriented stage. However, the expression of XACS3A was not able to rescue complete polarization of these cells as it did for cells expressing active LIMK1 (Tables 4.3 and 4.4).

CAmDia1-expressing CECFs have a higher phosphoAC/cofilin ratio than the control cells

Dissociated CECFs that were infected with CAmDia1, CALIMK, or XAC-S3E, or treated with jasplakinolide were blocked at the same stage, i.e. the circumferential stage, and they develop the same phenotype (C.D. morphology). All of these cells progressed to the oriented phenotype or beyond through the expression of XAC-S3A. We hypothesized that the overexpression of CAmDia1 could have enhanced phosphorylation of AC proteins in CECFs. To test this hypothesis, chick cardiac explants were infected with CAmDia1 adenovirus that was constructed using the pShuttle vector system so that there was no fluorescent protein expression. Forty-eight hours post infection, the explants were dissociated and cells plated on matrigel-coated coverslips for

Table 4.3 Co-infection of CAmDia1 with XAC-A3 rescued the increase in circumferential actin bundle formation caused by CAmDia1 expression in CECF, but failed to rescue the loss of polarization. Scoring of cells in each category was done 1 h post plating.

	Control Uninfected	CAmDia1-expressing	CAmDia1+ XAC-A3 expressing
Adherent	4.4% ± 0.7	10.1% ± 2.0	2.9%
Radial	4.8% ± 0.6	4.0% ± 2.0	5.1%
Circumferential	18.7% ± 3.0	[illegible]	[illegible]
Oriented	26.6% ± 8.0	10.9% ± 1.0	28.5%
Break of symmetry	1.1% ± 0.2	5.8% ± 1.0	5.1%
Lateral loss of lamellipodium	6.1% ± 0.2	8.6% ± 1.0	4.4%
Complete polarization	31.0% ± 2.0	[illegible]	[illegible]
Non-polarized	3.7% ± 0.6	12.3% ± 5.0	37.9%
Disorganized	3.6% ± 0.6	1.6% ± 0.8	2.2%

Table 4.4 Co-infection of CAmDia1 with XAC-A3 rescued the increase in circumferential actin bundle formation caused by CAmDia1 expression in CECF

	Control Uninfected	CAmDia1-expressing	CAmDia1+ XAC-A3 expressing
Disorganized	4.7% ± 0.6	3.5% ± 2.0	5.1%
Radial	19.0% ± 4.0	7.0% ± 5.0	11.9%
Circumferential	22.7% ± 3.0	[illegible]	16.4%
Oriented	53.0% ± 4.0	22.5% ± 3.0	[illegible]

1 h at 37°C, and then fixed and stained for actin, cofilin, and total phosphorylated ADF/cofilin. The same protocol was followed with control uninfected CECFs. We could not use control infected cells, i.e. GFP-expressing only, because we had to use three fluorescent colors in immunostaining, FITC- and Alexa-647- conjugated secondary antibodies for cofilin and pAC staining, respectively, and Alexa-350 phalloidin for actin to identify the circumferential stage (Figure 4.7). The average intensity of total pAC and cofilin staining was measured. CAmDia1-infected dissociated CECFs that were blocked at the circumferential stage had a 40% increase in phosphoAC/total cofilin ratio (0.82, n = 47 cells, two separate experiment) than the control uninfected cells (0.58, n = 42 cells, two separate experiments) (Figure 4.8).

Discussion

To assess the role(s) played by mDia1 in the initiation of cell polarity, dissociated fibroblasts were used. These cells must reestablish polarity after plating and thus can be used for studying the earliest steps in initiation of polarization, which cannot be observed for fibroblasts migrating out of an explant. Furthermore, polarized CECFs round up when treated with 5μM LatA for 1h, but when LatA is removed the cells undergo the same stages of actin organization observed in plated dissociated explants and the same percentages of cells re-polarize (50-75%). Thus, by either dissociating chick cardiac explants before plating or treating plated explants with LatA after cells have migrated out, one can follow the steps of cell polarization from the fried egg morphology to the onset of migration and all cells that polarize appear to undergo the same stages of actin organization in sequence (Figure 4.4).

Figure 4.7
pAC/cofilin staining in dissociated CECFs at the circumferential stage. Dissociated control uninfected (A-C) and CAmDia1-infecetd (D-F) were fixed and stained for pAC (A and D), cofilin (B and E), and actin (C and F). Actin filament staining was performed to identify the circumferential stage.

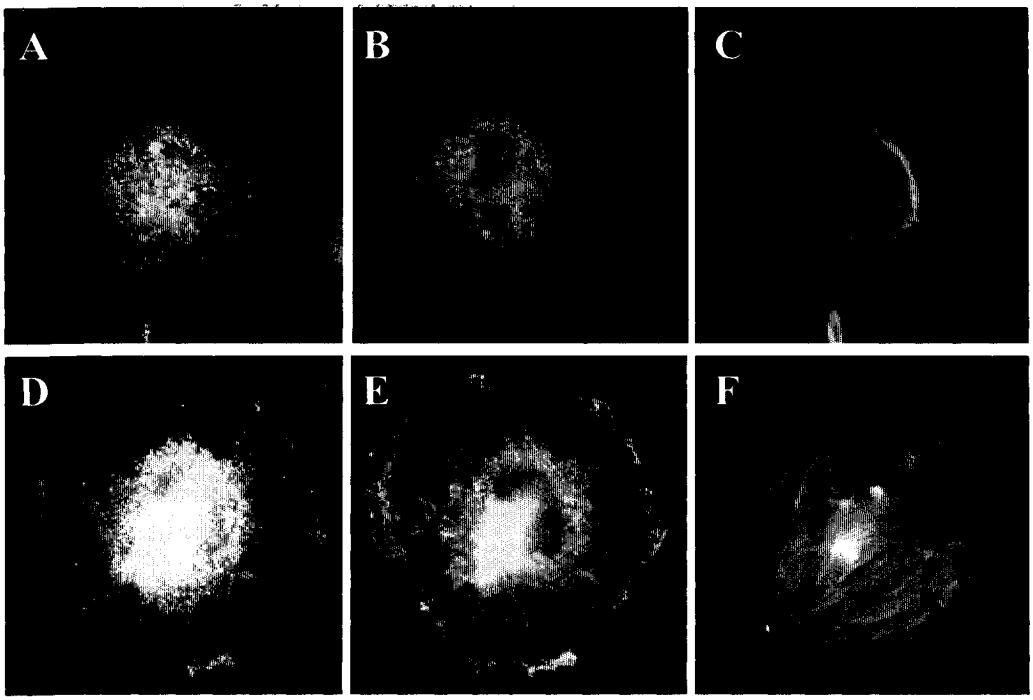

Figure 4.8
CAmDia1-infected dissociated CECFs blocked at the circumferential stage had a higher phosphoAC/cofilin ratio than the control uninfected cells. The average intensity of total pAC and cofilin staining was measured using Metamorph software, and the ratio of total pAC/cofilin intensities was calculated. CAmDia1-expressing dissociated CECFs that were blocked at the circumferential stage had a higher phosphoAC/cofilin ratio (0.82, n = 47 cells, two separate experiment) than the control uninfected cells (0.58, n = 42 cells, two separate experiments) ($P < 0.001$).

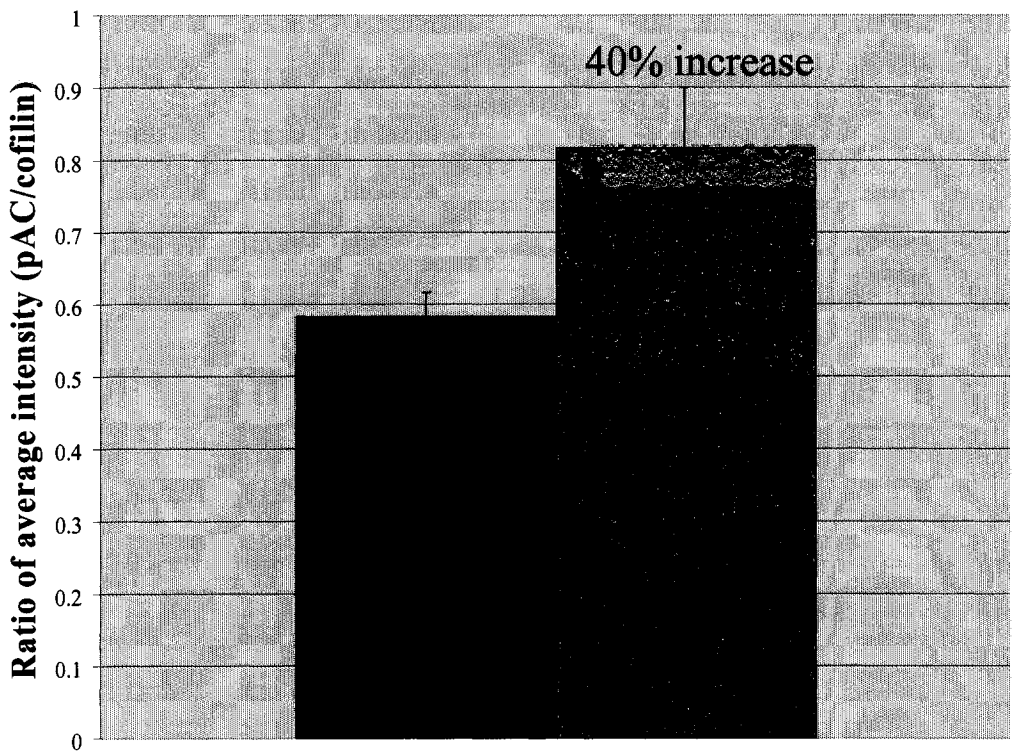

In order for CECFs to attain a polarized morphology, those with circumferential actin, CD phenotype, must go through the oriented stage in order for the break symmetry to occur. It was shown that both the severing and depolymerizing activities of AC were required for the dissociated CECFs to progress from the circumferential to the oriented stage (Dawe, Ph.D. thesis). CAmDia1-expressing cells co-infected with adenovirus expressing XAC-S3A progressed from the circumferential phenotype to the oriented stage (Table 4.3 and 4.4). CAmDia1-infected dissociated CECFs that were blocked at the circumferential stage had a 40% increase in phosphoAC/total cofilin ratio when compared to the control uninfected cells (Figure 4.8).

There are several possible ways in which mDia overexpression could affect ADF/cofilin phosphorylation. mDia1 upregulates Rac via two Src-mediated pathways. The first pathway is through Cas/Crk/DOCK180 (Tsuji *et al.,* 2002), and the second is via DIP/Vav2 (Meng *et al.,* 2004) (See Figure 4.3). We propose that overexpression of mDia1 activates Rac, which in turn activates PAK. Phosphorylation and inactivation of ADF/cofilin could be mediated by activation of LIMK (Edwards *et al.,* 1999) or inhibition of SSH-1L (Soosairajah *et al.,* 2005). Inhibition of AC proteins in CAmDia1-infected dissociated CECFs resulted in the block of progression from the circumferential to the oriented stage (Figure 4.9).

Alternatively, microtubule dynamics apparently are required for maintaining a pool of active ADF/cofilin at the leading edge of migrating CECFs (Cramer *et al.,* submitted). The stabilization of microtubules plus ends by mDia overexpression could decrease the dynamics needed for maintaining active ADF/cofilin. Whether dynamic

Figure 4.9
A proposed model for the relation between mDia1 and AC during the initiation of polarization of CECFs. mDia1 upregulates Rac via two Src-mediated pathways; the first is through Cas/Crk/DOCK180, and the second is via DIP/Vav2. We propose that overexpression of mDia1 activated Rac, which in turn activated PAK; this activation resulted in phosphorylation of AC proteins and thus inhibiting them. Phosphorylation of AC could have been mediated by activation of LIMK or inhibition of SSH. Inhibition of AC proteins in CAmDia1-infected dissociated CECFs resulted in the block of progression from the circumferential to the oriented stage.

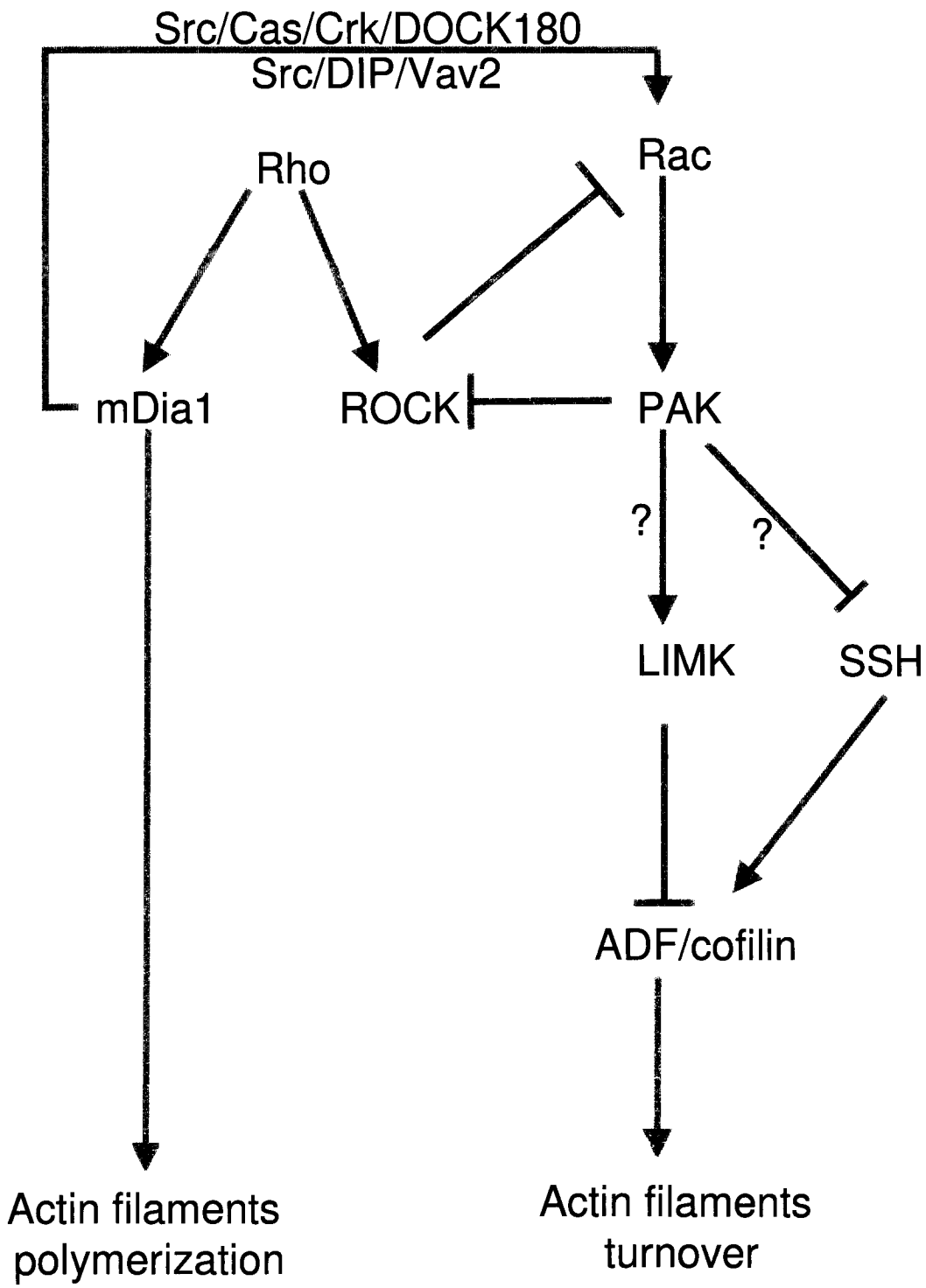

microtubule plus ends are involved in activating an ADF/cofilin phosphatase or inhibiting a kinase is unknown at this time.

Chapter five

General discussion

Summary

The first main objective of the work presented here was to assess the role of mDia1 in the cytoskeleton reorganization during the migration of spontaneously polarized cells, i.e. chick embryo cardiac fibroblasts (CECFs). mDia1 involvement in actin and microtubule dynamics has been studied in adherent cells such as HeLa and COS-7 cells (Watanabe *et al.,* 1997; 1999; Ishizaki *et al.*, 2001), and in cells that have been induced to polarize either by wounding a confluent monolayer of NIH 3T3 cells (wound healing assay; Magdalena *et al.,* 2003), or chemokine-induced migration in lymphocytes (Vicente-Manzanares *et al.,* 2003). We found that overexpression of a constitutively active mutant (CA) of mDia1 induced the loss of polarization in CECFs and slowed down the motility of chick fibroblasts, while DNmDia1-expressing CECFs failed to migrate out of an explant.

CAmDia1-infected CECFs showed an increase in focal adhesion area (both in number and size). This would result in making the CAmDia1-expressing cells more adhesive to the matrigel substrate and could slow down migration rates. We also found that CAmDia1 expression in CECFs caused a 73% increase in microtubule plus ends penetrating the lamellipodium, more than 60% of which were classified as stabilized due

to the appearance of Glu-tubulin at their plus ends. This enhanced microtubule stabilization could in turn reduce the pool of active ADF/cofilin needed for protrusion and migration of CECFs (Dawe *et al.,* 2003; Cramer *et al.,* submitted), and will also restrict the ability of microtubules to target focal adhesions, which has been implicated in focal adhesion disassembly (Kaverina *et al.,* 1999; Small *et al.,* 2002; Ezratty *et al.,* 2005).

The second objective was to investigate the role of mDia1 during the initiation of cell polarization. We used the dissociated CECF system, which allowed us to study the earliest steps of polarization. We found a three fold increase in the numbers of CAmDia1-expressing cells that accumulated in the circumferential actin stage compared to the controls and these cells had a higher pAC/cofilin ratio (less active AC) than control uninfected cells. Co-expressing the non-phosphoregulated mutant of Xenopus AC (XAC-S3A) allowed the CAmDia1-expressing cells to proceed to the next step of polarization, the oriented actin stage. This finding suggests that overexpression of CAmDia1 in dissociated CECFs resulted in the inactivation of AC proteins, which prevented their progression from the circumferential to the oriented stage.

Future directions

Investigating the role of mDia1 during CECF migration and initiation of polarization in the absence of ROCK activity

When CECFs were treated with 10 μM Y-27632 (ROCK inhibitor), they polarized normally but they had aberrant tail formation (an abnormally large tail region), and the tail failed to retract (Dawe, Ph.D. thesis). It would be interesting to study cell

polarization in CAmDia1-expressing cells in the absence of ROCK activity, because ROCK and mDia activation are the only two known direct downstream effector targets of active Rho (Watanabe *et al.,* 1999). The ROCK pathway activates myosin II, so in the presence of the ROCK inhibitor the CAmDia effects should be less complicated to interpret. Thus we would like to investigate if the reduced ROCK activity could prevent the accumulation of circumferential actin cables caused by CAmDia1 overexpression, since the C.D. morphology may result in part through myosin II contractile mechanisms. Also, polarized CECFs do not form tails in the presence of blebbistatin, a myosin II inhibitor (Dawe Ph.D., Thesis). Thus, it would be of great interest to see what effect CAmDia1 would have on tail morphology in the absence of ROCK activity, where some myosin II might be activated via ROCK independent mechanisms (e.g. calcium activation of myosin light chain kinase). Treating NIH 3T3 fibroblasts overexpressing CAmDia1 with Y-27632 increased their migration rate in a wound healing assay (Magdalena *et al.,* 2003), suggesting the presence of other mechanisms for myosin II activation. However, the simplicity of the formin family proteins expressed in the CECFs will make it easier to follow and interpret mDia-dependent events, especially in the analysis of lamellipodial protrusion.

Studies on mDia function in the absence of endogenous mDia

Studies in which we express different mDia domains would be enhanced further if we could develop an siRNA for the single cytoplasmic CECF mDia homolog, Gg2. Such an siRNA construct could be expressed as a hairpin RNA using adenovirus, as has been done by Kevin Flynn in our lab for downregulating cofilin. The cardiac explant system is ideal for these studies because explant cells can be infected with 100% efficiency in

suspension and held in suspension for up to 5 days before plating with no loss in the number of cells initially establishing polarity (Louise Cramer, personal communication). Even for relatively stable proteins (turnover half live of 24 h), this time period should allow for significant down regulation in Gg2 levels (<5% of starting level). Thus, in these cells we could fully analyze the role in cell polarization and migration of the different mDia isoforms found in mammalian cells in the absence of endogenous interfering proteins.

Testing the hypothesis that dynamic microtubule tips are associated with ADF/cofilin phosphatase

In chapter three, we found that 65% of the microtubule plus ends penetrating the lamellipodium in CAmDia1-expressing CECFs were stabilized. Cramer *et al.,* (submitted) provide evidence that that dynamic microtubules deliver to the leading edge signaling molecules, either an ADF/cofilin phosphatase (e.g. slingshot) or molecules that work upstream to activate the phosphatase. Three lines of evidence were presented. First, dynamic microtubules are found penetrating into polarized, but not non-polarized, lamellipodia where they are associated with regions of activated (dephosphorylated) AC. Second, taxol stabilized microtubules do not have the region of active AC around their tips. Third, polarized cells lose their directional migration when nocodazole, is added and microtubules disappear. However, polarized migration is rescued in nocodazole by overexpression of active AC, strongly suggesting that the function of microtubules in leading edge protrusion is to provide this pool of active AC.

Therefore, stabilization of microtubule tips should minimize the localized activation of AC required for lamellipodium protrusion. We can test this hypothesis in

two ways. First, we can infect CECFs with CAmDia1 adenovirus, and then localize the active pool of AC through image ratioing after immunostaining for phosphoAC and total cofilin. By staining for Glu-microtubules along with phosphoAC we can identify location of stable and dynamic microtubule tips and see if the amount of phosphoAC differs in the vicinity of each. Alternatively, we can treat CECFs with low levels of taxol to stabilize only a small percentage of microtubule tips. If we do these studies in cells expressing a fluorescently labeled EB1 (e.g. EB1-GFP; Figure 5.1) we can differentiate dynamic microtubules (have EB1 associated) versus stable microtubules (no EB1 label). Cells can be fixed and immunostained for ratio imaging to directly observe the pAC/cofilin ratios found around the ends of dynamic microtubules. If our hypothesis is correct, then CAmDia1-expressing and taxol-treated CECFs should have a higher pAC/cofilin ratio around stable microtubule tips than around the dynamic tips.

Dissecting the pathway from mDia1 to ADF/cofilin

The results from chapter four indicate that overexpression of CAmDia1 results in an increase in pAC/cofilin ratio when compared to uninfected CECFs. We proposed a model in which we predict that the overexpression of CAmDia1 activates Rac (Tsuji *et al.,* 2002; Meng *et al.,* 2004), which in turn activates PAK (Edwards *et al.,* 1999); this activation results in phosphorylation of AC proteins thus inhibiting them. Phosphorylation of AC could be mediated via activation of LIMK (Arber *et al.,* 1998; Yang *et al.,* 1998), or inhibition of slingshot (Soosairajah *et al.,* 2005). We can test several steps of this pathway. First we can directly measure Rac activity in cell by a Rac FRET assay (Nishiya *et al.,* 2005). Alternatively, we can express DN-PAK or DN-LIMK

Figure 5.1
EB1.GFP-expressing CECF. Still images (A-C) of CECF expressing EB1.GFP, D) image overlay of A,B, and C. Time is min: sec.

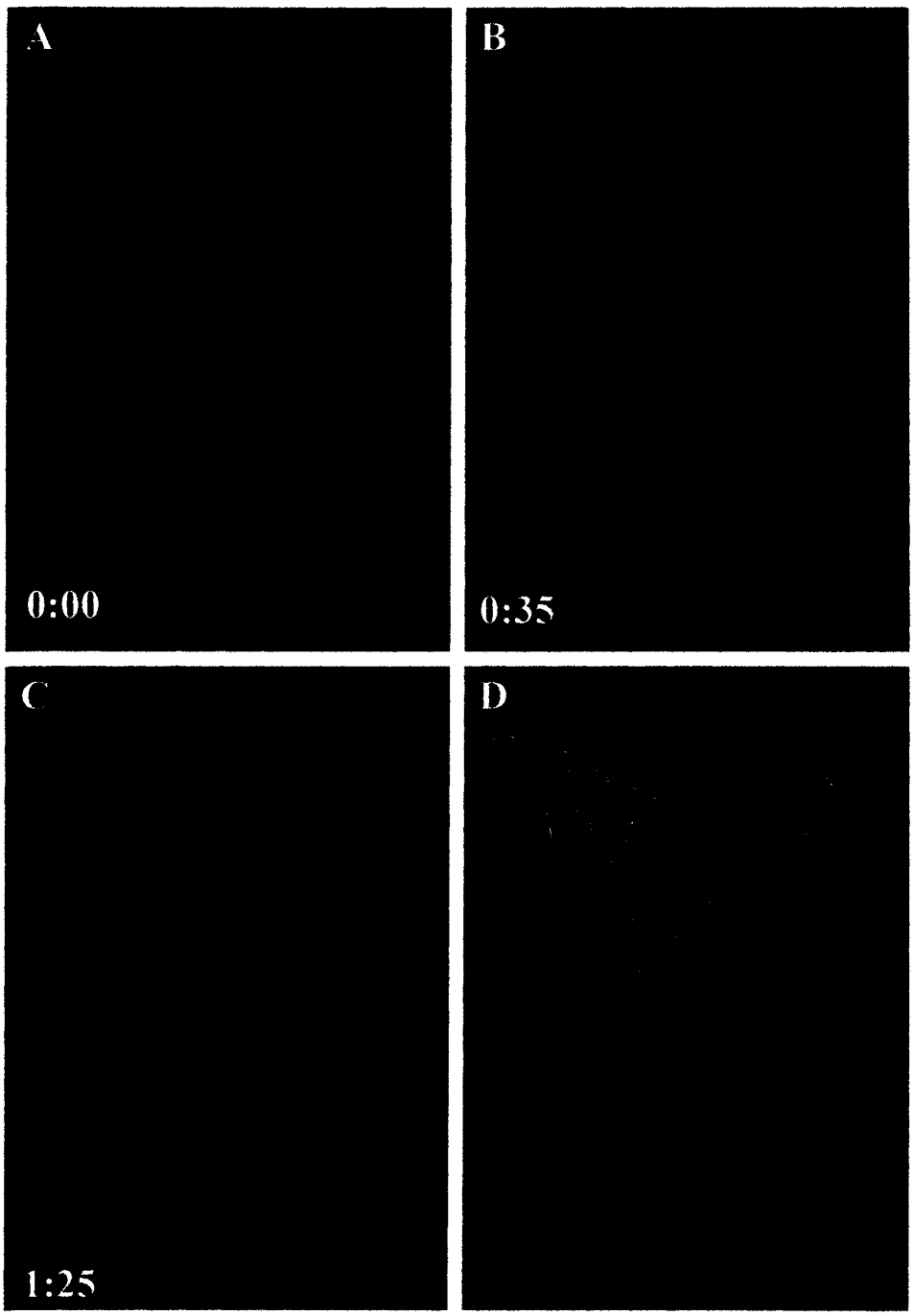

to see if we can block the cell accumulation at the circumferential stage caused by CAmDia1 overexpression.

Studying the role of stathmin during the migration of CECFs

Overexpression of a non-phosphorylatable stathmin (a microtubule depolymerizing protein) in CECFs could have an effect on microtubules similar to nocodazole and thus cause formation of multiple lamellipodia through reducing the pool of active AC required for leading edge protrusion (Cramer *et al.,* submitted). Stathmin is regulated by phosphorylation on multiple sites by at least three different kinases (Beretta *et al.,* 1993; Leighton *et al.,* 1993; Brattsand *et al.,* 1994; Marklund *et al.,* 1994; le Gouvello *et al.,* 1998), each of which decreases its ability to destabilize microtubules. To see if stathmin and mDia work in opposite ways to regulate cell polarity through microtubule dynamics and AC activity regulation, we can determine the effects of overexpressing the non-phosphorylatable stathmin (CA-stathmin) on establishing cell polarity in CECFs and see if co-expression of CAmDia antagonizes the effect.

Further studies on rescued DNmDia1-expressing CECFs

In chapter three, we found that co-expressing DNmDia1 with wt-paxillin rescued the ability of DNmDia1-expressing CECFs to migrate out of the explants, but almost all of the cells were non-polarized. In order to study actin dynamics (using fluorescent-actin adenoviruses), or microtubule-plus end dynamics (EB1.GFP), we need to test the efficiency of infecting CECFs with three viruses simultaneously, because the only migrating cells are the ones that co-express DNmDia1 and paxillin. If we can get reasonable infectivity with three viruses, then we can investigate microtubule-plus ends dynamics, if the tips are more dynamic than in control cells, this could suggest the

frequency of focal adhesion targeting by microtubules in DNmDia1-expressing CECFs is higher than control cells which could explain the faulty adhesion phenotype. Also, we can stain for stabilized microtubules in the rescued cells and if the percentage of stable microtubules is lower in these cells, then this would confirm that the absence of mDia1 in DNmDia1-expressing cells caused the reduction in microtubule stabilization which in turn led to the increase in the frequency of focal adhesion targeting by microtubules.

REFERENCES

Abe, H., Ohshima, S., Obinata, T. (1989). A cofilin-like protein is involved in the regulation of actin assembly in developing skeletal muscle. *J. Biochem (Tokyo)* **106**, 696-702.

Abe, H., Nagaoka, R., Obinata, T. (1993). Cytoplasmic localization and nuclear transport of cofilin in cultured myotubes. *Exp. Cell Res.* **206**, 1-10.

Adams, J.M., Houston, H., Allen, J., Lints, T., Harvey, R. (1992). The hematopoietically expressed vav proto-oncogene shares homology with the dbl GDP-GTP exchange factor, the bcr gene and a yeast gene (CDC24) involved in cytoskeletal organization. *Oncogene* **7**, 611-618.

Agnew, B.J., Minamide, L.S., Bamburg, J.R. (1995). Reactivation of phosphorylated actin depolymerizing factor and identification of the regulatory site. *J. Biol. Chem.* **270**, 17582-17587.

Aguda, A. H., Burtnick, L. D., Robinson, R.C. (2005).The state of the filament. *EMBO Rep.* **6**, 220-226.

Ahern-Djamali, S.M., Bachmann, C., Hua, P., Reddy, S.K., Kastenmeier, A.S., Walter, U., Hoffmann, F.M. (1999). Identification of profilin and src homology 3 domains as binding partners for Drosophila enabled. *Proc. Natl. Acad. Sci. U S A* **96**, 4977-4982.

Ahmad, F.J., Yu, W., McNally, F.J., Baas, P.W. (1999). An essential role for katanin in severing microtubules in the neuron. *J. Cell Biol.* **145**, 305-315.

Aizawa, H., Kawasaki, H., Murofushi, H., Kotani, S., Suzuki, K., Sakai, H.(1989). A common amino acid sequence in 190-kDa microtubule-associated protein and tau for the promotion of microtubule assembly. *J. Biol. Chem.* **264**, 5885-5890.

Akhmanova, A., Hoogenraad, C.C., Drabek, K., Stepanova, T., Dortland, B., Verkerk, T., Vermeulen, W., Burgering, B.M., De Zeeuw, C.I., Grosveld, F., Galjart, N. (2001). Clasps are CLIP-115 and -170 associating proteins involved in the regional regulation of microtubule dynamics in motile fibroblasts. *Cell* **104**, 923-935.

Alblas, J., Ulfman, L., Hordijk, P., Koenderman, L. (2001). Activation of Rhoa and ROCK are essential for detachment of migrating leukocytes. *Mol. Biol. Cell* **12**, 2137-2145.

Allen, C., Borisy, G.G. (1974). Structural polarity and directional growth of microtubules of Chlamydomonas flagella. *J. Mol. Biol.* **90**, 381-402.
Allen, W.E., Zicha, D., Ridley, A.J., Jones, G.E. (1998). A role for Cdc42 in macrophage chemotaxis. *J. Cell Biol.* **141**, 1147-1157.

Almenar-Queralt, A., Lee, A., Conley, C.A., Ribas de Pouplana, L., Fowler, V.M. (1999). Identification of a novel tropomodulin isoform, skeletal tropomodulin, that caps actin filament pointed ends in fast skeletal muscle. *J. Biol. Chem.* **274**, 28466-28475.

Amatruda, J.F., Cannon, J.F., Tatchell, K., Hug, C., Cooper, J.A. (1990). Disruption of the actin cytoskeleton in yeast capping protein mutants. *Nature* **344**, 352-354.

Amos, L., Klug, A. (1974). Arrangement of subunits in flagellar microtubules. *J. Cell Sci.* **14**, 523-549.

Arakawa, Y., Bito, H., Furuyashiki, T., Tsuji, T., Takemoto-Kimura, S., Kimura, K., Nozaki, K., Hashimoto, N., Narumiya, S. (2003). Control of axon elongation via an SDF-1alpha/Rho/mDia pathway in cultured cerebellar granule neurons. *J. Cell Biol.* **161**, 381-391.

Arber, S., Barbayannis, F.A., Hanser, H., Schneider, C., Stanyon, C.A., Bernard, O., Caroni, P. (1998). Regulation of actin dynamics through phosphorylation of cofilin by LIM-kinase. *Nature* **393**, 805-809.

Baas, P.W., Qiang, L. (2005). Neuronal microtubules: when the MAP is the roadblock. *Trends Cell Biol.* **15**, 183-187.

Bailly, M., Macaluso, F., Cammer, M., Chan, A., Segall, J.E., Condeelis, J.S. (1999). Relationship between Arp2/3 complex and the barbed ends of actin filaments at the leading edge of carcinoma cells after epidermal growth factor stimulation. *J. Cell Biol.* **145**, 331-345.

Ballweber, E., Hannappel, E., Huff, T., Mannherz, H.G. (1997). Mapping the binding site of thymosin beta4 on actin by competition with G-actin binding proteins indicates negative co-operativity between binding sites located on opposite subdomains of actin. *Biochem. J.* **327**, 787-793.

Ballweber, E., Giehl, K., Hannappel, E., Huff, T., Jockusch, B.M., Mannherz, H.G. (1998). Plant profilin induces actin polymerization from actin: beta-thymosin complexes and competes directly with beta-thymosins and with negative co-operativity with DNase I for binding to actin. *FEBS Lett.* **425**, 251-255.

Bamburg J.R. (1999). Proteins of the ADF/cofilin family: essential regulators of actin dynamics. *Annu. Rev. Cell Dev. Biol.* **15**, 185-230.

Bamburg, J.R., Wiggan, O.P. (2002). ADF/cofilin and actin dynamics in disease. *Trends Cell Biol.* **12**, 598-605.
Banerjee, M., Worth, D., Prowse, D.M., Nikolic, M. (2002). Pak1 phosphorylation on t212 affects microtubules in cells undergoing mitosis. *Curr. Biol.* **12**, 1233-1239.

Baorto, D.M., Mellado, W., Shelanski, M.L. (1992). Astrocyte process growth induction by actin breakdown. *J. Cell Biol.* **117**,357-367.

Barth, A.I., Siemers, K.A, Nelson, W.J. (2002). Dissecting interactions between EB1, microtubules and APC in cortical clusters at the plasma membrane. *J. Cell Sci.* **115**, 1583-1590.

Bashour, A.M., Fullerton, A.T., Hart, M.J., Bloom, G.S. (1997). IQGAP1, a Rac- and Cdc42-binding protein, directly binds and cross-links microfilaments. *J. Cell Biol.* **137**, 1555-1566.

Belmont, L.D., Orlova, A., Drubin, D.G., Egelman, E.H. (1999). A change in actin conformation associated with filament instability after Pi release. *Proc. Natl. Acad. Sci. U S A* **96**, 29-34.

Beretta, L., Dobransky, T., Sobel, A. (1993). Multiple phosphorylation of stathmin. Identification of four sites phosphorylated in intact cells and in vitro by cyclic AMP-dependent protein kinase and p34cdc2. *J. Bio.l Chem.* **268**, 20076-20084.

Berkner, K.L., Sharp, P.A. (1983). Generation of adenovirus by transfection of plasmids. *Nucleic Acids Res.* **11**, 6003-6020.

Bernard, O., Ganiatsas, S., Kannourakis, G., Dringen, R. (1994). Kiz-1, a protein with LIM zinc finger and kinase domains, is expressed mainly in neurons. *Cell Growth Differ.* **5**, 1159-1171.

Bernstein, B.W., Bamburg, J.R. (1982). Tropomyosin binding to F-actin protects the F-actin from disassembly by brain actin-depolymerizing factor (ADF). *Cell Motil.* **2**, 1-8.

Bershadsky, A.D., Tint, I.S., Neyfakh, A.A. Jr., Vasiliev, J.M. (1985). Focal contacts of normal and RSV-transformed quail cells. Hypothesis of the transformation-induced deficient maturation of focal contacts. *Exp. Cell Res.* **158**, 433-444.

Best, A., Ahmed, S., Kozma, R., Lim, L. (1996). The Ras-related GTPase Rac1 binds tubulin. *J. Biol. Chem.* **271**, 3756–3762.

Bienz, M., Hamada, F. (2004). Adenomatous polyposis coli proteins and cell adhesion. *Curr. Opin. Cell Biol.* **16**, 528-535.

Bito, H., Furuyashiki, T., Ishihara, H., Shibasaki, Y., Ohashi, K., Mizuno, K., Maekawa, M., Ishizaki, T., Narumiya, S. (2000). A critical role for a Rho-associated kinase,

p160ROCK, in determining axon outgrowth in mammalian CNS neurons. *Neuron* **26**, 431-441.

Blanchoin, L., Pollard, T.D. (1998). Interaction of actin monomers with Acanthamoeba actophorin (ADF/cofilin) and profilin. *J. Biol. Chem.* **273**, 25106-25111.

Brabek, J., Constancio, S.S/, Siesser, P.F., Shin, N.Y., Pozzi, A., Hanks, S.K. (2005). Crk-associated substrate tyrosine phosphorylation sites are critical for invasion and metastasis of SRC-transformed cells. *Mol. Cancer Res.* **3**, 307-315.

Brattsand, G., Marklund, U., Nylander, K., Roos, G., Gullberg, M. (1994). Cell-cycle-regulated phosphorylation of oncoprotein 18 on Ser16, Ser25 and Ser38. *Eur. J. Biochem.* **220**, 359-68.

Bretscher, A. (2003). Polarized growth and organelle segregation in yeast: the tracks, motors, and receptors. *J. Cell Biol.* **160**, 811-816.

Brieher, W.M., Coughlin, M., Mitchison, T.J. (2004). Fascin-mediated propulsion of Listeria monocytogenes independent of frequent nucleation by the Arp2/3 complex. *J. Cell Biol.* **165**, 233-242.

Brown, A., Li, Y., Slaughter, T., Black, M.M. (1993). Composite microtubules of the axon: quantitative analysis of tyrosinated and acetylated tubulin along individual axonal microtubules. *J. Cell Sci.* **104**, 339-52.

Bryce, N.S., Schevzov, G., Ferguson, V., Percival, J.M., Lin, J.J., Matsumura, F., Bamburg, J.R., Jeffrey, P.L., Hardeman, E.C., Gunning, P., Weinberger, R.P. (2003). Specification of actin filament function and molecular composition by tropomyosin isoforms. *Mol. Biol. Cell* **14**, 1002-1016.

Bulinski, J.C., Gundersen, G.G. (1991). Stabilization of post-translational modification of microtubules during cellular morphogenesis. *Bioessays* **13**, 285-293.

Burns, R. G. (1991). Alpha-, beta-, and gamma-tubulins: sequence comparisons and structural constraints. *Cell Motil. Cytoskeleton* **20**, 181–189.

Burridge, K., Chrzanowska-Wodnicka, M. (1996). Focal adhesions, contractility, and signaling. *Annu. Rev. Cell Dev. Biol.* **12**, 463-518.

Cai, G., Zhang, J., Liu, L., Shen, Q. (2005). Successful treatment of experimental autoimmune myocarditis by adenovirus-mediated gene transfer of antisense CIITA. *J. Mol. Cell Cardiol.* **38**, 593-605.

Calderwood, D.A., Tuckwell, D.S., Eble, J., Kuhn, K., Humphries, M.J. (1997). The integrin alpha1 A-domain is a ligand binding site for collagens and laminin. *J. Biol. Chem.* **272**, 12311-12317.

Casella, J.F., Torres, M.A. (1994). Interaction of Cap Z with actin. The NH2-terminal domains of the alpha 1 and beta subunits are not required for actin capping, and alpha 1 beta and alpha 2 beta heterodimers bind differentially to actin. *J. Biol. Chem.* **269**, 6992-6998.

Castrillon, D.H., Gonczy, P., Alexander, Sh., Rawson, R., Eberhart, Ch., Viswanathan, S., DiNardot, S., Wasserman, S. (1993). Toward a molecular genetic analysis of spermatogenesis in *Drosophila melanogastec* characterization of male-sterile mutants generated by single P element mutagenesis. *Genetics* **135**, 489-505.

Castrillon, D.H., Wasserman, S.A. (1994). Diaphanous is required for cytokinesis in Drosophila and shares domains of similarity with the products of the limb deformity gene. *Development* **120**, 3367-3377.

Chan, D.C., Wynshaw-Boris, A., Leder, P. (1995). Formin isoforms are differentially expressed in the mouse embryo and are required for normal expression of fgf-4 and shh in the limb bud. *Development* **121**, 3151-3162.

Chang, F. (1999). Movement of a cytokinesis factor cdc12p to the site of cell division. *Curr. Biol.* **9**, 849-852.

Chang, F., Peter, M. (2002). Formins Set the Record Straight. *Science* **297**, 531-532.

Chang, W., Webster, D.R., Salam, A.A., Gruber, D., Prasad, A., Eiserich, J.P., Bulinski, J.C. (2002). Alteration of the C-terminal amino acid of tubulin specifically inhibits myogenic differentiation. *J. Biol. Chem.* **277**, 30690-30698.

Chen, H., Bernstein, B.W., Bamburg, J.R. (2000). Regulating actin-filament dynamics in vivo. *Trends Biochem. Sci.* **25**, 19-23.

Chhabra, D., Bao, S., dos Remedios, C.G. (2002) The distribution of cofilin and DNase I in vivo. *Cell Res.* 12, 207-214.

Chen, H., Bernstein, B.W., Bamburg, J.R. (2000). Regulating actin-filament dynamics in vivo. *Trends Biochem. Sci.* **25**, 19-23.

Chrzanowska-Wodnicka, M., Burridge, K. (1996). Rho-stimulated contractility drives the formation of stress fibers and focal adhesions. *J. Cell Biol.* **133**, 1403-1415.

Clark, E.A., King, W.G., Brugge, J.S., Symons, M., Hynes, R.O. (1998). Integrin-mediated signals regulated by members of the rho family of GTPases. *J. Cell Biol.* **142**, 573-586.

Copeland, J.W., Treisman, R. (2002). The Diaphanous-related formin mDia1 controls serum response factor activity through its effects on actin polymerization. *Mol. Biol. Cell* **13**, 4088-4099.

Copeland, J.W., Copeland, S.J., Treisman, R. (2004). Homo-oligomerization is essential for F-actin assembly by the formin family FH2 domain. *J. Biol. Chem.* **279**, 50250-50256.

Corsi, A., Perry, S.V. (1958). Some observations on the localization of myosin, actin and tropomyosin in the rabbit myofibril. *Biochem. J.* **68**, 12-17.

Cramer, L.P., Siebert, M., Mitchison, T.J. (1997). Identification of novel graded polarity actin filament bundles in locomoting heart fibroblasts: implications for the generation of motile force. *J. Cell Biol.* **136**, 1287-1305.

Cramer, L.P. (1999). Organization and polarity of actin filament networks in cells: implications for the mechanism of myosin-based cell motility. *Biochem. Soc. Symp.* **65**, 173-205.

Cramer, L.P, Bamburg, J.R., Mseka, T. Microtubules spatially regulate ADF/cofilin to control cell polarity and directed migration. *Nat. Cell. Biol.*, Submitted.

Crespo, P., Schuebel, K.E., Ostrom, A.A., Gutkind, J.S., Bustelo, X.R. (1997). Phosphotyrosine-dependent activation of Rac-1 GDP/GTP exchange by the vav proto-oncogene product. *Nature* **385**, 169-172.

Critchley, D.R. (2000). Focal adhesions - the cytoskeletal connection. *Curr. Opin. Cell Biol.* **12**,133-139.

Curmi, P.A., Maucuer, A., Asselin, S., Lecourtois, M., Chaffotte, A., Schmitter, J.M., Sobel, A. (1994). Molecular characterization of human stathmin expressed in Escherichia coli: site-directed mutagenesis of two phosphorylatable serines (Ser-25 and Ser-63). *Biochem. J.* **300**, 331-8.

Curmi, P.A., Andersen, S.S., Lachkar, S., Gavet, O., Karsenti, E., Knossow, M., Sobel, A. (1997). The stathmin/tubulin interaction in vitro. *J. Biol. Chem.* 272, 25029-25036.

Dammermann, A., Desai, A., Oegema, K. (2003). The minus end in sight. *Curr. Biol.* **13**, R614-R624.

David-Pfeuty, T., Erickson, H.P., Pantaloni, D. (1977). Guanosinetriphosphatase activity of tubulin associated with microtubule assembly. *Proc. Natl. Acad. Sci. U S A* **74**, 5372-5376.

Dawe, H.R., Minamide, L.S., Bamburg, J.R., Cramer, L.P. (2003). ADF/cofilin controls cell polarity during fibroblast migration. *Curr. Biol.* **13**, 252-257.

Dawe, H.R. Ph.D. thesis. MRC Molecular and Cellular Biology Laboratory and Department of Biology, University College London, London, UK.

de la Pompa, J.L., James, D., Zeller, R. (1995). Limb deformity proteins during avian neurulation and sense organ development. *Dev. Dyn.* **204**, 156-167.

De Maria, A., Arruti, C. (2003). Bovine DNase I: gene organization, mRNA expression, and changes in the topological distribution of the protein during apoptosis in lens epithelial cells. *Biochem. Biophys. Res. Commun.* **312**, 634-641.

Dermardirossian, C., Bokoch, G.M. (2005). GDIs: central regulatory molecules in Rho GTPase activation. *Trends Cell Biol.* [Epub ahead of print].

Derry, J.M., Ochs, H.D., Francke, U. (1994). Isolation of a novel gene mutated in Wiskott-Aldrich syndrome. *Cell* **78**, 635-644.

Desai, A., Mitchison, T.J. (1997). Microtubule polymerization dynamics. *Annu. Rev. Cell Dev. Biol.* **13**, 83-117.

DesMarais, V., Ichetovkin, I., Condeelis, J., Hitchcock-DeGregori, S.E. (2002). Spatial regulation of actin dynamics: a tropomyosin-free, actin-rich compartment at the leading edge. *J. Cell Sci.* **115**, 4649-4660.

DesMarais, V., Ghosh, M., Eddy, R., Condeelis, J. (2005). Cofilin takes the lead. *J. Cell Sci.***118**, 19-26.

Diamantopoulos, G.S., Perez, F., Goodson, H.V., Batelier, G., Melki, R., Kreis, T.E., Rickard, J.E. (1999). Dynamic localization of CLIP-170 to microtubule plus ends is coupled to microtubule assembly. *J. Cell Biol.* **144**, 99-112.

Didry, D., Carlier, M.F., Pantaloni, D. (1998). Synergy between actin depolymerizing factor/cofilin and profilin in increasing actin filament turnover. *J. Biol. Chem.* **273**, 25602-25611.

Doe, C.Q. (2001). Cell polarity: the PARty expands. *Nat. Cell Biol.* **3**, E7-E9.

Domanski, M., Hertzog, M., Coutant, J., Gutsche-Perelroizen, I., Bontems, F., Carlier, M.F., Guittet, E., van Heijenoort, C. (2004). Coupling of folding and binding of thymosin beta4 upon interaction with monomeric actin monitored by nuclear magnetic resonance. *J. Biol. Chem.* **279**, 23637-23645.

dos Remedios, C.G., Chhabra, D., Kekic, M., Dedova, I.V., Tsubakihara, M., Berry, D.A., Nosworthy, N.J. (2003). Actin binding proteins: regulation of cytoskeletal microfilaments. *Physiol. Rev.* **83**, 433-473.

Doucas, H., Garcea, G., Neal, C.P., Manson, M.M., Berry, D.P. (2005). Changes in the Wnt signalling pathway in gastrointestinal cancers and their prognostic significance. *Eur. J. Cancer* **41**, 365-379.

Drewes, G., Trinczek, B., Illenberger, S., Biernat, J., Schmitt-Ulms, G., Meyer, H.E., Mandelkow, E.M., Mandelkow, E. (1995). Microtubule-associated protein/microtubule affinity-regulating kinase (p110mark). A novel protein kinase that regulates tau-microtubule interactions and dynamic instability by phosphorylation at the Alzheimer-specific site serine 262. *J. Biol .Chem.* **270**, 7679-2688.

Duncan, F.E., Moss, S.B., Schultz, R.M., Williams, C.J. (2005). PAR-3 defines a central subdomain of the cortical actin cap in mouse eggs. *Dev. Biol.* **280**, 38-47.

Ebashi, S., Kodama, A. (1966). Native tropomyosin-like action of troponin on trypsin-treated myosin B. *J. Biochem.* **60**, 733-734.

Eddy, R.J, Pierini, L.M., Maxfield, F.R. (2002). Microtubule asymmetry during neutrophil polarization and migration. *Mol. Biol. Cell* **13**, 4470-4483.

Eden, S., Rohatgi, R., Podtelejnikov, A.V., Mann, M., Kirschner, M.W. (2002). Mechanism of regulation of WAVE1-induced actin nucleation by Rac1 and Nck. *Nature* **418**, 790-793.

Edwards, D.C., Sanders, L.C., Bokoch, G.M., Gill, G.N. (1999). Activation of LIM-kinase by Pak1 couples Rac/Cdc42 GTPase signalling to actin cytoskeletal dynamics. *Nat. Cell Biol.* **1**, 253-259.

Etienne-Manneville, S. (2004). Actin and Microtubules in Cell Motility: Which One is in Control? *Traffic* **5**, 470-477.

Etienne-Manneville, S., Hall, A. (2001). Integrin-mediated activation of Cdc42 controls cell polarity in migrating astrocytes through PKCzeta. *Cell* **106**, 489-498.

Etienne-Manneville, S., Hall, A. (2002). Rho GTPases in cell biology. *Nature* **420**, 629-635.

Etienne-Manneville, S., Hall, A. (2003). Cdc42 regulates GSK-3beta and adenomatous polyposis coli to control cell polarity. *Nature* **421**, 753-756.

Evangelista, M., Blundell, K., Longtine, M.S., Chow, C.J., Adames, N., Pringle, J.R., Peter, M., Boone, C. (1997). Bni1p, a yeast formin linking cdc42p and the actin cytoskeleton during polarized morphogenesis. *Science* **276**, 118-122.

Evangelista, M., Pruyne D., Amberg, D.C., Boone, C., Bretscher, A. (2002). Formins direct Arp2/3-independent actin filament assembly to polarize cell growth in yeast. *Nat. Cell Biol.* **4**, 260-269.

Evangelista, M., Zigmond, S., Boone, C. (2003). Formins: signaling effectors for assembly and polarization of actin filaments. *J. Cell Sci.* **116**, 2603-2611.

Evans, L., Mitchison, T., Kirschner, M. (1985). Influence of the centrosome on the structure of nucleated microtubules. *J. Cell Biol.* **100**, 1185-1191.

Feierbach, B., Chang, F. (2001). Roles of the fission yeast formin for3p in cell polarity, actin cable formation and symmetric cell division. *Curr. Biol.* **11**, 1656-1665.

Fischer, R.S., Fowler, V.M. (2003). Tropomodulins: life at the slow end. *Trends Cell Biol.* **13**, 593-601.

Frickey, T., Lupas, A.N. (2004). Phylogenetic analysis of AAA proteins. *J. Struct. Biol.* **146**, 2-10.

Fujiwara, T., Tanaka, K., Inoue, E., Kikyo, M., Takai, Y. (1999). Bni1p regulates microtubule-dependent nuclear migration through the actin cytoskeleton in Saccharomyces cerevisiae. *Mol. Cell Biol.* **19**, 8016-8027.

Fujiwara, T., Mammoto, A., Kim, Y., Takai, Y. (2000). Rho small G-protein-dependent binding of mDia to a Src homology 3 domain-containing IRSp53/BAIAP2. *Biochem. Biophys. Res. Commun.* **271**, 626-629.

Fujiwara, I., Takahashi, S., Tadakuma, H., Funatsu, T., Ishiwata, S. (2002). Microscopic analysis of polymerization dynamics with individual actin filaments. *Nat. Cell Biol.* **4**, 666-673.

Fukata, M., Kuroda, S., Fujii, K., Nakamura, T., Shoji, I., Matsuura, Y., Okawa, K., Iwamatsu, A., Kikuchi, A., Kaibuchi. K. (1997). Regulation of cross-linking of actin filament by IQGAP1, a target for Cdc42. *J. Biol. Chem.* **272**, 29579-29583.

Fukata, M., Watanabe, T., Noritake, J., Nakagawa, M., Yamaga, M., Kuroda, S., Matsuura, Y., Iwamatsu, A., Perez, F., Kaibuchi, K. (2002). Rac1 and Cdc42 capture microtubules through IQGAP1 and CLIP-170. *Cell* **109**, 873-885.

Fukata, M., Nakagawa, M., Kaibuchi, K. (2003). Roles of Rho-family GTPases in cell polarisation and directional migration. *Curr. Opin. Cell Biol.* **15**, 590-597.

Funamoto, S., Milan, K., Meili, R., Firtel, R.A. (2001). Role of phosphatidylinositol 3' kinase and a downstream pleckstrin homology domain-containing protein in controlling chemotaxis in dictyostelium. *J. Cell Biol.* **153**, 795-810.

Funamoto, S., Meili, R., Lee, S., Parry, L., Firtel, R.A. (2002). Spatial and temporal regulation of 3-phosphoinositides by PI 3-kinase and PTEN mediates chemotaxis. *Cell* **109**, 611-623.

Gagnoux-Palacios, L., Hervouet, C., Spirito, F., Roques, S., Mezzina, M., Danos, O., Meneguzzi, G. (2005). Assessment of optimal transduction of primary human skin keratinocytes by viral vectors. *J. Gene Med.* [Epub ahead of print]

Gasman, S., Kalaidzidis, Y., Zerial, M. (2003). RhoD regulates endosome dynamics through Diaphanous-related Formin and Src tyrosine kinase. *Nat. Cell Biol.* **5**, 195-204.

Gavet, O., Ozon, S., Manceau, V., Lawler, S., Curmi, P., Sobel, A. (1998). The stathmin phosphoprotein family: intracellular localization and effects on the microtubule network. *J. Cell Sci.* **111**, 3333-3346.

Geneste, O., Copeland, J.W., Treisman, R. (2002). LIM kinase and Diaphanous cooperate to regulate serum response factor and actin dynamics. *J. Cell Biol.* **157**, 831-838.

Gohla, A., Birkenfeld, J., Bokoch, G.M. (2005). Chronophin, a novel HAD-type serine protein phosphatase, regulates cofilin-dependent actin dynamics. *Nat. Cell Biol.* **1**, 21-29.

Goldschmidt-Clermont, P.J., Machesky, L.M., Baldassare, J.J., Pollard, T.D. (1990). The actin-binding protein profilin binds to PIP2 and inhibits its hydrolysis by phospholipase C. *Science* **247**, 1575-1578.

Graham, F.L., Smiley, J., Russell, W.C., Nairn, R. (1977). Characteristics of a human cell line transformed by DNA from human adenovirus type 5. *J. Gen. Virol.* **36**, 59-74.

Grosse, R., Copeland, J.W., Newsome, T.P., Way, M., Treisman, R (2003). A role for VASP in RhoA-Diaphanous signalling to actin dynamics and SRF activity. *EMBO J.* **22**, 3050-3061.

Gundersen, G.G., Kalnoski, M.H., Bulinski, J.C. (1984). Distinct populations of microtubules: tyrosinated and nontyrosinated alpha tubulin are distributed differently in vivo. *Cell* **38**, 779-789.

Gundersen, G.G. Microtubule capture: IQGAP and CLIP-170 expand the repertoire. (2002). *Curr. Biol.* **12**, R645-R647.

Gungabissoon, R.A., Bamburg, J.R. (2003). Regulation of growth cone actin dynamics by ADF/cofilin. *J. Histochem. Cytochem.* **51**, 411-420.

Gunning, P., Hardeman, E., Jeffrey, P., Weinberger, R. (1998). Creating intracellular structural domains: spatial segregation of actin and tropomyosin isoforms in neurons. *Bioessays* **20**, 892-900.

Habas, R., Kato, Y., He,X. (2001). Wnt/Frizzled Activation of Rho Regulates Vertebrate Gastrulation and Requires a Novel Formin Homology Protein Daam1. *Cell* **107**, 843-845.

Haj-Ahmad, Y., Graham, F.L. (1986). Characterization of an adenovirus type 5 mutant carrying embedded inverted terminal repeats. *Virology* **153**, 22-34.

Haque, N., Gong, C.X., Sengupta, A., Iqbal, K., Grundke-Iqbal, I. (2004). Regulation of microtubule-associated proteins, protein kinases and protein phosphatases during differentiation of SY5Y cells. *Brain Res. Mol. Brain Res.* **129**, 163-170.

Harui, A., Suzuki, S., Kochanek, S., Mitani, K. (1999). Frequency and stability of chromosomal integration of adenovirus vectors. *J. Virol.* **73**, 6141-6146.

Hartwig, J.H., Bokoch, G.M., Carpenter, C.L., Janmey, P.A., Taylor, L.A., Toker, A., Stossel, T.P. (1995). Thrombin receptor ligation and activated Rac uncap actin filament barbed ends through phosphoinositide synthesis in permeabilized human platelets. *Cell* **82**, 643-653.

Hawkins, M., Pope, B., Maciver, S.K., Weeds, A.G. (1993). Human actin depolymerizing factor mediates a pH-sensitive destruction of actin filaments. *Biochemistry* **32**, 9985-9993.

Hayden, J.H., Bowser, S.S., Rieder, C.L. (1990). Kinetochores capture astral microtubules during chromosome attachment to the mitotic spindle: direct visualization in live newt lung cells. *J. Cell Biol.* **111**, 1039-1045.

Hayden, S.M., Miller, P.S., Brauweiler, A., Bamburg, J.R. (1993). Analysis of the interactions of actin depolymerizing factor with G- and F-actin. *Biochemistry* **32**, 9994-10004.

Heath, J.P., Dunn, G.A. (1978). Cell to substratum contacts of chick fibroblasts and their relation to the microfilament system. A correlated interference-reflexion and high-voltage electron-microscope study. *J. Cell Sci.* **29**, 197-212.

Helfman, D.M., Levy, E.T., Berthier, C., Shtutman, M., Riveline, D., Grosheva, I., Lachish-Zalait, A., Elbaum, M., Bershadsky, A.D. (1999). Caldesmon inhibits nonmuscle cell contractility and interferes with the formation of focal adhesions. *Mol. Biol. Cell* **10**, 3097-3112.

Higgs, H.N., Peterson, K.J. (2005). Phylogenetic analysis of the formin homology 2 domain. *Mol. Biol. Cell.* **16**, 1-13.

Higgs, H.N., Pollard, T.D. (2000). Activation by Cdc42 and PIP (2) of Wiskott-Aldrich syndrome protein (WASp) stimulates actin nucleation by Arp2/3 complex. *J. Cell Biol.* **150**, 1311-1320.

Holmes, K.C., Popp, D., Gebhard, W., Kabsch, W. (1990). Atomic model of the actin filament. *Nature* **347**, 44-49,

Holy, T.E., Leibler, S. (1994). Dynamic instability of microtubules as an efficient way to search in space. *Proc. Natl. Acad. Sci. U S A* **91**, 5682-5685.

Honnappa, S., John, C.M., Kostrewa, D., Winkler, F.K., Steinmetz, M.O. (2005). Structural insights into the EB1-APC interaction. *EMBO J.* **24**, 261-269.

Hoogenraad, C.C., Akhmanova, A., Grosveld, F., De Zeeuw, C.I., Galjart, N. (2000). Functional analysis of CLIP-115 and its binding to microtubules. *J. Cell Sci.* **113**, 2285-2297.

Horio, T., Hotani, H. (1986). Visualization of the dynamic instability of individual microtubules by dark-field microscopy. *Nature* **321**, 605-607.

Howard, J., Hyman, A.A. (2003). Dynamics and mechanics of the microtubule plus end. *Nature* **422**, 753-758.

Howell, B., Larsson, N., Gullberg, M., Cassimeris, L. (1999). Dissociation of the tubulin-sequestering and microtubule catastrophe-promoting activities of oncoprotein 18/stathmin. *Mol. Biol. Cell* **10**, 105-118.

Hu, H., Li, M., Labrador, J.P., McEwen, J., Lai, E.C., Goodman, C.S., Bashaw, G.J. (2005). Cross GTPase-activating protein (CrossGAP)/Vilse links the Roundabout receptor to Rac to regulate midline repulsion. *Proc. Natl. Acad. Sci. U S A* **102**, 4613-4618.

Huff, T., Rosorius, O., Otto, A.M., Muller, C.S., Ballweber, E., Hannappel, E., Mannherz, H.G. (2004). Nuclear localisation of the G-actin sequestering peptide thymosin beta4. *J. Cell Sci.* **117**, 5333-5341.

Huxley, H.E. (1963). Electron microscope studies on the structure of natural and synthetic protein filaments from striated muscles. *J. Mol. Biol.* **7**, 281-308.

Illenberger, S., Drewes, G., Trinczek, B., Biernat, J., Meyer, H.E., Olmsted, J.B., Mandelkow, E.M., Mandelkow, E. (1996). Phosphorylation of microtubule-associated proteins MAP2 and MAP4 by the protein kinase p110mark. Phosphorylation sites and regulation of microtubule dynamics. *J. Biol. Chem.* **271**, 10834-10843.

Ishizaki, T., Naito, M., Fujisawa, K., Maekawa, M., Watanabe, N., Saito, Y., Narumiya, S. (1997). p160ROCK, a Rho-associated coiled-coil forming protein kinase, works downstream of Rho and induces focal adhesions. *FEBS Lett.* **404**, 118-124.

Ishizaki, T., Uehata, M., Tamechika, I., Keel, J., Nonomura, K., Maekawa, M., Narumiya, S. (2000). Pharmacological properties of Y-27632, a specific inhibitor of rho-associated kinases. *Mol. Pharmacol.* **57**, 976-983.

Ishizaki, T., Morishima, Y., Okamoto, M., Furuyashiki, T., Kato, T., Narumiya, S. (2001). Coordination of microtubules and the actin cytoskeleton by the Rho effector mDia1. *Nat. Cell Biol.* **3**, 8-14.

Jackson-Grusby, L., Kuo, A., Leder, P. (1992). A variant limb deformity transcript expressed in the embryonic mouse limb defines a novel formin. *Genes Dev.* **6**, 29-37.

Jessup, C.F., Brereton, H.M., Coster, D.J., Williams, K.A. (2005). In vitro adenovirus mediated gene transfer to the human cornea. *Br. J. Ophthalmol.* **89**, 658-661.

Kann, M.L., Soues, S., Levilliers, N., Fouquet, J.P. (2003). Glutamylated tubulin: Diversity of expression and distribution of isoforms. *Cell Motil. Cytoskeleton* **55**, 14-25.

Karabay, A., Yu, W., Solowska, J.M., Baird, D.H., Baas, P.W. (2004). Axonal growth is sensitive to the levels of katanin, a protein that severs microtubules. *J. Neurosci.* **24**, 5778-5788.

Kato, T., Watanabe, N., Morishima, Y., Fujita, A., Ishizaki, T., Narumiya, S. (2001). Localization of a mammalian homolog of diaphanous, mDia1, to the mitotic spindle in HeLa cells. *J. Cell Sci.* **114**, 775-784.

Katz, B.Z., Zamir, E., Bershadsky, A., Kam, Z., Yamada, K.M., Geiger, B. (2000). Physical state of the extracellular matrix regulates the structure and molecular composition of cell-matrix adhesions. *Mol. Biol. Cell* **11**, 1047-1060.

Kawano Y., Fukata Y., Oshiro N., Amano M., Nakamura T., Ito M., Matsumura F., Inagaki M., Kaibuchi K. (1999). Phosphorylation of myosin-binding subunit (MBS) of myosin phosphatase by Rho-kinase in vivo. *J. Cell Biol.* **147**, 1023-38.

Khaitlina, S., Walloscheck, M., Hinssen, H. (2004). Calcium-induced conformational changes in the C-terminal half of gelsolin stabilize its interaction with the actin monomer. *Biochemistry* **43**, 12838-12845.

Khyrul, W.A., LaLonde, D.P., Brown, M.C., Levinson, H., Turner, C.E. (2004). The integrin-linked kinase regulates cell morphology and motility in a rho-associated kinase-dependent manner. *J. Biol. Chem.* **279**, 54131-54139.

Kimura, K., Ito, M., Amano, M., Chihara, K., Fukata, Y., Nakafuku, M., Yamamori, B., Feng, J., Nakano, T., Okawa, K., Iwamatsu, A., Kaibuchi, K. (1996). Regulation of myosin phosphatase by Rho and Rho-associated kinase (Rho-kinase). *Science* **273**, 245-248.

Kiyokawa, E., Hashimoto, Y., Kobayashi, S., Sugimura, H., Kurata, T., Matsuda, M. (1998). Activation of Rac1 by a Crk SH3-binding protein, DOCK180. *Genes Dev.* **12**, 3331-3336.
Kleinebrecht, J., Selow, J., Winkler, W. (1982). The mouse mutant limb-deformity (ld). *Anat. Anz.* **152**, 313-324.

Klinghoffer, R.A., Sachsenmaier, C., Cooper, J.A., Soriano, P. (1999). Src family kinases are required for integrin but not PDGFR signal transduction. *EMBO J.* **18**, 2459-2471.

Kodama, A., Lechler, T., Fuchs, E. (2004). Coordinating cytoskeletal tracks to polarize cellular movements. *J. Cell Biol.* **167**, 203-207.

Kosako, H., Yoshida, T., Matsumura, F., Ishizaki, T., Narumiya, S., Inagaki, M. (2000). Rho-kinase/ROCK is involved in cytokinesis through the phosphorylation of myosin light chain and not ezrin/radixin/moesin proteins at the cleavage furrow. *Oncogene* **19**, 6059-6064.

Kostyukova, A.S., Rapp, B.A., Choy, A., Greenfield, N.J., Hitchcock-DeGregori, S.E. (2005). Structural requirements of tropomodulin for tropomyosin binding and actin filament capping. *Biochemistry* **44**, 4905-4910.

Kotani, K., Yonezawa, K., Hara, K., Ueda, H., Kitamura, Y., Sakaue, H., Ando, A., Chavanieu, A., Calas, B., Grigorescu, F. (1994). Involvement of phosphoinositide 3-kinase in insulin- or IGF-1-induced membrane ruffling. *EMBO J.* **13**, 2313-2321.

Kovacs, G.G., Laszlo, L., Kovacs, J., Jensen, P.H., Lindersson, E., Botond, G., Molnar, T., Perczel, A., Hudecz, F., Mezo, G., Erdei, A., Tirian, L., Lehotzky, A., Gelpi, E., Budka, H., Ovadi, J. (2004). Natively unfolded tubulin polymerization promoting protein TPPP/p25 is a common marker of alpha-synucleinopathies. *Neurobiol. Dis.* **17**, 155-162.

Kovar, D.R., Pollard, T.D. (2004). Insertional assembly of actin filament barbed ends in association with formins produces piconewton forces. *Proc. Natl. Acad. Sci. U S A* **101**, 14725-14730.

Kozlov, M.M., Bershadsky, A.D. (2004). Processive capping by formin suggests a force-driven mechanism of actin polymerization. *J. Cell Biol.* **167**, 1011-1017.

Kozma, R., Ahmed, S., Best, A., Lim, L. (1995). The Ras-related protein Cdc42Hs and bradykinin promote formation of peripheral actin microspikes and filopodia in Swiss 3T3 fibroblasts. *Mol. Cell Biol.* **15**, 1942-1952.

Kraehenbuhl, J.P., Racine, L., Jamieson, J.D. (1977). Immunocytochemical localization of secretory proteins in bovine pancreatic exocrine cells. *J. Cell Biol.* **72**, 406-423.

Krebs, A., Rothkegel, M., Klar, M., Jockusch, B.M. (2001). Characterization of functional domains of mDia1, a link between the small GTPase Rho and the actin cytoskeleton. *J. Cell Sci.* **114**, 3663-3672.

Krendel, M., Zenke, F.T., Bokoch, G.M. (2002). Nucleotide exchange factor GEF-H1 mediates cross-talk between microtubules and the actin cytoskeleton. *Nat. Cell Biol.* **4**, 294-301.

Kress, M., Huxley, H.E., Faruqi, A.R., Hendrix, J. (1986). Structural changes during activation of frog muscle studied by time-resolved X-ray diffraction. *J. Mol. Biol.* **188**, 325-342.

Kureishi, Y., Kobayashi, S., Amano, M., Kimura, K., Kanaide, H., Nakano, T., Kaibuchi, K., Ito, M. (1997). Rho-associated kinase directly induces smooth muscle contraction through myosin light chain phosphorylation. *J. Biol. Chem.* **272**, 12257-12260.

Laemmli, U.K. (1970). Cleavage of structural proteins during the assembly of the head of bacteriophage T4. *Nature* **227**, 680-685.

Lambrechts, A., Braun, A., Jonckheere, V., Aszodi, A., Lanier, L.M., Robbens, J., Van Colen, I., Vandekerckhove, J., Fassler, R., Ampe, C. (2000). Profilin II is alternatively spliced, resulting in profilin isoforms that are differentially expressed and have distinct biochemical properties. *Mol. Cell Biol.* **20**, 8209-8219.

Landry, J., Huot, J. (1995). Modulation of actin dynamics during stress and physiological stimulation by a signaling pathway involving p38 MAP kinase and heat-shock protein 27. *Biochem. Cell Biol.* **73**, 703-707.

Lansbergen, G., Komarova, Y., Modesti, M., Wyman, C., Hoogenraad, C.C., Goodson, H.V., Lemaitre, R.P., Drechsel, D.N., van Munster, E., Gadella, T.W. Jr., Grosveld, F., Galjart, N., Borisy, G.G., Akhmanova, A. (2004). Conformational changes in CLIP-170 regulate its binding to microtubules and dynactin localization. *J. Cell Biol.* **166**, 1003-1014.

Larson, L., Arnaudeau, S., Gibson, B., Li, W., Krause, R., Hao, B., Bamburg, J.R., Lew, D.P., Demaurex, N., Southwick, F. (2005). Gelsolin mediates calcium-dependent disassembly of Listeria actin tails. *Proc. Natl. Acad. Sci. USA.* **102**, 1921-1926.

Le Clainche, C., Pantaloni, D., Carlier, M.F. (2003). ATP hydrolysis on actin-related protein 2/3 complex causes debranching of dendritic actin arrays. *Proc. Natl. Acad. Sci. USA* **100**, 6337-6342.

Lee, L., Klee, S.K., Evangelista, M., Boone, C., Pellman, D. (1999). Control of mitotic spindle position by the Saccharomyces cerevisiae formin Bni1p. *J. Cell Biol.* **144**, 947-961.

le Gouvello S, Manceau V, Sobel A. (1998). Serine 16 of stathmin as a cytosolic target for Ca2+/calmodulin-dependent kinase II after CD2 triggering of human T lymphocytes. *J. Immunol.* **161**, 1113-1122.

Lehotzky, A., Tirian, L., Tokesi, N., Lenart, P., Szabo, B., Kovacs, J., Ovadi, J. (2004). Dynamic targeting of microtubules by TPPP/p25 affects cell survival. *J. Cell Sci.* **117**, 6249-6259.

Leighton, I.A., Curmi, P., Campbell, D.G., Cohen, P., Sobel, A. (1993). The phosphorylation of stathmin by MAP kinase. *Mol. Cell Biochem.* **127-128**, 151-156.

Lepley, D., Paik, J.H., Hla, T., Ferrer, F. (2005). The G protein-coupled receptor S1P2 regulates Rho/Rho kinase pathway to inhibit tumor cell migration. *Cancer Res.* **65**, 3788-3795.

Leung, T., Chen, X.Q., Manser, E., Lim, L. (1996). The p160 RhoA-binding kinase ROK alpha is a member of a kinase family and is involved in the reorganization of the cytoskeleton. *Mol. Cell Biol.* **16**, 5313-5327.

Li, F., Higgs, H.N. (2003). The mouse Formin mDia1 is a potent actin nucleation factor regulated by autoinhibition. *Curr. Biol.* **13**, 1335-1340.

Li, F., Higgs, H.N. (2005). Dissecting requirements for auto-inhibition of actin nucleation by the formin, mDia1. *J. Biol. Chem.* **280**, 6986-6992.

Lin, K.M., Mejillano, M., Yin, H.L. (2000). Ca^{2+} regulation of gelsolin by its C-terminal tail. *J. Biol. Chem.* **275**, 27746-27752.

Lodish, H., Berk, A., Zipursky, S.L., Matsudaira, P., Paltimore, D., Darnell, J.E. (2000). Molecular Cell Biology, 4th edition. W.H. Freeman and Co.: New York.

Louie, R.K., Bahmanyar, S., Siemers, K.A., Votin, V., Chang, P., Stearns, T., Nelson, W.J., Barth, A.I. (2004). Adenomatous polyposis coli and EB1 localize in close proximity of the mother centriole and EB1 is a functional component of centrosomes. *J. Cell Sci.* **117**, 1117-1128.

Lu, J., Pollard, T.D. (2001). Profilin binding to poly-L-proline and actin monomers along with ability to catalyze actin nucleotide exchange is required for viability of fission yeast. *Mol. Biol. Cell* **12**, 1161-1175.

Lu, B., Roegiers, F., Jan, L.Y., Jan, Y.N. (2001). Adherens junctions inhibit asymmetric division in the Drosophila epithelium. *Nature* **409**, 522-525.

Machesky, L.M., Atkinson, S.J., Ampe, C., Vandekerckhove, J., Pollard, T.D. (1994). Purification of a cortical complex containing two unconventional actins from Acanthamoeba by affinity chromatography on profilin-agarose. *J. Cell Biol.* **127**, 107-

115.

Machesky, L.M., Reeves, E., Wientjes, F., Mattheyse, F.J., Grogan, A., Totty, N.F., Burlingame, A.L., Hsuan, J.J., Segal, A.W. (1997). Mammalian actin-related protein 2/3 complex localizes to regions of lamellipodial protrusion and is composed of evolutionarily conserved proteins. *Biochem. J.* **328**, 105-112.

Machesky, L.M., Cooper, J.A. (1999). Cell motility. Bare bones of the cytoskeleton. *Nature* **401**, 542-543.

Maekawa, M., Ishizaki, T., Boku, S., Watanabe, N., Fujita, A., Iwamatsu, A., Obinata, T., Ohashi, K., Mizuno, K., Narumiya, S. (1999). Signaling from Rho to the actin cytoskeleton through protein kinases ROCK and LIM-kinase. *Science* **285**, 895-898.

Magdalena, J., Millard, T.H., Machesky, L.M. (2003). Microtubule involvement in NIH 3T3 Golgi and MTOC polarity establishment. *J. Cell Sci.* **116**, 743-756.

Marklund, U., Larsson, N., Gradin, H.M., Brattsand, G., Gullberg, M. (1996). Oncoprotein 18 is a phosphorylation-responsive regulator of microtubule dynamics. *EMBO J.* **15**, 5290-5298.

Margolis, R.L., Wilson, L. (1978). Opposite end assembly and disassembly of microtubules at steady state in vitro. *Cell* **13**, 1-8.

Marston, S.B., Redwood, C.S. (2003). Modulation of thin filament activation by breakdown or isoform switching of thin filament proteins: physiological and pathological implications. *Circ. Res.* **93**, 1170-1178.

Mass, R.L., Zeller, R., Woychik, R.P., Vogt, T.F., Leder, P. (1990). Disruption of formin-encoding transcripts in two mutant limb deformity alleles. *Nature* **346**, 853-855.

Massoumi, R., Larsson, Ch., Sjölander, A. (2002). Leukotriene D_4 induces stress-fibre formation in intestinal epithelial cells via activation of RhoA and PKCδ. J. Cell Sci. **115**, 3509-3515.

Mateer, S.C., Morris, L.E., Cromer, D.A., Bensenor, L.B., Bloom, G.S. (2004). Actin filament binding by a monomeric IQGAP1 fragment with a single calponin homology domain. *Cell Motil. Cytoskeleton* **58**, 231-241.

Matsushima, K., Aosaki, M., Tokuraku, K., Hasan, M.R., Nakagawa, H., Kotani, S. (2005). Identification of a neural cell specific variant of microtubule-associated protein 4. *Cell Struct. Funct.* **29**, 111-124.

Maucuer, A., Moreau, J., Mechali, M., Sobel, A. (1993). Stathmin gene family: phylogenetic conservation and developmental regulation in Xenopus. *J. Biol. Chem.* **268**, 16420-16429.

Maun, N.A., Speicher, D.W., DiNubile, M.J., Southwick, F.S. (1996). Purification and properties of a Ca(2+)-independent barbed-end actin filament capping protein, CapZ, from human polymorphonuclear leukocytes. *Biochemistry* **35**, 3518-3524.

McKean, P.G., Baines, A., Vaughan, S., Gull, K. (2003). Gamma-tubulin functions in the nucleation of a discrete subset of microtubules in the eukaryotic flagellum. *Curr. Biol.* **13**, 598-602.

McNally, F.J. (1996). Modulation of microtubule dynamics during the cell cycle. *Curr. Opin. Cell Biol.* **8**, 23-29.

McNally, K.P., Buster, D., McNally, F.J. (2002). Katanin-mediated microtubule severing can be regulated by multiple mechanisms. *Cell Motil. Cytoskeleton* **53**, 337-349.

Meberg, P.J., Ono, S., Minamide, L.S., Takahashi, M., Bamburg, J.R. (1998). Actin depolymerizing factor and cofilin phosphorylation dynamics: response to signals that regulate neurite extension. *Cell Motil. Cytoskeleton* **39**, 172-190.

Meng, W., Numazaki, M., Takeuchi, K., Uchibori, Y., Ando-Akatsuka, Y., Tominaga, M., Tominaga, T. (2004). DIP (mDia interacting protein) is a key molecule regulating Rho and Rac in a Src-dependent manner. *EMBO J.* **23**, 760-771.

Meyer, G., Kim, B., van Golen, C., Feldman, E.L. (2005). Cofilin activity during insulin-like growth factor I-stimulated neuroblastoma cell motility. *Cell Mol. Life Sci.* **62**, 461-470.

Miki, H., Takenawa, T. (2003). Regulation of actin dynamics by WASP family proteins. *J. Biochem. (Tokyo)* **134**, 309-313.

Miller, R.K., Cheng, S.C., Rose, M.D. (2000). Bim1p/Yeb1p mediates the Kar9p-dependent cortical attachment of cytoplasmic microtubules. *Mol. Biol Cell* **11**, 2949-2959.

Mimori-Kiyosue, Y., Tsukita, S. (2003). "Search-and-capture" of microtubules through plus-end-binding proteins (+TIPs). *J. Biochem. (Tokyo)* **134**, 321-326.

Minamide, L.S., Painter, W.B., Schevzov, G., Gunning, P., Bamburg, J.R. (1997). Differential regulation of actin depolymerizing factor and cofilin in response to alterations in the actin monomer pool. *J. Biol. Chem.* **272**, 8303-8309.

Minamide, L.S., Shaw, A.E., Sarmiere, P.D., Wiggan, O., Maloney, M.T., Bernstein, B.W., Sneider, J.M., Gonzalez, J.A., Bamburg, J.R. (2003). Production and use of replication-deficient adenovirus for transgene expression in neurons. *Methods Cell Biol.* **71**, 387-416.

Mitchison, T., Kirschner, M. (1984). Dynamic instability of microtubule growth. *Nature* **312**, 237-242.

Mitchison, T.J., Cramer, L.P. (1996). Actin-based cell motility and cell locomotion. *Cell* **84**, 371-379.

Morgan, T.E., Lockerbie, R.O., Minamide, L.S., Browning, M.D., Bamburg, J.R. (1993). Isolation and characterization of a regulated form of actin depolymerizing factor. *J. Cell Biol.* **122**, 623-633.

Mori, S., Yasuda, T., Takeshita, H., Nakajima, T., Nakazato, E., Mogi, K., Kaneko, Y., Kishi, K. (2001). Molecular, biochemical and immunological analyses of porcine pancreatic DNase I. *Biochim. Biophys. Acta.* **1547**, 275-287.

Morsy, M.A., Gu, M., Motzel, S., Zhao, J., Lin, J., Su, Q., Allen, H., Franlin, L., Parks, R.J., Graham, F.L., Kochanek, S., Bett, A.J., Caskey, C.T. (1998). An adenoviral vector deleted for all viral coding sequences results in enhanced safety and extended expression of a leptin transgene. *Proc. Natl. Acad. Sci. U S A* **95**, 7866-7781.

Morsy, M.A., Caskey, C.T. (1999). Expanded-capacity adenoviral vectors--the helper-dependent vectors. *Mol. Med. Today* **5**, 18-24.

Moseley, J.B., Sagot, I., Manning, A.L., Xu, Y., Eck, M.J., Pellman, D., Goode, B.L. (2004). A conserved mechanism for Bni1- and mDia1-induced actin assembly and dual regulation of Bni1 by Bud6 and profilin. *Mol. Biol. Cell* **15**, 896-907.

Mullins, R.D., Stafford, W.F., Pollard, T.D. (1997). Structure, subunit topology, and actin-binding activity of the Arp2/3 complex from Acanthamoeba. *J. Cell Biol.* **136**, 331-43.

Mullins, R.D., Heuser, J.A., Pollard, T.D. (1998). The interaction of Arp2/3 complex with actin: nucleation, high affinity pointed end capping, and formation of branching networks of filaments. *Proc. Natl. Acad. Sci. U S A* **95**, 6181-6186.

Nachmias, V.T., Huxley, H.E. (1970). Electron microscope observations on actomyosin and actin preparations from Physarum polycephalum, and on their interaction with heavy meromyosin subfragment I from muscle myosin. *J. Mol. Biol.* **50**, 83-90.

Nagata-Ohashi, K., Ohta, Y., Goto, K., Chiba, S., Mori, R., Nishita, M., Ohashi, K., Kousaka, K., Iwamatsu, A., Niwa, R., Uemura, T., Mizuno, K. (2004). A pathway of neuregulin-induced activation of cofilin-phosphatase Slingshot and cofilin in lamellipodia. *J. Cell Biol.* **165**, 465-471.

Nakagawa, H., Miki, H., Nozumi, M., Takenawa, T., Miyamoto, S., Wehland, J., Small, J.V. (2003). IRSp53 is colocalised with WAVE2 at the tips of protruding lamellipodia and filopodia independently of Mena. *J. Cell Sci.* **116**, 2577-2583.

Nakano, K., Takaishi, K., Kodama, A., Mammoto, A., Shiozaki, H., Monden, M., Takai, Y. (1999). Distinct actions and cooperative roles of ROCK and mDia in Rho small G protein-induced reorganization of the actin cytoskeleton in Madin-Darby canine kidney cells. *Mol. Biol. Cell.* **10**, 2481-2491.

Napirei, M., Karsunky, H., Zevnik, B., Stephan, H., Mannherz, H.G., Moroy, T. (2000). Features of systemic lupus erythematosus in Dnase1-deficient mice. *Nat. Genet.* **25**, 177-81.

Narumiya, S., Ishizaki, T., Watanabe, N. (1997). Rho effectors and reorganization of actin cytoskeleton. *FEBS Lett.* **410**, 68-72.

Nevins, J.R., DeGregori, J., Jakoi, L., Leone, G. (1997). Functional analysis of E2F transcription factor. *Methods Enzymol.* **283**, 205-219.

Nielsen, M.G., Turner, F.R., Hutchens, J.A., Raff, E.C. (2001). Axoneme-specific beta-tubulin specialization: a conserved C-terminal motif specifies the central pair. *Curr. Biol.* **11**, 529-533.

Nishida, E., Iida, K., Yonezawa, N., Koyasu, S., Yahara, I., Sakai, H. (1987). Cofilin is a component of intranuclear and cytoplasmic actin rods induced in cultured cells. *Proc. Natl. Acad. Sci. U S A* **84**, 5262-5266.

Nishimura, T., Yamaguchi, T., Kato, K., Yoshizawa, M., Nabeshima, Y., Ohno, S., Hoshino, M., Kaibuchi, K. (2005) PAR-6-PAR-3 mediates Cdc42-induced Rac activation through the Rac GEFs STEF/Tiam1. *Nat. Cell Biol.* **7**, 270-277.

Nishiya, N., Kiosses, W.B., Han, J., Ginsberg, M.H. (2005). An alpha4 integrin-paxillin-Arf-GAP complex restricts Rac activation to the leading edge of migrating cells. *Nat. Cell Biol.* **7**, 343-352.

Niwa, R., Nagata-Ohashi, K., Takeichi, M., Mizuno, K., Uemura, T. (2002). Control of actin reorganization by Slingshot, a family of phosphatases that dephosphorylate ADF/cofilin. *Cell* **108**, 233-246.

Nobes, C.D., Hall, A. (1995). Rho, rac, and cdc42 GTPases regulate the assembly of multimolecular focal complexes associated with actin stress fibers, lamellipodia, and filopodia. *Cell* **81**, 53-62.

Nobes, C.D. and Hall, A. (1999). Rho GTPases control polarity, protrusion, and adhesion during cell movement. *J. Cell Biol.* **144**, 1235-1244.

Noda, M., Yasuda-Fukazawa, C., Moriishi, K., Kato, T., Okuda, T., Kurokawa, K., Takuwa, Y. (1995). Involvement of rho in GTP gamma S-induced enhancement of

phosphorylation of 20 kDa myosin light chain in vascular smooth muscle cells: inhibition of phosphatase activity. *FEBS Lett.* **367**, 246-250.

Noiges, R., Eichinger, R., Kutschera, W., Fischer, I., Nemeth, Z., Wiche, G., Propst, F. (2002). Microtubule-associated protein 1A (MAP1A) and MAP1B: light chains determine distinct functional properties. *J. Neurosci.* **22**, 2106-2114.

Nyakern-Meazza, M., Narayan, K., Schutt, C.E., Lindberg, U. (2002). Tropomyosin and gelsolin cooperate in controlling the microfilament system. *J. Biol. Chem.* **277**, 28774-28779.

Ohta, Y., Kousaka, K., Nagata-Ohashi, K., Ohashi, K, Muramoto, A., Shima, Y., Niwa, R., Uemura, T., Mizuno, K. (2003). Differential activities, subcellular distribution and tissue expression patterns of three members of Slingshot family phosphatases that dephosphorylate cofilin. *Genes Cells* **8**, 811-824.

Okada, K., Takano-Ohmuro, H., Obinata, T., Abe, H. (1996). Dephosphorylation of cofilin in polymorphonuclear leukocytes derived from peripheral blood. *Exp. Cell Res.* **227**, 116-122.

Okazaki, T., Wang, H., Masliah, E., Cao, M., Johnson, S.A., Sundsmo, M., Saitoh, T., Mori, N. (1995). SCG10, a neuron-specific growth-associated protein in Alzheimer's disease. *Neurobiol. Aging* **16**, 883-894.

Omelchenko, T., Vasiliev, J.M, Gelfand, I.M., Feder, H.H, Bonder, E.M (2002). Mechanisms of polarization of the shape of fibroblasts and epitheliocytes: Separation of the roles of microtubules and Rho-dependent actin–myosin contractility. *Proc. Natl. Acad. Sci. U S A* **99**, 10452-10457.

O'Neill, G.M., Fashena, S.J., Golemis, E.A. (2000). Integrin signalling: a new Cas(t) of characters enters the stage. *Trends Cell Biol.* **10**, 111-119.

Ono, S., Ono, K. (2002). Tropomyosin inhibits ADF/cofilin-dependent actin filament dynamics. *J. Cell Biol.* **156**, 1065-1076.

Ono, S., Abe, H., Nagaoka, R., Obinata, T. (1993). Colocalization of ADF and cofilin in intranuclear actin rods of cultured muscle cells. *J. Muscle Res. Cell Motil.* **14**, 195-204.

Orosz, F., Kovacs, G.G., Lehotzky, A., Olah, J., Vincze, O., Ovadi, J. (2004). TPPP/p25: from unfolded protein to misfolding disease: prediction and experiments. *Biol. Cell.* **96**,701-711.

Otterbein, L.R., Graceffa, P., Dominguez, R. (2001). The crystal structure of uncomplexed actin in the ADP state. *Science* **293**, 708-711.

Ozon, S., Byk, T., Sobel, A. (1998). SCLIP: a novel SCG10-like protein of the stathmin family expressed in the nervous system. *J. Neurochem.* **70**, 2386-2396.

Palazzo, A.F., Cook, T.A., Alberts, A.S., Gundersen, G.G. (2001). mDia mediates Rho-regulated formation and orientation of stable microtubules. *Nat. Cell Biol.* **3**, 723-729.

Palazzo, A.F., Eng, C.H., Schlaepfer, D.D., Marcantonio, E.E., Gundersen, G.G. (2004). Localized stabilization of microtubules by integrin- and FAK-facilitated Rho signaling. *Science* **303**, 836-839.

Pantaloni, D., Boujemaa, R., Didry, D., Gounon, P., Carlier, M.F. (2000). The Arp2/3 complex branches filament barbed ends: functional antagonism with capping proteins. *Nat. Cell Biol.* **2**, 385-391.

Peitsch, M.C., Polzar, B., Stephan, H., Crompton, T., MacDonald, H.R., Mannherz, H.G., Tschopp, J. (1993). Characterization of the endogenous deoxyribonuclease involved in nuclear DNA degradation during apoptosis (programmed cell death). *EMBO J.* **12**, 371-377.

Peng, J., Wallar, B.J., Flanders, A., Swiatek, P.J., Alberts, A.S. (2003). Disruption of the Diaphanous-related formin Drf1 gene encoding mDia1 reveals a role for Drf3 as an effector for Cdc42. *Curr. Biol.* **13**, 534-545.

Perez, F., Diamantopoulos, G.S., Stalder, R., Kreis, T.E. (1999). CLIP-170 highlights growing microtubule ends in vivo. *Cell* **96**, 517-527.

Perry, S.V. (2001). Vertebrate tropomyosin: distribution, properties and function. *J. Muscle Res. Cell Motil.* **22**, 5-49.

Pollard, T.D., Blanchoin, L., Mullins, R.D. (2000). Molecular mechanisms controlling actin filament dynamics in nonmuscle cells. *Annu. Rev. Biophys. Biomol. Struct.* **29**, 545-576.

Pollard, T.D. (2002). Formins initiate new actin filaments. *Nat. Cell Biol.* **4**, E191-E192.

Ponti, A., Machacek, M., Gupton, S.L., Waterman-Storer, C.M., Danuser, G. (2004). Two distinct actin networks drive the protrusion of migrating cells. *Science* **305**, 1782-1786.

Pring, M., Evangelista, M., Boone, C., Yang, C., Zigmond, SH. (2003). Mechanism of formin-induced nucleation of actin filaments. *Biochemistry* **42**, 486-496.

Pruyne, D., Evangelista, M., Yang, C., Bi, E., Zigmond, S., Bretscher, A., Boone, C. (2002). Role of formins in actin assembly: nucleation and barbed-end association. *Science* **297**, 612-615.

Raftopoulou, M., Hall, A. (2004). Cell migration: Rho GTPases lead the way. *Dev. Biol.* **265**, 23-32.

Raman, N., Atkinson, S.J. (1999). Rho controls actin cytoskeletal assembly in renal epithelial cells during ATP depletion and recovery. *Am. J. Physiol.* **276**, C1312-C1324.

Rauch, F., Polzar, B., Stephan, H., Zanotti, S., Paddenberg, R., Mannherz, H.G.(1997). Androgen ablation leads to an upregulation and intranuclear accumulation of deoxyribonuclease I in rat prostate epithelial cells paralleling their apoptotic elimination. *J. Cell Biol.* **137**, 909-923.

Reinhard, M., Giehl, K., Abel, K., Haffner, C., Jarchau, T., Hoppe, V., Jockusch, B.M., Walter, U. (1995). The proline-rich focal adhesion and microfilament protein VASP is a ligand for profilins. *EMBO J.* **14**, 1583-1589.

Rekosh, D.M., Russell, W.C., Bellet, A.J., Robinson, A.J. (1977). Identification of a protein linked to the ends of adenovirus DNA. *Cell* **11**, 283-95.

Ren, Y., Li, R., Zheng, Y., Busch, H. (1998). Cloning and characterization of GEF-H1, a microtubule-associated guanine nucleotide exchange factor for Rac and Rho GTPases. *J. Biol. Chem.* **273**, 34954-34960.

Ridley, A.J., Hall, A. (1992). Distinct patterns of actin organization regulated by the small GTP-binding proteins Rac and Rho. *Cold Spring Harb. Symp. Quant. Biol.* **57**, 661-671.

Ridley, A.J., Paterson, H.F., Johnston, C.L., Diekmann, D., Hall, A. (1992). The small GTP-binding protein rac regulates growth factor-induced membrane ruffling. *Cell* **70**, 401-410.

Riveline, D., Zamir, E., Balaban, N.Q., Schwarz, U.S., Ishizaki, T., Narumiya, S., Kam, Z., Geiger, B., Bershadsky, A.D. (2001). Focal contacts as mechanosensors: externally applied local mechanical force induces growth of focal contacts by an mDia1-dependent and ROCK-independent mechanism. *J. Cell Biol.* **153**, 1175-1186.

Rohatgi, R., Ho, H.Y., Kirschner, M.W. (2000). Mechanism of N-WASP activation by CDC42 and phosphatidylinositol 4, 5-bisphosphate. *J. Cell Biol.* **150**, 1299-1310.

Rottner, K., Hall, A., Small, J.V. (1999). Interplay between Rac and Rho in the control of substrate contact dynamics. *Curr. Biol.* **9**, 640-648.

Rubinfeld, B., Albert, I., Porfiri, E., Fiol, C., Munemitsu, S., Polakis, P. (1996). Binding of GSK3beta to the APC-beta-catenin complex and regulation of complex assembly. *Science* **272**, 1023-1026.

Russell, W. C. (2000). Update on adenovirus and its vectors. *J. Gen. Virol.* **81**, 2573–2604.

Safer, D., Sosnick, T.R., Elzinga, M. (1997). Thymosin beta 4 binds actin in an extended conformation and contacts both the barbed and pointed ends. *Biochemistry* **36**, 5806-5816.

Sagot, I., Klee, S.K., Pellman, D. (2002). Yeast formins regulate cell polarity by controlling the assembly of actin cables. *Nat. Cell Biol.* **4**, 42-50.

Sagot, I., Rodal, A.A., Moseley, J., Goode, B.L., Pellman, D. (2002). An actin nucleation mechanism mediated by Bni1 and profilin. *Nat. Cell Biol.* **4**, 626-631.

Sambrook, J., Fritsch, E.F., Maniatis, T. (1989). Molecular Cloning: A laboratory manual, 2nd edition. Cold Spring Harbor Laboratory Press, Cold Spring Harbor, New York.

Sambrook, J., Russell, D.W. (2001) Molecular cloning: A laboratory manual. 3rd edition. Cold Spring Harbor Laboratory Press, Cold Spring Harbor, New York.

Satoh, S., Tominaga, T. (2001). mDia-interacting protein acts downstream of Rho-mDia and modifies Src activation and stress fiber formation. *J. Biol. Chem.* 2001, **276**, 39290-39294.

Schafer, D.A., Cooper, J.A. (1995). Control of actin assembly at filament ends. *Annu. Rev. Cell Dev. Biol.* **11**, 497-518.

Schafer, D.A., Jennings, P.B., Cooper, J.A. (1996). Dynamics of capping protein and actin assembly in vitro: uncapping barbed ends by polyphosphoinositides. *J. Cell Biol.* **135**, 169-179.

Schirenbeck, A., Bretschneider, T., Arasada, R., Schleicher, M., Faix, J. (2005). The Diaphanous-related formin dDia2 is required for the formation and maintenance of filopodia. *Nat. Cell Biol.* **7**, 619-625.

Schluter, K., Jockusch, B.M., Rothkegel, M. (1997). Profilins as regulators of actin dynamics. *Biochim. Biophys. Acta.* **1359**, 97-109.

Schmidt, M.R., Piekos, B., Cabatingan, M.S., Woodland, R.T. (2000). Expression of a human coxsackie/adenovirus receptor transgene permits adenovirus infection of primary lymphocytes. *J. Immun.* **165**, 4112-4119.

Schuyler, S.C., Pellman, D. (2001). Microtubule "plus-end-tracking proteins": The end is just the beginning. *Cell* **105**, 421-424.

Servant, G., Weiner, O.D., Herzmark, P., Balla, T., Sedat, J.W., Bourne, H.R. (2000). Polarization of chemoattractant receptor signaling during neutrophil chemotaxis. *Science* **287**, 1037-1040.

Severson, A.F., Baillie, D.L., Bowerman, B. (2002). A Formin Homology protein and a profilin are required for cytokinesis and Arp2/3-independent assembly of cortical microfilaments in C. elegans. *Curr. Biol.* **12**, 2066-2075.

Schutt, C.E., Myslik, J.C., Rozycki, M.D., Goonesekere, N.C., Lindberg, U. (1993). The structure of crystalline profilin-beta-actin. *Nature* **365**, 810-816.

Sherwood, N.T., Sun, Q., Xue, M., Zhang, B., Zinn, K. (2004). Drosophila spastin regulates synaptic microtubule networks and is required for normal motor function. *PLoS Biol.* **2**, e429.

Shimada, A., Nyitrai, M., Vetter, I.R., Kuhlmann, D., Bugyi, B., Narumiya, S., Geeves, M.A., Wittinghofer, A. (2004). The core FH2 domain of diaphanous-related formins is an elongated actin binding protein that inhibits polymerization. *Mol. Cell* **13**, 511-522.

Shimada, O., Suzuki, S., Tosaka-Shimada, H., Ishikawa, H. (1998). Detection of deoxyribonuclease I in a hormone-secretory pathway of pituitary cells in humans and rats. *Cell Struct. Funct.* **23**, 49-56.

Smith, H.C., Berezney, R., Brewster, J.M., Rekosh, D. (1985). Properties of adenoviral DNA bound to the nuclear matrix. *Biochemistry* **24**, 1197-1202.

Soltani, M.H., Pichardo, R., Song, Z., Sangha, N., Camacho, F., Satyamoorthy, K., Sangueza, O.P., Setaluri, V. (2005). Microtubule-associated protein 2, a marker of neuronal differentiation, induces mitotic defects, inhibits growth of melanoma cells, and predicts metastatic potential of cutaneous melanoma. *Am. J. Pathol.* **166**, 1841-1850.

Soosairajah, J., Maiti, S., Wiggan, O., Sarmiere, P., Moussi, N., Sarcevic, B., Sampath, R., Bamburg, J.R., Bernard, O. (2005). Interplay between components of a novel LIM kinase-slingshot phosphatase complex regulates cofilin. *EMBO J.* **24**, 473-486.

Spiegelman, B.M., Penningroth, S.M., Kirschner, M.W. (1977). Turnover of tubulin and the N site GTP in Chinese hamster ovary cells. *Cell* **12**, 587-600.

Steigerwald, K., Behbehani, G.K., Combs, K.A., Barton, M.C., Groden, J. (2005). The APC tumor suppressor promotes transcription-independent apoptosis in vitro. *Mol. Cancer Res.* **3**, 78-89.

Steinmetz MO, Stoffler D, Hoenger A, Bremer A, Aebi U. (1997). Actin: from cell biology to atomic detail. *J. Struct. Biol.***119**, 295-320.

Stepanova, T., Slemmer, J., Hoogenraad, C.C., Lansbergen, G., Dortland, B., De Zeeuw, C.I., Grosveld, F., van Cappellen, G., Akhmanova, A., Galjart, N. (2003). Visualization of microtubule growth in cultured neurons via the use of EB3-GFP (end-binding protein 3-green fluorescent protein). *J. Neurosci.* **23**, 2655-2664.

Stillman, B.W., Bellett, A.J., Robinson, A.J. (1977). Replication of linear adenovirus DNA is not hairpin-primed. *Nature* **269**, 723-725.

Stradal, T.E., Rottner, K., Disanza, A., Confalonieri, S., Innocenti, M., Scita, G. (2004). Regulation of actin dynamics by WASP and WAVE family proteins. *Trends Cell Biol.* **14**, 303-311.

Su, L.K., Burrell, M., Hill, D.E., Gyuris, J., Brent, R., Wiltshire, R., Trent, J., Vogelstein, B., Kinzler, K.W. (1995). APC binds to the novel protein EB1. *Cancer Res.* **55**, 2972-2977.

Suetsugu, S., Miki, H., Takenawa, T. (1998). The essential role of profilin in the assembly of actin for microspike formation. *EMBO J.* **17**, 6516-6526.

Sumi, T., Matsumoto, K., Takai, Y., Nakamura, T. (1999). Cofilin phosphorylation and actin cytoskeletal dynamics regulated by rho- and Cdc42-activated LIM-kinase 2. *J. Cell Biol.* **147**, 1519-1532.

Sumi, T., Matsumoto, K., Nakamura, T. (2001). Specific activation of LIM kinase 2 via phosphorylation of threonine 505 by ROCK, a Rho-dependent protein kinase. *J. Biol. Chem.* **276**, 670-676.

Svenson, I.K., Kloos, M.T., Jacon, A., Gallione, C., Horton, A.C., Pericak-Vance, M.A., Ehlers, M.D., Marchuk, D.A. (2005). Subcellular localization of spastin: implications for the pathogenesis of hereditary spastic paraplegia. *Neurogenetics* [Epub ahead of print].

Svitkina, T.M., Verkhovsky, A.B., McQuade, K.M., Borisy, G.G. (1997). Analysis of the actin-myosin II system in fish epidermal keratocytes: mechanism of cell body translocation. *J. Cell Biol.* **139**, 397-415.

Svitkina, T.M., Borisy, G.G. (1998). Correlative light and electron microscopy of the cytoskeleton of cultured cells. *Methods Enzymol.* **298**, 570-592.

Svitkina, T.M., Borisy, G.G. (1999). Arp2/3 complex and actin depolymerizing factor/cofilin in dendritic organization and treadmilling of actin filament array in lamellipodia. *J. Cell Biol.* **145**, 1009-1026.

Svitkina, T.M., Bulanova, E.A., Chaga, O.Y., Vignjevic, D.M., Kojima, S., Vasiliev, J.M., Borisy, G.G. (2003). Mechanism of filopodia initiation by reorganization of a dendritic network. *J. Cell Biol.* **160**, 409-421.

Symons, M., Derry, J.M., Karlak, B., Jiang, S., Lemahieu, V., Mccormick, F., Francke, U., Abo, A. (1996). Wiskott-Aldrich syndrome protein, a novel effector for the GTPase CDC42Hs, is implicated in actin polymerization. *Cell* **8**, 723-734.

Takaishi, K., Matozaki, T., Nakano, K., Takai, Y. (2000). Multiple downstream signalling pathways from ROCK, a target molecule of Rho small G protein, in reorganization of the actin cytoskeleton in Madin-Darby canine kidney cells. *Genes Cells* **5**, 929-936.

Tawil, N., Wilson, P., Carbonetto, S. (1993). Integrins in point contacts mediate cell spreading: factors that regulate integrin accumulation in point contacts vs. focal contacts. *J. Cell Biol.* **120**, 261-271.

Theriot, J.A., Mitchison, T.J. (1991). Actin microfilament dynamics in locomoting cells. *Nature* **352**, 126-131.

Tirian L, Hlavanda E, Olah J, Horvath I, Orosz F, Szabo B, Kovacs J, Szabad J, Ovadi J. (2003). TPPP/p25 promotes tubulin assemblies and blocks mitotic spindle formation. *Proc. Natl. Acad. Sci. U S A* **100**, 13976-13981.

Tirnauer, J.S., Bierer, B.E. (2000). EB1 proteins regulate microtubule dynamics, cell polarity, and chromosome stability. *J. Cell Biol.* **149**, 761-766.

Tolliday, N., VerPlank, L., Li, R. (2002). Rho1 directs formin-mediated actin ring assembly during budding yeast cytokinesis. *Curr. Biol.* **12**, 1864-1870.

Tominaga, T., Sahai, E., Chardin, P., McCormick, F., Courtneidge, S.A., Alberts, A.S. (2000). Diaphanous-related formins bridge Rho GTPase and Src tyrosine kinase signaling. *Mol. Cell.* **5**, 13-25.

Trumpp, A., Blundell, P.A., de la Pompa, J.L., Zeller, R. (1992). The chicken limb deformity gene encodes nuclear proteins expressed in specific cell types during morphogenesis. *Genes Dev.* **6**, 14-28.

Tsuji, T., Ishizaki, T., Okamoto, M., Higashida, C., Kimura, K., Furuyashiki, T., Arakawa, Y., Birge, R.B., Nakamoto, T., Hirai, H., Narumiya, S. (2002). ROCK and mDia1 antagonize in Rho-dependent Rac activation in Swiss 3T3 fibroblasts. *J. Cell Biol.* **157**, 819-830.

Vallee, R.B., Borisy, G.G. (1977). Removal of the projections from cytoplasmic microtubules in vitro by digestion with trypsin. *J. Biol. Chem.* **252**, 377-382.

Van Aelst, L., Symons, M. (2002). Role of Rho family GTPases in epithelial morphogenesis. *Genes Dev.* **16**, 1032-1054.

Vartiainen, M.K., Machesky, L.M. (2004). The WASP-Arp2/3 pathway: genetic insights. *Curr. Opin. Cell Biol.* **16**, 174-181.

Verma, I.M., Somia, N. (1997). Gene therapy -- promises, problems and prospects. *Nature* **389**, 239-242.

Vicente-Manzanares, M., Rey, M., Perez-Martinez, M., Yanez-Mo, M., Sancho, D., Cabrero, J.R., Barreiro, O., de la Fuente, H., Itoh, K., Sanchez-Madrid, F. (2003). The RhoA effector mDia is induced during T cell activation and regulates actin polymerization and cell migration in T lymphocytes. *J. Immunol.* **171**, 1023-1034.

Vogt, T.F., Jackson-Grusby, L., Rush, J., Leder, P. (1993). Formins: phosphoprotein isoforms encoded by the mouse limb deformity locus. *Proc. Natl. Acad. Sci. U S A* **90**, 5554-5558.

Walker, R. A., O'Brien, E.T., Pryer, N.K., Soboeiro, M., Voter, W.A., Erickson, H.P., Salmon, E.D. (1988). Dynamic instability of individual microtubules analyzed by video light microscopy: rate constants and transition frequencies. *J. Cell Biol.* **107**, 1437-1448.

Wallar, B.J., Alberts, A.S. (2003). The formins: active scaffolds that remodel the cytoskeleton. *Trends Cell Biol.* **13**, 435-446.

Wasserman, S. (1998). FH proteins as cytoskeletal organizers. *Trends Cell Biol.* **8**, 111-115.

Watanabe, N., Madaule, P., Reid, T., Ishizaki, T., Watanabe, G., Kakizuka, A., Saito, Y., Nakao, K., Jockusch, B.M., Narumiya, S. (1997). p140mDia, a mammalian homolog of Drosophila diaphanous, is a target protein for Rho small GTPase and is a ligand for profilin. *EMBO J.* **16**, 3044-3056.

Watanabe, N., Kato, T., Fujita, A., Ishizaki, T., Narumiya, S. (1999). Cooperation between mDia1 and ROCK in Rho-induced actin reorganization. *Nat. Cell Biol.* **1**, 136-143.

Watanabe, N., Higashida, C. (2004). Formins: processive cappers of growing actin filaments. *Exp. Cell Res.* **301**, 16-22.

Weaver, A.M., Heuser, J.E., Karginov, A.V., Lee, W.L., Parsons, J.T., Cooper, J.A. (2002). Interaction of cortactin and N-WASp with Arp2/3 complex. *Curr. Biol.* **12**, 1270-1278.

Wegner, A. (1982). Treadmilling of actin at physiological salt concentrations. An analysis of the critical concentrations of actin filaments. *J. Mol. Biol.* **161**, 607-615.

Wedlich-Soldner, R., Li, R. (2004). Closing the loops: new insights into the role and regulation of actin during cell polarization. *Exp. Cell Res.* **301**, 8-15.

Wen, Y., Eng, C.H., Schmoranzer, J., Cabrera-Poch, N., Morris, E.J., Chen, M., Wallar, B.J., Alberts, A.S., Gundersen, G.G. (2004). EB1 and APC bind to mDia to stabilize microtubules downstream of Rho and promote cell migration. *Nat. Cell Biol.* **6**, 820-830.

Wittmann, T., Waterman-Storer, C.M. (2001). Cell motility: can Rho GTPases and microtubules point the way? *J. Cell Sci.* **114**, 3795-3803.

Wittmann, T., Bokoch, G.M., Waterman-Storer, C.M. (2004). Regulation of microtubule destabilizing activity of Op18/stathmin downstream of Rac1. *J. Biol. Chem.* **279**, 6196-6203.

Wodarz, A. (2002). Establishing cell polarity in development. *Nat. Cell Biol.* **4**, E39-44.

Worthylake, R.A., Burridge, K. (2003). RhoA and ROCK promote migration by limiting membrane protrusions. *J. Biol. Chem.* **278**, 13578-13584.

Xu, Y., Moseley, J.B., Sagot, I., Poy, F., Pellman, D., Goode, B.L., Eck, M.J. (2004). Crystal structures of a Formin Homology-2 domain reveal a tethered dimer architecture. *Cell* **116**, 711-723.

Yamada, A., Hara, A., Inoue, M., Kamizono, S., Higuchi, T., Itoh, K. (1997). Beta 2-integrin-mediated signal up-regulates counterreceptor ICAM-1 expression on human monocytic cell line THP-1 through tyrosine phosphorylation. *Cell Immunol.* **178**, 9-16.

Yano, H., Uchida, H., Iwasaki, T., Mukai, M., Akedo, H., Nakamura, K., Hashimoto, S., Sabe, H. (2000). Paxillin alpha and Crk-associated substrate exert opposing effects on cell migration and contact inhibition of growth through tyrosine phosphorylation. *Proc. Natl. Acad. Sci. U S A* **197**, 9076-9081.

Yeh, P., Perricaudet, M. (1997). Advances in adenoviral vectors: from genetic engineering to their biology. *FASEB J.* **11**, 615-623.

Yonezawa, N., Nishida, E., Sakai, H. (1985). pH control of actin polymerization by cofilin. *J. Biol. Chem.* **260**, 14410-14412.

Yonezawa, N., Nishida, E., Iida, K., Yahara, I., Sakai, H. (1990). Inhibition of the interactions of cofilin, destrin, and deoxyribonuclease I with actin by phosphoinositides. *J. Biol. Chem.* **265**, 8382-8386.

Yu, F.X., Lin, S.C., Morrison-Bogorad, M., Atkinson, M.A., Yin, H.L. (1993). Thymosin beta 10 and thymosin beta 4 are both actin monomer sequestering proteins. *J. Biol. Chem.* **268**, 502-509.

Zamir, E., Katz, B.Z., Aota, S., Yamada, K.M., Geiger, B., Kam, Z. (1999). Molecular diversity of cell-matrix adhesions. *J. Cell Sci.* **112**, 1655-1669.

Zamir, E., Katz, M., Posen, Y., Erez, N., Yamada, K.M., Katz, B.Z., Lin, S., Lin, D.C., Bershadsky, A., Kam, Z., Geiger, B. (2000). Dynamics and segregation of cell-matrix adhesions in cultured fibroblasts. *Nat. Cell Biol.* **2**, 191-196.

Zenke, F.T., Krendel, M., DerMardirossian, C., King, C.C., Bohl, B.P., Bokoch, G.M. (2004). p21-activated kinase 1 phosphorylates and regulates 14-3-3 binding to GEF-H1, a microtubule-localized Rho exchange factor. *J. Biol. Chem.* **279**, 18392-18400.

Zheng Y. (2001). Dbl family guanine nucleotide exchange factors. *Trends Biochem. Sci.* **26**, 724-732.

Zigmond, S.H., Evangelista, M., Boone, C., Yang, C., Dar, A.C., Sicheri, F., Forkey, J., Pring, M. (2003) Formin leaky cap allows elongation in the presence of tight capping proteins. *Curr. Biol.* **13**, 1820-1823.

Zumbrunn, J., Kinoshita, K., Hyman, A.A., Nathke, I.S. (2001). Binding of the adenomatous polyposis coli protein to microtubules increases microtubule stability and is regulated by GSK3 beta phosphorylation. *Curr. Biol.* **11**, 44-49.